Manganese Deposits of the Cape Peninsula, South Africa

Duncan Graeme MacGregor
MCGDUN004

Thesis presented for the degree of Master of Science

In the Department of Geological Sciences
University of Cape Town
May 2013

ABSTRACT

The outcrops, petrography and geochemistry of manganese deposits were studied at several sites on the Cape Peninsula (Skeleton Gorge, Kasteelpoort Path, Kommetjie and Hout Bay) as well as at Rooi Els on the opposite side of False Bay. The purpose of this study was to understand the origin and depositional history of these manganese deposits. Manganese ore samples contain between 16 and 86 wt% MnO, 0.3 to 29 wt% Fe_2O_3, 1.2 and 5.6 wt% K_2O and a P_2O_5 content of 0.3 to 1.8 wt%. The primary manganese oxide mineral present is cryptomelane (KMn_8O_{16}). The iron and quartz content of bulk rock samples have a positive correlation, and a negative correlation to manganese. From the field data, petrography and chemistry by electron microprobe analysis, it was established that the method of deposition was lateral secretion and the deposits fit into Harrison's (1998) manganese classification as a Type 1 deposit. Lateral secretion involves the reduction of manganese and iron oxides within the soil profile by acidified rain water, further leaching of oxides as reducing groundwaters flow through regolith and bedrock, and the eventual precipitation as oxides at groundwater seeps and springs.

Field observations and the chemistry of water and rock samples support the lateral secretion model in which the manganese and iron are chemically leached from the Peninsula Formation quartz arenite sandstone bedrock and transported along fractures and faults to be deposited as oxides upon emergence at the surface. Minor surface coatings of iron and manganese oxides are ubiquitous in the study area but can become concentrated in locally historic economic deposits where the groundwater flow is focused by topography, aquitards and faults. Trace element composition of the manganese-rich deposits indicates that they are low-temperature, hydrogenous freshwater deposits. The proposed Eh-pH evolution of surface and ground water flow paths is consistent with the reduction of manganese and iron within the soil profile, and the precipitation of first iron and then manganese at springs and seeps. The Rare Earth Element (REE) patterns suggest variable sources and transport of the manganese and iron. The manganese deposits of the Cape Peninsula are no longer economic but do provide insights into the remobilisation of metals by low temperature groundwaters during the process of lateral secretion.

Manganese , Skeleton Gorge , Lateral Secretion, Cape Peninsula

PLAGIARISM DECLARATION

I know that plagiarism is wrong. Plagiarism is to use another's work and pretend that it is one's own. Each significant contribution to, and quotation in this thesis from the work of other people has been attributed and has been cited and referenced. I have not allowed, and will not allow anyone to copy my work with the intention of passing it off as his or her own work.

Signature: _____

Date: _____

ACKNOWLEDGEMENTS

I would like to sincerely thank all the people that have been influential in this dissertation.

My supervisor John Compton, for dedicating so much of his time in helping me complete this thesis and in sharing his wealth of knowledge.

My colleague Ed Swindell, for the use of his vast manganese knowledge and library.

My wife, for her unwavering support and patience.

TABLE OF CONTENTS

1. INTRODUCTION 1

1.1 MANGANESE IN THE CAPE PENINSULA 1
1.2 GEOLOGICAL SETTING 3
1.3 MANGANESE DEPOSIT CLASSIFICATIONS 7
1.4 MANGANESE, ITS PURPOSES AND APPLICATIONS 14
1.5 STUDY OBJECTIVES 17

2 METHODS 18

2.1 FIELD WORK AND SAMPLING 18
2.2 PETROGRAPHY 23
2.3 MINERAL AND CHEMICAL ANALYSIS 25

3 RESULTS 28

3.1 FIELD ANALYSIS 28
3.1.1 CONTOUR PATH SITE 28
3.1.2 SKELETON GORGE SITE 28
3.1.3 KASTEELPOORT PATH 38
3.1.4 ROOI ELS 39
3.1.5 KOMMETJIE 45
3.1.6 HOUT BAY MANGANESE MINE 47
3.1.7 PHYSICAL VARIATIONS AMONG DEPOSITIONAL SITES 48
3.2 CHEMICAL ANALYSIS 50
3.2.1 X-RAY FLUORESCENCE RESULTS 50
3.2.2 X-RAY DIFFRACTION RESULTS 59
3.2.3 INDUCTIVELY COUPLED PLASMA MASS SPECTROPHOTOMETER RESULTS 61
3.2.4 CHEMICAL VARIATIONS BETWEEN DEPOSITIONAL SETTING 66
3.3 THIN SECTION ANALYSIS 69
3.3.1 PETROGRAPHIC DESCRIPTIONS 69

3.3.2 Microprobe Analysis 75

4 DISCUSSION 94

4.1 Lateral Secretion as a Depositional Model 94
4.1.1 Field Evidence Supporting the Lateral Secretion Model 95
4.1.2 Redox Reaction of Manganese and Iron 96
4.1.3 Environment of Manganese Deposition 103
4.2 Fluid Flow Dynamics 106
4.2.1 Porosity of the Rocks 106
4.2.2 Fault Bounded Deposits 108
4.2.3 Mass Balance 111
4.3 Type 1 or Type 8 Deposit 112
4.3.1 Source of the Manganese 113
4.3.2 Type 8 Deposit 116
4.4 REE Analysis 117

5 CONCLUSION 120

REFERENCES 124

APPENDIX A 131

APPENDIX B 133

APPENDIX C 139

LIST OF TABLES

TABLE 1: STRATIGRAPHIC SUCCESSION OF THE TABLE MOUNTAIN GROUP (JIA ET AL, 2009). 4
TABLE 2: EFFECTIVE POROSITY OF ROCK TYPES FOUND IN THE CAPE PENINSULA (WEB2).... 6
TABLE 3: CLASSIFICATION SYSTEM COMPILED BY HARRISON (1998)..... 8
TABLE 4: WORLD PRODUCTION OF MANGANESE ORES AND CONCENTRATES 1970 – 2010 (TONS·10^3) (UNITED NATIONS, 2003; WEB 1). 15
TABLE 5: TYPICAL COMPOSITIONS IN WEIGHT PERCENT OF METALLURGICAL MANGANESE ORES REPRESENTATIVE OF THE VARIOUS DIFFERENT SEDIMENTARY DIAGENETIC TYPES 8A, 8B, 8D AND 8F DEFINED BY HARRISON (1998) (TANGSTAD ET AL. 2004).....16
TABLE 6: SAMPLE NUMBERS AND GPS LOCATION OF THE DIFFERENT LOCALITIES SAMPLED IN THE CAPE PENINSULA AREA.....19
TABLE 7: SAMPLES CLASSIFIED BY SAMPLE TYPE, ROCK TYPE (SST = SANDSTONE) AND SAMPLE NUMBER. 20
TABLE 8: SITE, LOCATION, NUMBERS AND LOCALITY OF SKELETON GORGE SAMPLES. 21
TABLE 9: SAMPLES CLASSIFIED BY SAMPLE TYPE, DEPOSITIONAL SETTING AND SAMPLE NUMBER. 21
TABLE 10: WATER SAMPLE SITE NUMBERS AND LOCATIONS. 23
TABLE 11: SAMPLES USED FOR PETROGRAPHIC ANALYSIS. 24
TABLE 12: NUMBER OF PRIMARY MICROPROBE MAPS AND ELEMENT (MN, FE, SI) LINE SCANS COMPLETED FOR THE DIFFERENT SAMPLE LOCALITIES. 24
TABLE 13: ROCK SAMPLES ANALYSED BY XRF AND ICP-MS ANALYSIS. 25
TABLE 14: THE MAJOR (WT%) AND TRACE (PPM) ELEMENT COMPOSITION OF UNMINERALISED SAMPLES BY XRF. 52
TABLE 15: THE MAJOR (WT %) AND TRACE (PPM) ELEMENT COMPOSITION OF TRANSITIONAL MANGANESE ROCKS BY XRF. 53
TABLE 16: THE MAJOR (WT %) AND TRACE (PPM) ELEMENT COMPOSITION OF TRANSITIONAL IRON ROCKS BY XRF. 54
TABLE 17: THE MAJOR (WT %) AND TRACE (PPM) ELEMENT COMPOSITION OF MANGANESE AND IRON RICH ROCKS BY XRF. 55
TABLE 18: ICP-MS RESULTS FOR THE UNMINERALISED SAMPLES (PPM). 61
TABLE 19: ICP-MS RESULTS FOR THE IRON AND MANGANESE TRANSITION SAMPLES (PPM). 62
TABLE 20: ICP-MS RESULTS FOR MANGANESE AND IRON RICH SAMPLES (PPM).....63
TABLE 21: ICP-MS RESULTS FOR THE WATER SAMPLES (PPM), ND = NOT DETECTED. 65
TABLE 22: SAMPLES ANALYSED BY XRF AND ICP-MS AND MICROPROBE SORTED BY TYPE OF MANGANESE DEPOSIT.....66
TABLE 23: ELEMENT COMPOSITION OF HIGHLY ENRICHED MANGANESE ROCKS PLOTTED IN FIGURES 73-75. 103
TABLE 24: CALCULATION OF TIME REQUIRED TO FORM THE SKELETON GORGE MANGANESE DEPOSIT FROM PRESENT-DAY WATERS. 111
TABLE 25: MANGANESE ABUNDANCE IN COMMON ROCKS BASED ON MANGANESE CONTENT OF COMMON MINERAL ASSEMBLAGES. ADAPTED FROM GRAHAM ET AL. (1988). 114
TABLE 26: MAJOR ELEMENTS OF UNMINERALISED TMG ROCKS (WT%). 115
TABLE 27: APPROXIMATE VOLUME CALCULATIONS OF POTENTIAL TOTAL MANGANESE IN THE PENINSULA FM AND GRAAFWATER FM..... 116
TABLE 28: WORLDWIDE MANGANESE DEPOSITS COMPARED WITH THE CAPE PENINSULA DEPOSITS, ADAPTED FROM SCHAEFER ET AL. (2001). 123

LIST OF FIGURES

Figure 1: Diagram showing an idealised cross section through TMG bedrock and the flow of groundwater in the lateral secretion model of iron and manganese deposition in the Cape Peninsula (Compton, 2004). 2

Figure 2: Stratigraphic column of South Africa (Anhaeusser et al., 2006), the highlighted formation is the formation within which the Cape Peninsula manganese deposits are formed 3

Figure 3: Topography of the Cape Peninsula area (far left) and areas surrounding and to the east of False Bay (image courtesy of Computamaps). 5

Figure 4: Lithology and structural controlled aquifers, a) Syncline, the Baths hot spring model, b) Fault and basement bounded outcrop model (Jia et al., 2009). In both images the Peninsula Fm acts as the aquifer and the other formations act as aquitards. 6

Figure 5: Scale of manganese deposits based on Harrison's classification, Type 8F is a sedimentary diagenetic (chemical) deposit. On this scale individual volcanic and hydrothermal deposits do not feature. Adapted from Schaefer et al. (2001). 8

Figure 6: Geological Map adapted from Compton (2004), showing the location (yellow stars) and names of sites sampled for this study. 19

Figure 7: Satellite images from Google Maps showing the sites sampled along Skeleton Gorge. 20

Figure 8: Satellite image from Google Maps showing water sampling locations. . 22

Figure 9: The absolute differences between duplicate samples for element oxide analysis by XRF. 25

Figure 10: Average percentage relative standard deviation (%RSD) and total procedural blank (tpb) achieved for both ICP-MS runs for the rock samples. 27

Figure 11: Geological map showing the sample location sites on Table Mountain (Council for Geoscience Cape Town Geological Map 1:50 000). 1 = Skeleton Gorge; 2 = Kasteelpoort Path; 3 = Contour Path. 29

Figure 12: Sketch of the Skeleton Gorge deposit. Facing North West looking up towards sample site 3&4, with sample site 5 in the foreground and sample site 2 in the background. The trail is indicated by the rectangular blocks. Vertical Exaggeration (VE) of 1:1. 30

Figure 13: Iron staining within the veins of a loose boulder found at the top of Skeleton Gorge. 31

Figure 14: Manganese coating found at Site 2 associated with a perennial seep. Photo on left is of the outcrop face and on the right of a close up of the exposed rock face with deep orange (iron) and black (manganese) stained Peninsula Fm sandstone. 32

Figure 15: The siltstone layer (spray painted orange) below the overhang at Skeleton Gorge with a black manganese surface coating along a groundwater seep (immediately below the hammer) slightly south of Sample Site 4. 33

Figure 16: The "dry" southernmost portion of Site 3. Photo on left is of moss overgrown manganese and on the right the weathered and crumbling manganese and iron exposure. 34

Figure 17: Manganese drip structures on the overhang in the "wet" portion of the Site 4. 34
Figure 18: The extent of the talus slope (left) and green moss and fern coating the exposed surface of the deposit (right). 35
Figure 19: Deposit of manganese occurring south of the Skeleton Gorge fault associated with a seasonal seep. 36
Figure 20: The botryoidal manganese crystal habit found at site 7. 37
Figure 21: Heavily weathered manganese and iron deposits along the Kasteelpoort Path cementing loose slope talus. 38
Figure 22: Sketch of the Kasteelpoort Path depositional site. The iron and manganese are deposited in the centre of gorge as part of the seasonal river and talus slope. VE of 1:1. 39
Figure 23: Geological map of the Rooi Els sampling site (Council for Geoscience Cape Town Geological Map 1:50 000). Point 1 shows the full extent of the manganese and iron occurrence, and Point 2 shows the manganese rich addit where the sampling was conducted. 40
Figure 24: Sketch of the total Rooi Els depositional site as exposed along the R45 road cuts. VE of 1:1. 41
Figure 25: The manganese "rubified" talus slopes on the R45 road 3 km north of Rooi Els. 42
Figure 26: Veins filled with manganese oxides found in the Peninsula Fm bedrock near the addit at the Rooi Els site. 43
Figure 27: Cross section of the addit in Rooi Els showing the fracture frequency, size, and the dominant mineral being precipitated out. VE of 1:5. 44
Figure 28: A massive manganese boulder above the addit at the Rooi Els site. 44
Figure 29: Geological map of the Kommetjie site (Council for Geoscience Cape Town Geological Map 1:50 000) showing the location of the Site (1) and a nearby fault (2). 45
Figure 30: The weathered surface texture of manganese-rich boulders found at the Kommetjie site where the visible ridges are rich in manganese. 46
Figure 31: Sketch of the Kommetjie deposit. The boulders are not in situ but appear old and highly weathered. VE of 1:1. 46
Figure 32: Sketch of the Hout Bay deposit. VE of 1:1.5. 47
Figure 33: Geological map showing the location (1) of one of the addits of the Hout Bay manganese mine (Council for Geoscience Cape Town Geological Map 1:50 000). 48
Figure 34: Variations in silica, iron and manganese content across all rock types. 56
Figure 35: Correlation between aluminium and iron across all enriched rock types. 57
Figure 36: Correlation between aluminium and manganese across all enriched rock types. 57
Figure 37: Correlation between manganese and potassium across all enriched rock types. 58
Figure 38: Correlation between potassium and aluminium across all rock types. 58
Figure 39: The XRD profile (blue line) of sample B6 from Rooi Els. The peaks associated with green spikes are attributed to cryptomelane and peaks associated with the red spikes to quartz. 60

Figure 40: Average REE profiles normalised to PAAS for each sample type. 64
Figure 41: Average REE profiles normalised to PAAS for each sample locality... 64
Figure 42: Box plots showing the range of manganese, silica and iron content (wt%) in the different types of manganese deposits studied. The black dots represent the outliers. The black outlined sections the 1st and 4th interquartile range, and the grey shaded blocks the 2nd and 3rd interquartile range. The black line in the middle represents the mean of the data..... 67
Figure 43: Box plots showing the ranges of aluminium and potassium in the different types of manganese deposits studied. 68
Figure 44: Thin Section of sample D3 of Peninsula Fm sandstone. Equigranular medium to coarse sub round quartz grains, minor micaceous material and some small sub rounded detrital isotropic minerals cemented by quartz. Polarised light (left) and plane light (right)..... 70
Figure 45: Thin Section of sample D1 of Graafwater Fm sandstone. Note the reduced grain size of the quartz and the increase in micaceous material as opposed to sample D3, Figure 27. Polarised light (left) and plane light (right)..... 70
Figure 46: Thin Section of sample B1 (plane light). In comparison to Figure 27 there is more micaceous material in between the grain boundaries..... 71
Figure 47: Thin Section of sample C3 on the left, showing manganese (black) and iron (red) cements surrounding quartz. Thin section of B4 on the right, shows filled fractures of quartz grains, both images in plane light. .. 72
Figure 48: Thin section of B4, showing the vein of manganese material in plane light..... 72
Figure 49: Thin section images of sample A4 (left) and B4 (right) showing the high grade manganese relationship with quartz and iron..... 73
Figure 50: Thin section of sample B6 on the left, and B2 on the right in plane light showing the patterns developed through the deposition of the iron by chemical variations within the fluids..... 74
Figure 51: Thin section of sample B2, showing the zonation of the iron in plane light..... 74
Figure 52: Peninsula Fm sandstone sample 1. Note the slight occurrence of iron within the potassium and aluminium mineral, potentially mica. Reflected light image shown in lower right-hand corner with dark mineral interpreted to be a mica grain rich in K, Al, Si and some Fe but no appreciable Mn. Colours relate to counts per pixel ranging from blue (low) to red (high) shown on the far right scales. The dark lines in the reflective light image represent fractures or grain boundaries between the quartz grains. 76
Figure 53: Peninsula Fm sandstone sample D4. The occurrence of iron and some manganese is associated with the darker grain in the lower right-hand image. The dark mark in the lower right hand quadrant of the reflected light image is a blemish formed on the carbon coating post the laser burn. 77
Figure 54: Graafwater Fm siltstone sample D1. Iron is concentrated with the dark mineral, which is similar to sample 1 (Figure 53), suggesting the dark mineral is potassium and aluminium rich. Manganese is slightly more

concentrated along with iron but also occurs homogeneously throughout the image. 78
Figure 55: Peninsula Fm siltstone sample 30, from the overhang in Skeleton Gorge. Relatively high concentrations of the aluminium and potassium rich mineral, most probably mica, occur within this siltstone, the iron follows the potassium while the manganese shows a homogenous distribution. 79
Figure 56: Iron precipitating around quartz grains, sample C6. As in earlier images some of the grain boundaries and fractures occurring within the Si grains are not associated with Mn or Fe precipitation. 81
Figure 57: Iron and manganese precipitation between quartz grains, sample C2. 82
Figure 58: Dominant manganese and secondary iron precipitation in sample B4. . 83
Figure 59: Two scans of Transitional sample A5 showing transitional deposition of manganese and iron. 84
Figure 60: Sample E4 from Hout Bay displays a mixture of nearly highly concentrated but separate precipitation of manganese and iron. 86
Figure 61: Sample C6 from Kasteelpoort Path consists of very rich iron having traces of manganese. 87
Figure 62: Sample C5 from Kasteelpoort Path shows evidence for multiple iron and manganese precipitates which are not defined in the homogeneous texture of the reflected light image. 88
Figure 63: Four compositionally different precipitates of high concentrate manganese in sample 8 from Skeleton Gorge Site 3 and 4. 89
Figure 64: Three compositionally different precipitates of high concentrate manganese in sample 10 from Skeleton Gorge Site 3 and 4. 90
Figure 65: Textural variations shown in lower right image that do not correspond to chemical differences, sample B6 from Skeleton Gorge. . 91
Figure 66: Sample 10 from Skeleton Gorge Site 3 and 4, showing nearly iron deposition surrounded by quartz and mica, and manganese deposition isolated in the centre. Note that high manganese area is also enriched in potassium which is reflecting the composition of the manganese mineral (refer to following section). 92
Figure 67: Sample E4 from Hout Bay, showing silica sharing precipitation space with the iron. 93
Figure 68: Correlation of molybdenum and manganese suggesting the presence of a redox reaction. 97
Figure 69: Dissolution pattern within an average soil profile with depth. Adapted from Martin (2003). 97
Figure 70: Redox equations of the reduction of manganese and iron within the soil horizon (Lovley, 1991). 98
Figure 71: Eh-pH diagrams for manganese and iron (Dill et al., 2010). The blue represents aqueous phases, the yellow solid phases and the red lines boundaries between the different compounds. The white represents where the fluid would become unstable. The green line shows the suggested evolution of the fluids moving through the TMG as rainwater forms subsurface groundwater which eventually emerge at surface seeps. 100

FIGURE 72: SCHEMATIC SHOWING THE CHANGE IN EH-PH FOR MN AND FE DURING THE FLOW PATH OF THE FLUIDS WITH THE LATERAL SECRETION MODEL. RAINFALL (A) PERCOLATES THROUGH THE SOIL PROFILE AND BECOMES ACIDIC AND REDUCING AND LEACHES MN AND FE FROM THE SOIL INTO SOLUTION (B). THE FLUID CONTINUES TO MOVE THROUGH THE REGOLITH AND BEDROCK FRACTURE FLUID PATHWAYS DISSOLVING ADDITIONAL MN AND FE AS WELL AS K FROM MICA MINERAL DISSOLUTION (C). WHEN THE FLUID EVENTUALLY FLOWS LATERALLY TO AN OXIDATION FRONT WHERE FIRST FE AND THEN MN ARE PRECIPITATED OUT AS OXIDES MN(IV) AND FE(III) (D) AND FINALLY THE FLUIDS STABILISE WITH STREAMS CARRYING THE REMAINING MN(II) AND FE (II) IN SOLUTION. 102
FIGURE 73: ENVIRONMENT CLASSIFICATION OF THE MANGANESE DEPOSITS OF THIS STUDY BASED ON NICHOLSON (1992). NA CONTENT OF THE ORES IS PLOTTED AGAINST THE MG CONTENT TO DIFFERENTIATE BETWEEN FRESH, SHALLOW MARINE AND MARINE DEPOSITS. 104
FIGURE 74: URANIUM VS. THORIUM CONTENT OF SAMPLES FROM TABLE 23 COMPARED TO FIELDS OF MANGANESE FORMATION DEFINED BY BONATTI ET AL. (1972). 105
FIGURE 75: TERNARY PLOT AS DEVISED BY BONATTI ET AL. (1972) DIFFERENTIATING BETWEEN HYDROTHERMAL AND HYDROGENOUS MANGANESE FORMATION. SAMPLES FROM THIS STUDY (TABLE 23) PLOTTED AS RED POINTS. 105
FIGURE 76: GROUNDWATER FLOW PATHS THROUGH AQUIFERS AND AROUND AQUITARDS WITHIN TABLE MOUNTAIN, FROM JIA ET AL. (2009)..... 107
FIGURE 77: CROSS SECTION OF THE SKELETON GORGE DEPOSIT (AS SHOWN IN THE GEOLOGICAL MAP INSERT, A-B) SHOWING THE INFLUENCE OF THE FAULT ON THE FLUID DYNAMICS OF THE DEPOSIT. THE BLUE ARROWS INDICATE THE APPROXIMATE FLUID FLOW PATHS. RAINWATER MOVES INTO THE AQUIFER (PENINSULA FM) AND THEN FLOWS ALONG DIP ABOVE THE LESS POROUS GRAAFWATER FM AND CAPE GRANITE SUITE FM, TOWARDS THE MORE POROUS FAULTED BEDROCK WHICH ALLOWS FOR FASTER AND HIGHER LEVELS OF FLUID FLOW. FINALLY THE FLUIDS REACH THE FAULT ZONE WHICH ACTS AS AN AQUITARD FORCING THE FLUIDS TO SEEP OUT OF THE ROCK. 109
FIGURE 78: THIN SECTION OF SAMPLE D3 OF PENINSULA FM SANDSTONE (LEFT) SAMPLE B6 (RIGHT) IN PLANE LIGHT. SAMPLE D3 SHOWS THE TYPICAL ROUNDED TO SUBROUNDED QUARTZ GRAINS, WHILE B6 SHOWS MORE SUBANGULAR QUARTZ GRAINS WITH A HIGHER DEGREE OF FRACTURES. 110
FIGURE 79: CONCENTRATIONS OF THE KEY ELEMENTS WITHIN POSSIBLE SOURCE ROCKS OF THE MANGANESE DEPOSITS. DUE TO THE LOW CONCENTRATIONS OF THE MANGANESE (MNO) IT WAS MULTIPLIED BY A FACTOR OF TEN IN ORDER TO SHOW THE VARIATIONS ON THE GRAPH. 115
FIGURE 80: PAAS NORMALISED REE PLOTS OF THE TABLE MOUNTAIN REGION SITES. 118
FIGURE 81: SOURCE (SILICA RICH) ROCK PAAS NORMALISED REE PATTERNS FROM ICP-MS ANALYSES. 119

1. INTRODUCTION

1.1 Manganese in the Cape Peninsula

Manganese deposits are common throughout the Cape Peninsula. The vast majority of these are superficial staining of rock outcrops. In some locations, Rooi Els and Hout Bay, old artisanal manganese mines exist where deep vein deposits of high grade manganese were mined. Rooi Els also hosts a talus slope style of manganese deposit which can be seen for a long section of the road. These three unique styles of manganese deposition, surface, veined and talus, were suggested, by Compton (2004), to have formed through groundwater being reduced within the soil profile and then leaching out of the metals (manganese and iron) contained in the bedrock. The mountainous terrain then facilitates springs and seeps which upon exiting the mountain re-oxygenate these reduced fluids and allow for the precipitation of these metals on the surface of the rocks (Figure 1). This suggestion has not been proven in any studies of the Cape Peninsula. The presence of hot springs throughout the Cape Peninsula (Diamond and Harris, 2000) and the lack of a source rock for the manganese raise questions concerning Compton's model.

The manganese-rich deposits found in the Cape Peninsula are locally of high-grade, and are highly variable and inconsistent deposits which were mined at the turn of the 20th century (Welsh, 1917). However, due to their highly variable nature and their high content of the deleterious element phosphorus, the economic extraction of manganese from these deposits was stopped once they were mined out at Hout Bay and Rooi Els and no further mining activity of similar type deposits was carried out in the region.

The variations in the major oxide composition of sandstone surrounding the Hout Bay manganese mine were documented by Duncan et al. (1978), but there is no existing body of work that looks specifically into the manganese deposits found throughout the Cape Peninsula. The reason for the lack of work on these deposits is twofold. The economic viability of these deposits currently in relation to the other types of deposits is very low. Another reason why little information exists on this deposit is to do with the deleterious elements which are elevated in this deposit making it uneconomic. The main deleterious element documented in these deposits is phosphorus, which negates the affect that manganese has on steel, making the steel brittle. The general accepted maximum phosphorus content of a manganese ore is 0.2 wt% P (Tangstad et al., 2004) while deposits on the Cape Peninsula have a phosphorus content of between 0.13 wt% and 0.88wt% P with an average of 0.38wt% P which is outside the acceptable range for phosphorous.

However, this in no way means that the knowledge gained from this deposit is of no value. Understanding the genesis of the manganese not only adds to the body of work around manganese deposits, but could also add to the understanding of the mechanisms of the formation of the Cape Peninsula. If necessary, the high phosphorus content could be blended out with a low

phosphorus material making this a saleable manganese product to be used in the manufacture of manganese alloys and steel.

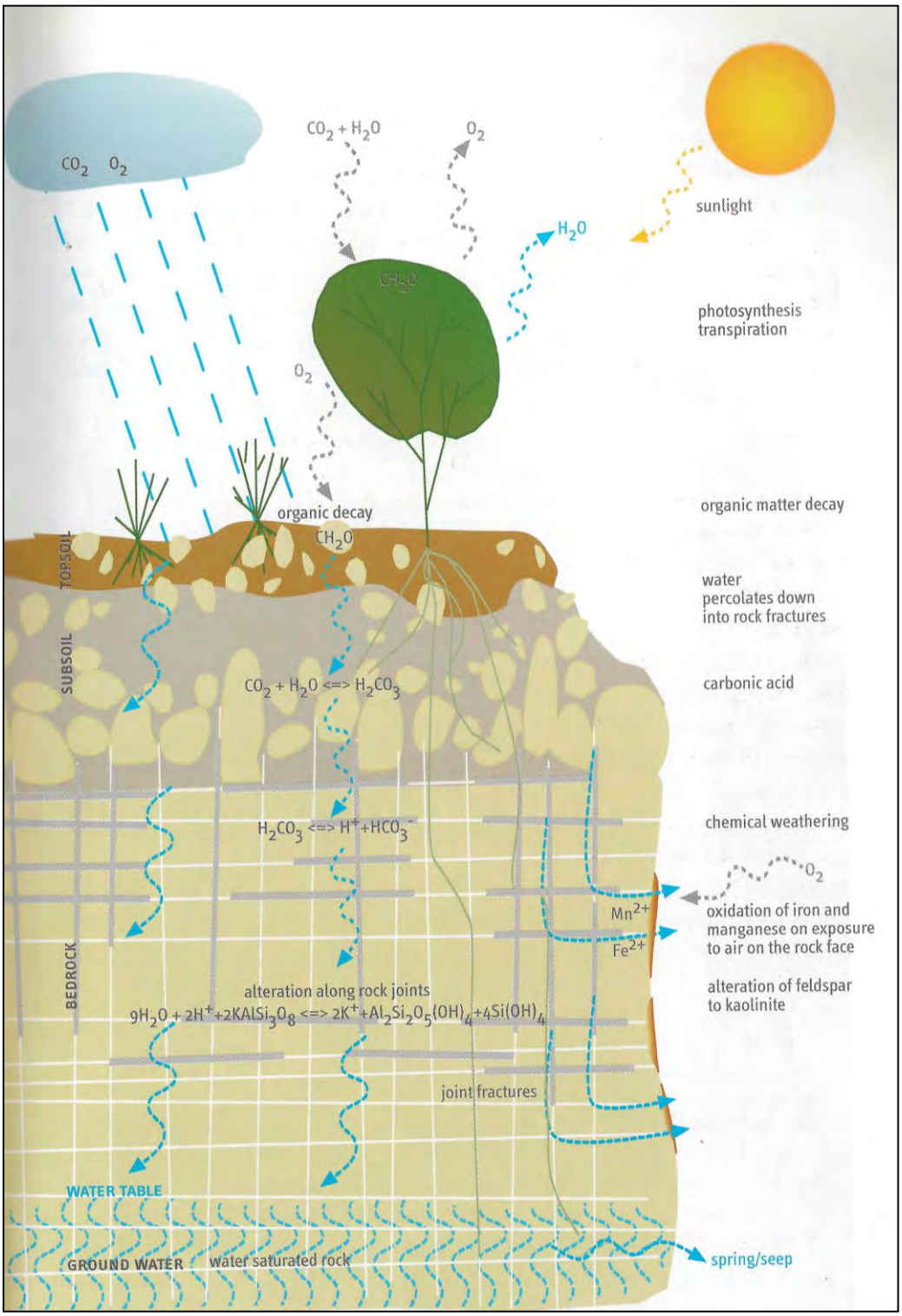

Figure 1: Diagram showing an idealised cross section through TMG bedrock and the flow of groundwater in the lateral secretion model of iron and manganese deposition in the Cape Peninsula (Compton, 2004).

1.2 Geological Setting

Stratigraphy

The geology of the Cape Peninsula consists of three major rock groups, the Malmesbury Group, the Cape Granite Suite, and the Table Mountain Group (TMG) (Figure 2, Table 1) with a variable thickness of Quaternary sediment cover. The Malmesbury Group is a 550 Ma interbedded shale and turbidite formed on the continental shelf and slope. The Malmesbury Group has been locally metamorphosed by the intrusion of the Cape Granite Suite at 540 Ma. The area then underwent erosion and uplift, which was followed by the subsidence and deposition of the TMG rocks between 520 and 450 Ma. The Graafwater and Peninsula formations constitute the base of the TMG in the study area.

The Graafwater Fm is interbedded maroon (red bed) mudstone and sandstone which is overlain by quartz arenite sandstone of the Peninsula Fm. Extensional tectonic forces during the Cretaceous break up of Gondwana caused multiple faults throughout the region (Anhaeusser et al., 2006).

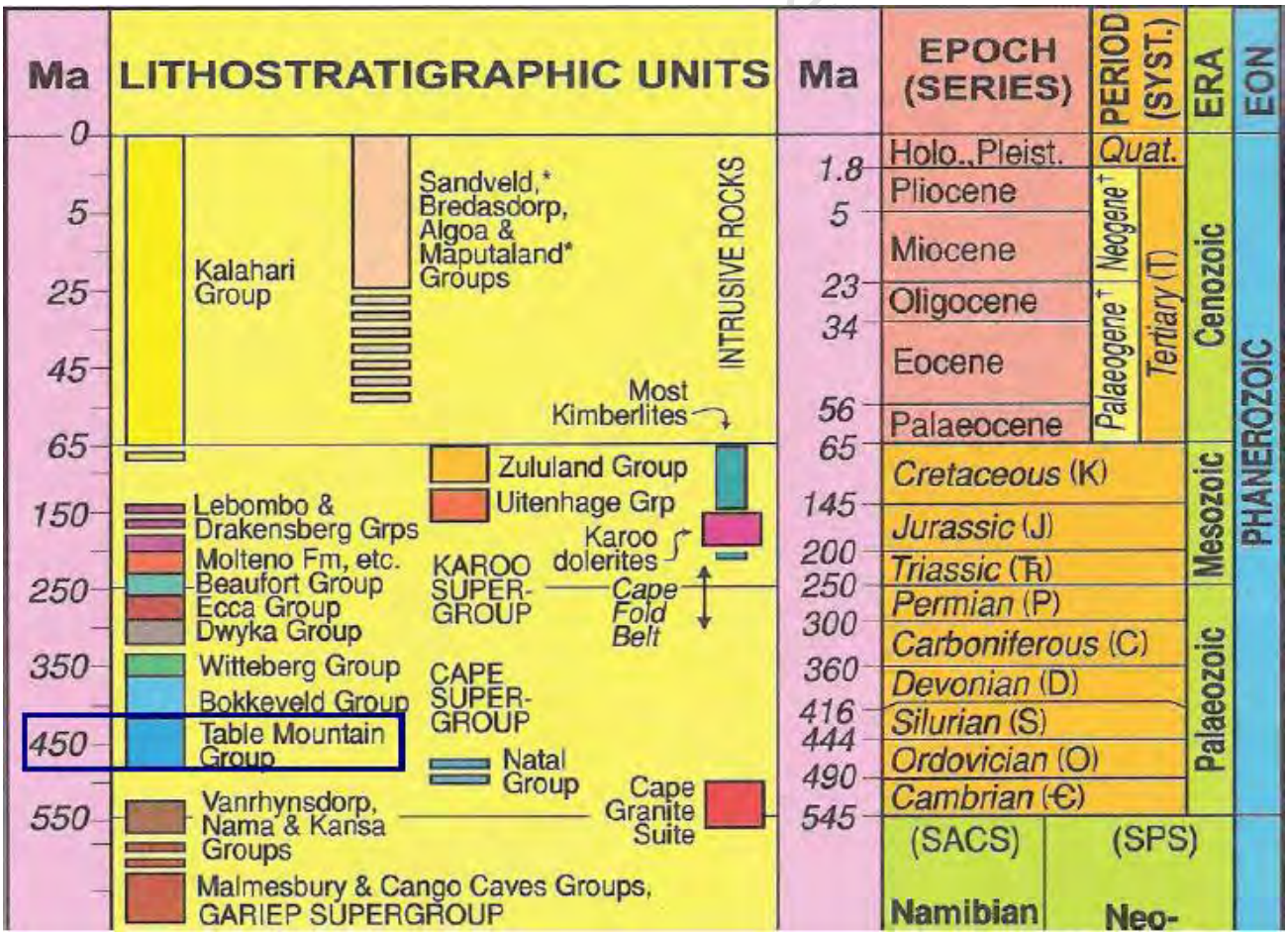

Figure 2: Stratigraphic column of South Africa (Anhaeusser et al., 2006), the highlighted formation is the formation within which the Cape Peninsula manganese deposits are formed.

Table 1: Stratigraphic succession of the Table Mountain Group (Jia et al, 2009).

Group	Subgroup	Formation	Geological symbol	Thickness (m) subtotal	Thickness (m)	Lithology
Bokkeveld			D	4000		Siltstones, shales, sandstones
Table Mountain	Nardouw	Rietvlei/Baviaanskloof	Dr/ S–Db	1200	300	Feldspathic quartz arenite
		Skurweberg	Ss		500	Quartz arenites
		Goudini	Sg		400	Arenite, minor siltstone, shale
		Cedarberg	O–Sc	70	50~150	Silty shales and shaly siltstone
	Peninsula	Pakhuis	Opa	2500~3100	100~150	Tillite, diamictite, quartz arenites
		Peninsula	Ope		1500~2000	Largely thick-bedded, coarse-grained quartzitic arenites
		Graafwater	Og		65~150	Thin-bedded sandstone, siltstone, shale and mudstone
		Piekenierskloof	Op		800	Quartzitic sandstone with coarse-grained to gritty zones and rudites
Basement		Underlying the TMG are the Malmesbury shales, the Gamtoos and the Kaaimans argillites, comprising a suite of moderately to lightly metamorphosed sedimentary rocks; and the Cape Granite Suite.				

Topography and Fluvial Characteristics of the Cape Peninsula

The Cape Peninsula is a faulted, deeply incised mountainous region that is part of the larger Cape Fold Belt. The mountains are mainly capped by Peninsula Fm sandstone (in the Cape Peninsula) and this hard rock weathers very slowly which helps to facilitate the formation of the mountains in the region (Figure 3). The Cape Peninsula is located along the South African coast line and has a Mediterranean-type climate. This means that most rainfall occurs in winter (Burgers et al., 2010). Water is channelled into multiple streams and rivers which flow perennially or seasonally. These rivers have a large impact on the topography of the Cape Peninsula by incising steep gorges and canyons.

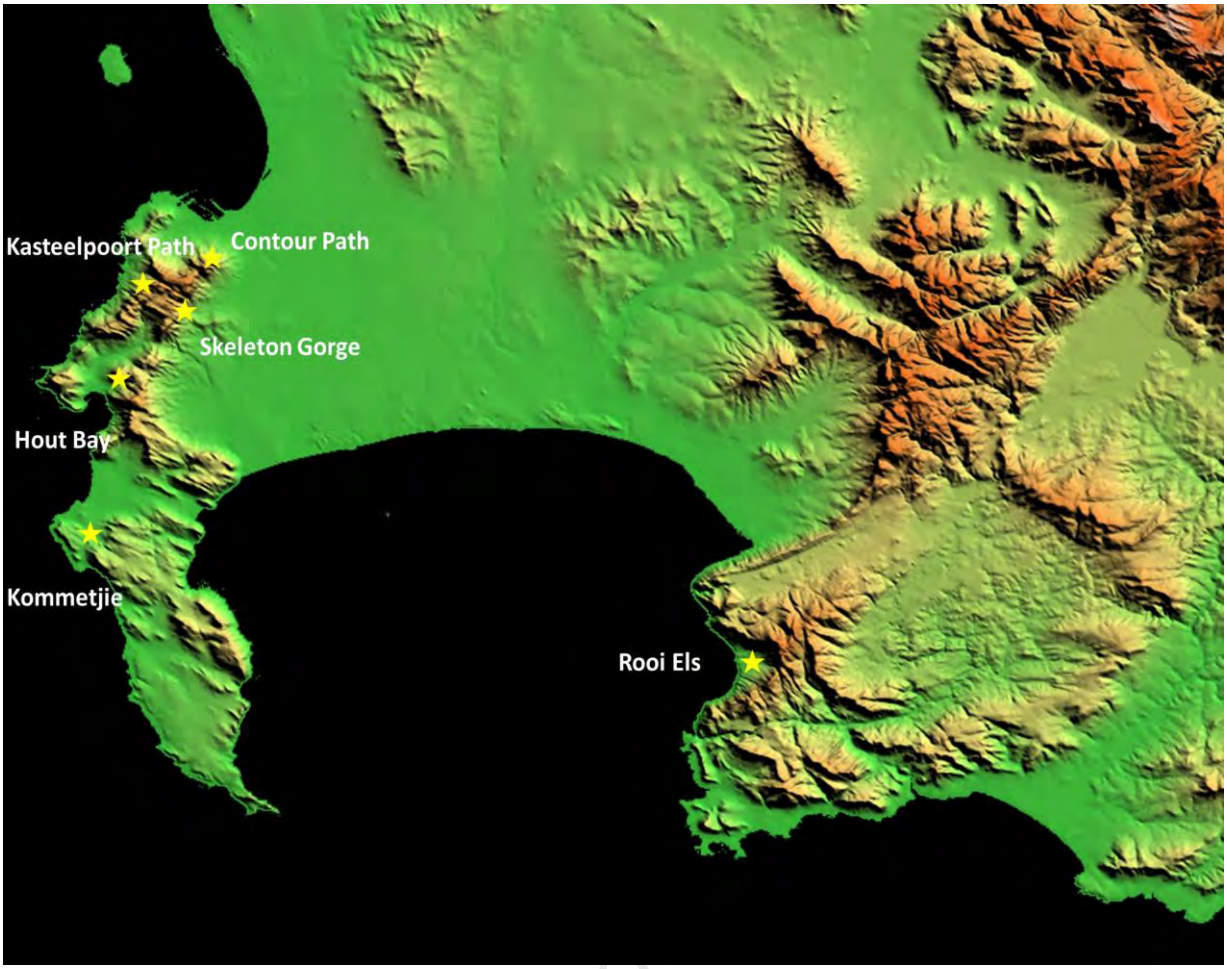

Figure 3: Topography of the Cape Peninsula area (far left) and areas surrounding and to the east of False Bay (image courtesy of Computamaps).

Not only does local topography assist with the fluvial system of the Cape Peninsula, the varying rock formations have different effective porosities making them excellent aquifers or aquitards. These mountains, slopes and gorges coupled with the climate and the effective porosity of the bedrock results in springs throughout the region. The presence of aquifers and aquitards either promote the formation of springs sourced from groundwater or surface flow over the soil regolith. Table 2 shows the summary of global estimates of porosity for typical samples of the lithology's found within the Cape Peninsula. Figure 4 shows the effect that these varying porosities have on the fluvial conditions of the Cape Peninsula, where the highly fractured Peninsula Fm sandstone acts as an aquifer, and the faults, granite and Malmesbury shale's act as aquitards.

Many of the springs which exist within the greater Cape Peninsula are thermal springs. Isotope compositions show that these springs are sourced from groundwater, and their oxygen isotope values suggest that these springs recharge at significantly higher altitudes than the level of the spring (Diamond and Harris, 2000). Figure 4 shows how these springs can move from high altitudes to great depths, heat up, and then return as hydrothermal springs.

In summary, the Cape Peninsula is a folded and faulted mountainous region which has been incised by rivers and streams with many natural low-temperature and hydrothermal springs and seeps.

Table 2: Effective porosity of rock types found in the Cape Peninsula (WEB2).

Global Term	Cape Peninsula	Porosity	Effective Porosity	
Granite	Cape Granite Suite	0.025		0.025
Medium Grained Sandstone	Peninsula Fm Sandstone	0.340		0.270
Shale	Malmesbury Shale	0.050		0.050
Shale	Graafwater Fm	0.050	0.050	
Fine Grained Sandstone		-	0.210	0.130
Unconsolidated Sediments (Sand - Coarse)	Quaternary Sediments	0.280		0.210
Aeolian Sand	-	-		0.380
Fault Breccia	Peninsula Fm	0.140		0.000
Siltstone	Peninsula Fm	0.350		0.120

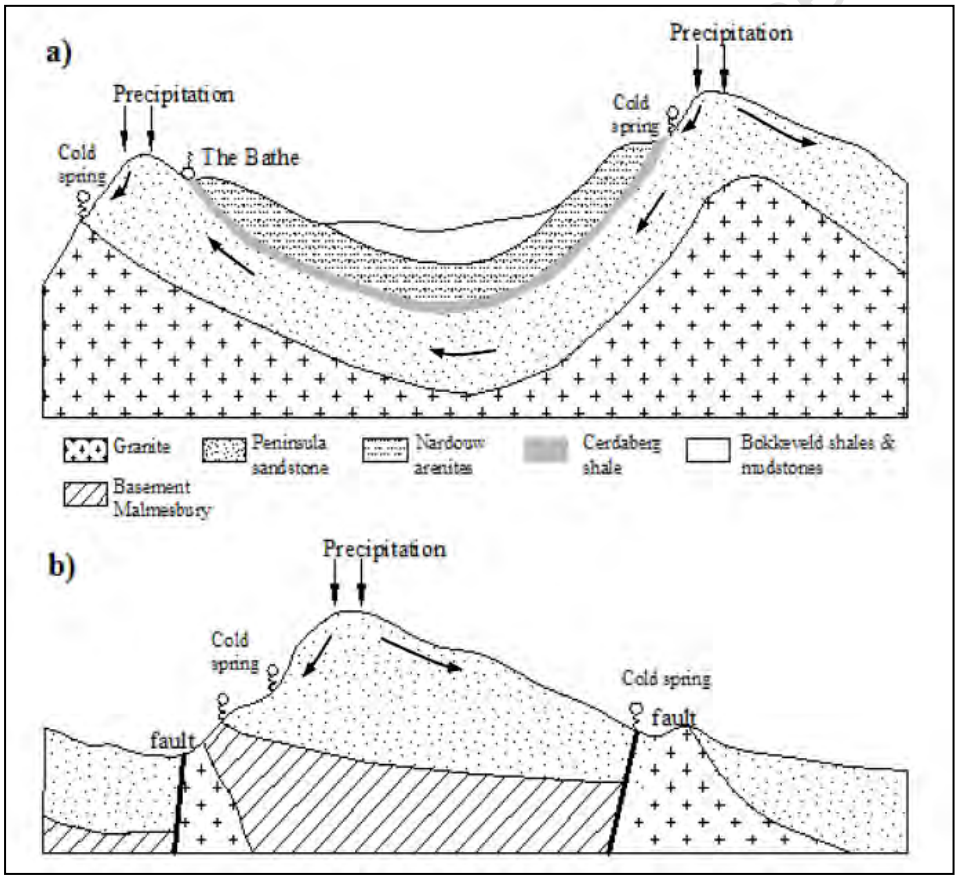

Figure 4: Lithology and structural controlled aquifers, a) Syncline, the Baths hot spring model, b) Fault and basement bounded outcrop model (Jia et al., 2009). In both images the Peninsula Fm acts as the aquifer and the other formations act as aquitards.

1.3 Manganese deposit classifications

Manganese deposits occur in sedimentary, volcanic and metamorphic rocks. Most manganese occurrences around the world are hydrothermal or volcanic in origin, but most economic deposits are not, the largest contributing manganese deposit type by volume is sedimentary diagenetic, chemical sedimentary deposits (Schaefer et al., 2001) (Figure 5). Multiple classification systems exist for manganese deposits, and multiple authors have created their own classification systems for various portions of these manganese deposits. The primary authors and classification systems used follow below.

Roy (1981, 1988, 1992, 1997) covers most manganese deposits, from terrestrial to marine and volcanogenic deposits. Roy divided these deposits based on their process of formation and age of deposit, hydrothermal, sedimentary or superficial deposits. Within these three broad genetic types occur sub types such as sedimentary volcanogenic and sedimentary non volcanogenic deposits and then their sedimentary metamorphic equivalents. Due to this broad classification system some of the subtleties of the different depositional environments are lost.

Machamer (1987) came up with a 5 fold classification system of economic manganese deposits. This was based on the host rocks, and the manganese minerals themselves (IE manganese carbonate within pillow lavas or intrusives, or schists). All non-economic deposits were excluded from this classification system, thus any small scale manganese deposit which might be of academic interest does not fall into this classification system.

Laznicka (1992) discussed 322 terrestrial manganese deposits throughout the world, and the need for a comprehensive singular classification system which covers all the existing classification systems. It was stated that this classification system needs to be dependent on three factors, the genesis of the deposit, the lithological association, and the geotechnical and environmental setting. Laznicka did not create a classification system, but listed all the requirements that the classification system would need to cover, from mineralogy through to age of the deposits.

Cox and Singer (1986) put together a comprehensive document for the classification of all non-fuel minerals, not only manganese. They based their classification primarily on the mechanism of formation, IE mafic and ultra maffic intrusions into a stable environment. They did not come up with their own classification system for any of the minerals, but rather listed all the possible depositional environments and depositional models.

The problem with all these classification systems is that there are multiple ways to classify a single deposit. For example a manganese deposits which was formed within a shallow marine non volcanogenic environment during an anoxic transgression would be classified as follows. Roy, Phanerozoic sedimentary; Machamer, Type V – Bedded to Nodular Manganese Oxide, Mixed Oxide-Carbonate and Carbonate hosted by Sands and Sandstones, Clays and Claystones, poorly consolidated limy sediments; Laznicka, marine sedimentary, non-volcanogenic, dominantly carbonate; Cox and Singer, Canon and Force

Model. In some of the classification systems the description is concise and fits the depositional model, and in others it is too broad.

Harrison (1998) summarised the various classification systems into a single comprehensive classification system for exploration and exploitation purposes. This summary has eight manganese types encompassing all potential economic or sub economic manganese deposits found throughout the world. Under this classification system a shallow marine non volcanogenic environment during an anoxic transgression would be classified as a Type 8A deposit. A summary of each type can be found below in Table 3 followed by a discussion on each type. All of this information was sourced from Harrison's comprehensive study.

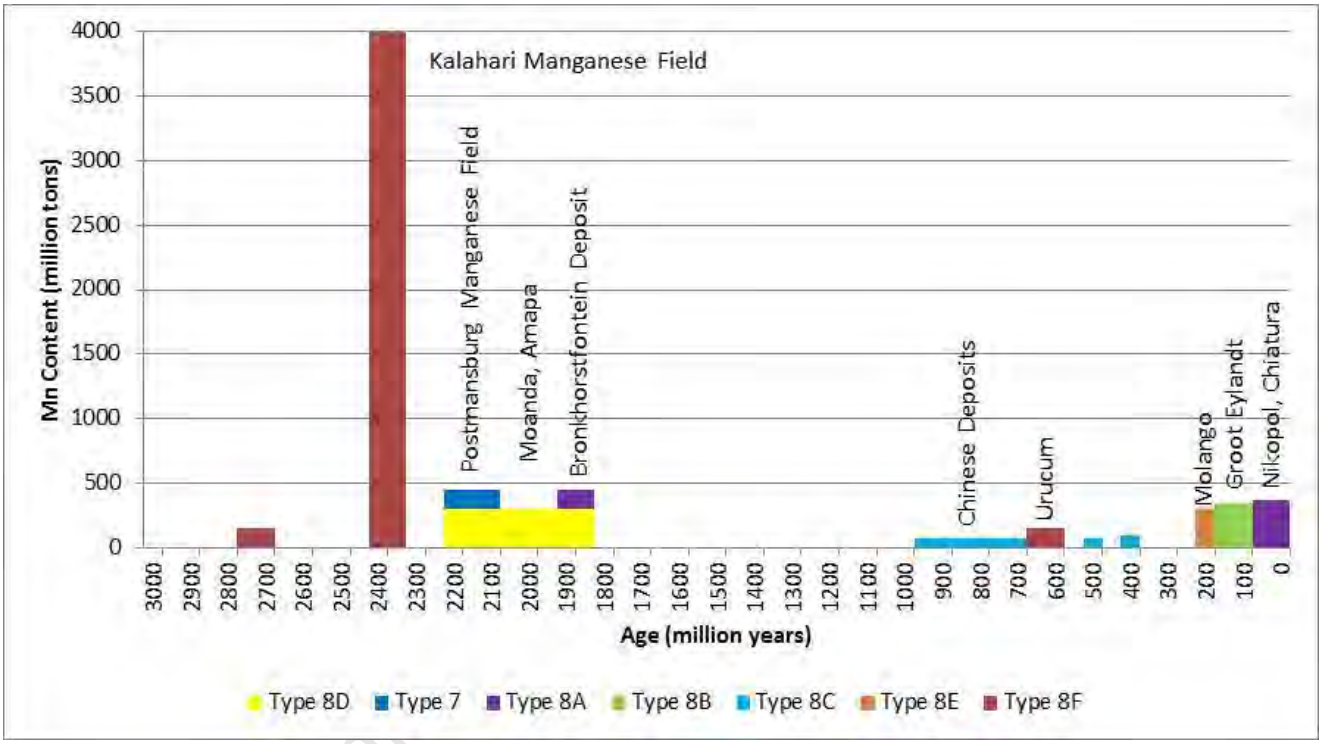

Figure 5: Scale of manganese deposits based on Harrison's classification, Type 8F is a sedimentary diagenetic (chemical) deposit. On this scale individual volcanic and hydrothermal deposits do not feature. Adapted from Schaefer et al. (2001).

Table 3: Classification system compiled by Harrison (1998).

Type		Sub Types	Brief Description
Type 1	Hydrothermal	0	Hydrothermal vein deposits, usually associated with hot springs.
Type 2	Carbonate Replacement	0	Carbonate replacement due to igneous intrusions.
Type 3	Carbonatite Associated	0	Carbonatite associated low grade manganese deposits.
Type 4	Volcanogenic Manganese	6	Volcanogenic exhalative process within a marine environment.
Type 5	Volcanogenic Sedimentary Manganese	2	Supergene enrichment of a volcanogenic deposit.
Type 6	Sedimentary Exhalative Deposits	2	Sedimentary exhalative (SEDEX) process within a marine environment.
Type 7	Karstic Deposits	0	Manganese rich carbonates, enriched through erosive processes.
Type 8	Sedimentary Diagenetic Type	7	Chemical sedimentary deposition of manganese.

Type 1

Type 1 deposits are generally hydrothermal vein deposits but include low temperature metasomatic and other hydrogenous processes. While this covers a large range of deposit styles, the majority of these deposits are sub economic. Those that are economic are only viable as local artisanal mining due to their small size, irregular nature, limited depth, and many of the associated elements within these deposits (sulphur, phosphorus) are deleterious to the smelting process. While the host rock varies, the tectonic system is usually an orogenic belt where faulting is present, the hydrothermal fluids are usually volcanic in origin, but can be from any source. Faults provide the ore control process, allowing the movement of the hydrothermal or groundwater fluids. In some cases permeability in the regolith can allow for sufficient fluid flow to form these deposits. Due to the hydrothermal nature of these deposits zonation is common as is alteration of the host rocks, however it is not a necessary factor. Essentially, the presence of faults and a hydrogenous source are the only common factors of these deposits.

These deposits have massive variations internally of the manganese type, but are dominated by manganese oxides. In relation to size and grade these deposits are usually 0.025 Million tonnes (Mt) with only 10% being greater than 0.26 Mt and 10% being less than 0.0024 Mt. The average grade is 30% Mn with only 10% being greater than 42% Mn and 10% being less than 20% Mn. There is no correlation between grade and size of deposit. Examples include the South western USA, Dzhezda (Russia), and Tarapaca Province (Chile).

Type 2

Type 2 deposits occur when the host rock is a carbonate and a volcanic intrusion occurs into the host rock, such as a small granite pluton intruding into a dolomite sequence. The intrusion either forms pathways through faulting and fracture formation or makes use of existing fractures in the host rock. The high temperature of the intrusion forms hydrothermal fluids, these fluids react with the host rock and a replacement process begins of different orders of hydrothermal minerals. The manganese occurs predominantly as a carbonate and due to its hydrothermal nature deleterious elements are generally high. Similar to Type 1 deposits there is a large variation in manganese grade and the scale of the deposit and as such they are only suitable for small scale artisanal mining. The mean size of these deposits is 0.022Mt with only 10% being greater than 0.53Mt and 10% being less than 0.0009Mt. Examples of these deposits include Phillipsburg (Montana, USA) and Janggun (Korea).

Type 3

Type 3 deposits occur in carbonatite volcanic intrusions which are rich in multiple trace elements (thorium, uranium, molybdenum, copper, lead, zinc, barium, etc.). The host rocks are generally Precambrian in age while the

intrusion is generally younger and occurs during the early stages of continental rifting. The ore body generally occurs within or alongside the carbonatite volcanic intrusion as steeply dipping dykes of manganiferrous sideritic soviet (manganese and iron rich siderite occurring within a course grained variety of the carbonate intrusion, soviet) which can get up to a few meters thick. The manganese is carbonate in origin and high in deleterious elements. The grade of these deposits is low, while the scale is large enough for small scale mining. The mean deposit is taken to be like the Mrima deposits in Kenya which contain 0.6 Mt of ore at a grade of 20 wt% Mn. The major examples include Mrima and Kiwara (Kenya) and Chilwa and Tundulu (Malawi).

Type 4

There are six subtypes within volcanogenic Type 4 manganese deposits. All six of these volcanogenic manganese types are formed due to submarine exhalative processes or 'Black Smokers' (Robb, 2005). The six different types are based around the volcanic source, or the tectonic setting. Franciscan Type is oceanic ridges and rifted marginal basins being obducted onto a continental margin. Cuban Type is an island arc being obducted onto a continental margin. Olympic Peninsula Type is a deep or shallow ocean basin with seamounts and volcanic islands being obducted onto a continental margin. Cyprus Type is an interarc basin and a mid-oceanic ridge being obducted onto a continental margin. Terrestrial or Shallow Water Acid Volcanic Type involves no obduction, but occurs within continental sediments on a continental margin. The Submarine Acid to Intermediate Volcanic Type is associated with very shallow volcanism which can be explosive within a continental setting.

The common denominator between all six types is that they involve a continental setting and sub marine exhalative processes. The variation comes from the depth, type of tectonic setting and the chemistry of the exhalative process. These are generally small scale deposits smaller than Type 2 deposits, but they occur in easily definable lenses and are therefore extractable. Not all subtypes are economic in terms of grade and the presence of deleterious elements. Examples of mines and deposits exist for all subtypes. Ladd Mines (California, USA) is a Franciscan Type; Quinto and Ponupo Mines (Cuba) are Cuban Type; Crescent Mine (Washington, USA) is an Olympic Peninsula Type; Troulii, Drapia, and Skouriotissa (Cyprus) are Cyprus Type; El Arrayan, Corral Quemado and Fragua (Chile) are Terrestrial or Shallow Water Acid Volcanic Type and Glib en Nam (Morocco) is a Submarine Water Acid Volcanic Type

Type 5

Two subtypes exist for volcanogenic sedimentary Type 5 manganese deposits. Both of these subtypes involve supergene enrichment of an existing manganese deposit. It is this supergene enrichment which makes these deposits economical. The difference between the two subtypes has nothing to do with the supergene process, but rather the formation of the original proto ore.

The first subtype (5A) is Supergene Enriched Metamorphosed Volcanogenic Sedimentary Associated with Greenstone Belts. The origin of this deposit is a sedimentary exhalative process similar to Type 4, but Archean in age. Post the exhalative deposition of the ore there has been metamorphism which makes the categorization of the exact exhalative process impossible, and finally within the last million years (Quaternary Period) a supergene enrichment process has upgraded the deposit to be highly economic. This results in a zoned manganese deposit with the original lower grade metamorphosed ore, the protore, a supergene depleted zone, and an upper supergene enriched zone. Not only is the supergene process critical to this subtype of deposit, but also the metamorphism, as Type 4 deposits are small scale, and the metamorphic process concentrates the individual lenses of Type 4 ore into single larger deposit, either through remobilisation or faulting and folding.

The second subtype is Supergene Enriched Metamorphosed Sedimentary Deposits (5B). These deposits are identical to the subtype 5A deposits except for the origin of the protore. In subtype 5A the basis of formation is that of Type 4 deposits. Subtype 5B more closely resembles Type 8 deposits, specifically chemical sedimentary precipitates in a shallow marine euxinic environment. Post the deposition of these protores in the Archean there is metamorphism followed by supergene enrichment during the Quaternary Period. In this subtype the original protore is already on a large enough scale to be classified as a large low grade deposit; it is the secondary enrichment which is critical to the economic viability of the deposit by high grading a section of the ore.

The size of both of these subtypes depends on the extent of the protore, and the grade depends on the supergene enrichment process. There appear to be two classes of deposits: those of 3Mt (majority of deposits) and those of 8Mt and greater. The protore is generally low grade, 20-30% Mn while the supergene enriched cap is 35-55% Mn.

There are many examples of world class operations throughout the world of both subtypes. Subtype 5A includes carbonate protore examples Nsuta (Ghana), Tambao (Burkina Faso) and silicate protore examples are Ansongo (Mali) and Montiambo, Naniango and Ziemougoula (Ivory Coast). Subtype 5B includes Kisenge (DRC), Matthews Ridge (Guyana), Serra do Navio and Morro da Mina (Brazil).

Type 6

Two subtypes exist for Type 6 sedimentary exhalative (SEDEX) manganese deposits. The two subtypes are Highly Metamorphosed Polymetallic SEDEX Type (Broken Hill Type Deposits) and Classical SEDEX or Shale Hosted Massive Sulphide Deposits. Both types start with a shallow marine or lacustrine environment at sufficient water depths to promote anoxia, but the first subtype involves metamorphism which changes the overall geology and geochemistry of the deposit. The host rock is generally a series of euxinic marine sediments, black shale, siltstone, sandstone, chert, dolomite, micritic limestone and

turbidites. The main host of the ore is laminated carbonate with a high organic component. The mineralization is secondary to the formation of the host rock through digenesis or epigenesis resulting in the formation of sulphides with zinc, lead and silver in dominance and iron and manganese secondary.

As in both cases the dominant mineral is not manganese, but rather lead, zinc and silver. These deposits are not really economic manganese deposits; as such they do not have an associated grade or size component. Examples of the non-metamorphosed SEDEX deposits are Meggen and Ramelsberg (Germany) and Sullivan (Australia). Examples of the metamorphosed SEDEX deposits include Cannington and Broken Hill (Australia) and Aggeneys (South Africa).

Type 7

Type 7 karstic deposits are manganese rich carbonates which are enriched through the natural sub aerial weathering process of the carbonate. As the deposit is weathered by rain water, the actual carbonate is dissolved and the other minerals occurring within the carbonate, including manganese, are left behind. This results in a pocketed ore body with remnant hills or unweathered carbonates and depressions with manganese and other detrital material occurring in these depressions. Due to the nature of the formation of these deposits, the ore bodies are irregular in size, continuity and grade, and lend themselves to small scale artisanal mining. Grades within a single deposit can vary between 20-50% and can contain varying amounts of silica and iron. Examples include Woodie-Woodie (Australia) and the Postmansburg manganese fields (South Africa).

Type 8

There are 7 subtypes of the sedimentary diagenetic Type 8 manganese deposit. These subtypes of deposit are all different sedimentary marine or sub marine processes resulting in some form of manganese deposition. All of them involve some oxic and anoxic transition, resulting in the reduction and oxidation of precipitates, namely manganese and iron within the marine environment. They are also divided between supergene enriched, and not supergene enriched and finally between the host rock type. This results in the following subtypes, Sandstone Claystone, Supergene Enriched Sandstone Claystone, Black Shale, Supergene Enriched Black Shale, Carbonate Type, Banded Iron Formation Type and Supergene Enriched Banded Iron Formation Type. The reason that no supergene enriched carbonate exists, is that this would become a Type 7 deposit.

There are four distinct host rocks each occurring within an oxic/anoxic transition zone. The oxic/anoxic boundary either facilitates the precipitation of manganese and iron during the entire deposition of the host rock, which means that the manganese and iron are part of the host rock (Black Shale and Banded Iron Formation Type), or the oxic/anoxic boundary shifts during the deposition

of the host rock resulting in a layer of manganese and iron precipitation (Sandstone Claystone and Carbonate) within the host rock.

Due to the nature of the deposits (large marine basins) and the interface (the oxic / anoxic transition) these deposits represent the largest scale and highest grade deposits out of all of the different types, and account for 70% of all the terrestrial manganese deposits in the world (Beukes et al., 2001). The Sandstone Claystone Type average size is 7.3 Mt with 10% greater than 280 Mt and 10% less than 0.19 Mt. The average grade of these deposits is around 20 – 40% Mn. Examples include Nikopol and Bolshoi Tokmak (Ukraine) and Chiatura (Georgia). The Supergene Enriched Sandstone Claystone is similar in scale to the Sandstone Claystone Type but with a supergene influenced higher grade. An example of this deposit is Groot Eylandt (Australia).

Black Shale Type deposits are large size deposits, but without the supergene enrichment they are generally too low grade for economic purposes. This coupled with the fact that the manganese is locked up within the shale means that without supergene enrichment the extraction of the manganese is nearly impossible. The scale of both the supergene and non-supergene deposits is similar to Sandstone Claystone deposits, while the grade of the non-supergene is around 10-20% Mn and the supergene enriched deposits grade is around 35-45% Mn. An example of a non-supergene Black Shale Type deposit is Ziangstan (China) and an example of a Supergene Black Shale Type deposit is Moanda (Gabon) and the Azul deposits (Brazil).

The Carbonate Type deposit is generally low grade, similar to the Black Shale type, however in some instances the lenses of manganese can be high grade and the added benefit of the deposit is that due to the high carbon content these ores can be calcined easily to produce a metallurgical product. They are the same scale as Sandstone Claystone deposits, with similar grades as Black Shale deposits. Examples include Imini (Morocco), Molango (Mexico) and Ulu Telyak (Russia).

Banded Iron Formation type deposits are higher grade as they are chemical sedimentary deposits of alternating manganese and iron. The Supergene Enriched Banded Iron Formation type results in a 'super grade' manganese deposit. This type is of the same size as the Sandstone Claystone deposit but, the largest known deposit falls within this category, the Kalahari Manganese Field accounts for 56% of the world's total terrestrial manganese resources. These deposits have an average grade of between 20-40% while the supergene deposits are between 35-50% Mn. Examples of this deposit type include the Kalahari Manganese Field (South Africa), Morro du Urucum (Brazil), Otjosondu (Namibia). An example of Supergene Enriched Banded iron Formation type is Rio das Velhas Series (Brazil).

Summary

Based on the host rock of the Cape Peninsula, the general nature of the deposit, and the suggested method of deposition by Compton (2004) there are two

possible Type categories into which the Cape Peninsula deposits could fall. Due to the hosting of the manganese deposits within the Peninsula Fm Sandstone it is possible that the manganese deposits within the Cape Peninsula are low tonnage versions of the Type 8 sandstone claystone deposit style, with the manganese being supergene enriched and concentrated in isolated locations. It is also possible that these are a Type 1 deposit which could either be a hydrothermal metasomatic process or a low temperature metasomatic groundwater formation process and the fact that they are hosted in a sandstone material is coincidental.

1.4 Manganese, its purposes and applications

Manganese is the 25th element on the periodic table and the 12th most abundant element in Earth's crust, although it only has an average concentration within Earth's crust of 0.1% (Cunat, 2004; Lindstad et al., 2007). While manganese is the 12th most abundant metal in the crust, it is the 4th most used metal in terms of tonnes mined (Lindstad et al., 2007). Manganese has many different applications and throughout history manganese has been used by many cultures for many different purposes. Paintings using manganese date back 17000 years, in Greece the Spartans used manganese in their steel weapons resulting in them being superior while the Egyptians and Romans used manganese in glass (Lindstad et al., 2007).

In the 1700's manganese was used in some chemicals, namely potassium permanganate and in the production of chlorine. In 1774 manganese was recognised by Carl Wilhelm Scheele as a separate chemical element. In the 19th century various experiments were conducted on an iron manganese alloy. In 1860 Sir Henry Bessemer came up with the self-named Bessemer process of the production of the current form of ferromanganese, where the manganese makes the iron harder and less brittle by bonding with the excess sulphur and oxygen (Lindstad et al., 2007).

The reason that ferromanganese is such an important metal is due to its relationship with iron in the production of steel. Almost 90% of all ferromanganese produced is used in the production of steel because manganese can replace nickel (Cunat, 2004; Lindstad et al., 2007). Nickel is harder to find and extract being the 28th element on the periodic table and only the 24th most abundant mineral in Earth's crust (Cunat, 2004) making it much more costly. Nickel, and its substitute manganese, gives steel its ductility, toughness, corrosion resistance and causes steel to be non-magnetic. With 90% of manganese being used in steel there is a very strong link to the steel demand globally and manganese demand globally. Due to modern advances in steelmaking an average of 7.5 kg of manganese is required per tonne of steel produced (Lindstad et al., 2007). According to World Steel Association (WEB7) there is a forecast growth of 6% for steel demand in 2012, this forecast can also be applied to manganese.

Table 4 shows the world production of manganese between 1970 and 2010. The tonnes produced are represented by ores and concentrates. An ore represents the actual tonnes of rock removed from earth while a concentrate requires a secondary process, such as washing, sieving or sintering, to extract or beneficiate the manganese which usually results in an enrichment of the ore. For example, Australia's GEMCO mines low grade ore (20% Mn) with many impurities. A simple sieving process based on the natural size fractionation of the ore results in a larger grain sized fraction (>1mm) concentrate with a substantially higher grade (47% Mn) than the original ore (Bryant and Hope, 2012). While reporting a concentrate as opposed to an ore will result in a lower reported tonnage figure, a higher manganese grade is reported. It is up to the prerogative of the company reporting the resource as to how they wish to represent the resource, as long as it is in line with an acceptable reporting standard such as Joint Ore Reserves Committee's (JORC) code (JORC, 2004). The supply percentage of Table 4 shows how much of the world's manganese is supplied by the main manganese producing countries (South Africa, Gabon, Ukraine, Australia and Brazil) as a percentage of global manganese production. China is excluded from these main manganese producers as their manganese is of a lower grade quality and none of its manganese reaches the seaborne market and is all sold internally.

Table 4: World production of manganese ores and concentrates 1970 – 2010 (tons·10^3) (United Nations, 2003; WEB 1).

Country / Year	1970	1975	1980	1985	1990	1995	1999	2003	2006	2010
Australia	739	1555	1999	2003	1950	2127	1912	2550	4556	6465
China	1121	2102	2332	2644	4060	8011	3186	4000	8000	13000
India	1820	1360	1692	1240	1393	1797	1596	1650	2084	2600
South Africa	3054	5897	5695	3601	4402	3199	3122	3501	5213	7172
Gabon	1615	2118	2146	2340	2423	1930	1910	2000	3000	3201
Ghana	356	357	246	357	364	187	612	1200	1659	1000
USSR (former)	6840	8459	10250	9900	8500					
Ukraine						3192	1985	2591	1606	1589
Georgia						42	48			
Kazakstan						492	944	2361	2531	3042
Brazil	2126	1800	2282	2523	2300	2398	1640	2600	3390	2400
Mexico	99	410	447	396	452	370	459	310	346	485
Others	1205	1627	113	190	754	875	519	455	752	1720
World Total	18975	25685	27202	25194	26598	24620	17933	23218	33137	42674
Supply Percentage	65%	67%	71%	69%	64%	39%	48%	46%	49%	45%

As manganese is used with iron to create hardened steel and manganese ores contain iron, a premium is paid for ores containing more manganese and less iron as less volume of manganese ore can be purchased to be added to the raw iron ore to produce steel. A higher grade manganese ore results in a higher price paid for that ore. Similarly the deleterious elements (such as phosphorus) negatively affect the price of the manganese ores. Due to the wide range of manganese deposit types and the wide range of steel applications, there are

many kinds of ferromanganese alloys, in some cases some suppliers list up to 20 different products.

These alloys need to be smelted from various manganese ores and from various manganese deposits around the world. Table 5 lists the most common metallurgical ores, ores containing >35% Mn, from around the world. This is a list of the products produced by the world's main manganese producers which make up roughly 40 – 70% of the world's manganese ore supply (depending on year of measure) but importantly these manganese resources make up 80% of the known global manganese resources. These listed metallurgical ores give a good indication as to what a competitive product on the manganese market would look like.

Table 5: Typical compositions in weight percent of metallurgical manganese ores representative of the various different sedimentary diagenetic types 8A, 8B, 8D and 8F defined by Harrison (1998) (Tangstad et al. 2004).

	Manganese Ore	Mn	Fe	SiO_2	Al_2O_3	MgO	CaO	BaO	K_2O	P	CO_2
Type 8A	Nikopol	48.0	2.9	9.1	1.8	1.0	2.4			0.19	
Type 8B	Groot Eylandt	48.8	6.0	6.9	4.2	0.1	0.1	0.3	2.00	0.09	0.5
Type 8D	Amapa Miudo 40	41.3	18.0	5.9	8.1	0.1	0.3	0.3	0.80	0.11	3.5
Type 8D	Amapa Sinter	49.1	12.5	7.6	7.6	0.5	0.8	0.3	0.30	0.10	-
Type 8D	Comilog MMA	50.5	3.9	4.0	5.5	0.3	0.2	0.2	0.70	0.11	0.1
Type 8D	Comilog MMD	44.5	6.7	7.7	7.2	-	0.1	0.2	0.75	0.09	0.1
Type 8D	Comilog MMR	48.5	5.1	5.0	6.1	0.1	0.1	0.3	0.75	0.11	0.1
Type 8D	Comilog MMS	46.5	5.5	7.7	7.5	-	-	0.1	0.75	0.09	0.1
Type 8D	Comilog Sinter	58.5	4.5	7.0	6.5	-	0.1	0.3	0.75	0.12	-
Type 8F	Asman 48	51.3	14.3	5.5	0.4	0.7	4.3	0.4	-	0.04	0.8
Type 8F	CVRD Lump	45.0	6.7	2.6	8.6	0.2	0.2		1.50	0.09	14.4
Type 8F	CVRD Sinter	54.5	6.1	5.4	8.7	0.5	1.9	0.3	1.40	0.11	0.2
Type 8F	Gloria	39.1	7.2	5.7	0.3	3.8	12.7	0.1	-	0.02	15.4
Type 8F	Mamatwan	37.8	6.6	4.0	0.5	3.5	14.7	-	-	0.02	17.0
Type 8F	Wessels 38%	42.3	18.9	4.9	2.5	1.0	6.0	0.3	0.10	0.04	3.6
Type 8F	Wessels 50%	50.2	14.5	3.6	0.4	1.0	5.6	0.3	0.10	0.04	2.6

The average cut-off grade for manganese ore is 27% (Maynard, 2010) while the average crustal concentration of manganese is 0.1% (Cunat, 2004). This large increase in manganese content to an acceptable product grade is caused through multiple enrichment scenarios linked to the depositional environment. Even in the case where the depositional environment forms a manganese rich ore body, it often does not have a high enough natural grade to be economically viable (Maynard, 2010). In this instance a secondary enrichment factor is necessary in order to further enrich the manganese to an acceptable product (Maynard, 2010). Processes that lead to this secondary enrichment normally take the form of hydrothermal fluids remobilizing the manganese or surface weathering enrichment of the manganese.

It is an understanding of the secondary weathering enrichment processes which is the focus of this thesis, particularly the impact of ground water flow and surface weathering on the transformation a low grade deposit into a high grade deposit.

1.5 Study Objectives

The primary objective of this study is to determine the origin of the manganese deposits of the Cape Peninsula and to test the hypothesis that they are Type 1 metasomatic deposits. It will also be shown that they are neither a Type 8 Sandstone Claystone Supergene Enriched deposit nor a Type 1 hydrothermal deposit.

This primary objective ties into a number of other questions:

What is the geochemistry of these deposits and what does it reveal about their origin?

What is the source of the manganese?

How was the manganese transported and deposited at the sites studied?

Was the formation of these manganese deposits controlled by groundwater flow, hydrothermal activity or bedrock structures and faults?

To answer these questions several of the major manganese deposits of the Cape Peninsula were studied. Field mapping of the existing deposits was conducted where the physical characteristics of the deposits was noted. Hand specimens were then collected for analysis in the lab including petrography, microprobe, and elemental (XRF and ICP-MS) analysis. Integration of field, petrographic and geochemical analysis provides detailed data to better understand many of the aspects of the deposits and to propose a model of their formation.

2 METHODS

2.1 Field Work and Sampling

A total of six sites were selected for study based on the known or hypothesised occurrence of significant amounts of manganese in the greater Cape Town area. The occurrence of manganese was described at the outcrop and representative rock samples were collected from each of the six sites (Figure 6) (Table 6). This initial batch of rock sampling was conducted along the noticeable manganese and iron precipitations, except for the Contour Path sample site. As such there were three groupings of samples collected, unmineralised samples, transitional samples (where iron and manganese precipitates are first apparent) and metal rich samples (Table 7). The Contour Path sample site was selected due to the presence of a recent rock fall and acted as a control group of unmineralised and unweathered and un-depleted host rock. The Contour Path samples were Peninsula Fm sandstone, and Graafwater Fm sandstone and siltstone.

A second round of samples were then collected from the Skeleton Gorge site as this was identified as the most extensive and best preserved site (Figure 7). While the initial sampling program was aimed at highlighting the transitional nature of the deposits, the second sampling program along Skeleton Gorge was conducted in order to document variations within the style of manganese deposition which had been noticed between the different sites throughout the Cape Peninsula. Certain hypotheses were also tested during this secondary phase of sampling through the gorge, so the positioning of the samples sites became crucial (Table 8). The variations within the manganese deposition were grouped into veined, surface, and talus slope styled mineralization (Table 9). While this second batch of samples had its own sample grouping, it could still fit within the overarching sample grouping described in Table 7. All samples collected within the Skeleton Gorge were hosted by the Peninsula Fm, however samples 10 to 14 and sample 30 occurred within a siltstone layer within the Peninsula Fm and seemed to be critical to the formation of the extensive manganese deposit within the gorge.

Wherever possible insitu rock samples were taken and the weathered surface was removed. GPS co-ordinates were taken at the sample sites, and notes were made about the locations geomorphology.

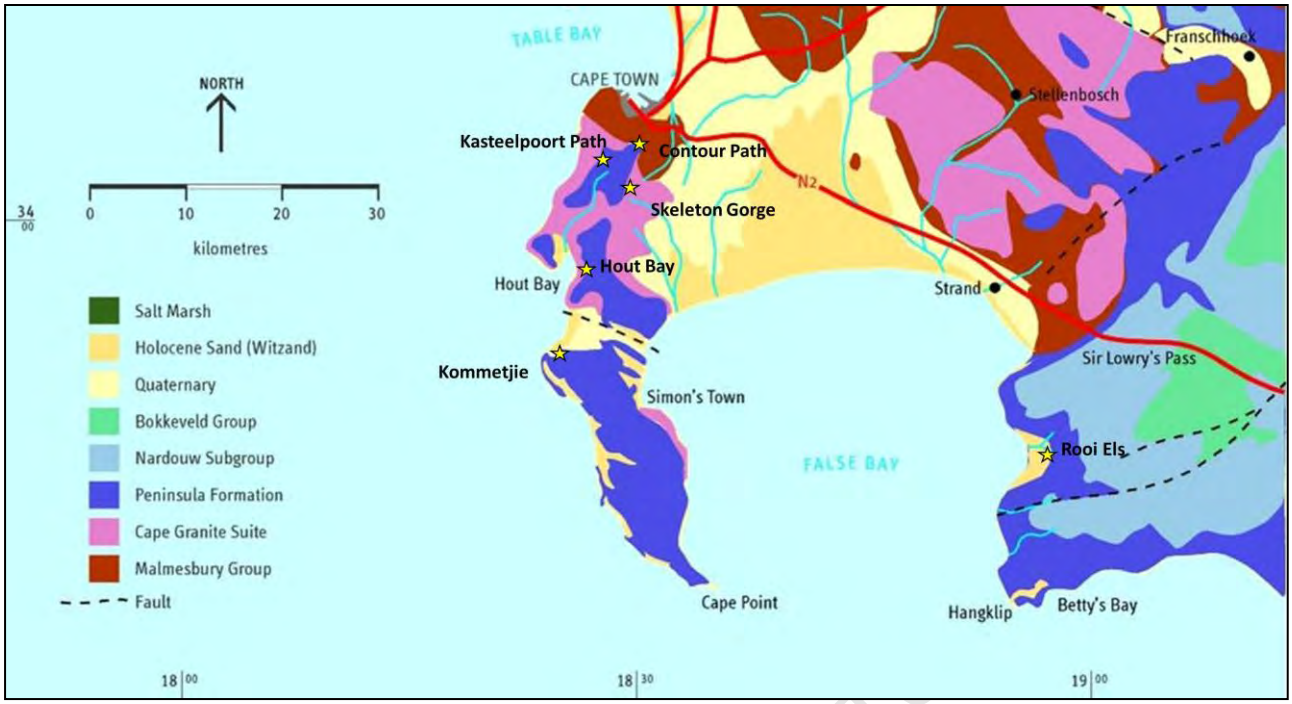

Figure 6: Geological Map adapted from Compton (2004), showing the location (yellow stars) and names of sites sampled for this study.

Table 6: Sample numbers and GPS location of the different localities sampled in the Cape Peninsula area.

Sample Numbers	GPS Coordinates of Site	Sample Locality
A1 – A7 1 – 31 (Table 8)	S – 33° 58.822' E – 018° 25.240'	Skeleton Gorge
B1 – B7	S – 34° 16.052' E – 018° 50.962'	Rooi Els
C1 – C7	S – 33° 58.385' E – 018° 23.519'	Kasteelpoort Path
D1 – D10	S – 33° 56.790' E – 018° 26.836'	Contour Path
E1 – E6	S – 34° 02.803' E – 018° 22.048'	Hout Bay
E7 – E8	S – 34°08.326' E – 018° 22.572'	Kommetjie

Table 7: Samples classified by sample type, rock type (SST = sandstone) and sample number.

Sample Type	Rock Type	Sample Numbers
Unmineralised Samples	Peninsula Fm Quartz Arenite Sandstone	A1,B1,D3,D4,D7,D8
	Graafwater Fm mudst/SST	D1,D2,D5,D6,D9,D10
Transitional Samples	Sandstone, Manganese and Iron	A2,A3,A5,A7,B2,B6, B7,C1,C3,C4,C6,C7,E6,E7
Metal Rich Samples	Manganese Rich	A4,A6,B4,C5,E3,E5,E8
	Iron Rich	B3,C2,E1,E2,E4

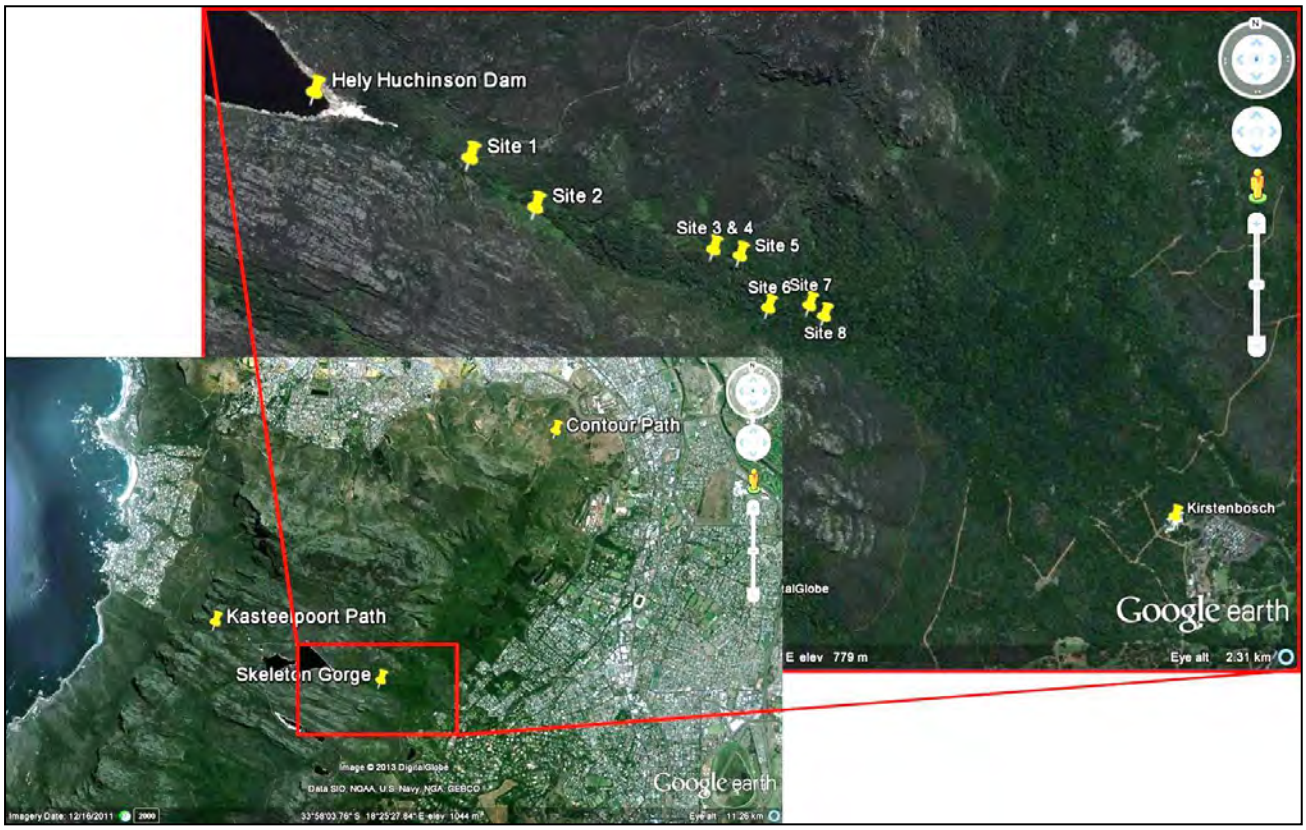

Figure 7: Satellite images from Google Maps showing the sites sampled along Skeleton Gorge.

Table 8: Site, location, numbers and locality of Skeleton Gorge samples.

Site Number	GPS Coordinates of Site	Sample Numbers	Sample Locality
1	S – 33° 58.767′ E – 018° 24.947′	1 – 2	Top of the Gorge
2	S – 33° 58.823′ E – 018° 25.011′	3 – 5	First manganese deposit, South of the Fault
3	S – 33° 58.797′ E – 018° 25.084′	6 – 18,30,31	Main Skeleton Gorge Deposit, North of the Fault
4	S – 33° 58.755′ E – 018° 25.097′		
5	S – 33° 58.911′ E – 018° 25.107′	19 - 23	Old deposit, Far North of the Fault
6	S – 33° 58.456′ E – 018° 25.137′	24 – 26	Seasonal Deposit, South of the Fault
7	S – 33° 58.891′ E – 018° 25.344′	NA	Current Seep (crystalline manganese) North of the Fault
8	S – 33° 58.896′ E – 018° 25.367′	27 – 29	Breccia Material, in the Fault

Table 9: Samples classified by sample type, depositional setting and sample number.

Sample Type	Depositional Setting	Sample Numbers
Unmineralised Samples	NA	1,2,30,31,A1
Transitional Samples	Veined	10,11,12,13,14,16,27,28,29,A2
	Surface	3,4,5,9,24,26,A3,A5,A7
	Talus	19,23
Metal Rich samples	Veined	15,17,18
	Surface	6,7,8,25,A4,A6
	Talus	20,21,22

Water samples were collected from Skeleton Gorge to determine how water chemistry (manganese content) relates to the features of the manganese deposit (Figure 8) (Table 10). Water samples were taken at springs, seeps, dams, and streams flowing on or nearby the deposit, and finally at water sources far downstream of the source of the water and the manganese deposits. A and B samples represent samples taken in a similar area. The water was collected in 500 ml polyurethane bottles and treated with 5ml of nitric acid to prevent the precipitation of any solids. The water sampling was conducted

during the winter of 2007. A complete elemental analysis was conducted on these water samples. GPS co-ordinates were taken at each water sample point.

Figure 8: Satellite image from Google Maps showing water sampling locations.

Table 10: Water sample site numbers and locations.

Site Number	Sample Locality	Water Sample Numbers	Coordinates of Site
1	Natural seep of water from the top of Kasteelpoort Path	1	S – 33° 58.421′ E – 018° 23.684′
2	Hely-Huchinson Dam	2a 2b	S – 33° 58.751′ E – 018° 24.471′
3	First crossing of stream along descent of Skeleton Gorge Path between rock sites 2 and 3	3a	S – 33° 58.814′ E – 018° 25.086′
4	Stream of water found at first manganese deposit (North of fault and rock site 3)	3b	S – 33° 58.82′ E – 018° 25.013′
5	Stream of water found at rock site 8	4a 4b	S – 33° 58.896′ E – 018° 25.367′
6	Stream of water found at the waterfall at the crossing of the Skeleton Gorge Path and the Contour Path.	5a 5b	S – 33° 58.982′ E – 018° 25.563′
7	Stream within Kirstenbosch Gardens	6	S – 33° 59.257′ E – 018° 25.879′

2.2 Petrography

Rock hand specimens collected in the field were examined in the lab. Based on the nature of their apparent manganese, iron and silica contents (unmineralised through to metal rich) as well as the apparent nature of deposition (talus slope, veined deposit, surface deposit), they were selected for petrographic and chemical analysis. A total of 50 of the 70 hand samples from the field were cut into polished sections (Table 11) for the dual purpose of both transmitted light petroscopy and microprobe analysis. The petrographic descriptions were done using transmitted light on a Nikon microscope. As many of the samples had a very low metal content and were highly friable due to extensive weathering of the host rock, cutting and polishing of mounted thin sections for the purpose of reflective light was not conducted. Mineral identification was conducted using XRD.

Table 11: Samples used for petrographic analysis.

Sample Numbers	Coordinates of Site	Sample Locality
A1 – A7 1-3,5,7,8,10,11,14,16,19,20,23,25,27,29-31	S – 33° 58.822′ E – 018° 25.240′	Skeleton Gorge
B1 – B7	S – 34° 16.052′ E – 018° 50.962′	Rooi Els
C1 – C7	S – 33° 58.385′ E – 018° 23.519′	Kasteelpoort Path
D1 – D4	S – 33° 56.790′ E – 018° 26.836′	Contour Path
E1 – E6	S – 34° 02.803′ E – 018° 22.048′	Hout Bay
E7	S – 34°08.326′ E – 018° 22.572′	Kommetjie

Microprobe analysis of the thin sections was done on a JEOL JXA-8000. Primary analysis was done in the form of elemental maps (80µm by 80µm) and line scans. The elements analysed were silicon, manganese and iron. Secondary analysis was done on a larger map scale size (150µm by 150µm) for silicon, manganese, iron, aluminium and potassium. The primary analysis was done on the initial regional deposits (Table 12). The purpose of this was to determine the microscopic relationships between the known bulk minerals and the elements silica, manganese and iron between different sites. The secondary analysis was carried out on the samples taken exclusively from Skeleton Gorge, a total of 75 maps and 19 line scans were done. **Appendix A** contains a complete list of samples analysed by microprobe and their maps and line scans.

Table 12: Number of primary microprobe maps and element (Mn, Fe, Si) line scans completed for the different sample localities.

Sample Locality	Number of maps constructed (80µm by 80µm)	Number of line scans done
Skeleton Gorge	5	1
Rooi Els	23	3
Kasteelpoort Path	19	11
Contour Path	8	0
Hout Bay	6	5
Kommetjie	0	0

2.3 Mineral and Chemical Analysis

Samples were selected for geochemical analysis (Table 13) based on petrography and the two classification systems. Bulk rock samples were crushed to a fine powder using a Siebtechnik vibratory disc mill. Homogeneous splits of the bulk sample powders were then analysed. All analyses were done at the University of Cape Town (UCT). The elemental composition of the powders was determined by X-ray fluorescence spectroscopy (XRF) using the XRF facility at UCT. Duplicate XRF analyses (rock samples 10 and 11) indicate an error of 3.13% for manganese, 3.57% for iron, 2.90% for silica, 2.93% for aluminium and 2.86% for potassium (Figure 9).

Table 13: Rock samples analysed by XRF and ICP-MS analysis.

XRF Analysis	Sample Locality	ICP-MS Analysis
A1;A4;A5;A6;1;2;3;5;6;7;8;9;10;11;12;13;14;15;16;18;19;20;21;22;23;25;27;29;30;31	Skeleton Gorge	A1;A4;A5;A6;1;2;3;5;25;30;31
B1;B2;B3;B4;B6	Rooi Els	B1;B2;B3;B4;B6
C2;C5;C6;C7	Kasteelpoort Path	C2;C5;C6;C7
D1;D2;D3;D4;D7;D8;D9;D10	Contour Path	D1;D2;D3;D4;D9;D10
E2;E3;E4;E5;E6	Hout Bay	E2;E3;E4;E5;E6
E7;E8	Kommetjie	E7;E8

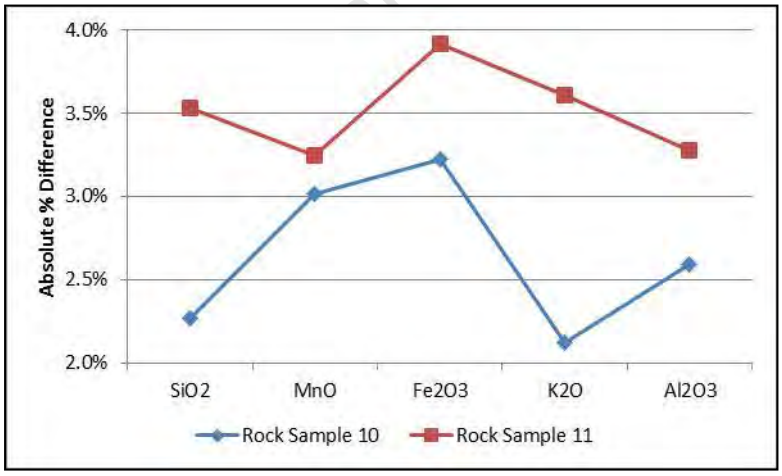

Figure 9: The absolute differences between duplicate samples for element oxide analysis by XRF.

Based on the results of the XRF, the samples with the highest manganese and silica contents were analysed for mineralogy using X-Ray Diffraction (XRD). The XRD instrument used was a Philips PW1390 Powder X-Ray Diffractometer, which uses a Copper K-α X-ray tube with wavelength of 1.542 Å. Bulk sample powders A4, B6 and E6 were run through the XRD. Quartz was used as an internal standard on the XRD profiles. The manganese minerals present were determined by combining bulk rock chemistry (XRF data) and the XRD profiles and by comparison to reported manganese minerals (Fleischer and Hewett, 1960).

Trace element analysis was conducted for both rock (Table 13) and all water samples using Inductively Coupled Plasma Mass Spectrophotometry (ICP-MS) on a Thermo-Fisher X Series2 instrument. For ICP-MS analysis 50 mg of the sample powder was dissolved in a 4:1 HF/HNO_3 acid mixture in a sealed Savilex beaker on a hotplate for 48 hours. This was followed by evaporation of the sample to incipient dryness and then two treatments of 2 mL concentrated HNO_3. The final dried product was then taken up in 5% HNO_3 solution containing 10 ppb Rhenium (Re), Indium (In), Rhodium (Rh), and Bismuth (Bi) as internal standards. Standardisation was against artificial multi-element standards. Along with the internal standard, a blank sample was included to determine the shift in readings. Figure 10 shows the average total procedural blank (tpb) achieved for both ICP-MS runs and the average percentage relative standard deviation (%RSD) achieved for each element tested. Some of the samples which were intended for ICP-MS did not completely dissolve and could not be analysed.

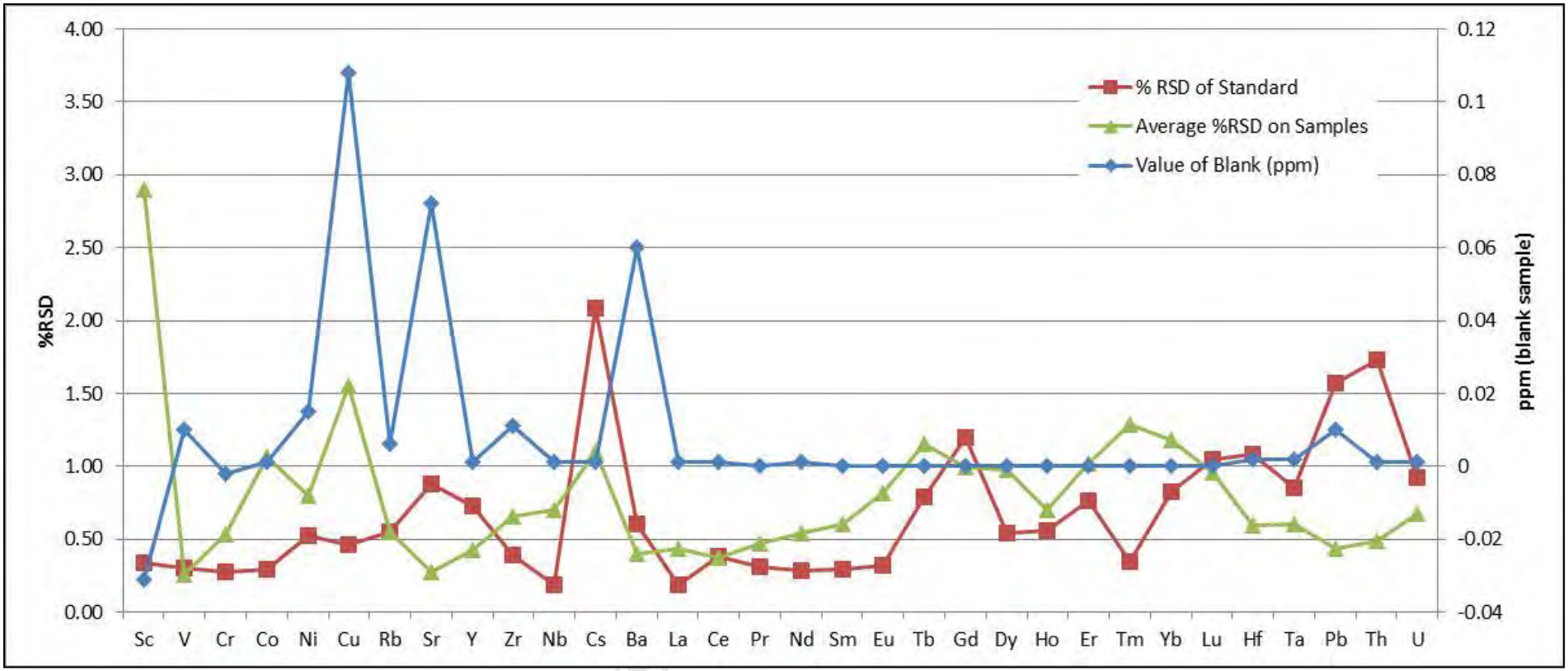

Figure 10: Average percentage relative standard deviation (%RSD) and total procedural blank (tpb) achieved for both ICP-MS runs for the rock samples.

3 RESULTS

3.1 Field Analysis

Multiple manganese rich sites were found during the field survey. Some sites were known deposits such as Hout Bay and Rooi Els which had been mined for manganese (Welsh, 1917); and others were previously not described or were unknown. Three sample types were collected: samples containing no obvious iron or manganese mineralisation from the Peninsula Fm sandstone and Graafwater Fm sandstone and siltstone, samples containing a variable and transitional mix of iron and manganese mineralisation, and samples enriched in manganese and iron.

Six Sites were investigated. The Contour Path site provided rocks which had no evidence of manganese or iron mineralisation. The Skeleton Gorge site was the largest and most extensive manganese deposit sampled, containing surface, veined and talus slope style of deposition. The Kasteelpoort Path site is linked to the Skeleton Gorge site by a fault and was a previously unknown, small and iron-rich talus slope style of deposit. The Rooi Els site occurs within a talus slope, with the manganese "rubifying" the slopes and also has a veined deposit which was mined in the past. The Kommetjie site is an old erosional remnant consisting of manganese boulders. The Hout Bay manganese site is a veined deposit and was mined in the past.

3.1.1 Contour Path Site

Samples from the Contour Path site are the least manganese or iron mineralised and is considered to represent the general or background composition of TMG bedrock. Peninsula Fm sandstone samples were collected from a recent rock fall to obtain fresh samples. The rock fall sampled occurs along the Contour Path near the cableway station (Figure 11 – point 3). The rocks in this area showed some surface weathering, thus boulders were broken up to get unweathered samples from the interior of the rocks for analysis. Graafwater Fm samples were collected from an in situ, outcrop exposure near to the rock fall site.

3.1.2 Skeleton Gorge Site

Rock Samples

There are multiple deposits of manganese along Skeleton Gorge from thin, surface coatings to massive vein and nodular manganese deposits. The gorge is situated along a fault (Figure 11 – point 1), and manganese deposits occur on either side of the fault. The largest manganese deposits occur on the northern side of the fault, while smaller manganese deposits occur on the southern side of the fault. The manganese deposits are hosted in Peninsula Fm sandstone with

beds dipping slightly (3-6 degrees) to the south west. The northern gorge outcrops had multiple seeps and springs flowing into the gorge (Figure 12).

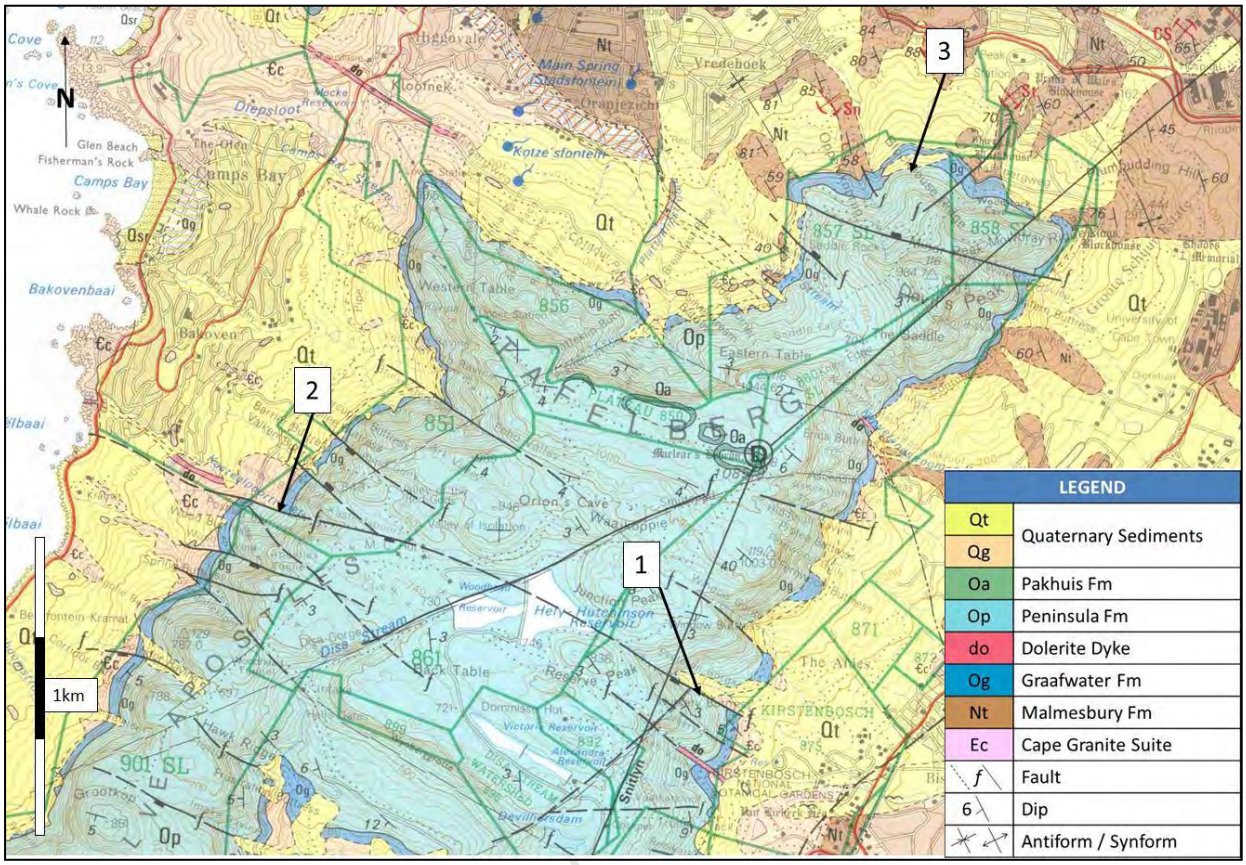

Figure 11: Geological map showing the sample location sites on Table Mountain (Council for Geoscience Cape Town Geological Map 1:50 000). 1 = Skeleton Gorge; 2 = Kasteelpoort Path; 3 = Contour Path.

Table 8 lists all the sites from which rock samples were taken from Skeleton Gorge. Additional deposits were found throughout the gorge but were not sampled due to inaccessibility or being similar in nature to already collected samples. Moving from the top of the gorge down, the first observed occurrence of manganese or iron mineralisation was a large boulder of Peninsula Fm sandstone not in situ (site 1 – 735 m). Iron staining was observed within small fractures (Figure 13) too recessed in the rock to sample.

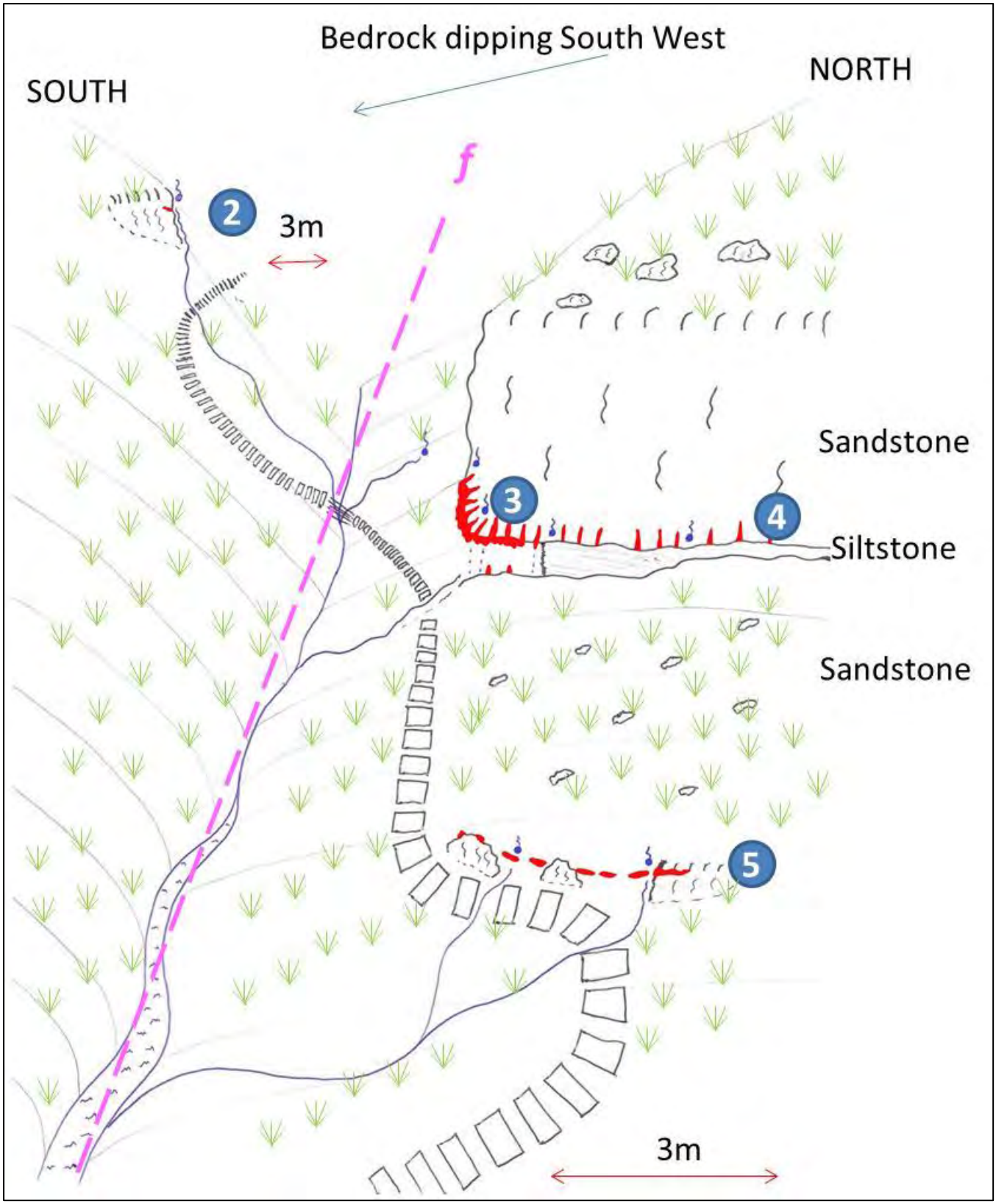

Figure 12: Sketch of the Skeleton Gorge deposit. Facing North West looking up towards sample site 3&4, with sample site 5 in the foreground and sample site 2 in the background. The trail is indicated by the rectangular blocks. Vertical Exaggeration (VE) of 1:1.

Site 2 occurs at the highest elevation within the gorge (690 m) where an in situ deposit of manganese was observed. This site is south of the fault and is associated with a small seep which flowed all year round. The manganese occurs in rock joints and as thin surface coatings. The host rock is Peninsula Fm sandstone and the site is along a small, steep cliff face, approximately 15 m wide and 4 m high. The surface coating of manganese is approximately 1 mm thick and localised along areas of active fluid flow (Figure 12). In between Site 2 and Sites 3 & 4, a deposit of manganese (not sampled) associated with a large seep was observed on the north side of the fault. The site was along a sloped rock face covered by a large amount of plant and moss growth which made it difficult to determine the extent of the deposit.

Figure 13: Iron staining within the veins of a loose boulder found at the top of Skeleton Gorge.

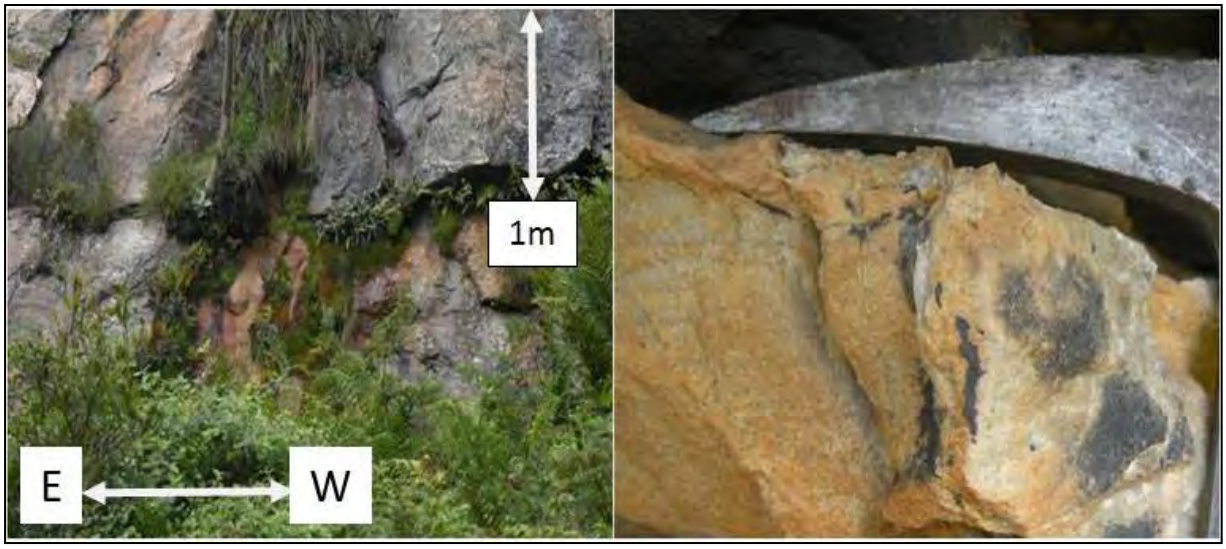

Figure 14: Manganese coating found at Site 2 associated with a perennial seep. Photo on left is of the outcrop face and on the right of a close up of the exposed rock face with deep orange (iron) and black (manganese) stained Peninsula Fm sandstone.

Sites 3 & 4 span the most extensive manganese deposit observed in Skeleton Gorge with Site 3 occurring at the highest elevation (550 m) of the manganese deposit and Site 4 occurring at the lowest elevation (531 m). The deposit occurs along a small water seep on the north side of the fault. The geology of this site is unique within Skeleton Gorge. The host rock is Peninsula Fm sandstone, however at the base of the deposit is a unit of fine grained siltstone, below which no manganese is found (Figure 15). The siltstone is softer than the sandstone, and resulted in an overhang forming. The manganese deposit extends laterally for at least 150 m along the overhang cliff face 30 m high.

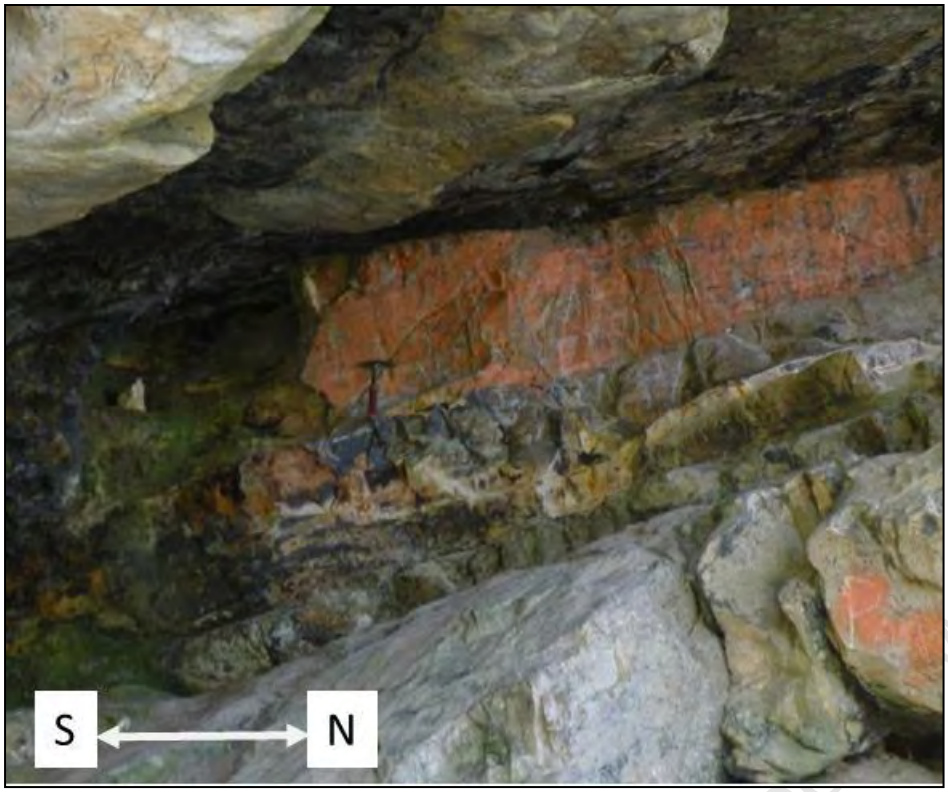

Figure 15: The siltstone layer (spray painted orange) below the overhang at Skeleton Gorge with a black manganese surface coating along a groundwater seep (immediately below the hammer) slightly south of Sample Site 4.

The manganese deposit of sites 3 & 4 varied. Along the cliff face the manganese and iron fill cracks, joints, and veins within the host rock. In some locations layers of surface coating up to 5 cm thick have formed. Overhang drip structures of manganese were observed, and on the floor below are smaller drip structures. Moving laterally away from the overhang the amount of manganese diminished, but all along the sheer cliff face is a manganese surface coating. Toward the north away from the overhang and away from the gorge, the manganese deposit varies between weathered and fresh exposures with the fresh manganese deposits associated with active water seeps.

Seeps between sites 3 and 4 varied in their flow intensity and seasonal variation in flow. The southernmost seep, nearest to Site 3 had no water flow in the summer and minimal water flow in the winter season which resulted in weathering and moss growth in the areas with less water flow (Figure 16). The middle portion between sites 3 and 4, under the overhang, had fluid flow throughout the year with an increase in the winter season; this constant water flow resulted in drip structures (Figure 17). The northernmost point of the deposit, Site 4, is seasonal, dry in the summer and wet in the winter.

Figure 16: The "dry" southernmost portion of Site 3. Photo on left is of moss overgrown manganese and on the right the weathered and crumbling manganese and iron exposure.

Figure 17: Manganese drip structures on the overhang in the "wet" portion of the Site 4.

Below sites 3 & 4 is site 5 on the northern side of the fault and not associated with a water seep. Site 5 showed extensive weathering, and similar to the manganese found in between sites 2 and 3, the manganese was covered in lichen and moss. As opposed to being in an exposed bedrock face, site 5 is along a talus slope at the base of the cliff of sites 3 & 4 (Figure 18). Based on the elevation difference this slope extended for approximately 50 m and consisted of manganese covered sandstone boulders, sandstone boulders without manganese, and a few centimetres thick layer of quartz-rich soil. There was significant plant growth covering the entire slope. At the point where in situ manganese occurs (site 5) there is a small overhang present which exposes a soil profile. The manganese is being deposited in the soil along the slope giving the manganese a granular texture with abundant included quartz grains. If the

manganese rocks are broken open, then loose soil is found trapped in voids in the rock. The moss and plants bind the soil as well as the manganese cement.

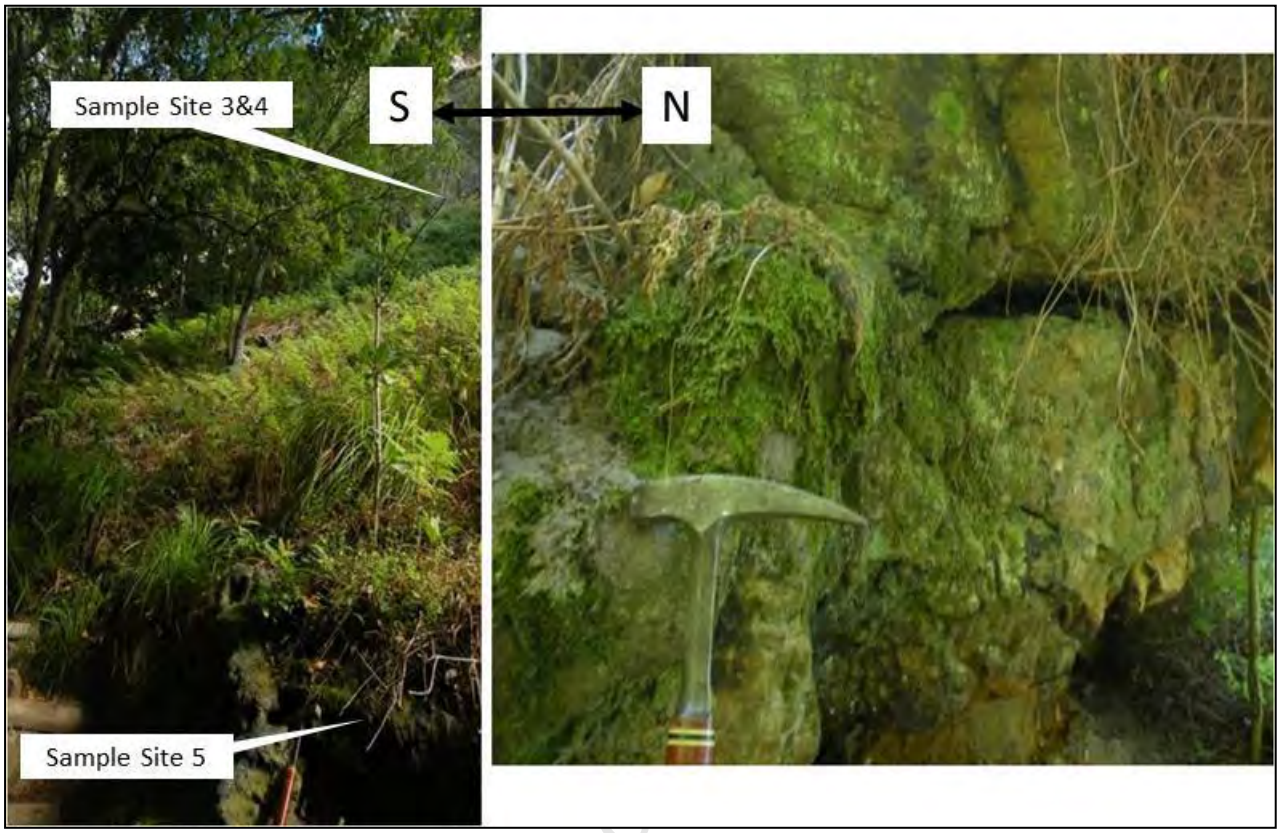

Figure 18: The extent of the talus slope (left) and green moss and fern coating the exposed surface of the deposit (right).

Further down the gorge the trail path is made up of multiple boulders of manganese, and manganese stained sandstone. It was not always possible to determine which boulders containing manganese were in situ, and which were part of the talus slope. Manganese deposits were observed wherever there were visible water seeps flowing into the gorge. The majority of these seep deposits occur on the north side of the fault. However, two additional deposits to site 2 were found south of the fault. One was site 6, the other was at a slightly higher elevation than site 6, but inaccessible to sampling. In both cases the geomorphology was the same, a slightly sloped cliff face of Peninsula Fm sandstone which had a wide but thin water flow down the width of the manganese deposit. The water flow was seasonal, and the manganese deposit forms only a thin surface coating along the flow path of the water (Figure 19).

Figure 19: Deposit of manganese occurring south of the Skeleton Gorge fault associated with a seasonal seep.

Significant manganese deposition appears to stop at an elevation of approximately 430 m within Skeleton Gorge. The water flow of the stream within the gorge at this point increases to form a constant flow. Along the cliff faces thin manganese surface coatings occur, and in one locality, site 7, where there was a constant slow flow of water over the surface of the rock, a thin crystalline botryoidal manganese deposit was found but not sampled (Figure 20). Site 8 at 410 m occurs where the stream cuts down deep into the bedrock and exposes bedrock fault breccia's full of iron stained joints and cracks, but with no significant manganese deposits.

In summary, deposits of manganese occur throughout Skeleton Gorge generally on the northern side of the fault and along seeps. There were 3 types of manganese deposits found, surface coating, vein deposits and intergranular talus slope deposits.

Figure 20: The botryoidal manganese crystal habit found at site 7.

Water Samples

Water was sampled from all possible sources along Skeleton Gorge to compare the trace element composition of the water to that of the rocks and to determine if the water transports sufficient manganese and iron to form the deposits to which they are associated. Water was taken from the top of the mountain down through the river valley to track the changes that occur to the water as it flows from the top of the mountain down through the rocks, out the seeps and into the streams. During subsequent rock sampling in different seasons the flow of water through the gorge was monitored.

The flow of water in summer was low and many seeps were inactive. The water in summer was darker in colour than in winter. The colour of the water is attributed to soluble organic tannins that are leached from the fynbos biome soils. The flow of water in winter was high with a large number of active seeps flowing in places where deposits of manganese were not noted. Water sampled during the winter season from seeps and the dam at the top of the mountain was dark in colour. The water during either season from the seeps where the most manganese was found (sites 3 & 4) was clear. The water from lower down in the gorge was a darker brown colour than waters higher in the gorge during either season.

3.1.3 Kasteelpoort Path

Based on one of the hypotheses, that manganese deposits may be fault controlled, the fault through Skeleton Gorge was followed to the other side of Table Mountain to Kasteelpoort Path (Figure 11 – point 2). This resulted in the discovery of a new manganese deposit within the Kasteelpoort Path gorge. There are however a couple of significant differences between this depositional site and Skeleton Gorge. The overall gorge is far narrower and steeper than Skeleton Gorge. The dip of the strata is to the south east, away from the deposit, and there was no fluid flow visible at any point along the gorge during the summer season. The manganese deposit also differed from that of Skeleton Gorge. The manganese is vertically extensive, but the deposit is at most 2 m wide, whereas in the Skeleton Gorge deposit is up to 150 m wide. The Kasteelpoort Path deposit also appears to be episodic, with sites having fresh deposits of manganese over weathered deposits and vice versa (Figure 21). The deposits are red in colour suggesting high iron content. Some manganese deposition occurs along fracture zones and elsewhere into unconsolidated sediments. None of the manganese deposits appears to be very thick in comparison to the deposits at Skeleton Gorge.

Figure 21: Heavily weathered manganese and iron deposits along the Kasteelpoort Path cementing loose slope talus.

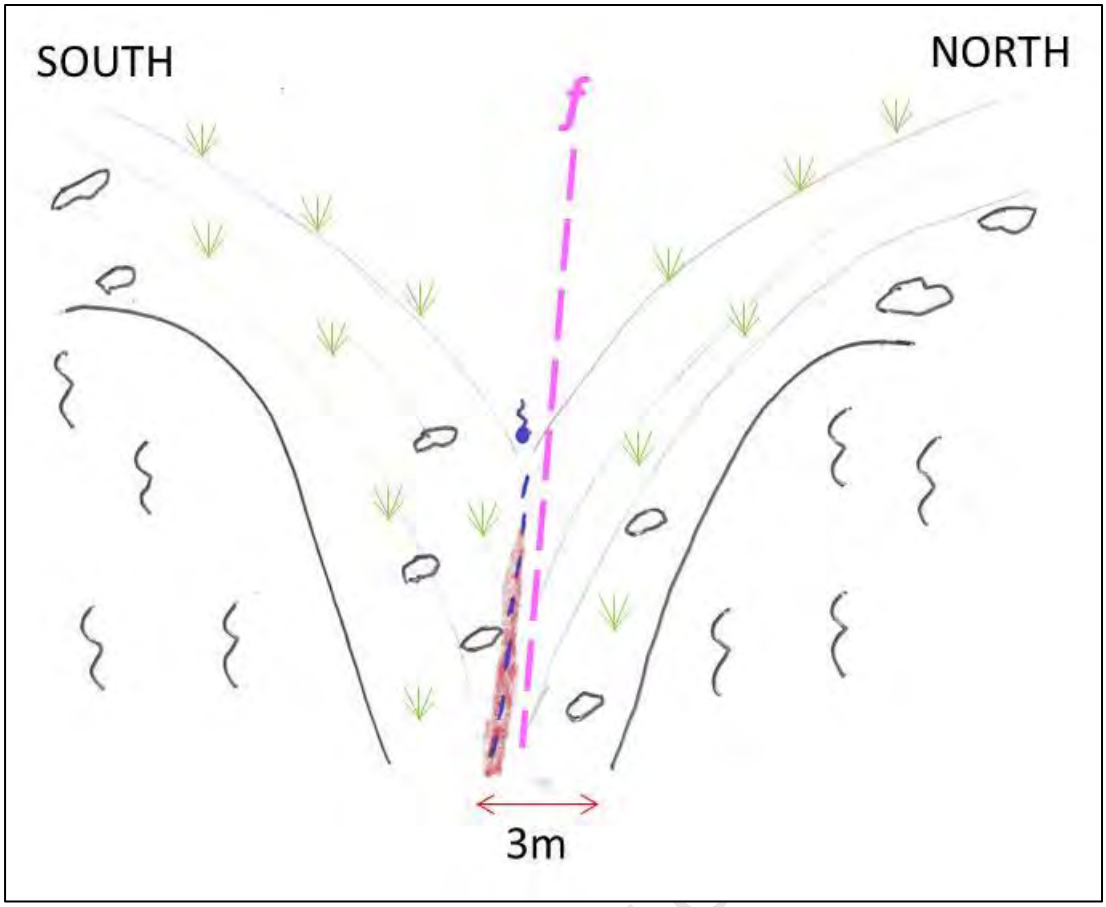

Figure 22: Sketch of the Kasteelpoort Path depositional site. The iron and manganese are deposited in the centre of gorge as part of the seasonal river and talus slope. VE of 1:1.

3.1.4 Rooi Els

The Rooi Els manganese deposit occurs along the road (R45) to the coastal town of Rooi Els, and is located between two large faults (Figure 23 – Point 1). The manganese deposit is not in a gorge, but rather occurs in the talus slope off of an exposed spur of Peninsula Fm sandstone. The Peninsula Fm beds dip to the east away from the depositional site into the mountain. Water was observed in summer to percolate through the loose sediment that makes up the talus slope. The deposit extends from Koeël Baai till Rooi Els Baai (2 km). Throughout most of the deposit, boulders and sediment which make up the talus slope, have been cemented together by manganese and iron oxides, in a process similar to "rubified slopes" described by Hutcheson (2004) (Figure 24 & 25).

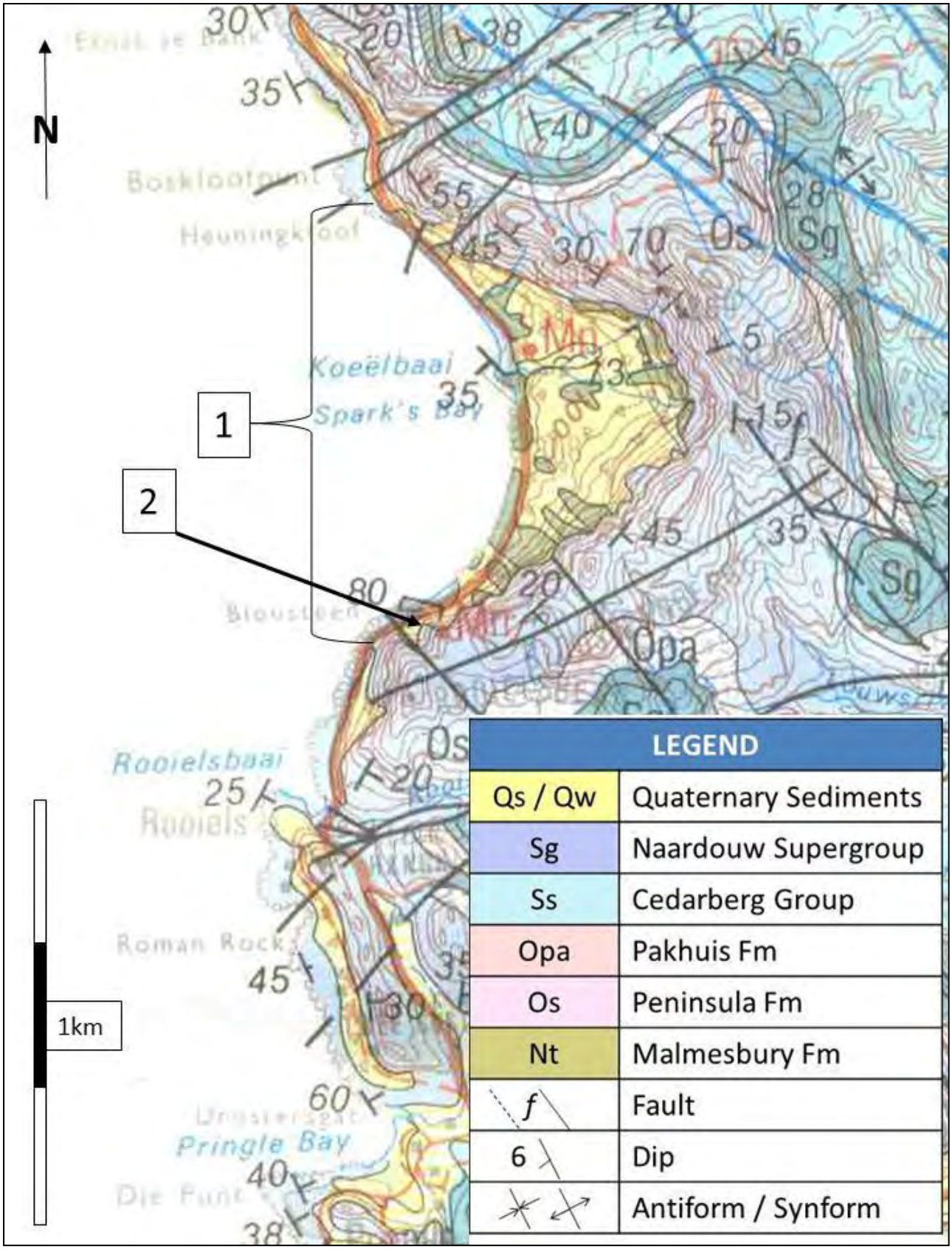

Figure 23: Geological map of the Rooi Els sampling site (Council for Geoscience Cape Town Geological Map 1:50 000). Point 1 shows the full extent of the manganese and iron occurrence, and Point 2 shows the manganese rich addit where the sampling was conducted.

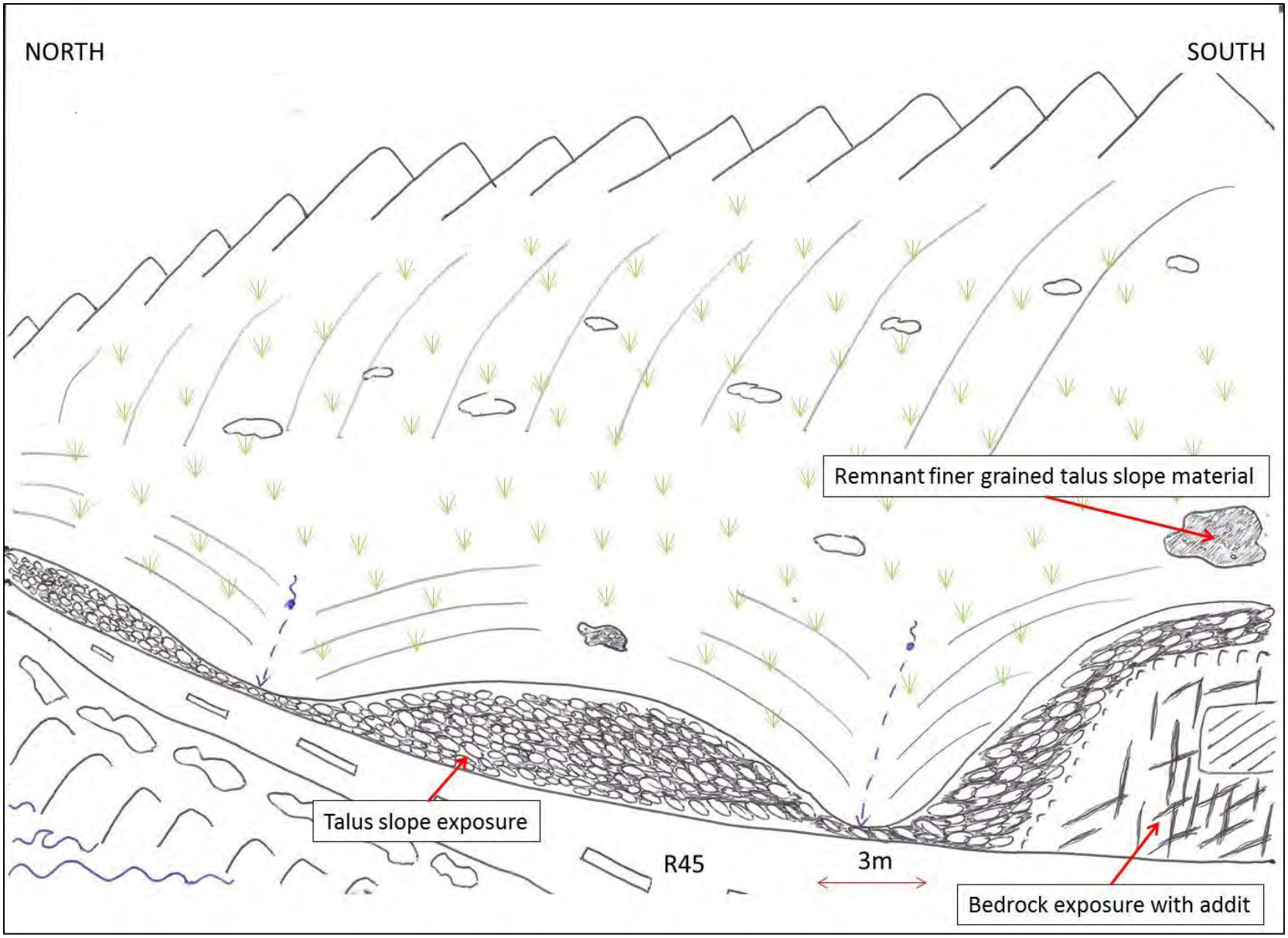

Figure 24: Sketch of the total Rooi Els depositional site as exposed along the R45 road cuts. VE of 1:1.

Figure 25: The manganese "rubified" talus slopes on the R45 road 3 km north of Rooi Els.

There is one location within the deposit where massive manganese deposition is observed (Figure 23 – Point 2). This is the only location in the road cutting where in situ Peninsula Fm sandstone bedrock is exposed. This location is where an addit was dug into the rock face in order to extract manganese rich ore (Welsh, 1917). This addit exploits a natural vein, within which massive manganese precipitated. While the manganese within this vein is no longer present, having been mined out, the remaining rock face is covered in veins of manganese and iron (Figure 26). From the entrance of the addit moving deeper into the bedrock the size and frequency of the fractures decreases and the occurrence of manganese decreases while the occurrence of iron increases (Figure 27). Moving laterally away from the deposit, the veins of manganese disappear within the exposed outcrop of Peninsula Fm sandstone which becomes covered by sandstone talus slope material cemented together by manganese and iron.

Figure 26: Veins filled with manganese oxides found in the Peninsula Fm bedrock near the addit at the Rooi Els site.

Above the addit there are large remnant eroded boulders of what appears to be primarily manganese with a matrix of fine grained to pebble sized quartz grains (Figure 28). The majority of the talus slope has cobble sized Peninsula Fm sandstone with the manganese acting as a matrix (Figure 25). In both cases the manganese acts as cement holding the loose particles together.

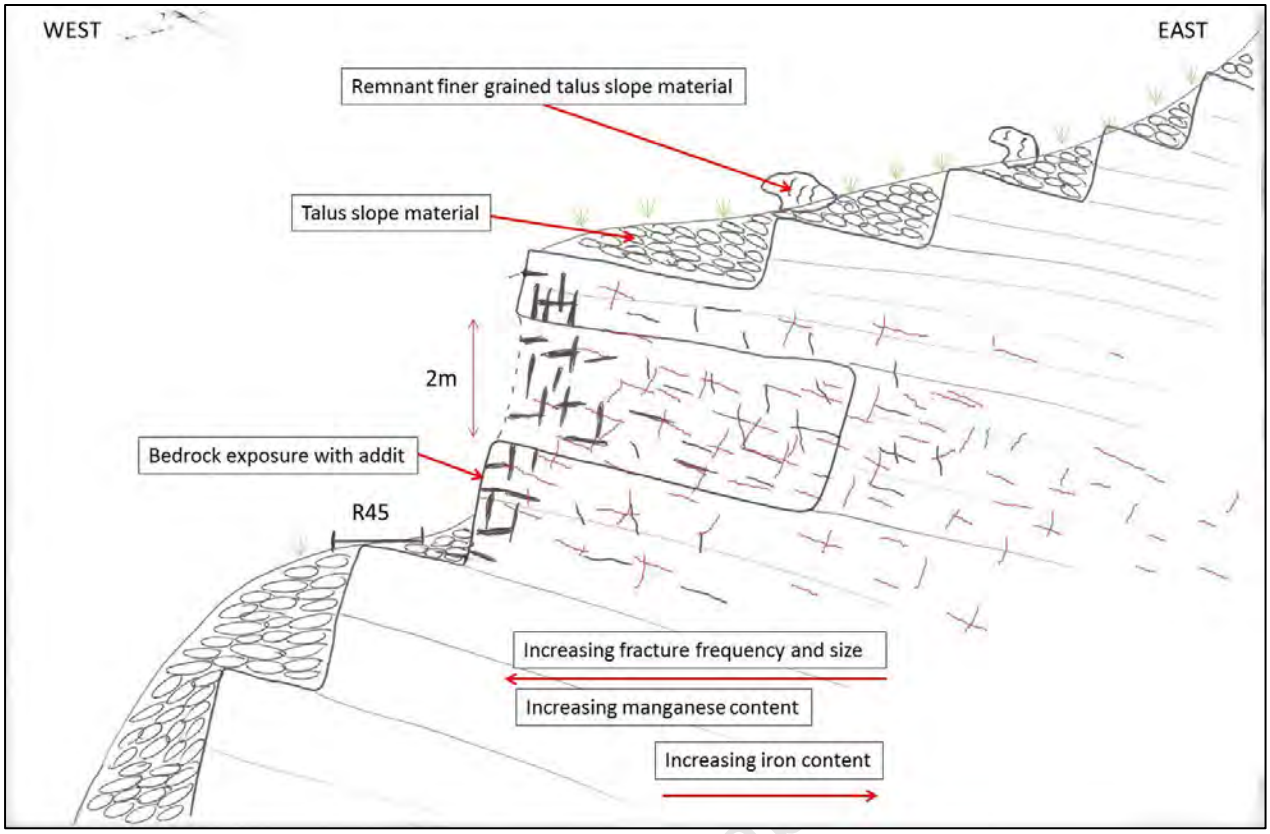

Figure 27: Cross section of the addit in Rooi Els showing the fracture frequency, size, and the dominant mineral being precipitated out. VE of 1:5.

Figure 28: A massive manganese boulder above the addit at the Rooi Els site.

3.1.5 Kommetjie

The deposit at Kommetjie consists of a couple of large boulders of massive manganese. None of these boulders are in situ. The massive manganese boulders appear to be remnants of manganese infilling of cracks between Peninsula Fm sandstone blocks (Figure 29 – point 1). The largest of these boulders is 10m wide, 20m long and 4m thick. There is still some sandstone present within the rock, but the majority of the sandstone has either been replaced by manganese or weathered away. The manganese is cracked and flaking which suggests that it is slowly weathering away (Figure 30). The bedrock in the Kommetjie area is Peninsula Formation sandstone with a surficial cover of Quaternary sand (Figure 31).

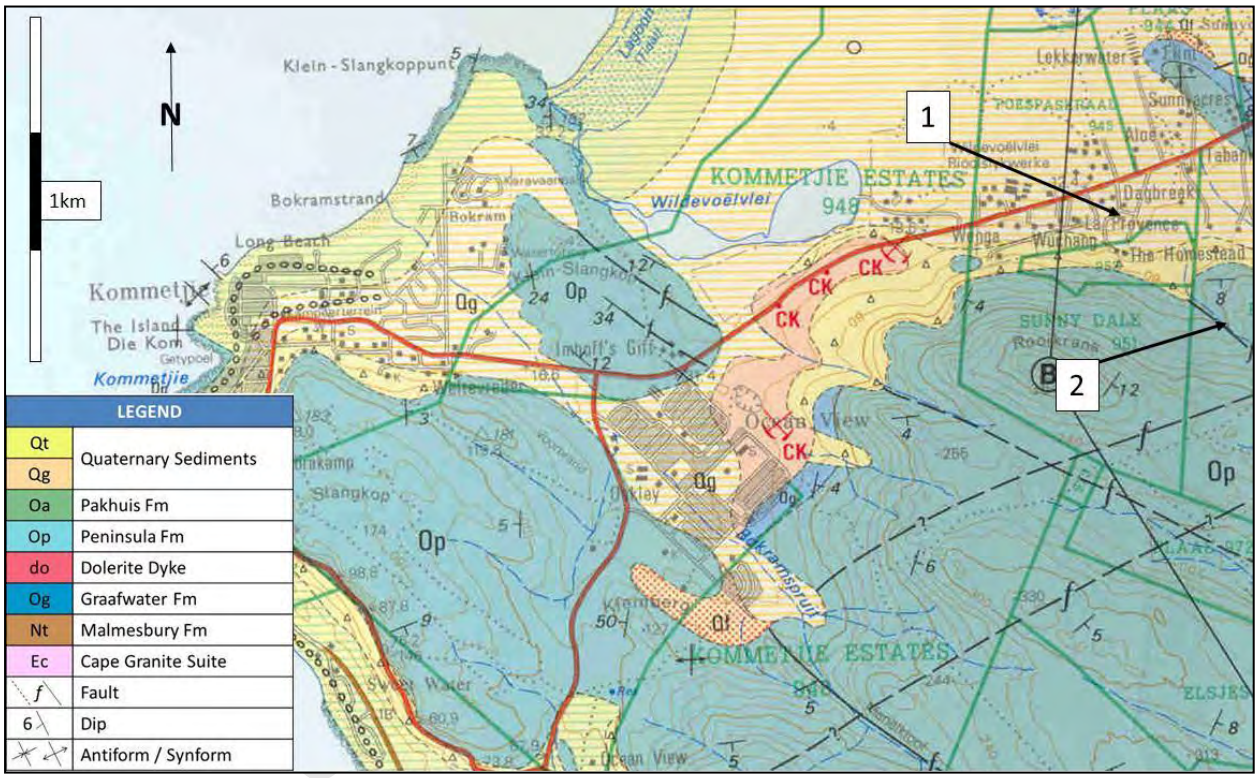

Figure 29: Geological map of the Kommetjie site (Council for Geoscience Cape Town Geological Map 1:50 000) showing the location of the Site (1) and a nearby fault (2).

Figure 30: The weathered surface texture of manganese-rich boulders found at the Kommetjie site where the visible ridges are rich in manganese.

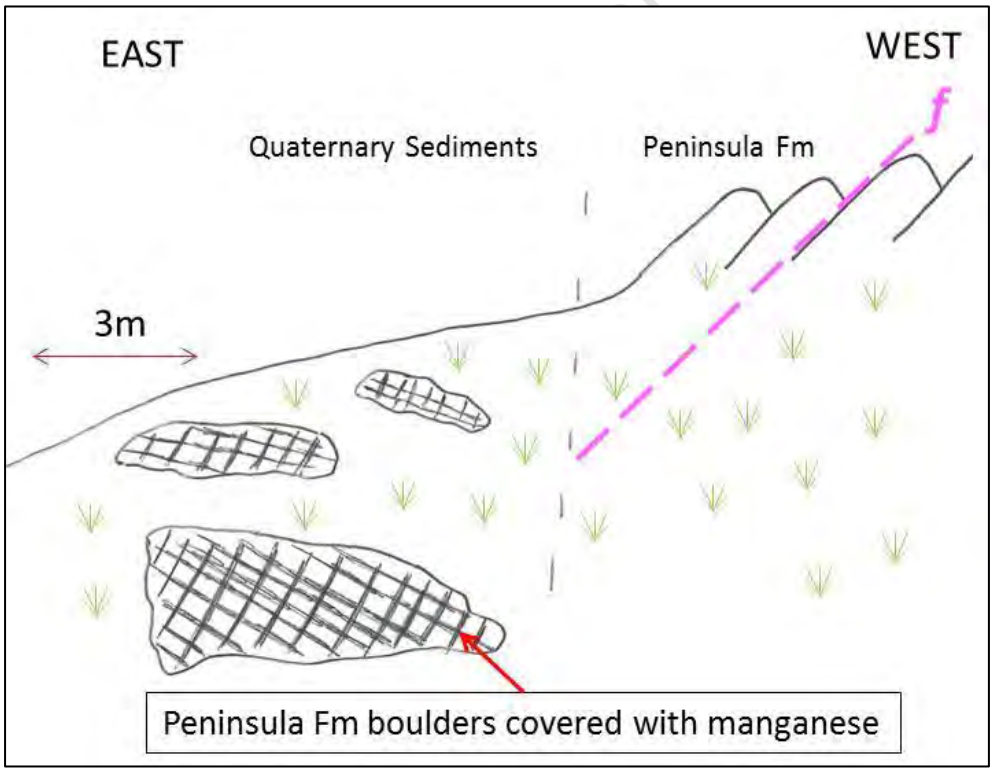

Figure 31: Sketch of the Kommetjie deposit. The boulders are not in situ but appear old and highly weathered. VE of 1:1.

3.1.6 Hout Bay Manganese Mine

The Hout Bay manganese mine deposit was heavily exploited for its manganese in the late 19th and early 20th century thus most of the manganese has been removed (Welsh, 1917). This meant that samples could only be collected from the dumps that occur in the area, making analysis of in situ samples difficult. This site occurs along a small fault, below an anticline and an old thrust fault with the Peninsula Fm bedrock dipping towards the site (Figure 32 & 33). The site is not in a gorge but on a mountain spur. The point where manganese was extracted is similar to that of Rooi Els, a thick vein of manganese which cuts through the Peninsula Fm. The addit exposes a similar view into the bedrock, with fracture frequency and size and manganese increasing towards the opening of the addit, and with iron being in more abundance deeper into the bedrock and a decrease in fracture frequency and size.

All the large veins have been exploited. No significant fluid flow was noticed during multiple visits to the site. This site was extensive enough for small scale mining, but there appears to be little to no recent manganese deposition, even within the soil profile.

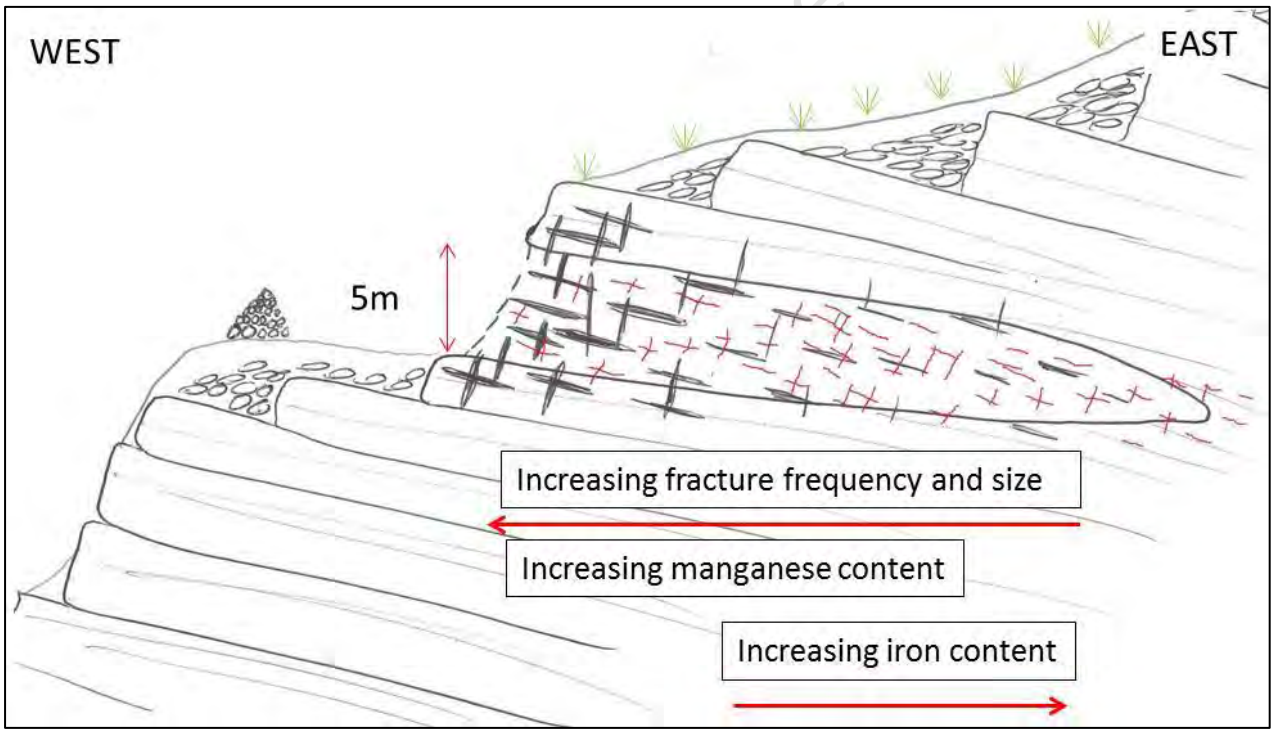

Figure 32: Sketch of the Hout Bay deposit. VE of 1:1.5.

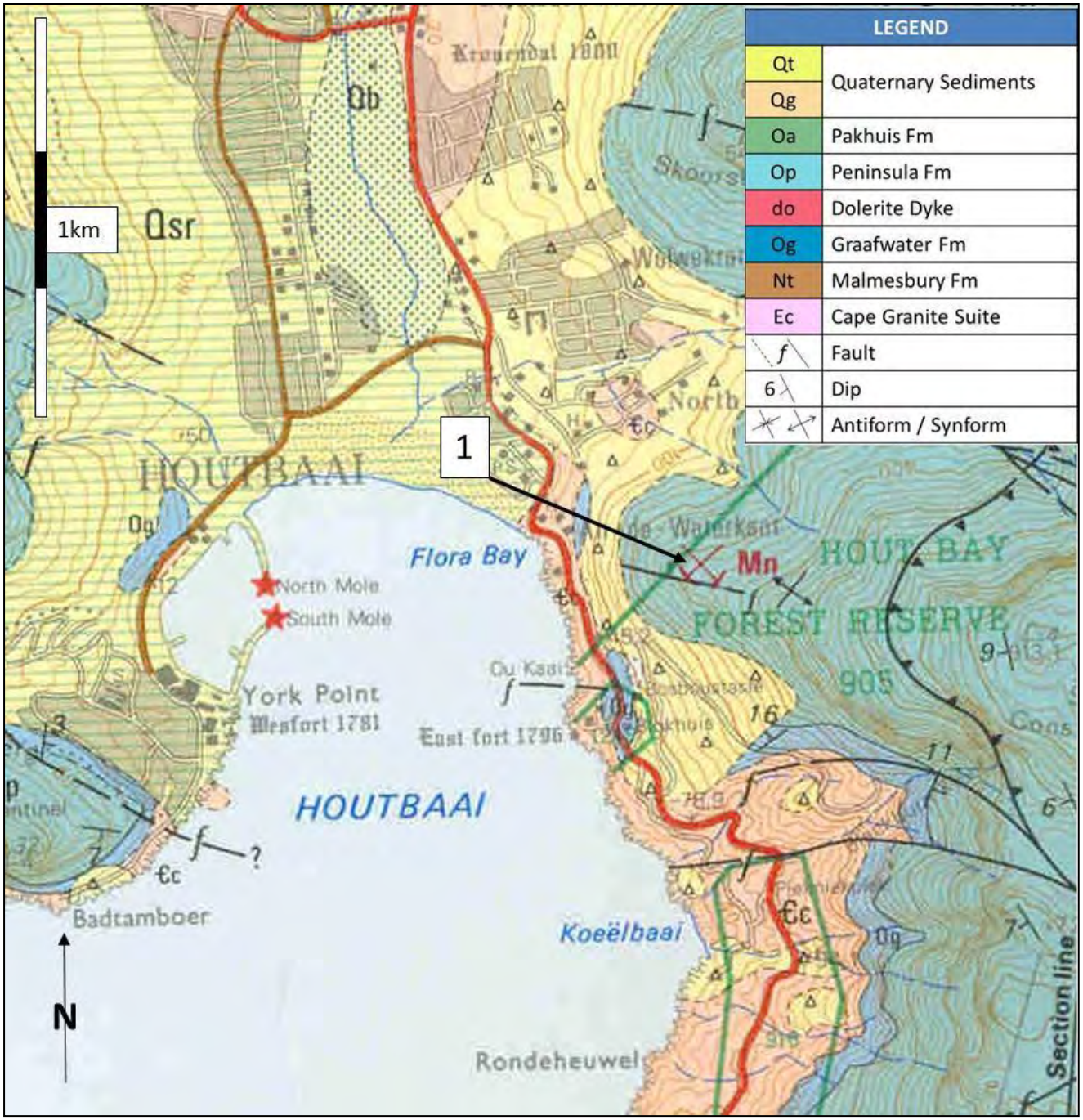

Figure 33: Geological map showing the location (1) of one of the addits of the Hout Bay manganese mine (Council for Geoscience Cape Town Geological Map 1:50 000).

3.1.7 Physical Variations among Depositional Sites

Three unique depositional settings were observed at multiple sample sites. In all cases, but Kommetjie where the boulders weren't in situ, the deposits were hosted by Peninsula Fm sandstone. The deposits can be split into active deposits where manganese and iron is still accumulating and deposits which are no

longer active. The contributing factor to the activity at the depositional site appears to be presence of water. Skeleton Gorge, Kasteelpoort and Rooi Els are active sites while Hout Bay and Kommetjie are no longer active. The following section summarizes the physical properties of the three depositional settings, veined, surface and talus slope deposits.

Veining

This appears to be the precursor to all of the deposits, regardless of type. The deeper, narrower veins are coated with iron, while the wider, shallower veins are coated with manganese. There appears to be a correlation with the size of the fracture, and the degree of manganese precipitation. For this reason the exceptionally large veins, Hout Bay and Rooi Els, formed massive 30m deep by 2-3m high by 2m wide manganese rich deposits which were suitable for artisanal mining. These large scale veined deposits are rare however and the majority of vein deposits are small scale along the joints and fractures of the bedrock as seen in Figure 13. For this reason it is difficult to quantify the full extent of these vein deposits as they mostly occur within the bedrock.

The position of the vein defines the next depositional setting. A vein beneath the soil profile would result in a talus slope style of deposit and a vein beneath an exposed rock surface would results in a surface coating of manganese and iron.

Surface Coating

Surface coatings can be divided into two categories, massive and minor. Minor surface coatings of manganese and iron are common throughout the entire Cape Peninsula with most rock outcrops having a thin, several millimetres thick surficial coating evident as orange (iron oxide) and black (manganese oxide) stains. The surface coating is the end result of the veined style of deposit with the manganese and iron coming out of the rock and precipitating on the surface of the rock.

In general the volumes of water seeping from the bedrock are so low or only seasonal that the surface coating is only noticeable as a surficial staining restricted to the uppermost several millimetres of the rock (Figure 14 – right hand image). In the event that the volumes of water and manganese are increased, layer upon layer of manganese can be deposited resulting in a potentially thick deposit of manganese (Figure 17). The only reason that these deposits would not be economic is owing to the limited lateral extent and inconsistency of the thickness of the layer of deposited manganese. In some instances the manganese layer could be up to 10 cm thick, and in other instances it reverts back to a superficial millimetre thick surface coating. It is the combination of specific geomorphological controls that create the necessary environment to form massive surface coatings as found, for example, at the Kommetjie and Skeleton Gorge sites.

To preserve the surface coatings, the erosion rate of Peninsula Fm sandstone needs to be slower than the accumulation rate of the manganese. Similarly to build up a massive surface coating then the accumulation rate of the manganese would have to far exceed the erosion rate of the Peninsula Fm sandstone. In most areas of the Cape Peninsula the erosion is fast enough in comparison to manganese deposition that only thin, millimetre scale surface coatings exist at any given time.

Talus Slopes

This is the final type noticed in the field and occurred when there was no bedrock but rather only loose unconsolidated sediment. The fluids moving through the regolith seep out into this loosely consolidated talus slope which will have a highly porous nature. As this talus slope is so porous it will act as an exposed rock surface and causes the formation of manganese within the soil profile which cements the unconsolidated sediment together, as seen in Rooi Els, Kasteelpoort Path and site 5 of Skeleton Gorge.

3.2 Chemical Analysis

3.2.1 X-Ray Fluorescence Results

The major and trace element composition of bulk rock samples determined by X-Ray Fluorescence is presented for silica rich rocks (Table 14), Transitional manganese rich rocks (Table 15), Transitional iron rich rocks (Table 16), manganese rich rocks and iron rich rocks (Table 17). The colouration in the tables is linked to the line colours for all the graphs. Silica content is highlighted in yellow, aluminium in blue, iron in red, manganese in green and potassium in purple. The results are ordered based on decreasing silica content.

Unmineralised samples were sandstone, except for sample 30 a siltstone from Skeleton Gorge. Samples D1, D2, D9 and D10 are Graafwater Fm sandstone exclusively from the Contour Path Site and the remaining samples are Peninsula Fm sandstone from various sites. The aluminium and potassium are very low in the Peninsula Fm sandstone, slightly increased in the Graafwater Fm sandstone and significantly increased in the Peninsula Fm siltstone.

In both the transitional iron and manganese rocks, a steady increase of iron and manganese is noticed, with either iron or manganese becoming more predominant and associated with a decline in silica and an increase in aluminium and potassium. Aluminium shows a slight positive correlation to iron and a slight negative correlation to manganese. Potassium shows a slight positive correlation to manganese. There is a slight negative correlation between the iron and manganese. In the metal rich iron and manganese samples (as defined by the high concentrations of either iron or manganese), the iron and manganese show a negative correlation. Aluminium and iron show a better correlation as do potassium and manganese, whereas aluminium and potassium

show a completely negative correlation and aluminium and manganese a flat correlation (Figures 34 – 38).

From the field analysis and the microscopy work some observations into the correlations of the different major elements can be made. The potassium and manganese's positive correlation is due to the manganese mineral which is being formed, Cryptomelane (Chapter 3.2.2). Similarly the flat to negative correlation between the aluminium and manganese is due to the replacement of manganese by aluminium within the Cryptomelane mineral. The positive correlation between the iron and aluminium is more than likely due to the presence of micaceous minerals in the region where the iron is being deposited. The correlation between potassium and aluminium is dependent on the region within the deposit that the sample occurs. Manganese rich samples will show poor correlation between the potassium and aluminium with elevated potassium (within the Cryptomelane) and depleted micaceous minerals (containing aluminium). High correlations between potassium and aluminium in the transition samples are due to the high amount of micaceous minerals containing aluminium and potassium.

The correlations of the minor elements are as follows, phosphorus has a positive correlation with manganese. Calcium and strontium are correlated as are potassium and rubidium. Among the trace elements, molybdenum has a strong positive correlation (0.59) with manganese. The remaining elements show no strong correlation to iron or manganese content.

Table 14: The major (wt%) and trace (ppm) element composition of unmineralised samples by XRF.

	Unmineralised Samples																		
Sample	A1	18	1	2	3	5	16	27	29	D7	D8	D3	D4	B1	D2	D9	D1	D10	30
SiO_2	94.36	83.69	96.45	96.60	95.34	95.08	90.98	93.43	92.23	95.77	97.52	96.32	95.72	94.30	93.46	88.55	89.16	82.09	81.89
TiO2	0.10	0.18	0.17	0.22	0.12	0.14	0.21	0.23	0.08	0.15	0.11	0.08	0.12	0.11	0.16	0.30	0.23	0.47	0.79
Al2O3	2.70	2.24	1.23	1.15	2.01	1.63	2.15	2.97	0.84	2.02	0.81	1.11	0.98	3.18	3.19	4.28	6.15	9.07	11.82
Fe_2O_3	0.50	0.89	0.28	0.41	0.42	1.28	1.14	1.10	3.33	0.52	0.78	0.93	0.99	0.48	0.60	1.40	0.86	2.57	1.21
MnO	0.03	7.76	0.08	0.03	0.02	0.06	3.02	0.04	0.07	0.07	0.03	0.03	0.04	0.05	0.03	0.06	0.03	0.04	0.04
MgO	0.17	0.21	0.20	0.24	0.25	0.20	0.25	0.19	0.20	0.18	0.20	0.21	0.20	0.17	0.28	0.38	0.42	0.84	0.34
CaO	0.03	0.09	0.02	0.03	0.13	0.04	0.11	0.02	0.03	0.11	0.03	0.06	0.04	0.02	0.05	0.05	0.02	0.07	0.04
Na2O	0.14	0.35	0.08	0.16	0.21	0.23	0.17	0.15	0.21	0.24	0.15	0.19	0.20	0.11	0.16	0.13	0.11	0.19	0.13
K_2O	0.65	0.57	0.23	0.21	0.44	0.36	0.68	0.76	0.04	0.14	0.17	0.25	0.18	0.75	0.81	2.06	1.66	3.76	1.87
P_2O_5	0.02	0.21	0.02	0.02	0.01	0.09	0.08	0.05	0.19	0.06	0.03	0.03	0.03	0.02	0.02	0.05	0.03	0.09	0.12
SO3	0.03	0.18	0.01	0.02	0.01	0.03	0.03	0.02	0.02	0.12	0.01	0.01	0.01	0.00	0.02	0.00	0.02	0.01	0.02
Cr2O3	0.01	0.02	0.01	0.01	0.02	0.02	0.02	0.02	0.01	0.02	0.01	0.01	0.01	0.01	0.01	0.01	0.01	0.01	0.03
NiO	0.00	0.00	0.01	0.01	0.00	0.01	0.00	0.02	0.00	0.00	0.00	0.00	0.00	0.00	0.00	0.00	0.00	0.00	0.02
H2O-	0.05	0.10	0.07	0.16	0.28	0.16	0.12	0.32	0.38	0.02	0.01	0.04	0.08	0.06	0.05	0.25	0.13	0.06	0.13
LOI	0.53	2.61	0.41	0.36	0.57	0.75	0.97	0.73	1.50	0.18	0.44	0.77	1.34	0.65	0.39	1.51	0.62	0.41	0.92
Total	99.32	99.11	99.29	99.63	99.84	100.07	99.94	100.04	99.14	99.61	100.29	100.04	99.93	99.91	99.22	99.03	99.44	99.70	99.36
Mo	2	6	1	1	1	2	7	1	1	1	1	2	2	2	2	2	2	2	2
Nb	7	17	6	7	5	5	6	4	4	4	7	6	7	7	8	11	9	16	7
Zr	36	192	66	126	48	57	66	30	38	31	61	25	30	49	62	335	99	280	52
Y	11	31	4	5	5	5	4	15	9	4	8	6	6	13	13	22	17	31	5
Sr	13	144	18	17	13	21	27	6	6	4	6	3	3	13	8	28	16	26	19
U	6	4	4	4	4	4	4	4	5	4	4	6	6	6	6	6	6	6	4
Th	5	10	4	4	4	4	4	4	4	4	4	5	5	5	5	5	5	6	4
Rb	23	29	8	7	15	12	19	3	2	6	13	6	6	25	31	74	65	142	12
Pb	8	9	5	5	5	5	6	5	5	5	5	8	8	8	8	9	8	13	7

Table 15: The major (wt %) and trace (ppm) element composition of transitional manganese rocks by XRF.

	Mn Transition												
Sample	19	E6	23	9	25	21	7	A5	22	13	11	12	20
SiO2	89.13	80.43	79.78	69.12	65.80	65.03	58.67	53.57	57.48	47.66	41.38	35.96	55.25
TiO2	0.24	0.13	0.20	0.17	0.18	0.19	0.11	0.25	0.17	0.64	1.39	1.08	0.17
Al2O3	1.47	1.57	1.77	3.26	2.30	2.25	2.87	2.51	2.76	8.37	20.79	15.59	2.61
Fe2O3	1.12	1.25	1.99	0.34	2.01	1.46	7.47	14.05	1.92	13.53	3.10	7.91	1.77
MnO	0.03	12.80	8.09	19.74	26.05	22.86	20.22	20.17	27.71	16.87	15.99	22.28	33.13
MgO	0.23	0.15	0.19	0.22	0.25	0.23	0.26	0.15	0.23	0.36	0.58	0.53	0.21
CaO	0.04	0.04	0.03	0.05	0.06	0.06	0.14	0.09	0.06	0.05	0.08	0.32	0.09
Na2O	0.27	0.54	0.10	0.39	0.01	0.37	0.29	0.21	0.32	0.37	0.49	0.39	0.05
K2O	0.31	0.63	0.59	1.38	1.54	1.35	1.37	1.24	1.59	2.27	5.56	4.43	2.16
P2O5	0.03	0.22	0.21	0.44	0.47	0.43	0.96	1.05	0.48	0.97	0.50	0.91	0.96
SO3	0.02	0.02	0.02	0.07	0.04	0.18	0.07	0.01	0.12	0.06	0.06	0.13	0.03
Cr2O3	0.01	0.00	0.01	0.01	0.01	0.01	0.02	0.02	0.01	0.02	0.02	0.02	0.01
NiO	0.00	0.00	0.00	0.00	0.01	0.00	0.01	0.00	0.01	0.01	0.01	0.01	0.01
H2O-	0.88	0.11	1.57	0.16	0.24	0.15	0.35	0.35	0.15	0.36	0.85	0.44	0.97
LOI	6.55	2.49	5.30	4.61	0.74	5.20	6.38	5.83	6.34	7.80	9.12	9.72	2.36
Total	100.34	100.40	99.88	99.97	99.70	99.79	99.17	99.51	99.36	99.34	99.93	99.73	99.77
Mo	8	2	4	7	1	6	14	2	11	7	1	1	1
Nb	5	9	4	17	7	21	16	11	15	41	81	62	8
Zr	65	50	59	133	74	168	137	80	143	765	1 557	1 089	73
Y	8	10	12	38	4	33	20	19	42	88	194	150	4
Sr	78	34	72	123	15	189	246	136	168	254	602	527	18
U	4	6	4	4	4	4	5	6	4	28	13	31	4
Th	4	5	4	5	6	21	11	5	13	31	79	71	4
Rb	33	9	25	73	25	72	66	14	81	183	539	410	7
Pb	14	8	16	60	5	38	15	8	61	48	113	89	8

Table 16: The major (wt %) and trace (ppm) element composition of transitional iron rocks by XRF.

	Fe Transition							
Sample	31	C7	C6	E7	B2	14	B6	10
SiO2	87.25	86.02	85.19	58.10	67.00	47.41	38.94	38.66
TiO2	0.11	0.12	0.54	0.21	0.25	0.68	0.10	0.76
Al2O3	1.09	2.63	1.89	1.41	1.52	8.69	1.99	9.48
Fe2O3	6.90	6.49	8.19	29.50	19.23	20.64	15.45	20.33
MnO	0.48	0.13	0.09	1.79	5.48	10.61	33.78	16.02
MgO	0.15	0.14	0.12	0.19	0.13	0.34	0.11	0.35
CaO	0.02	0.01	0.02	0.14	0.04	0.06	0.09	0.06
Na2O	0.16	0.09	0.05	0.16	0.15	0.07	0.31	0.34
K2O	0.04	0.07	0.06	0.11	0.37	1.94	1.59	2.49
P2O5	0.37	0.26	0.33	1.47	1.26	1.13	1.11	1.33
SO3	0.02	0.02	0.02	0.01	0.02	0.02	0.06	0.14
Cr2O3	0.01	0.01	0.02	0.01	0.01	0.02	0.01	0.01
NiO	0.00	0.00	0.00	0.00	0.00	0.01	0.01	0.01
H2O-	0.71	0.06	0.07	0.80	0.30	0.80	0.48	0.54
LOI	2.77	3.21	2.63	5.66	4.17	7.20	6.23	9.25
Total	100.08	99.27	99.22	99.56	99.92	99.62	100.26	99.78
Mo	1	2	2	2	2	2	8	1
Nb	17	7	18	10	10	21	9	48
Zr	329	46	112	252	48	304	36	920
Y	28	9	21	8	5	36	9	106
Sr	65	19	46	43	22	90	84	304
U	4	6	6	6	6	12	9	47
Th	12	5	12	5	8	4	5	41
Rb	72	2	2	2	6	61	28	212
Pb	22	12	12	8	8	5	8	62

Table 17: The major (wt %) and trace (ppm) element composition of manganese and iron rich rocks by XRF.

	Mn Rich Rocks								Fe Rich Rocks					
Sample	B4	8	A4	A6	C5	E3	E5	E8	6	15	C2	E2	B3	E4
SiO2	54.76	51.62	42.76	41.36	1.12	1.84	0.28	7.44	59.28	53.85	12.11	15.55	11.56	8.37
TiO2	0.21	0.20	0.24	0.09	0.04	0.05	0.05	0.33	0.12	0.16	0.08	1.37	1.82	0.84
Al2O3	2.90	4.71	2.23	1.54	1.93	2.58	1.84	4.96	2.51	2.38	1.34	14.88	12.18	9.47
Fe2O3	1.72	0.70	5.36	3.00	25.60	0.51	0.20	29.08	28.93	33.49	77.24	55.71	67.98	62.97
MnO	31.12	30.56	38.95	44.16	61.52	82.20	86.40	48.66	0.80	0.47	0.59	2.53	1.20	10.09
MgO	0.16	0.25	0.14	0.13	0.14	0.13	0.12	0.22	0.21	0.27	0.13	0.19	0.16	0.18
CaO	0.06	0.09	0.13	0.10	0.15	0.14	0.13	0.10	0.18	0.22	0.06	0.06	0.04	0.06
Na2O	0.48	0.02	0.25	0.30	0.47	0.42	0.27	0.72	0.25	0.33	0.13	0.38	0.16	0.15
K2O	1.71	1.88	2.16	2.22	2.47	4.62	4.72	2.67	0.20	0.20	0.02	0.11	0.05	0.45
P2O5	0.32	0.73	0.75	0.65	1.82	1.01	1.06	1.61	1.35	1.89	3.15	2.58	0.93	1.06
SO3	0.03	0.03	0.01	0.01	0.04	0.06	0.04	0.11	0.07	0.14	0.01	0.04	0.02	0.06
Cr2O3	0.01	0.03	0.01	0.01	0.00	0.01	0.01	0.01	0.01	0.01	0.01	0.04	0.02	0.03
NiO	0.01	0.06	0.00	0.00	0.01	0.01	0.00	0.00	0.01	0.01	0.01	0.00	0.00	0.01
H2O-	0.68	0.94	0.29	0.19	0.62	0.31	0.18	0.67	0.24	0.21	0.73	1.60	1.57	1.05
LOI	5.74	7.30	6.61	6.46	4.29	6.11	4.59	4.04	5.69	6.14	4.07	4.23	1.79	4.57
Total	99.91	99.14	99.89	100.22	100.23	99.99	99.89	100.64	99.85	99.79	99.69	99.28	99.48	99.34
Mo	5	16	22	29	72	10	12	15	3	1	2	2	2	6
Nb	9	4	12	7	7	8	10	14	13	16	8	17	25	13
Zr	73	90	114	34	2	5	2	218	124	151	1	92	218	69
Y	18	16	22	9	10	16	14	30	29	27	4	7	8	14
Sr	67	71	162	77	98	56	58	146	75	130	6	22	50	47
U	6	4	6	6	17	7	6	13	15	8	6	6	36	6
Th	5	4	5	5	5	5	5	6	5	4	5	5	20	5
Rb	30	31	42	41	50	96	101	64	10	16	2	2	2	3
Pb	8	49	46	8	8	8	8	8	6	10	10	8	8	8

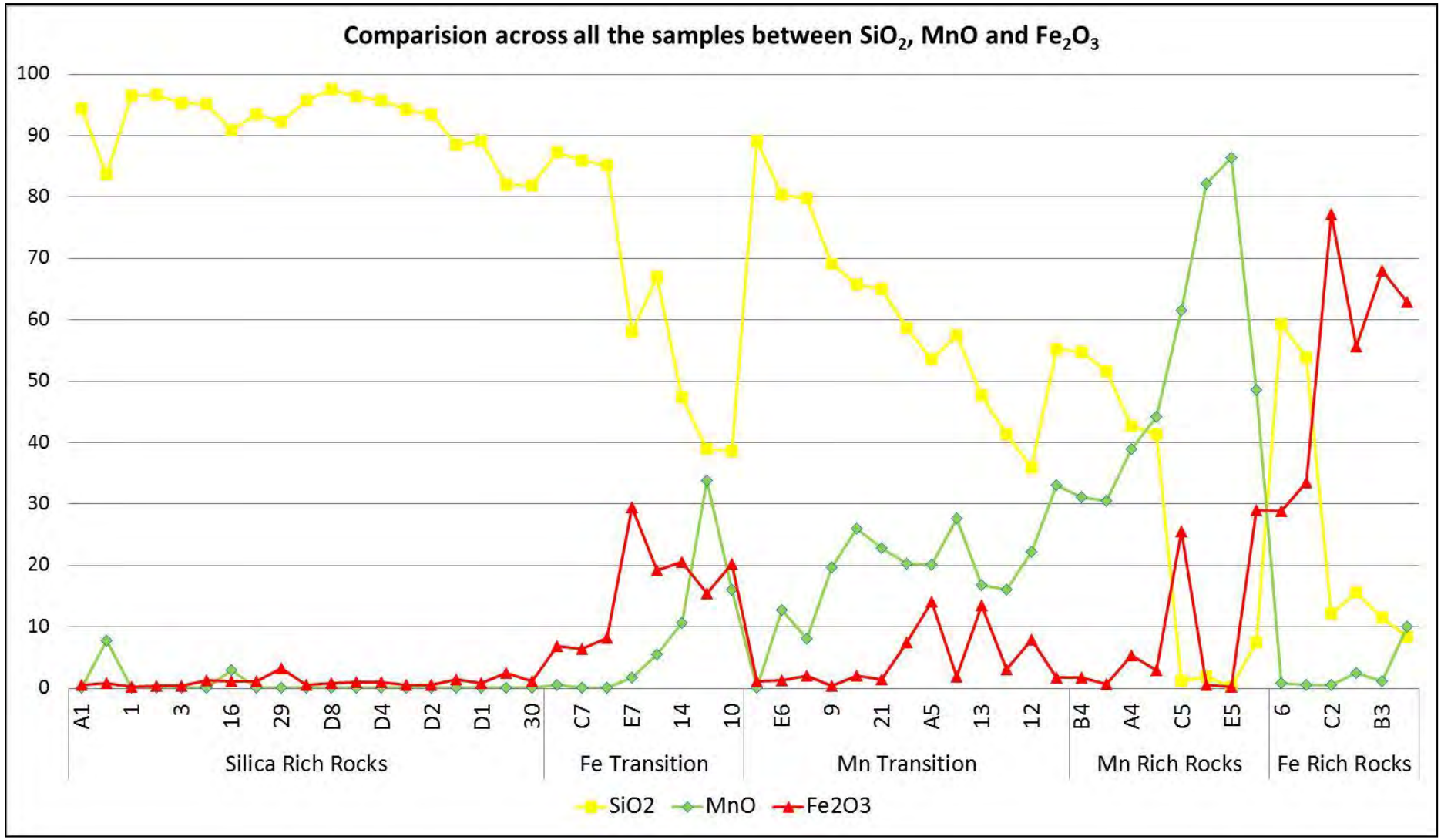

Figure 34: Variations in silica, iron and manganese content across all rock types.

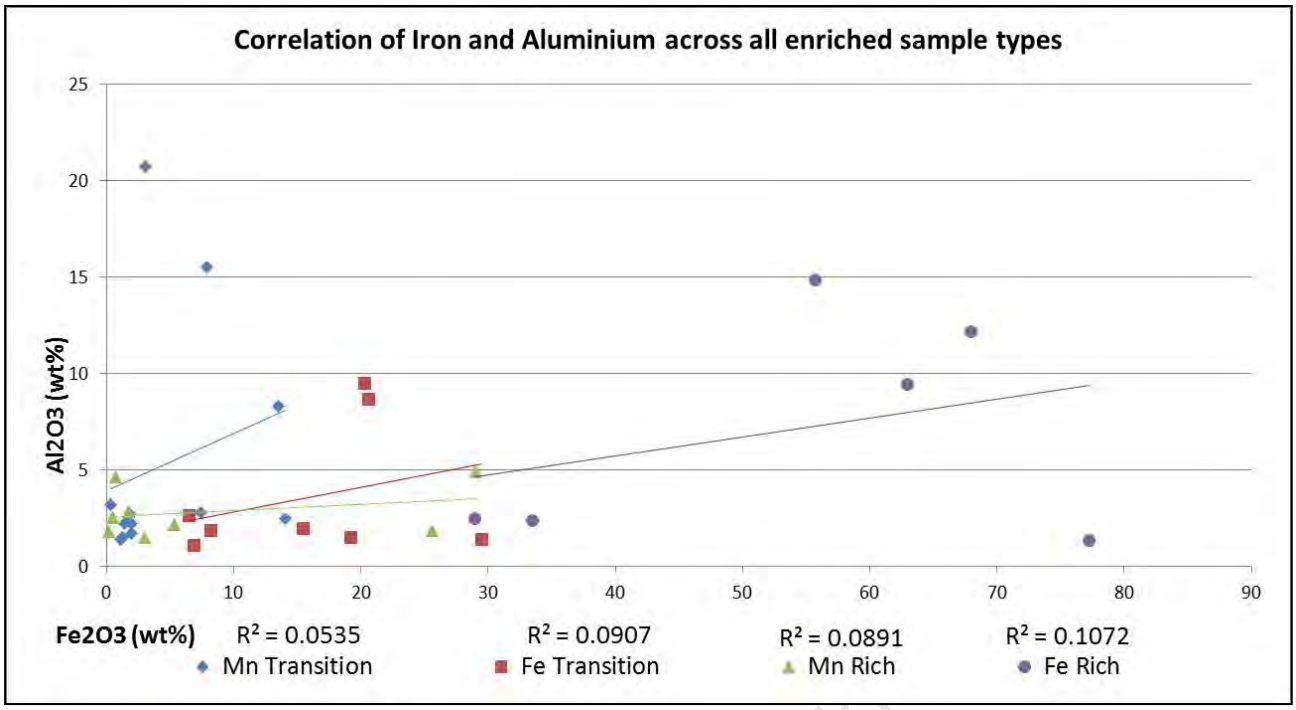

Figure 35: Correlation between aluminium and iron across all enriched rock types.

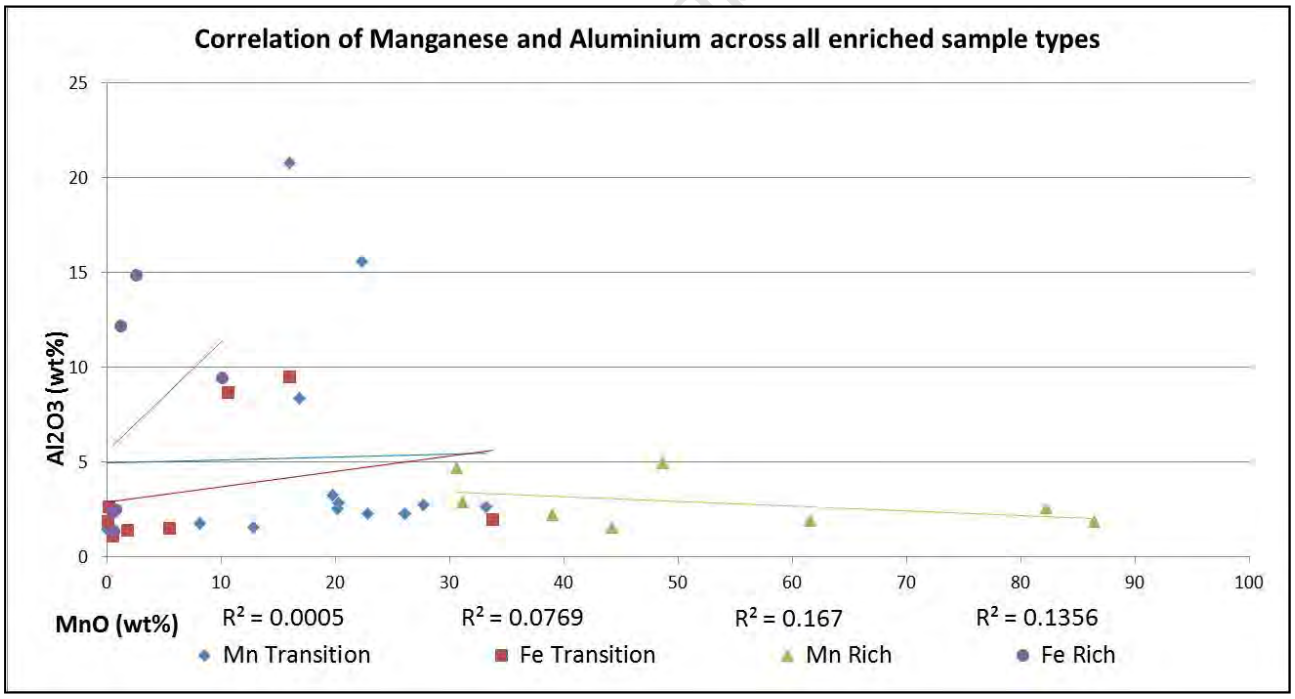

Figure 36: Correlation between aluminium and manganese across all enriched rock types.

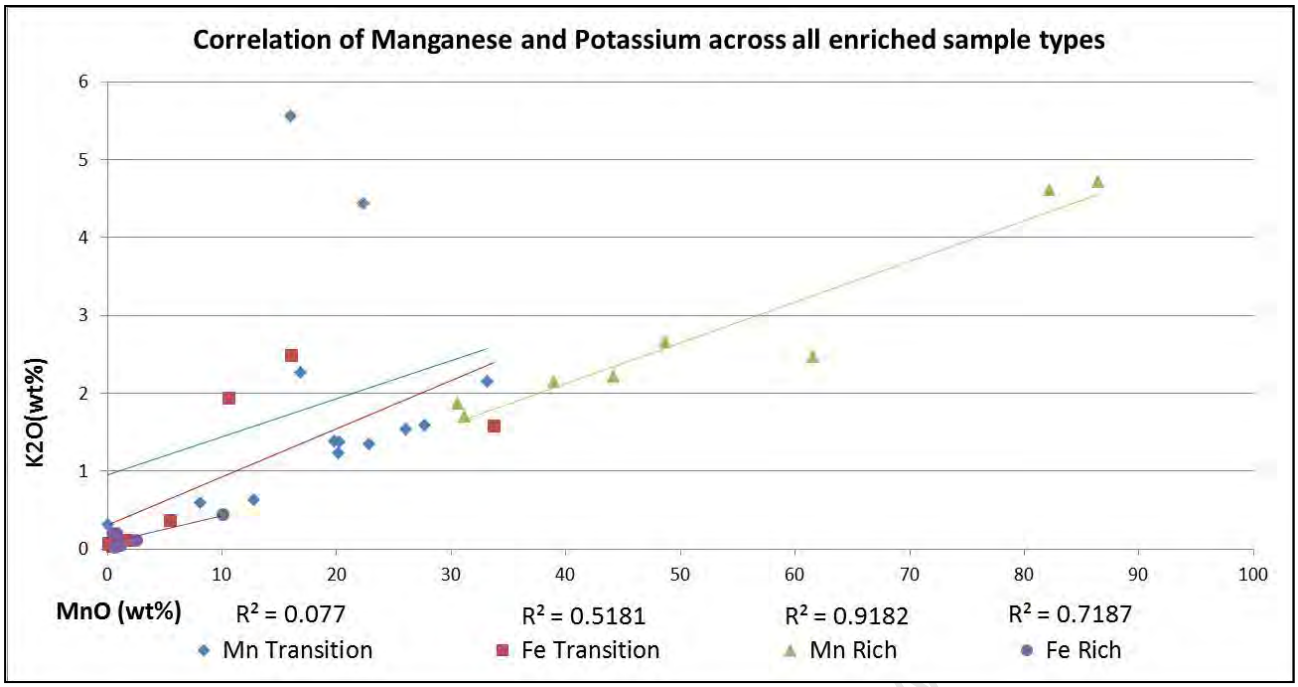

Figure 37: Correlation between manganese and potassium across all enriched rock types.

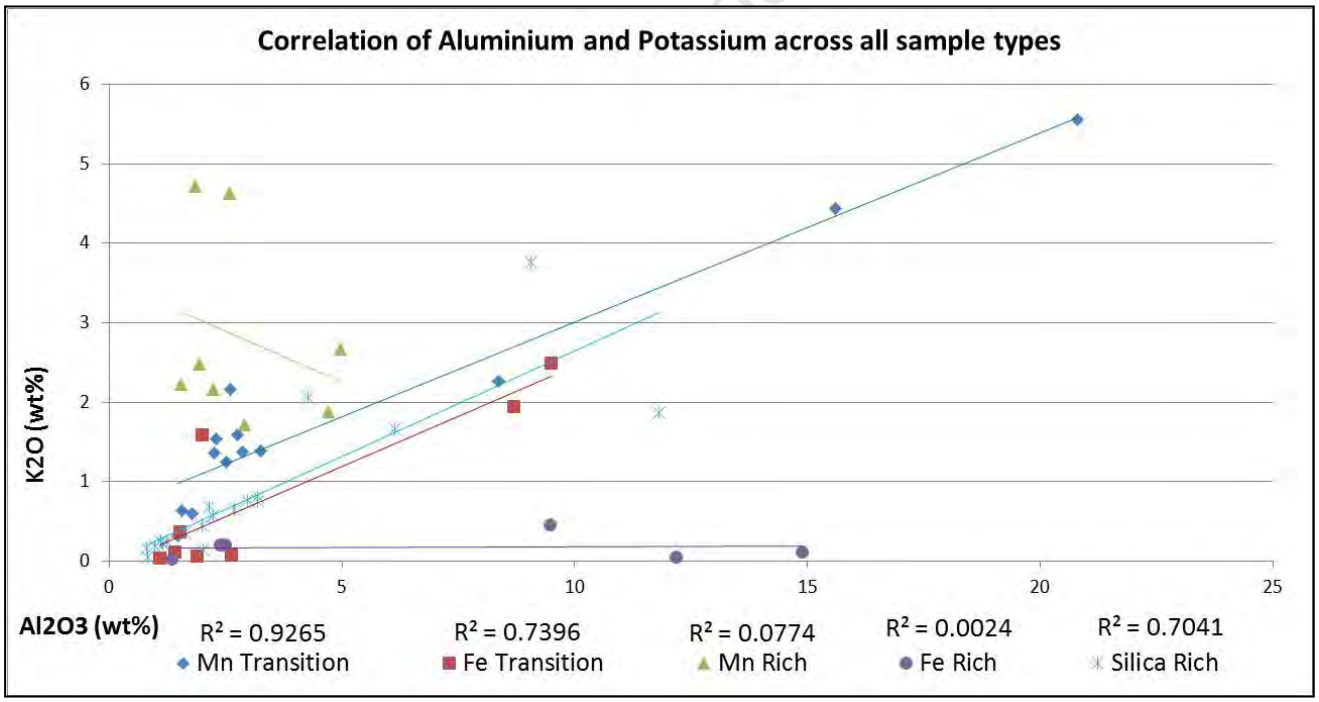

Figure 38: Correlation between potassium and aluminium across all rock types.

3.2.2 X-Ray Diffraction Results

Post the XRF results, three samples (A4, B6 and E6) were analysed by XRD to determine the mineralogy of these manganese rich rocks. The quartz was used as an internal standard from which to compare peaks of the XRD profile (Fleischer and Hewett, 1960). From the combined knowledge of the bulk mineral chemistry (XRF data) and the correlations of the various elements to the manganese, and the probable type of deposit (Type 1) it was possible to narrow down the possible manganese minerals. The studies done by Fleischer and Hewett (1960) and Nicholson (1992) were used to establish if any manganese minerals fit the chemical signature, the depositional environment, and the XRD profile. From the chemical data it was established that manganese and potassium content correlate (R^2 = 0.92 in Mn rich rocks, Figure 37). The XRD profiles confirm that the manganese rich samples contain the minerals quartz and cryptomelane (KMn_8O_{16}) (Figure 39). Other common manganese minerals were also tested against the scans to ensure that other minerals weren't present, and none of them correlated with the peaks in the profile. The remaining relatively minor peaks are probably related to unidentified iron and aluminium minerals present. In the other XRD scans done (**Appendix C**) the same mineral composition was noticed.

If the molar mass of manganese and potassium in KMn_8O_{16} is taken into account then the molar ratio of manganese to potassium in cryptomelane is 8:1 while the slope of the line in Figure 51 (in moles Mn:K) is 11.76. Thus there is insufficient potassium to supply all the required potassium to form pure KMn_8O_{16}. It is important to note that the psilomelane minerals, cryptomelane, hollandite and coronadite, are isostructural and can form isomorphous structures (Gruner, 1943) within the formula

$$Mn^{4+}_{8-(x/2+y/4+z/2)}\,(Mn^{2+}/R^{2+})_x\,(K,Na)_y\,(Ba,Pb)_z\,O_{16}\cdot(H_2O)_{2-(y+z)}$$

where R^2 represents Cu, Co, Zn, Al and Fe. While hollandite (barium variation) and coronadite (lead variation) have very similar XRD profiles to cryptomelane (potassium variation), it is the strong correlation of potassium to the manganese coupled with the XRD profile which suggests that cryptomelane is the main mineral occurring within these manganese deposits. It is possible that coronadite and hollandite also occur along with cryptomelane, but in very small quantities.

The average chemical formula for cryptomelane samples analysed by Gruner (1943) is:

$$Mn^{4+}_{7.42}(Mn^{2+},R^{2+})_{0.81}(K,Na)_{0.70}Ba_{0.02}O_{16}\cdot(H_2O)_{1.31}$$

This shows that while there may be insufficient potassium to account for all the manganese being precipitated out, the inclusion of minor amounts of sodium, barium and other elements (as represented by R) will make up for the lack of potassium and still allow for the formation of the mineral cryptomelane.

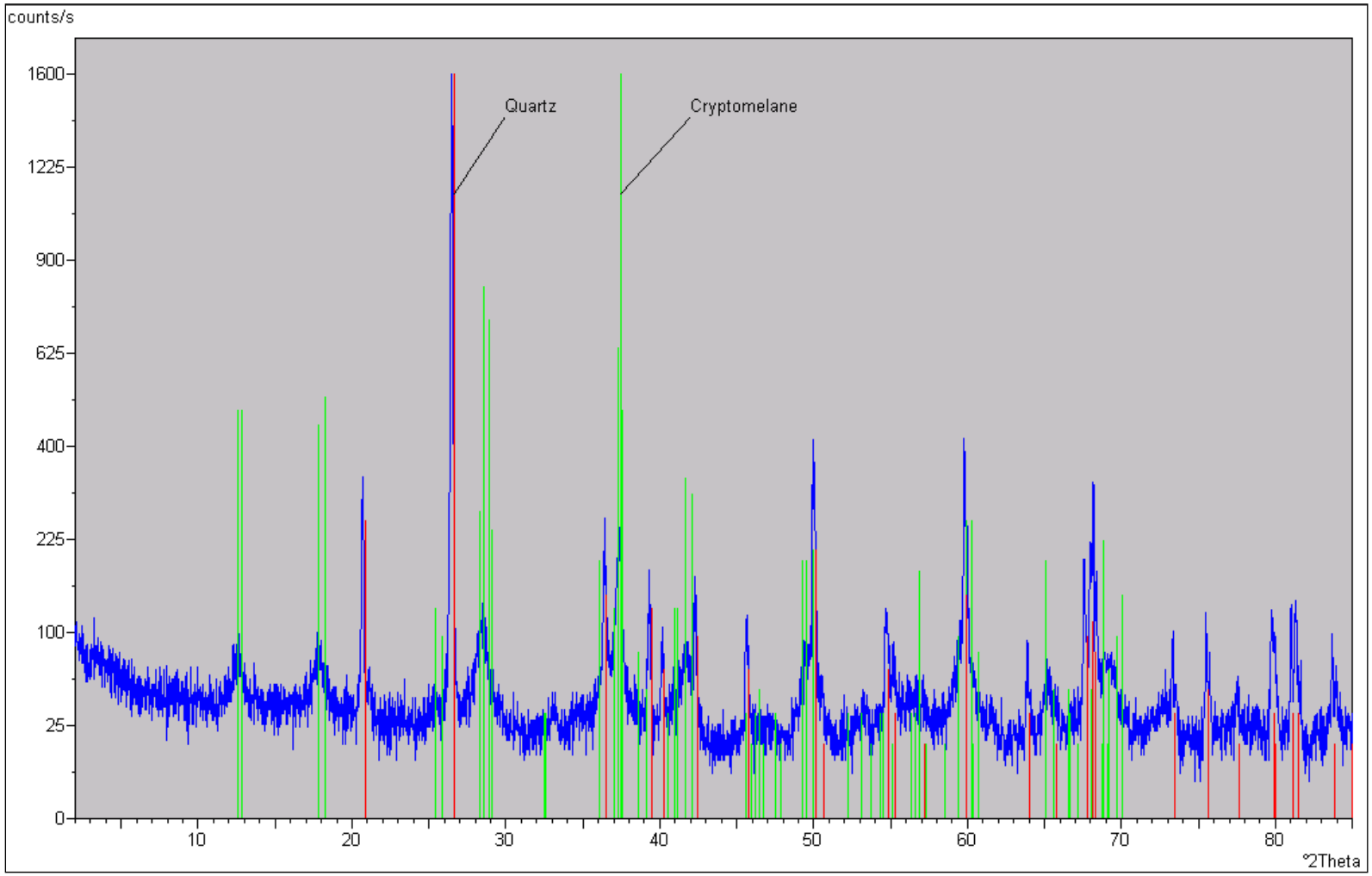

Figure 39: The XRD profile (blue line) of sample B6 from Rooi Els. The peaks associated with green spikes are attributed to cryptomelane and peaks associated with the red spikes to quartz.

3.2.3 Inductively Coupled Plasma Mass Spectrophotometer Results

The ICP-MS results are shown below for unmineralised samples (Table 18), transitional manganese and transitional iron (Table 19), as well as manganese and iron rich rocks (Table 20). The results are ordered by decreasing silica content. For evaluation purposes the ICP-MS results were normalised to Post Archean Australian Shale (PAAS) (McLennan and Taylor, 1985) because the TMG rocks are early Palaeozoic in age and sedimentary in origin. Figure 40 shows the average REE pattern relative to PAAS for all the rock samples analysed based on sample type and Figure 41 shows the average REE pattern relative to PAAS based on sample locality. Due to low concentrations of REE being present in the water samples only some of the elements were within the detection limit in all the samples, Table 21 shows the raw ICP-MS results for the water samples.

Table 18: ICP-MS results for the unmineralised samples (ppm).

	Unmineralised Samples													
	A1	1	2	3	5	29	30	D3	D4	B1	D2	D9	D1	D10
Sc	0.7	<1.5	<1.5	<1.5	0.2	<1.5	8.3	0.1	0.2	0.4	0.6	2.2	2.2	4.1
V	9.0	8.6	10.1	10.1	12.9	8.1	48.0	5.1	5.0	6.9	9.8	12.9	14.2	27.5
Cr	7.5	8.7	14.0	12.3	15.2	10.8	47.2	10.5	10.9	6.4	6.8	11.3	11.0	19.9
Co	0.3	0.3	0.4	0.4	3.3	5.1	1.0	0.7	0.7	0.3	0.6	2.9	1.1	4.2
Ni	3.3	2.6	4.0	4.2	6.8	9.6	5.6	4.1	4.0	2.1	2.7	6.3	4.1	9.2
Cu	5.9	2.0	1.8	2.1	5.6	7.9	4.8	6.2	5.4	5.6	6.4	9.6	9.1	8.1
Rb	18.5	6.9	6.5	13.6	11.2	0.7	64.8	7.4	5.9	12.2	25.3	67.2	61.8	107.1
Sr	10.8	16.8	17.3	12.8	21.2	7.7	61.7	4.4	4.0	6.6	6.4	26.4	16.1	23.9
Y	5.6	3.1	3.9	3.8	4.8	7.8	20.9	4.4	4.9	3.6	6.1	13.5	8.2	15.7
Zr	13.8	22.6	23.8	16.1	17.3	16.6	106.5	15.7	14.2	14.6	22.5	101.0	35.7	84.8
Nb	1.3	2.2	3.5	1.6	2.4	1.1	13.3	1.1	1.5	1.0	1.9	5.5	3.4	8.0
Cs	0.3	0.1	0.1	0.2	0.2	0.1	2.0	0.2	0.1	0.2	0.8	2.0	2.6	5.1
Ba	51.2	37.3	67.7	63.5	56.8	30.8	285.0	27.8	21.7	39.3	71.4	243.0	159.3	367.6
La	6.9	9.4	9.6	9.4	10.3	8.8	36.9	7.1	9.3	5.8	7.9	11.3	16.0	23.9
Ce	15.9	22.0	22.5	20.7	23.3	19.5	80.3	16.1	21.0	12.3	18.3	25.7	37.3	51.8
Pr	1.6	2.3	2.4	2.2	2.4	2.0	9.0	1.8	2.3	1.4	2.2	3.5	4.5	6.0
Nd	6.5	9.0	9.2	8.3	9.3	7.7	35.0	7.1	8.9	5.3	8.8	15.6	18.6	22.0
Sm	1.2	1.7	1.8	1.5	1.8	1.5	6.8	1.3	1.6	1.0	1.7	3.9	3.6	4.0
Eu	0.3	0.3	0.3	0.3	0.3	0.2	1.2	0.2	0.3	0.2	0.3	0.8	0.7	0.8
Gd	1.2	1.3	1.3	1.1	1.4	1.3	5.5	1.2	1.3	0.9	1.5	3.7	2.9	3.4
Tb	0.2	0.1	0.2	0.1	0.2	0.2	0.7	0.2	0.2	0.1	0.2	0.6	0.4	0.5
Dy	1.1	0.7	0.9	0.8	0.9	1.3	4.4	1.0	1.1	0.7	1.4	3.1	2.1	3.0
Ho	0.2	0.1	0.2	0.1	0.2	0.3	0.8	0.2	0.2	0.1	0.3	0.6	0.4	0.6
Er	0.6	0.4	0.5	0.4	0.5	0.7	2.2	0.5	0.5	0.4	0.7	1.6	1.0	1.7
Tm	0.1	0.1	0.1	0.1	0.1	0.1	0.3	0.1	0.1	0.1	0.1	0.2	0.1	0.3
Yb	0.5	0.4	0.5	0.4	0.6	0.6	2.1	0.5	0.6	0.4	0.6	1.5	0.8	1.7
Lu	0.1	0.1	0.1	0.1	0.1	0.1	0.3	0.1	0.1	0.1	0.1	0.2	0.1	0.3
Hf	0.4	0.7	0.8	0.5	0.5	0.6	3.2	0.5	0.4	0.4	0.7	3.0	1.1	2.2
Ta	n.d.	0.2	0.3	0.1	0.2	0.1	1.0	n.d.	n.d.	n.d.	n.d.	n.d.	0.0	0.6
Pb	2.1	3.9	4.1	3.3	3.9	4.3	17.3	3.7	3.9	1.5	4.3	14.7	8.4	15.5
Th	1.8	3.5	4.6	2.5	3.1	2.8	12.6	1.7	2.5	1.5	2.6	8.8	4.3	7.7
U	0.8	0.5	0.5	0.4	2.3	5.8	3.1	0.5	0.5	0.4	1.1	1.5	1.3	1.6

Table 19: ICP-MS results for the iron and manganese transition samples (ppm).

	Fe Transition						Mn Transition		
	31	**C7**	**C6**	**E7**	**B2**	**B6**	**E6**	**25**	**A5**
Sc	<1.5	1.3	1.6	2.3	0.3	3.6	1.2	0.3	1.0
V	8.6	14.2	16.8	14.6	6.9	64.6	4.0	18.2	10.7
Cr	14.4	18.5	23.0	9.8	7.0	8.3	5.5	13.5	36.7
Co	0.7	3.1	1.9	13.2	7.1	5.6	10.2	0.7	5.5
Ni	4.8	3.8	5.7	8.3	5.4	15.5	6.8	4.4	18.8
Cu	3.4	6.2	8.1	15.1	4.6	24.1	8.7	2.9	14.2
Rb	4.1	2.3	2.2	1.1	5.3	13.5	6.6	22.5	10.5
Sr	20.1	20.2	48.9	45.1	23.4	48.8	34.6	15.3	51.1
Y	5.2	6.1	13.1	6.6	4.5	5.8	8.5	4.9	10.9
Zr	36.2	25.6	59.4	49.3	28.9	12.5	25.7	26.4	19.7
Nb	2.0	2.0	12.3	3.9	5.5	1.0	1.3	4.0	4.3
Cs	0.1	0.1	0.1	0.1	0.4	0.4	0.6	0.3	0.3
Ba	23.4	20.2	25.3	216.3	29.5	152.2	42.7	67.3	435.6
La	10.8	13.5	37.4	2.5	19.6	5.8	16.4	13.3	13.5
Ce	24.4	28.9	79.3	6.0	41.5	12.8	33.1	28.7	31.0
Pr	2.6	3.1	8.9	0.7	4.5	1.4	3.5	2.8	3.2
Nd	10.5	11.0	30.4	2.5	15.3	4.8	12.7	10.2	12.1
Sm	2.1	1.9	5.2	0.5	2.6	0.9	2.3	1.5	2.2
Eu	0.4	0.3	0.8	0.1	0.4	0.2	0.4	0.3	0.4
Tb	1.7	1.5	3.7	0.6	1.5	0.8	1.8	1.1	2.0
Gd	0.2	0.2	0.5	0.1	0.2	0.1	0.3	0.1	0.3
Dy	1.2	1.1	2.7	0.8	0.9	0.9	1.6	0.9	1.8
Ho	0.2	0.2	0.5	0.2	0.2	0.2	0.3	0.2	0.4
Er	0.6	0.7	1.4	0.7	0.4	0.6	0.9	0.5	1.2
Tm	0.1	0.1	0.2	0.1	0.1	0.1	0.1	0.1	0.2
Yb	0.6	0.8	1.4	0.9	0.5	0.7	0.9	0.6	1.4
Lu	0.1	0.1	0.2	0.1	0.1	0.1	0.1	0.1	0.2
Hf	1.2	0.7	1.6	1.2	0.9	0.3	0.7	0.9	0.6
Ta	0.2	0.1	1.1	0.2	0.4	0.1	0.0	0.3	0.0
Pb	8.3	16.8	16.8	1.7	3.7	4.2	1.3	4.4	2.5
Th	3.2	4.3	15.3	0.9	7.3	2.1	3.9	4.9	4.3
U	0.9	1.9	2.9	2.8	2.3	11.5	2.2	1.5	5.2

Table 20: ICP-MS results for manganese and iron rich samples (ppm).

	Mn Rich Rocks							Fe Rich Rocks			
	B4	**A4**	**A6**	**C5**	**E3**	**E5**	**E8**	**C2**	**E2**	**B3**	**E4**
Sc	1.0	1.2	0.4	0.5	7.9	9.0	3.2	0.6	32.4	80.6	46.3
V	6.5	10.0	4.6	12.5	1.5	1.4	29.3	10.3	206.0	326.9	149.9
Cr	7.7	7.7	14.4	5.2	0.4	0.4	8.6	8.7	174.0	68.6	118.5
Co	54.4	7.6	4.9	8.0	32.7	29.9	19.7	18.7	23.3	5.6	58.0
Ni	39.8	6.5	5.0	18.2	5.2	3.9	10.0	63.2	27.4	6.1	105.0
Cu	22.8	13.3	7.0	15.3	23.7	17.2	15.0	52.0	77.0	80.3	95.2
Rb	19.2	18.6	11.0	17.5	29.1	30.0	32.0	0.5	0.7	0.9	4.5
Sr	55.3	77.7	26.3	40.5	27.8	21.0	87.7	6.6	21.3	47.0	38.7
Y	11.4	12.1	3.6	5.4	5.9	4.1	15.2	4.0	8.4	7.4	10.8
Zr	28.2	26.1	12.5	3.1	10.2	1.6	64.4	5.4	91.3	206.2	62.3
Nb	5.5	4.9	0.5	0.0	n.d.	n.d.	3.5	0.7	8.9	17.4	4.6
Cs	1.1	0.6	0.3	0.6	1.1	0.9	0.9	0.0	0.4	0.0	0.7
Ba	50.4	440.6	29.4	38.5	58.3	97.6	120.9	123.6	159.5	116.8	195.4
La	15.6	13.4	7.4	0.4	1.7	1.2	23.0	2.6	5.4	24.2	6.8
Ce	34.8	31.6	15.9	1.2	12.5	7.5	50.7	6.7	23.6	49.1	23.4
Pr	3.9	3.4	1.8	0.1	0.8	0.6	6.1	0.7	1.7	5.4	1.9
Nd	15.8	14.4	6.9	0.4	3.2	2.6	22.5	2.4	6.9	18.1	7.2
Sm	3.4	3.6	1.3	0.1	0.8	0.7	4.4	0.5	1.9	3.6	1.8
Eu	0.7	0.8	0.2	0.0	0.2	0.1	0.8	0.1	0.6	1.0	0.5
Tb	2.8	3.9	0.9	0.4	0.7	0.5	3.2	0.5	2.1	2.6	1.9
Gd	0.4	0.6	0.1	0.1	0.1	0.1	0.5	0.1	0.4	0.4	0.4
Dy	2.0	3.1	0.8	0.6	0.7	0.6	3.0	0.6	2.5	2.2	2.5
Ho	0.4	0.5	0.2	0.2	0.2	0.1	0.7	0.1	0.5	0.4	0.6
Er	1.5	1.4	0.4	0.5	0.5	0.4	1.9	0.4	1.5	1.0	1.7
Tm	0.2	0.2	0.1	0.1	0.1	0.1	0.3	0.1	0.2	0.2	0.3
Yb	1.8	1.3	0.4	0.6	0.6	0.5	2.1	0.4	1.7	1.1	2.0
Lu	0.3	0.2	0.1	0.1	0.1	0.1	0.3	0.1	0.2	0.2	0.3
Hf	0.8	0.8	0.4	0.1	0.3	0.0	1.8	0.1	2.2	5.8	1.5
Ta	n.d.	0.0	n.d.	n.d.	n.d.	n.d.	0.1	0.2	0.5	1.1	0.2
Pb	2.4	16.3	1.3	2.4	0.2	0.2	4.4	8.7	2.2	14.0	1.9
Th	7.7	4.9	1.3	0.2	1.7	0.1	6.4	1.2	1.0	21.2	1.8
U	3.7	3.8	1.4	18.1	1.9	1.2	11.4	3.3	0.6	35.6	9.6

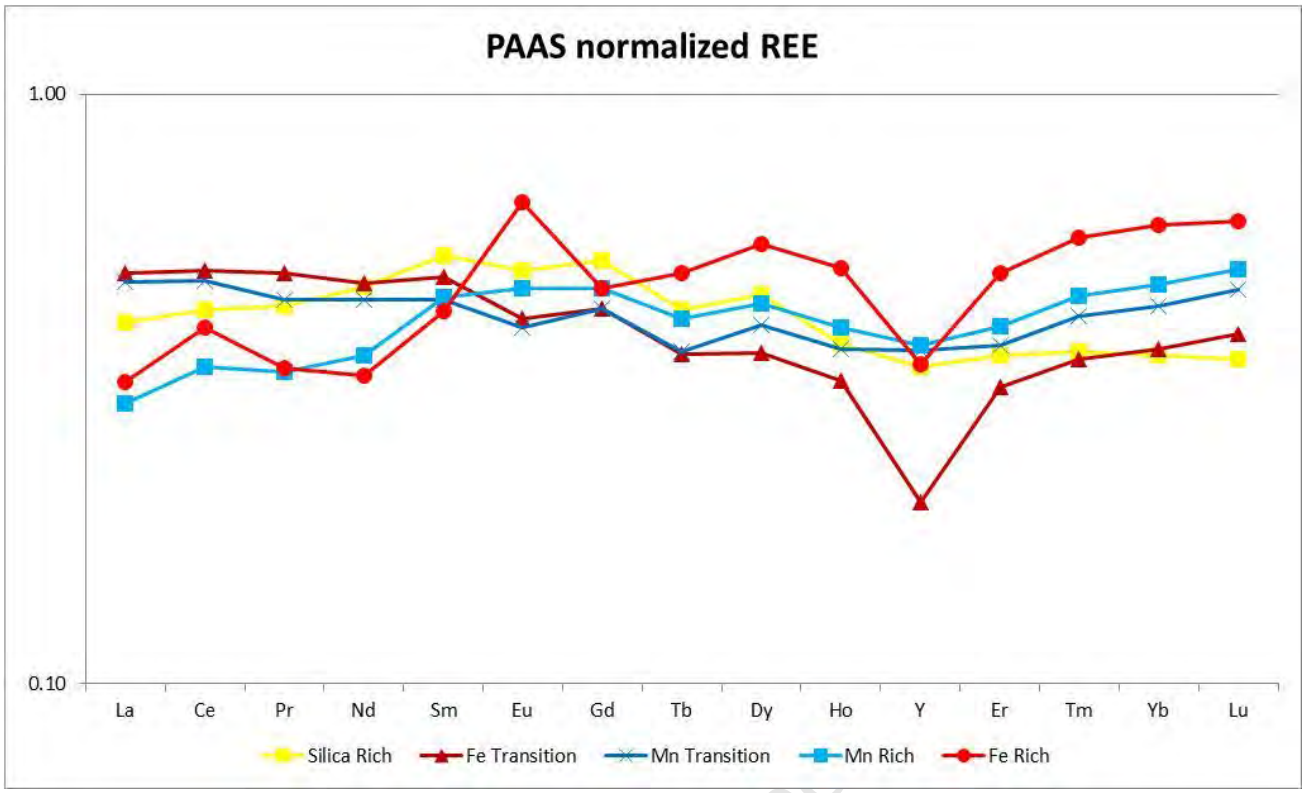

Figure 40: Average REE profiles normalised to PAAS for each sample type.

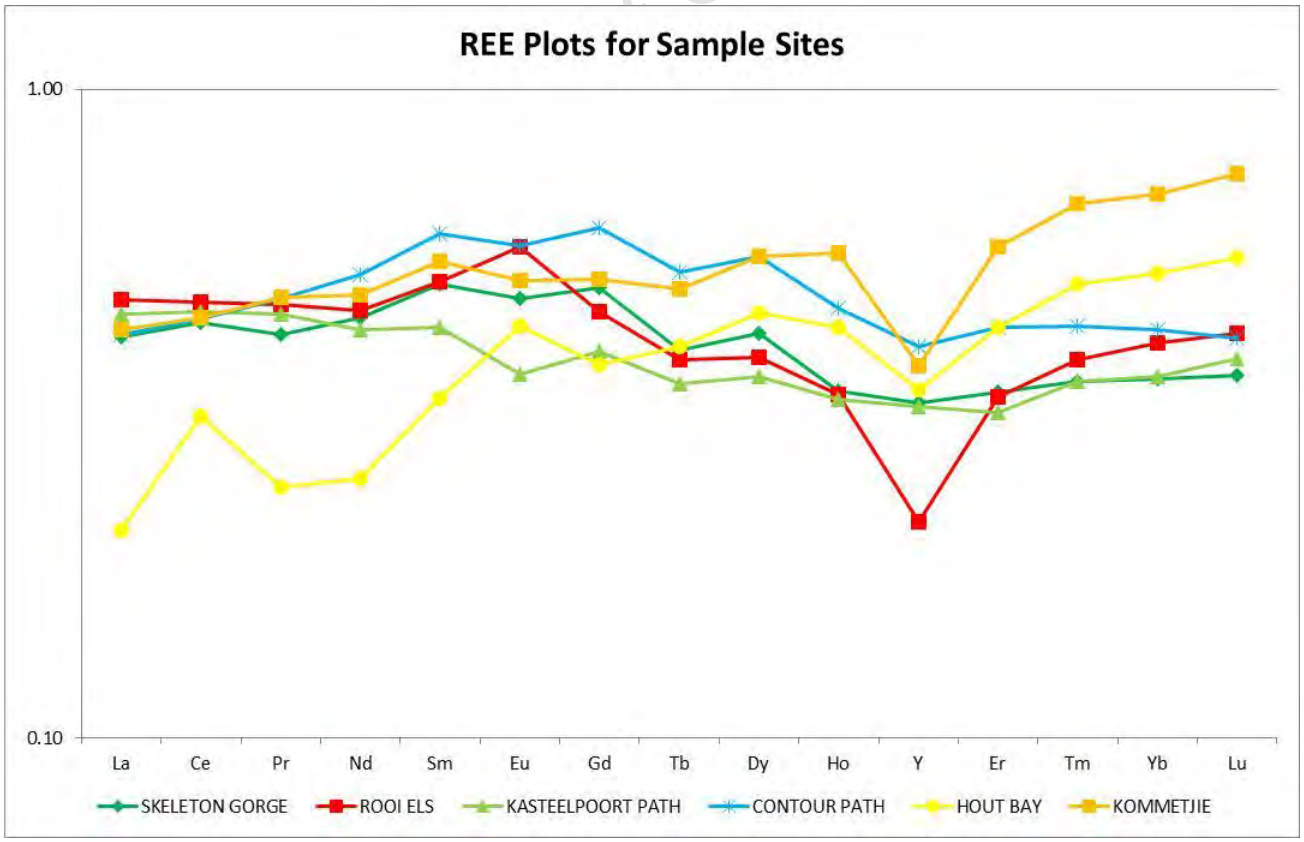

Figure 41: Average REE profiles normalised to PAAS for each sample locality.

Table 21: ICP-MS results for the water samples (ppm), nd = not detected.

	1	2a	2b	3a	3b	4a	4b	5a	5b	6
Li	1.6	0.3	0.3	1.2	1.1	1.4	1.4	1.7	1.6	1.7
Be	0.5	0.0	0.1	0.0	*n.d.*	*n.d.*	0.1	0.0	*n.d.*	0.2
Al	144.9	215.1	214.3	170.8	129.3	30.3	157.7	106.0	90.4	88.9
Sc	0.6	*n.d.*	*n.d.*	*n.d.*	*n.d.*	0.3	0.0	0.1	*n.d.*	0.1
Ti	2.8	6.4	6.6	7.1	6.3	2.4	3.5	3.1	3.3	4.7
V	0.9	0.7	0.6	0.8	0.4	0.2	0.8	0.3	0.2	0.6
Cr	7.3	*n.d.*	0.2	*n.d.*	*n.d.*	0.5	*n.d.*	*n.d.*	*n.d.*	1.3
Mn	40.9	3.1	2.6	40.4	41.8	83.3	1 005.8	68.9	173.5	31.1
Fe	469.4	77.6	129.0	159.0	101.8	636.9	4 648.8	286.1	70.3	274.4
Co	0.5	0.1	0.1	0.2	0.1	0.5	7.2	0.2	0.3	0.3
Ni	5.9	0.4	0.2	0.4	0.4	0.6	3.2	0.5	0.2	0.4
Cu	5.6	0.0	*n.d.*	0.4	0.3	0.4	2.3	2.3	0.8	0.4
Zn	18.3	5.2	2.6	6.7	6.8	9.0	11.4	3.9	3.2	5.4
Ga	0.2	0.1	0.1	0.2	0.1	0.0	0.2	0.2	0.1	0.8
As	0.5	0.3	0.3	0.2	0.2	0.4	0.9	0.2	0.1	0.7
Se	2.7	1.2	0.8	2.6	0.1	1.7	1.5	1.5	3.4	2.8
Rb	1.3	0.4	0.5	0.4	0.3	0.6	0.5	0.2	0.2	3.4
Sr	18.4	12.1	12.2	15.3	12.7	6.4	11.9	15.6	14.2	29.5
Y	0.2	0.1	0.1	0.1	0.1	0.1	0.8	0.1	0.0	0.2
Zr	0.6	0.8	0.5	0.2	1.1	0.3	0.6	0.6	0.2	0.3
Nb	0.2	0.1	0.1	0.0	0.0	*n.d.*	*n.d.*	*n.d.*	*n.d.*	*n.d.*
Mo	0.2	0.1	0.1	0.0	0.0	0.0	*n.d.*	0.0	*n.d.*	0.1
Ru	*n.d.*	*n.d.*	*n.d.*	*n.d.*	*n.d.*	*n.d.*	*n.d.*	*n.d.*	*n.d.*	*n.d.*
Rh	0.0	0.0	0.0	*n.d.*	*n.d.*	*n.d.*	*n.d.*	*n.d.*	*n.d.*	*n.d.*
Pd	0.0	0.0	0.0	0.0	0.0	0.0	0.0	0.0	*n.d.*	*n.d.*
Ag	0.2	0.1	0.1	0.1	0.1	0.1	0.1	0.0	0.1	0.0
Cd	0.1	0.0	*n.d.*	0.0	0.0	0.0	0.1	*n.d.*	0.0	0.0
Cs	0.1	*n.d.*	0.0	0.0	0.0	0.1	0.1	0.0	*n.d.*	0.1
Ba	4.2	1.3	1.4	2.4	2.2	1.2	5.1	3.2	2.3	16.9
La	0.1	0.1	0.1	0.1	0.1	0.0	0.1	0.1	0.0	0.1
Ce	0.3	0.3	0.3	0.2	0.2	0.1	0.2	0.1	0.1	0.2
Pr	0.0	0.0	0.0	0.1	0.0	0.0	0.1	0.1	0.0	0.0
Nd	0.1	0.1	0.1	0.1	0.1	0.0	0.1	0.1	0.0	0.1
Sm	0.0	0.0	0.0	*n.d.*	0.0	*n.d.*	0.0	*n.d.*	*n.d.*	0.0
Eu	*n.d.*	*n.d.*	*n.d.*	*n.d.*	*n.d.*	*n.d.*	*n.d.*	*n.d.*	*n.d.*	*n.d.*
Gd	0.0	*n.d.*	0.0	0.0	*n.d.*	*n.d.*	0.0	*n.d.*	*n.d.*	*n.d.*
Tb	*n.d.*	*n.d.*	*n.d.*	*n.d.*	*n.d.*	*n.d.*	*n.d.*	*n.d.*	*n.d.*	*n.d.*
Dy	0.0	0.0	*n.d.*	0.0	*n.d.*	*n.d.*	0.1	*n.d.*	*n.d.*	0.0
Ho	*n.d.*	*n.d.*	*n.d.*	*n.d.*	*n.d.*	*n.d.*	0.0	*n.d.*	*n.d.*	*n.d.*
Er	0.0	*n.d.*	*n.d.*	*n.d.*	*n.d.*	0.0	0.1	*n.d.*	*n.d.*	0.0
Tm	*n.d.*	*n.d.*	*n.d.*	*n.d.*	*n.d.*	*n.d.*	0.0	*n.d.*	*n.d.*	*n.d.*
Yb	0.0	*n.d.*	*n.d.*	*n.d.*	*n.d.*	0.0	0.1	0.0	*n.d.*	0.0
Lu	*n.d.*	*n.d.*	*n.d.*	*n.d.*	*n.d.*	*n.d.*	0.0	*n.d.*	*n.d.*	*n.d.*
Hf	0.0	0.0	0.0	*n.d.*	0.0	*n.d.*	*n.d.*	0.0	*n.d.*	*n.d.*
Ta	0.1	0.0	0.0	0.0	*n.d.*	*n.d.*	*n.d.*	*n.d.*	*n.d.*	*n.d.*
W	0.5	0.3	0.2	0.1	0.1	0.1	0.0	0.0	*n.d.*	0.1
Re	*n.d.*	*n.d.*	*n.d.*	*n.d.*	*n.d.*	*n.d.*	*n.d.*	*n.d.*	*n.d.*	*n.d.*
Ir	*n.d.*	*n.d.*	*n.d.*	*n.d.*	*n.d.*	*n.d.*	*n.d.*	*n.d.*	*n.d.*	*n.d.*
Pt	*n.d.*	*n.d.*	*n.d.*	*n.d.*	*n.d.*	*n.d.*	*n.d.*	*n.d.*	*n.d.*	*n.d.*
Au	0.3	0.1	0.1	0.0	*n.d.*	0.1	0.0	0.0	*n.d.*	*n.d.*
Tl	0.1	0.0	0.0	0.0	0.0	0.0	0.1	*n.d.*	*n.d.*	0.0
Pb	2.0	0.6	1.3	0.9	0.9	1.0	1.3	0.5	0.9	0.4
Th	0.1	0.1	0.1	0.0	0.0	0.0	0.0	0.0	0.0	0.0
U	0.1	0.0	0.0	0.0	0.0	0.0	0.1	0.0	0.0	0.1

3.2.4 Chemical Variations between Depositional Setting

The physical characteristics of the three depositional settings may result in quantifiable chemical differences. For this reason the chemical samples were divided into the different depositional settings and compared. Table 22 shows this division of the samples into their different depositional settings and Figures 42 and 43 show box plots of the XRF results for the major elements based on these groupings. Because Hout Bay and Rooi Els have examples of massive vein deposition, and there being both minor and major surface coatings recovered in Skeleton Gorge, this resulted in 5 different box plots: Deep Vein, Massive Vein, Minor Surface Coating, Massive Surface Coating and Talus Slope deposits.

Table 22: Samples analysed by XRF and ICP-MS and Microprobe sorted by type of manganese deposit.

Depositional Setting	Hand Samples	XRF Analysis	ICPMS Analysis	Microprobe Analysis
Minor Surface Coating	3, 5, D8	3, 5, D8	3, 5	3, 5
Massive Surface Coating	7, 8, 13, A3, A4, A5, C3, C4, C5, E7	7, 8, 13, A4, A5, C5, E7	A4, A5, C5, E7	7, 8, A3, A5, C3, C4, C5
Deep Veined Deposit	11, 20, A6, A7, B3, B4, C2, E1, E2, E3, E4, E5, E6	11, 20, A6, B3, B4, C2, E2, E3, E4, E5, E6	A6, B3, B4, C2, E2, E3, E4, E5, E6	11, 20, B4, C2, E3, E4
Massive Veined Deposit	16, 27, 29, C7, C9	16, 27, 29, C7, C9	C6, C7	16, 27, 29, C6
Talus Slope Deposit	19, 23, A2, B2, B6, B7	19, 23, B2, B6	B2, B6	19, 23, A2, B2, B6, B7

It is apparent that there is no chemical difference between the deep vein and minor surface coating deposits except in the absolute amounts of manganese and iron. The highly elevated silica content is linked to the extremely limited amount of iron and manganese precipitated out. The iron content of the deep veins is slightly elevated to the minor surface coatings and this fits with the overall physical observations where the iron is dominant in the narrow veins. The physical characteristics of the talus slope results in the manganese and iron cementing together soil and thus talus slope deposits have relatively high silica content from included quartz grains in comparison to the more massive surface and vein deposits. The iron and manganese are lowered as a result of the high silica, but importantly the values are more constrained than the other mechanisms. This could be due to the fact that only limited talus slope samples were taken, or due to the fact that as opposed to having a single point of precipitation resulting in either a massive deposit, or a minor deposit, the entire slope becomes a deposit resulting in a more blended deposit averaging out and constraining the values. With the massive surface mechanism the iron is tightly constrained, but the manganese varies hugely. This large variance is small in comparison to the massive vein deposits. Within the massive vein deposits the total variation is huge; large silica, iron and manganese variations. The manganese to iron ratios reflect this, with the deep vein and minor surface deposits having low ratios while the massive vein and massive surface deposits have a high ratio. The talus slope has a ratio of around 1:1.

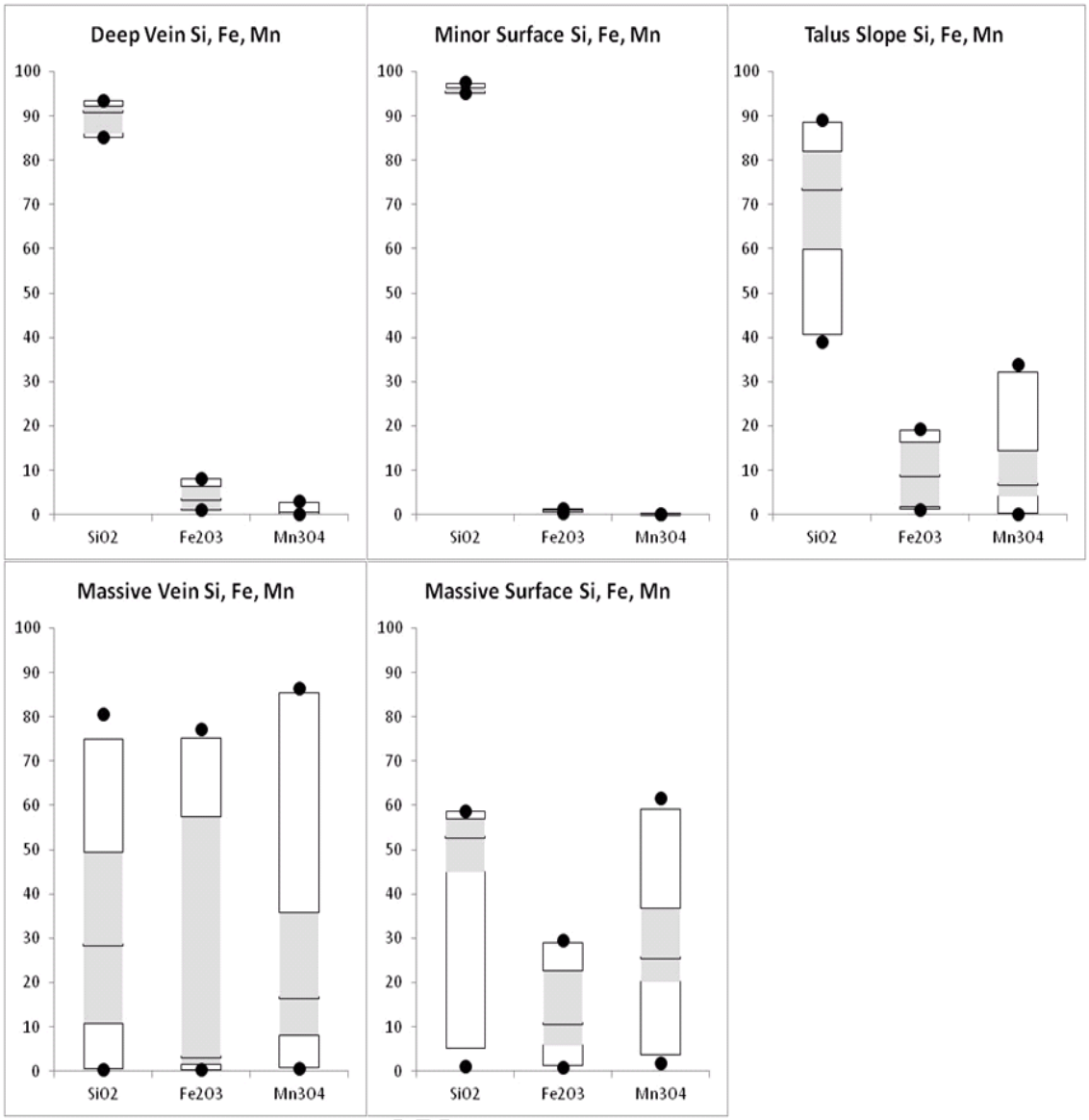

Figure 42: Box plots showing the range of manganese, silica and iron content (wt%) in the different types of manganese deposits studied. The black dots represent the outliers. The black outlined sections the 1st and 4th interquartile range, and the grey shaded blocks the 2nd and 3rd interquartile range. The black line in the middle represents the mean of the data.

In the second set of box plots, potassium and aluminium show a similar and invariant content for all the types except for massive vein deposits. Within the massive vein deposits the potassium and aluminium vary considerably, and they are overall slightly more enriched suggesting the presence of other unknown aluminium and potassium rich elements within the deposit. The ratio of potassium to aluminium shows that where the manganese to iron ratio is high (massive vein and massive surface deposits) the potassium to aluminium ratio is high, indicative of elevated potassium from an increase in cryptomelane.

ICP-MS analysis was done, but once again ordering the data in this format showed no real difference between the different types of deposits. Thus on a REE spectrum there is no difference between the mechanisms, and apart from

the expected differences in manganese, iron and silica between the different mechanisms, the only real chemical difference noted was the elevated aluminium and potassium of the massive vein deposits.

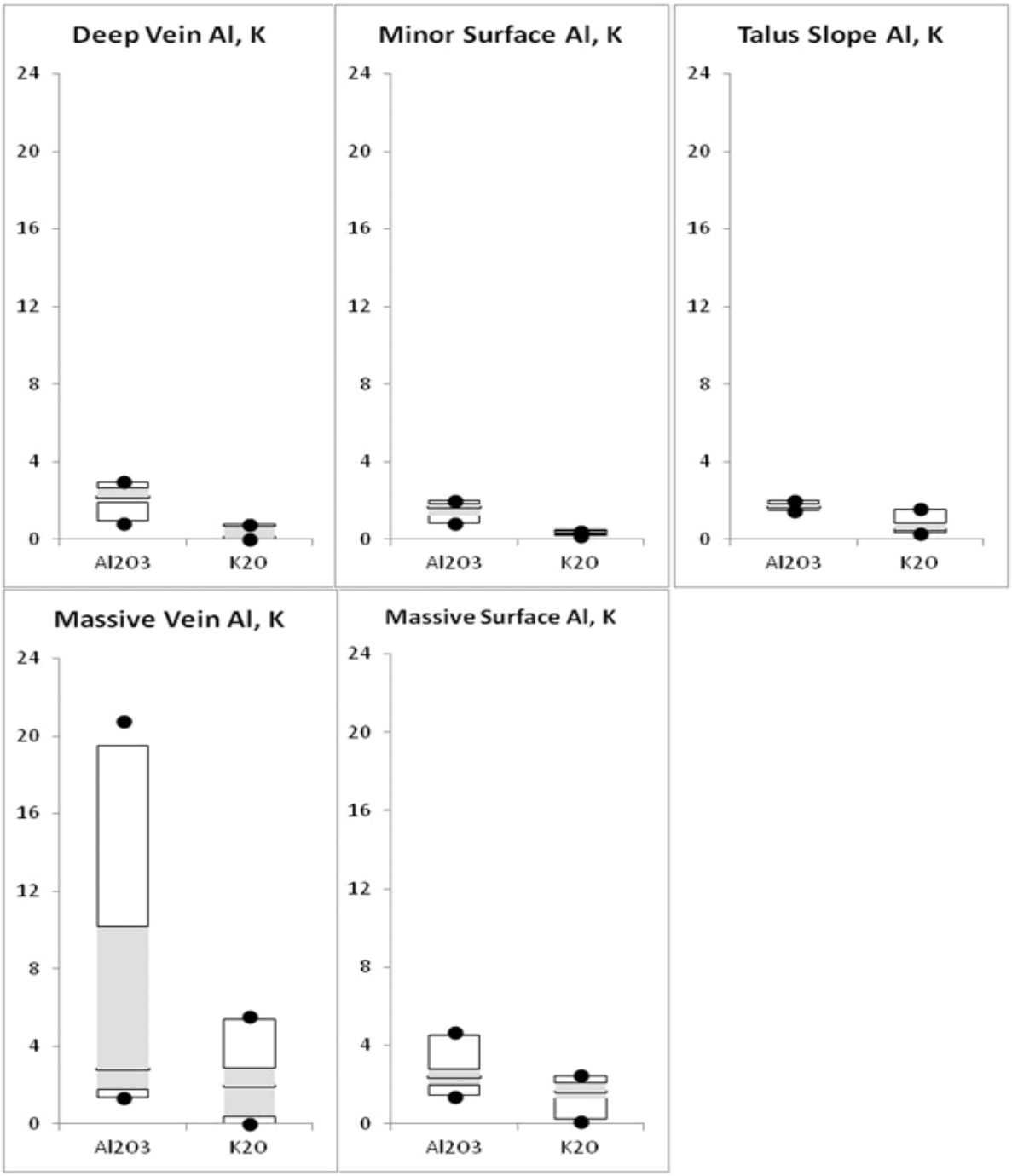

Figure 43: Box plots showing the ranges of aluminium and potassium in the different types of manganese deposits studied.

3.3 Thin Section Analysis

3.3.1 Petrographic Descriptions

Samples were cut into thin sections for petrographic analysis (Table 11). Three types of samples were selected (Table 7). Fresh unaltered and unmineralised rocks were cut perpendicular to bedding. Samples containing a transitional mix between silica, iron and manganese, were cut along the transitional contact. Samples highly enriched in manganese and iron was cut to best expose visible transitional features. At the microscopic level no real differences were noticed between the individual sample sites or the depositional settings suggesting that the mechanics which governed the deposits where similar across all depositional sites and the different depositional settings. It is possible at the microscopic level to see the interactions between the iron, manganese and silica, and to start to gain an understanding into the process of precipitation of the metals (unmineralised, transitional, metal rich samples). **Appendix B** lists all the petrographic descriptions.

Thin section analysis identified multiple minerals present within the samples, namely quartz, micaceous minerals, apatite and a red isotropic mineral and a black isotropic mineral and detrital black isotropic minerals. The red isotropic mineral was identified as iron, the black isotropic mineral was identified as manganese through the microprobe analysis while the detrital black isotropic mineral was shown to have slight occurrences of iron and manganese but the actual mineral was not identified.

Unmineralised Samples

Rocks showing no signs of manganese or iron mineralisation were sampled from the Peninsula Fm and Graafwater Fm. Samples were taken from the Contour Path site and from non-mineralised zones within depositional sites, for example, the siltstone found in the Peninsula Fm overhang of Skeleton Gorge (Figure 15).

Samples D3 and D4 are representative examples of unmineralised Peninsula Fm sandstone. In these samples quartz is dominant, making up 98% of the rock, with trace amounts of mica and rest of the thin sections is made up of detrital grains of an unidentified isotropic mineral. The quartz grains are equigranular, rounded to sub rounded, and medium to coarse grained. The micaceous material occurs between the grains and is not always present (Figure 44). The minor isotropic minerals were generally detrital in origin, fine sand sized and rounded. In the unmineralised Graafwater Fm samples (D1 and D2) mica is more abundant and the quartz grains are fine to medium rounded to sub rounded. Similar amounts of detrital isotropic minerals were found as with the Peninsula Fm (Figure 45).

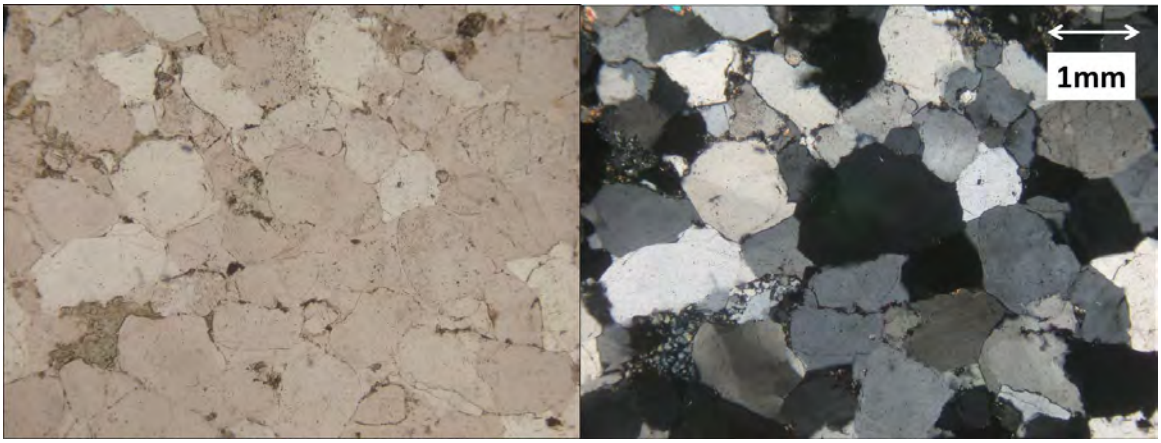

Figure 44: Thin Section of sample D3 of Peninsula Fm sandstone. Equigranular medium to coarse sub round quartz grains, minor micaceous material and some small sub rounded detrital isotropic minerals cemented by quartz. Polarised light (left) and plane light (right).

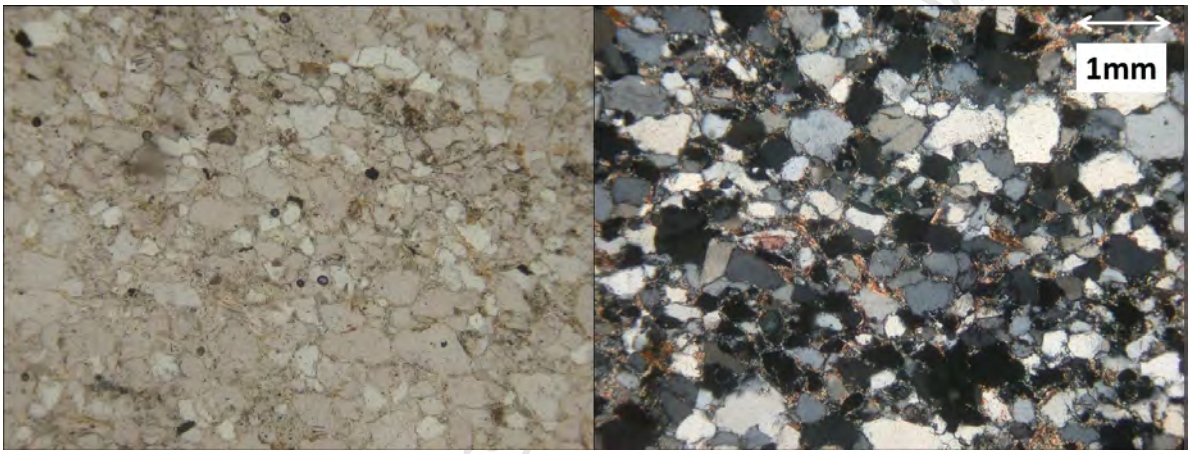

Figure 45: Thin Section of sample D1 of Graafwater Fm sandstone. Note the reduced grain size of the quartz and the increase in micaceous material as opposed to sample D3, Figure 27. Polarised light (left) and plane light (right).

There were additional samples of unmineralised Peninsula Fm sandstone rocks that were taken close to manganese rich deposits, such as samples A1, B1 and 31. These samples showed extensive weathering in hand specimen, when broken open the outer layers were a different colour to the inner layers and the outer layers were friable. Weathering was evident in the thin section as well as a slight increase in micaceous material, and greater intergranular porosity.

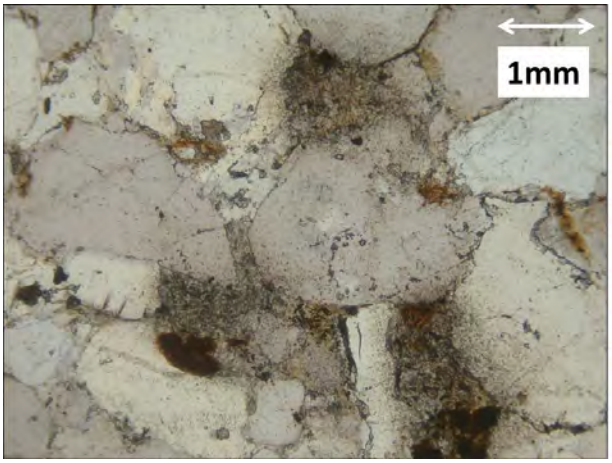

Figure 46: Thin Section of sample B1 (plane light). In comparison to Figure 27 there is more micaceous material in between the grain boundaries.

Transitional Rocks

Transitional rocks are those showing partial manganese and iron enrichment. The petrographic relationship between silica, manganese and iron is similar in the transitional rocks regardless of the sample location or depositional setting. The modal proportions of the different minerals (iron, manganese and quartz) are highly variable, but the deposition of the manganese and the iron appeared to be the same throughout the thin sections studied. Generally the quartz grains were sub rounded to sub angular, and had a bimodal coarse to fine grain size (Figure 47). The coarse grains were more tightly cemented, and no manganese was present, but partial iron staining was visible in places. The fine quartz grains are not as tightly cemented and are more angular than the coarse grains. Mineralised areas contained finer grained quartz with both iron and manganese occurring in between the quartz grains. The iron generally appeared to coat the edges of the quartz grains and the manganese filled the intergranular pore spaces or the larger fractures between the quartz grains.

In the majority of the samples the fine quartz grains coincide with fractures. Iron or manganese fills in the fractures of the grains, and then mainly manganese filled in the larger void spaces between the quartz grains. In all samples the fractures share the same orientation. Iron precipitates within the smallest fractures of the quartz, propagating along porous zones occasionally causing what appeared to be embayment's into the quartz. These embayments suggest the iron is replacing the quartz.

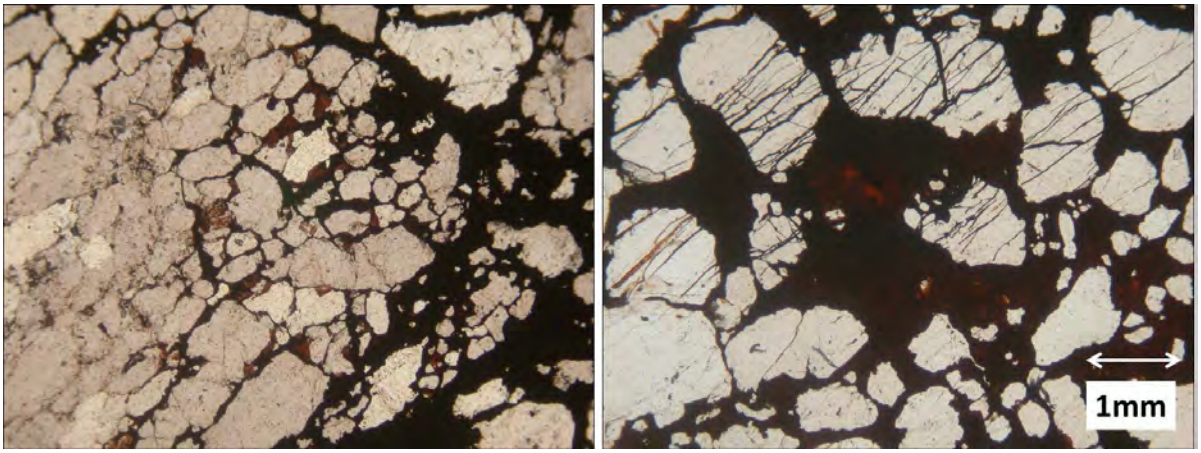

Figure 47: Thin Section of sample C3 on the left, showing manganese (black) and iron (red) cements surrounding quartz. Thin section of B4 on the right, shows filled fractures of quartz grains, both images in plane light.

The quartz-manganese boundary was less complicated, with the manganese infilling fractures in the quartz and some minor embayment's into the quartz grains. In sample B7 the manganese occurs adjacent to mica in between the quartz grains, with no replacement of the mica by the manganese. Some samples (B4, B6, B7, C2, C3, and C4) showed trace amounts of secondary veining. These veins were established to be highly concentrated manganese material (as determined by microprobe) are silver in hand specimen and completely isotropic under the microscope and cut through both the iron and the quartz grains. The textural relationships suggest that these veins are secondary to the iron (Figure 48). It only appears to occur in sites where massive vein deposits exist, such as at Rooi Els and Hout Bay.

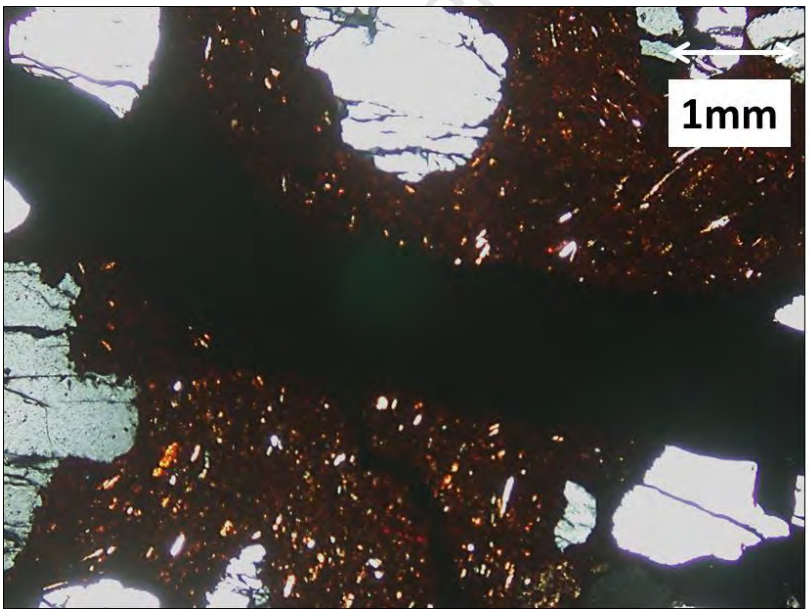

Figure 48: Thin section of B4, showing the vein of manganese material in plane light.

Manganese Rich Rocks

Manganese rich rocks contain greater than 50% modal proportions of manganese as determined by petrography. The manganese is isotropic, such that nothing is revealed when looking at manganese with transmitted light. Although nothing could be revealed about the inner textures of the manganese, the relationship between the manganese and the iron or quartz could still be studied. The iron and manganese share a sharp contact whilst the quartz and manganese have a more transitional contact. Initially the quartz is coarse grained and well cemented with few fractures. As the sandstone becomes less well cemented and the fractures increase, the manganese content increases and the quartz content decreases, as show in Figure 47, sample C3. This continues until the manganese could be classified as massive. Figure 49 shows how the manganese is completely separate from the iron and quartz, while the iron and quartz share the same space during larger scale precipitation of manganese.

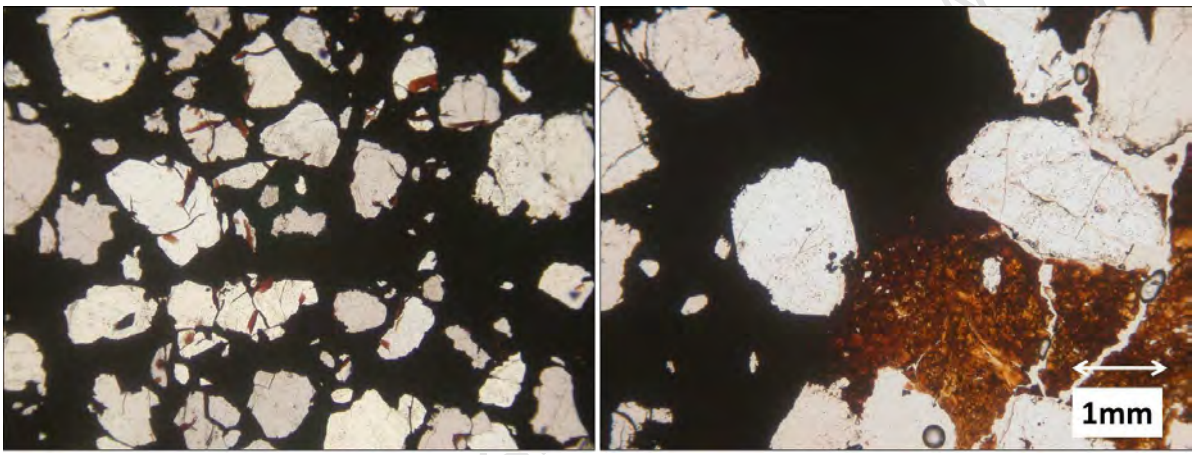

Figure 49: Thin section images of sample A4 (left) and B4 (right) showing the high grade manganese relationship with quartz and iron.

Iron Rich Rocks

Similar to the manganese rich rocks, iron rich rocks represent samples that have greater than 50% modal proportions of iron as determined by petrography. The iron had weak isotropy which and slight variations in the chemistry of the iron resulted in visible colour variations (Figure 50). These colour variations allow for visible zonation of the iron deposition which is linked to the variations in the fluids depositing the iron, and suggests multiple fluid phases.

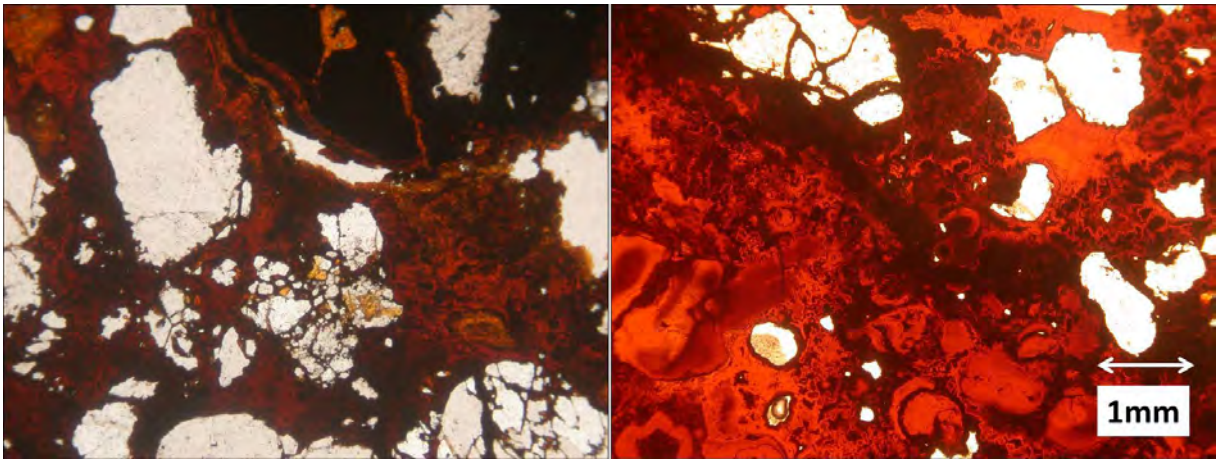

Figure 50: Thin section of sample B6 on the left, and B2 on the right in plane light showing the patterns developed through the deposition of the iron by chemical variations within the fluids.

The manganese and iron have a well-defined sharp contact, while the quartz and iron have a transitional contact. The iron initially occurs as a yellowish stain in between the grain boundaries of the quartz. As the grains of quartz become further apart the iron becomes a deeper red colour. Along the edges of some of the quartz grains with yellow staining were embayments of iron oxide. The progressive change from yellow to deep red colour did not only occur alongside the quartz grains, but also independent to the quartz grains. In this case the progression of colour was assumed to reflect changes in iron concentration related to different depositional fluids. In some samples concentrically banded grains occur (Figure 51). Formation of these grains may begin at a single point (potentially coating a quartz grain), and then grow as each successive ring is deposited over the previous ring, and as the concentration of iron within the fluids changes, so too does the concentration of the iron and the colour of the ring deposited.

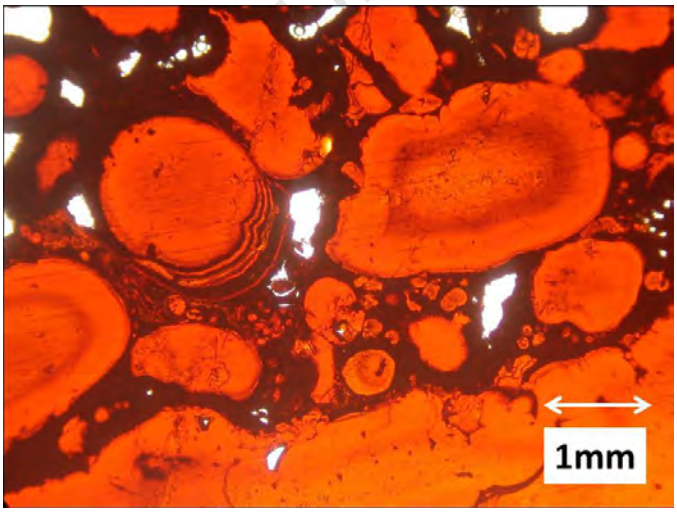

Figure 51: Thin section of sample B2, showing the zonation of the iron in plane light.

3.3.2 Microprobe Analysis

Similar to the objectives of the thin section analysis, the microprobe analysis attempted to generate information which would help in understanding the transitions from unmineralised rock to metal rich rock and the differences and similarities between the different depositional settings. The microprobe maps which were taken are essentially maps showing the spread of the element within the mapped area. While this does not give an absolute value of the element, it does allow for textural and basic chemical relationships to be established between the elements mapped. The analysis done on the unmineralised rocks was aimed to determine the location and relative concentration of manganese and iron in the rocks hosting the manganese deposits. The transitional rocks were analysed to determine the transitional changes between silica, iron, aluminium, potassium and manganese. Samples of metal rich manganese and iron were analysed to determine the elemental variations between iron, manganese, aluminium, potassium and silica.

Microprobe images were taken under reflected light, thus quartz appears clear, and iron has a slight yellow tint and manganese a slight blue tint while the isotropic minerals represent mica (potassium and aluminium rich) and oxide minerals (gangue). In all the images, a photo of the area being investigated is attached and the white block indicates the approximate area scanned.

Unmineralised Samples

As the majority of the host rocks were unmineralised quartz sandstone, the areas over which maps were produced were areas in between the quartz grains where minerals other than quartz were noticed. Figure 52 shows sample 1 from the top of Skeleton Gorge having very fine contacts between individual quartz grains and intergranular mica minerals which have low iron contents. In sample D4 (Figure 53) an isotropic mineral was found to have a high iron but low manganese content (5 counts maximum per pixel). The other potential source rock and host rock, the Graafwater Fm, had more mica minerals and more iron than the Peninsula Fm, but the petrographic fabric is the same. The siltstone sample 30, had no manganese present, but aluminium, potassium and iron were present (Figure 54).

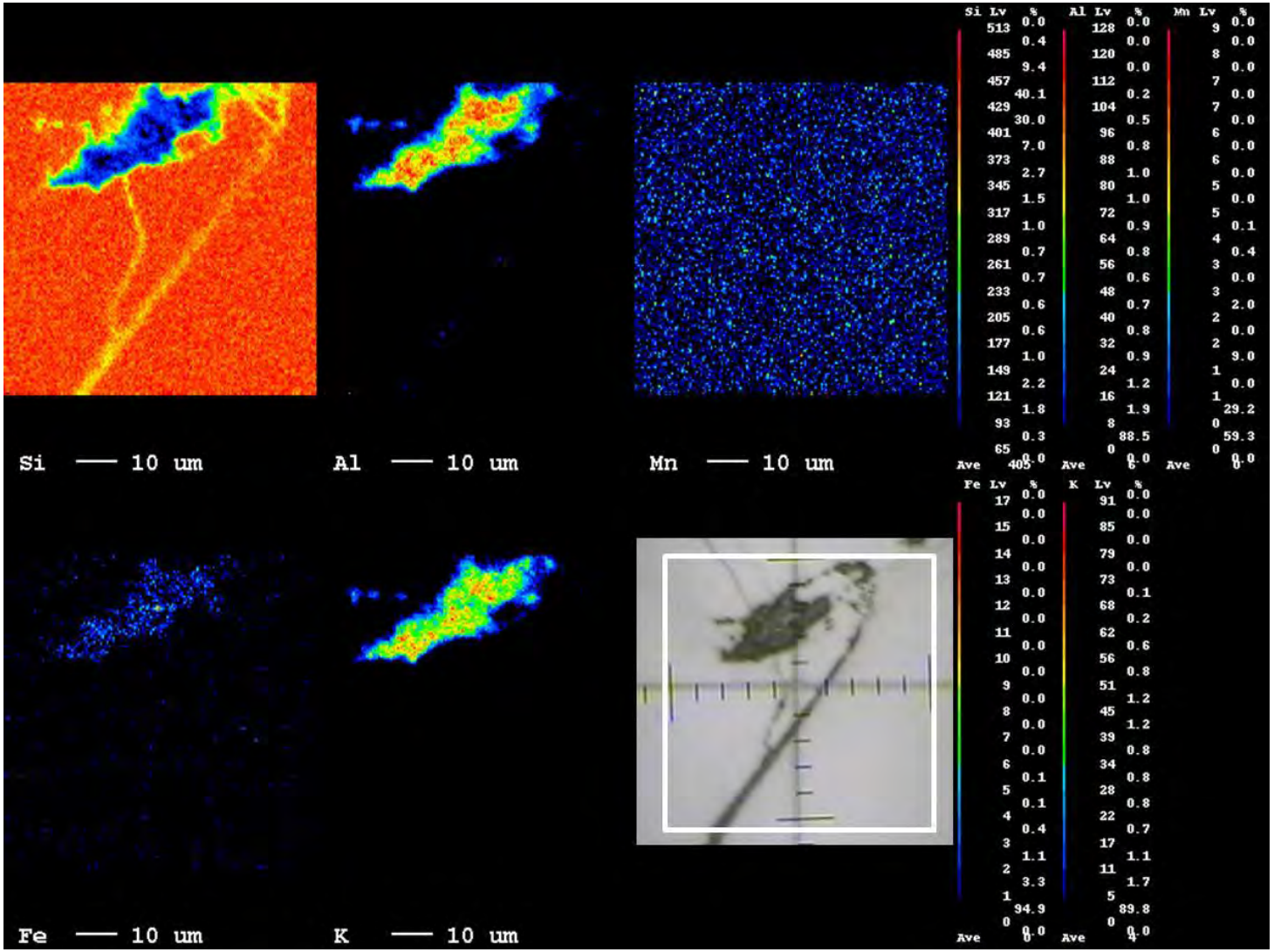

Figure 52: Peninsula Fm sandstone sample 1. Note the slight occurrence of iron within the potassium and aluminium mineral, potentially mica. Reflected light image shown in lower right-hand corner with dark mineral interpreted to be a mica grain rich in K, Al, Si and some Fe but no appreciable Mn. Colours relate to counts per pixel ranging from blue (low) to red (high) shown on the far right scales. The dark lines in the reflective light image represent fractures or grain boundaries between the quartz grains.

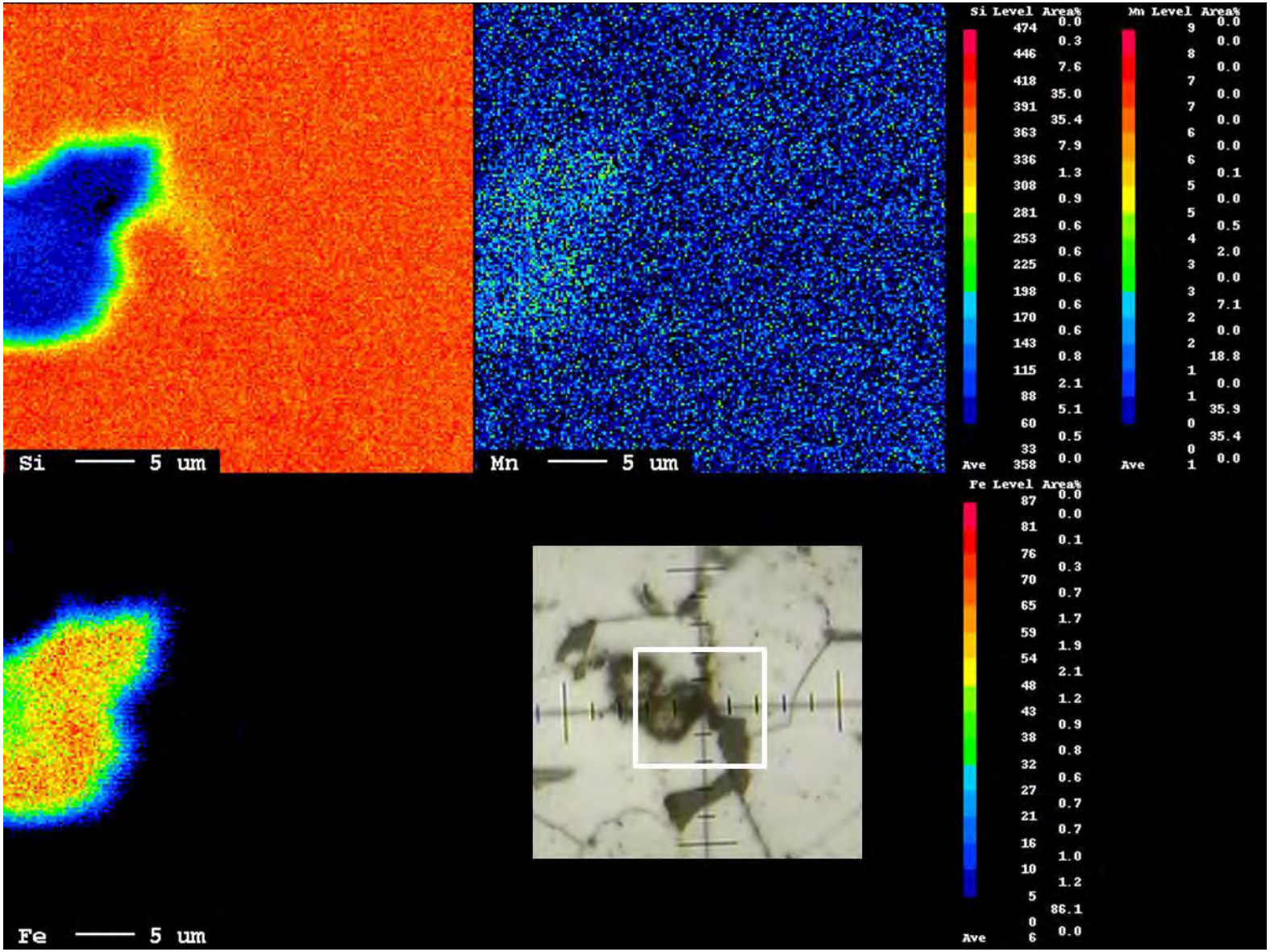

Figure 53: Peninsula Fm sandstone sample D4. The occurrence of iron and some manganese is associated with the darker grain in the lower right-hand image. The dark mark in the lower right hand quadrant of the reflected light image is a blemish formed on the carbon coating post the laser burn.

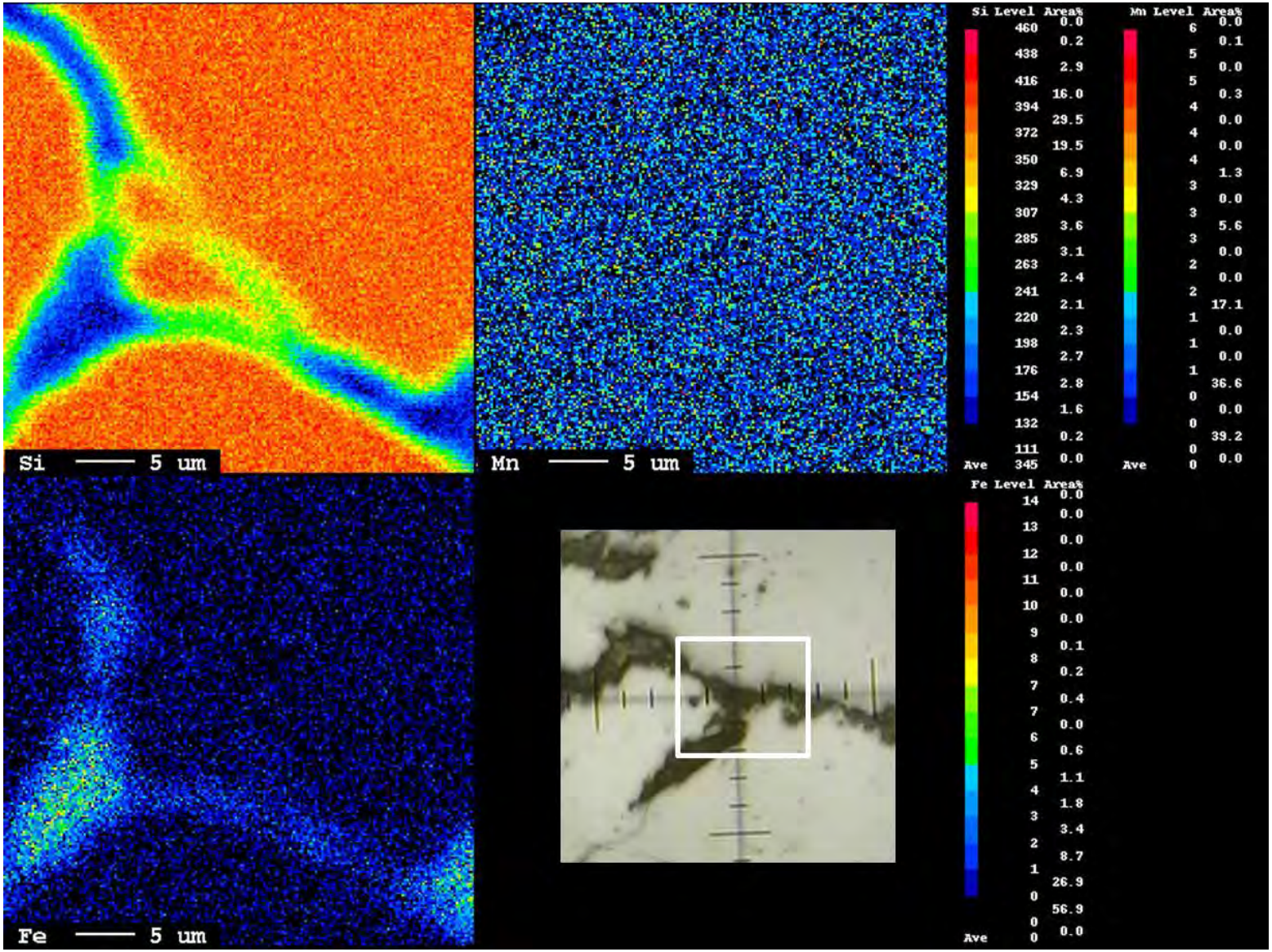

Figure 54: Graafwater Fm siltstone sample D1. Iron is concentrated with the dark mineral, which is similar to sample 1 (Figure 53), suggesting the dark mineral is potassium and aluminium rich. Manganese is slightly more concentrated along with iron but also occurs homogeneously throughout the image.

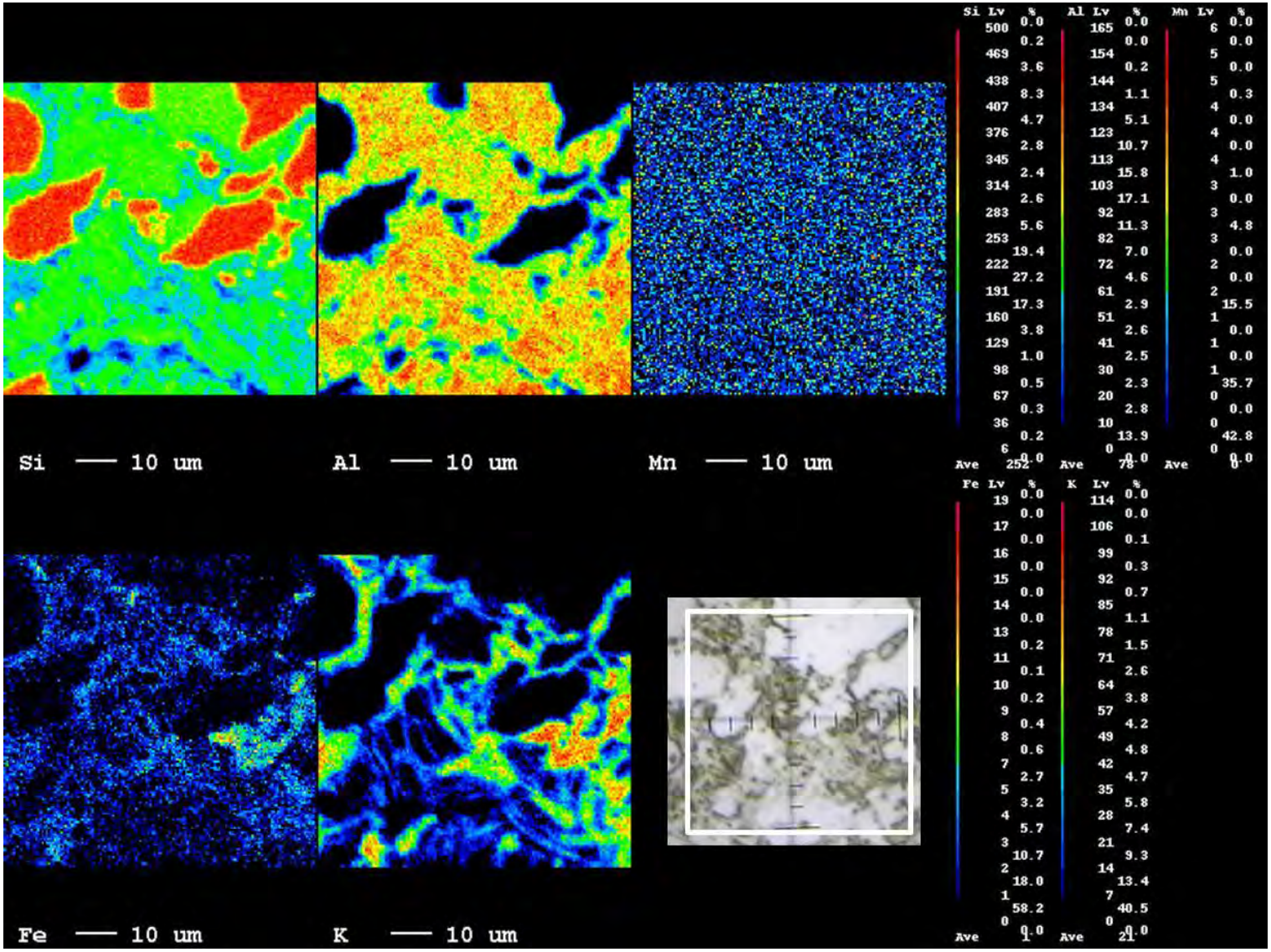

Figure 55: Peninsula Fm siltstone sample 30, from the overhang in Skeleton Gorge. Relatively high concentrations of the aluminium and potassium rich mineral, most probably mica, occur within this siltstone, the iron follows the potassium while the manganese shows a homogenous distribution.

Transitional Samples

Transitional samples all show the progression from the unmineralised quartz rich samples to the metal rich manganese and iron samples. Iron occurs along the grain boundaries of the quartz (Figure 56) with more iron occurring in the interstitial spaces of the quartz grains. In some rare instances manganese was observed along grain boundaries (Figure 57), but at significantly lower concentrations than the iron (68 counts per pixel for iron vs. 25 counts per pixel for manganese). As the interstitial void space increases, the textures of the iron and manganese precipitates become more variable. In some samples manganese is dominant and iron secondary (Figure 58). Figure 59 shows two scans from sample A5. In the bottom scan iron and manganese precipitated out at the same time, occupying the same space. In the top scan the manganese precipitated out along the grain boundaries first, followed by the iron. Iron appears to be more dominant in the transitional samples than manganese. In all of these transitional samples the iron and the manganese co-exist. As the intergranular space occupied by iron and manganese increases, this co-existence ends, and the iron and manganese exist completely separate from each other.

At this level of deposition the correlation between the potassium and manganese becomes evident, showing the formation of Cryptomelane.

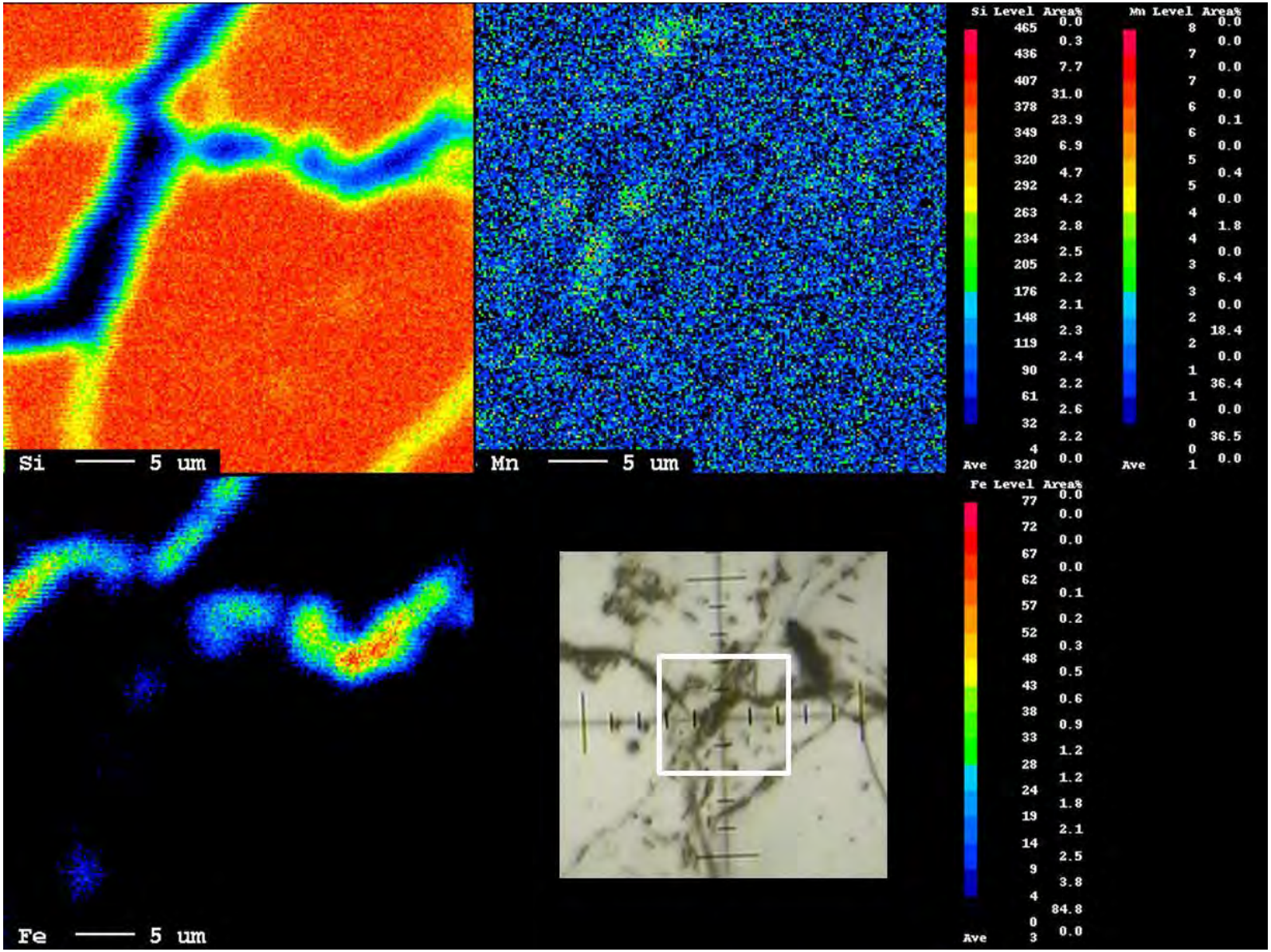

Figure 56: Iron precipitating around quartz grains, sample C6. As in earlier images some of the grain boundaries and fractures occurring within the Si grains are not associated with Mn or Fe precipitation.

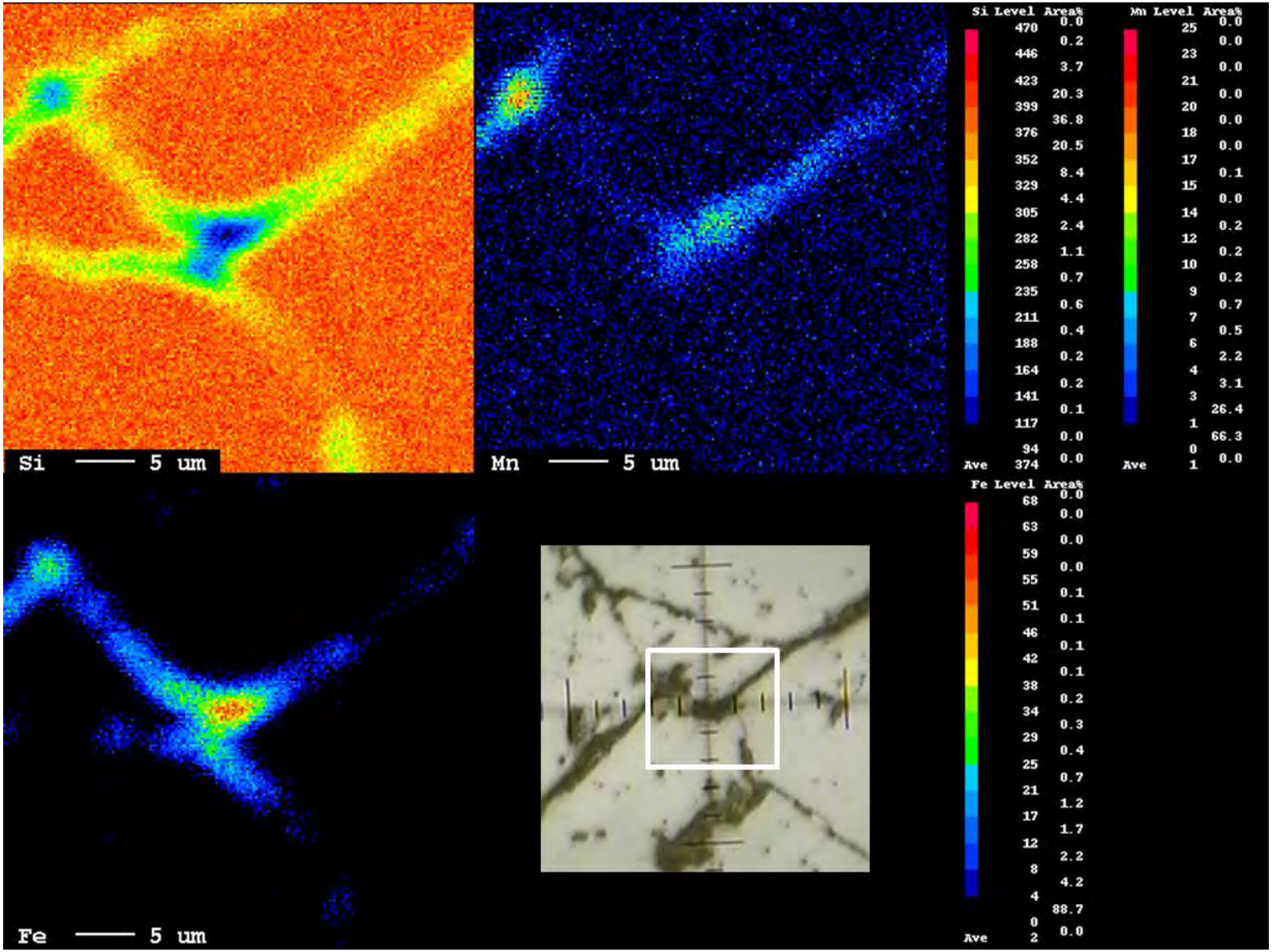

Figure 57: Iron and manganese precipitation between quartz grains, sample C2.

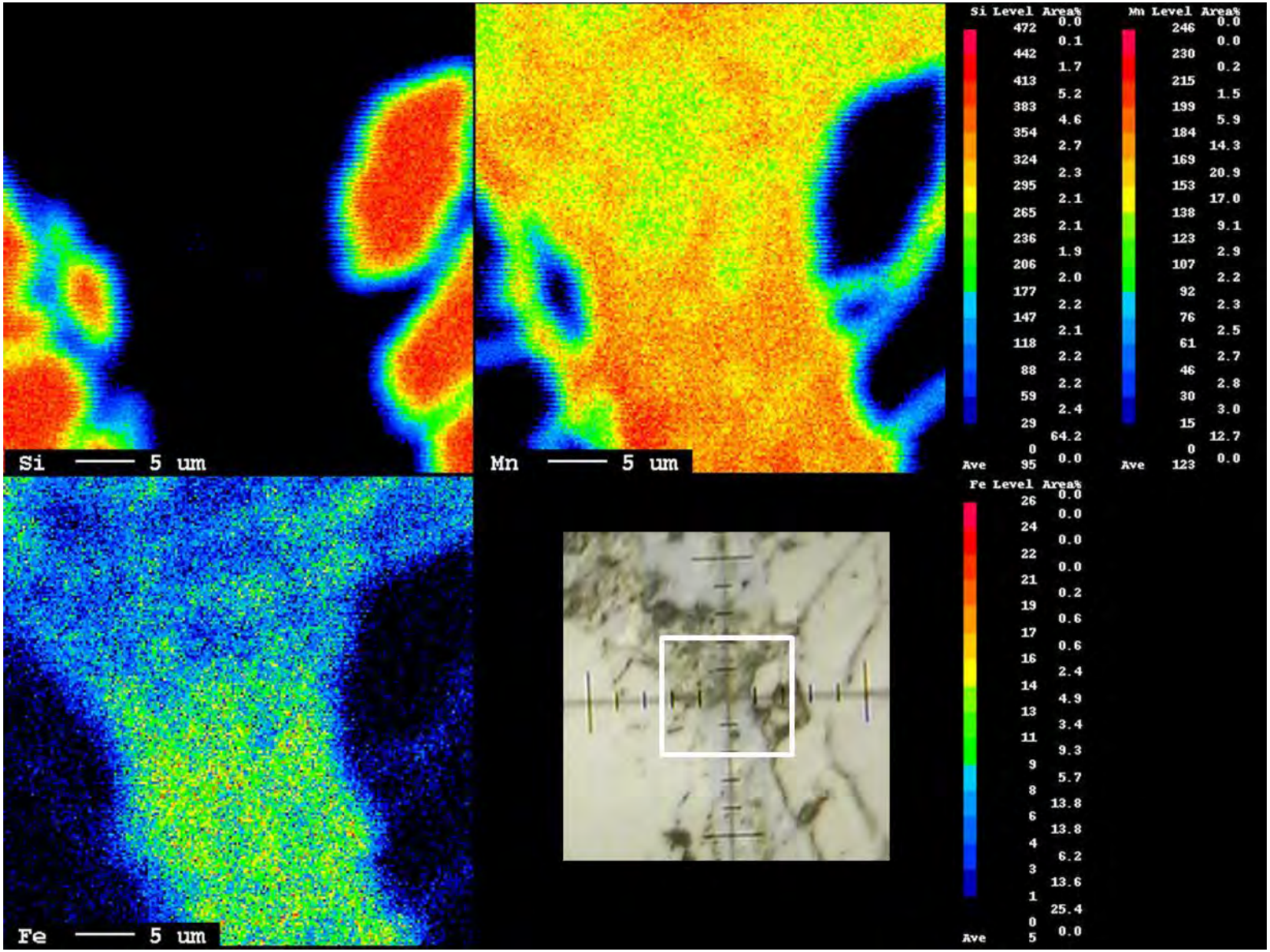

Figure 58: Dominant manganese and secondary iron precipitation in sample B4.

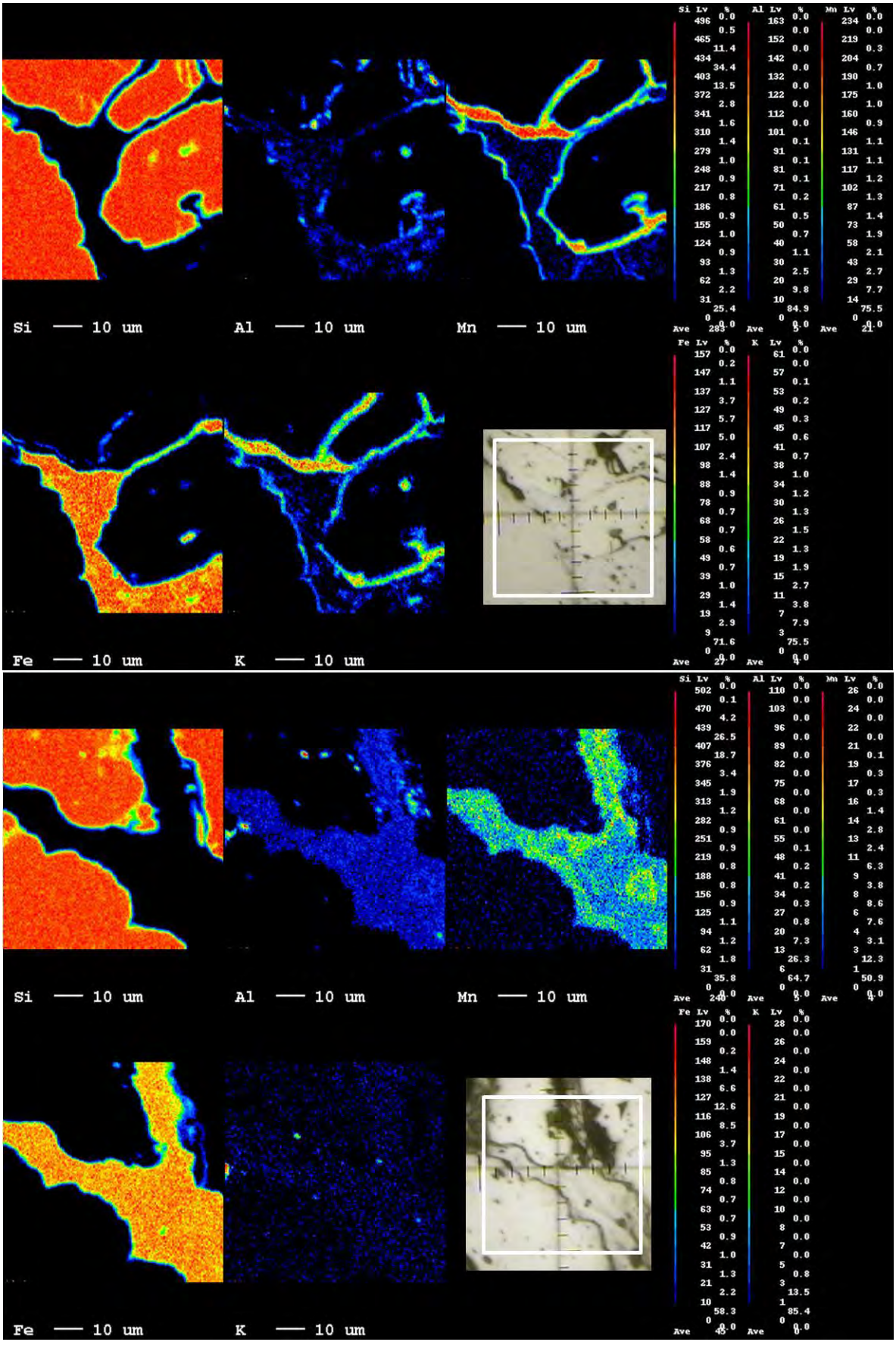

Figure 59: Two scans of Transitional sample A5 showing transitional deposition of manganese and iron.

Iron and Manganese Rich Samples

As the manganese and iron content of the rock increases, the manganese and iron no longer co-precipitate but occur in separate areas having sharp contacts (Figure 60). There are trace amounts of manganese in the iron and vice versa, but due to the high concentrations of these metal rich manganese or iron regions of the map, these trace amounts are not visible in the microprobe maps. Figure 61 shows an example where no manganese was found during the scan, but trace amounts manganese can be seen within the iron. The concentration of this manganese is at maximum 8 counts per pixel, compared to a maximum of 278 counts per pixel in Figure 60. Sample C5 suggests three periods of chemically different fluids moving through the voids resulting in different minerals being crystallised. The initial fluid phase deposited iron, the second fluid phase manganese and the final fluid iron and manganese together (Figure 62). In sample 8 (Figure 63), there are four visible stages in manganese deposition. While there is no appreciable iron present, variations in potassium and aluminium and manganese show four different phases of precipitation. Figure 64 shows only 3 phases, but the one phase shows potassium, manganese, and aluminium precipitating out together.

The XRD results showed that cryptomelane was the only mineral being precipitated out, and the accepted formula for cryptomelane (Gruner, 1943) has been shown to include aluminium as a substitute for manganese. Thus the drop in the manganese correlating with a rise in the aluminium content can still be explained within the mineral cryptomelane. It is important to note that the observation in Figure 63 where manganese is replaced by aluminium is common occurrence, but in general the manganese is associated with potassium.

Additional to the visible chemical differences on the maps, there are textural differences. Sample C5 shows chemical differences with no visible textural differences (Figure 62), but sample B6 shows visible textural differences in the photo image, but no chemical differences in the elemental map (Figure 65). It is important to note that iron precipitating with the manganese in sample C5 is not an isolated case, but it is a rare case at this level of the deposit. Generally at this level of deposition (metal rich) the iron and manganese precipitate out separately, the dual precipitation of iron and manganese is more noticed during the transition phase of deposition.

A siltstone from the Skeleton Gorge overhang (Sites 3&4) with visible iron and manganese staining in hand specimen has elemental maps which show similar behaviour of the iron and manganese precipitates (Figure 66).

Figure 67 shows an example of an occurrence where the iron and silica shared the same precipitation region. As this sample contained mostly metals (73%), this silica formed during the precipitation of the iron.

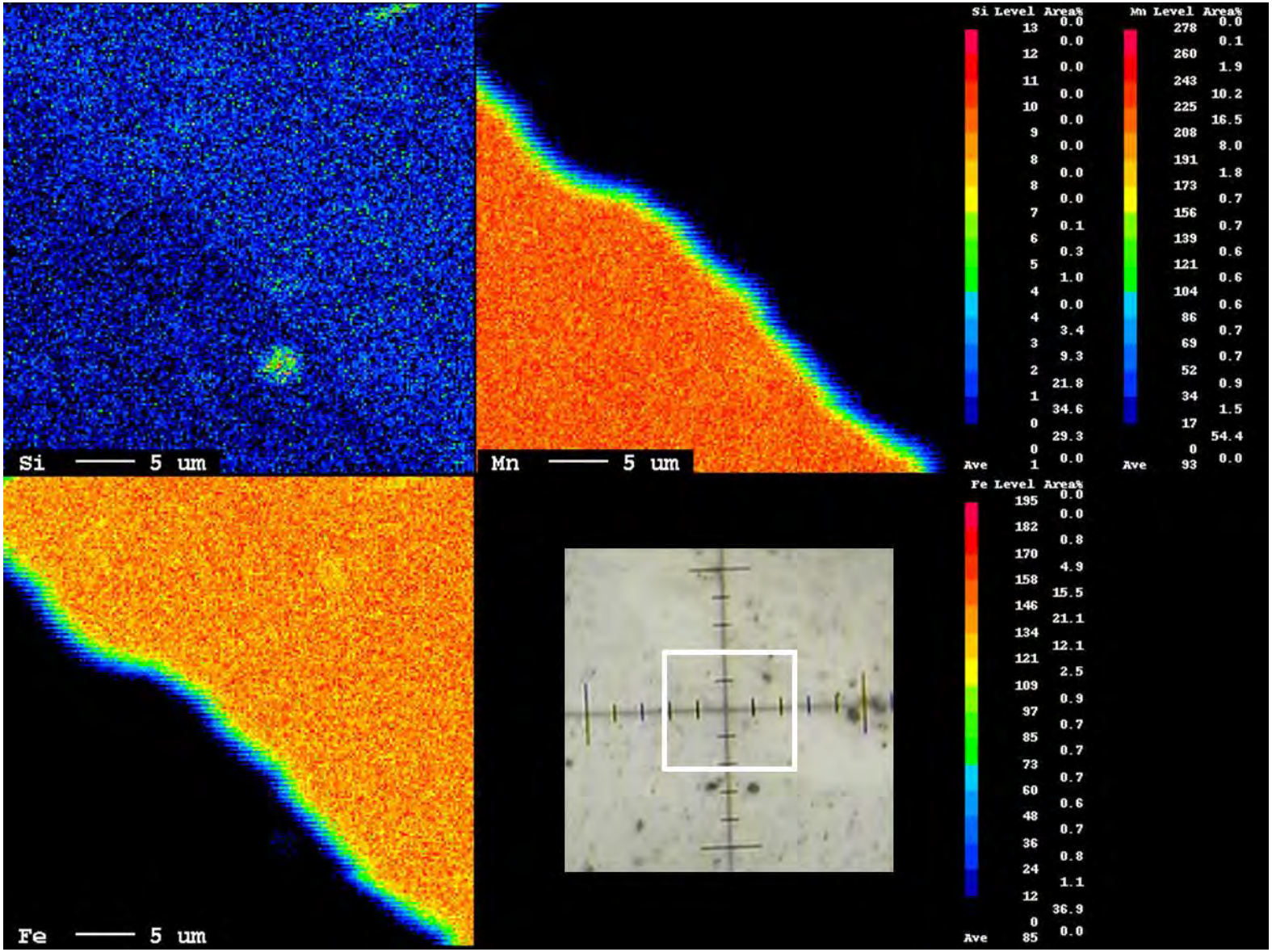

Figure 60: Sample E4 from Hout Bay displays a mixture of nearly highly concentrated but separate precipitation of manganese and iron.

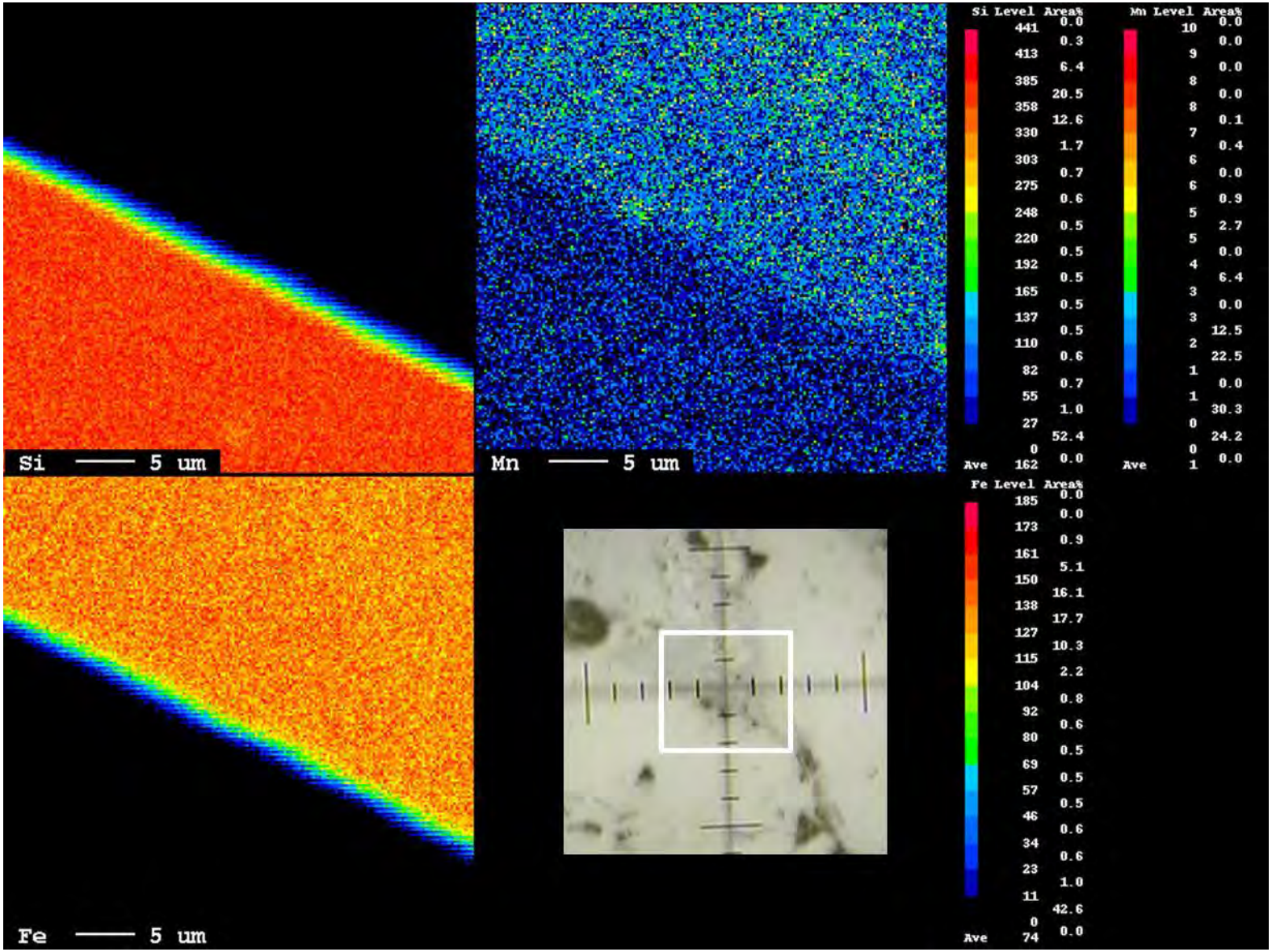

Figure 61: Sample C6 from Kasteelpoort Path consists of very rich iron having traces of manganese.

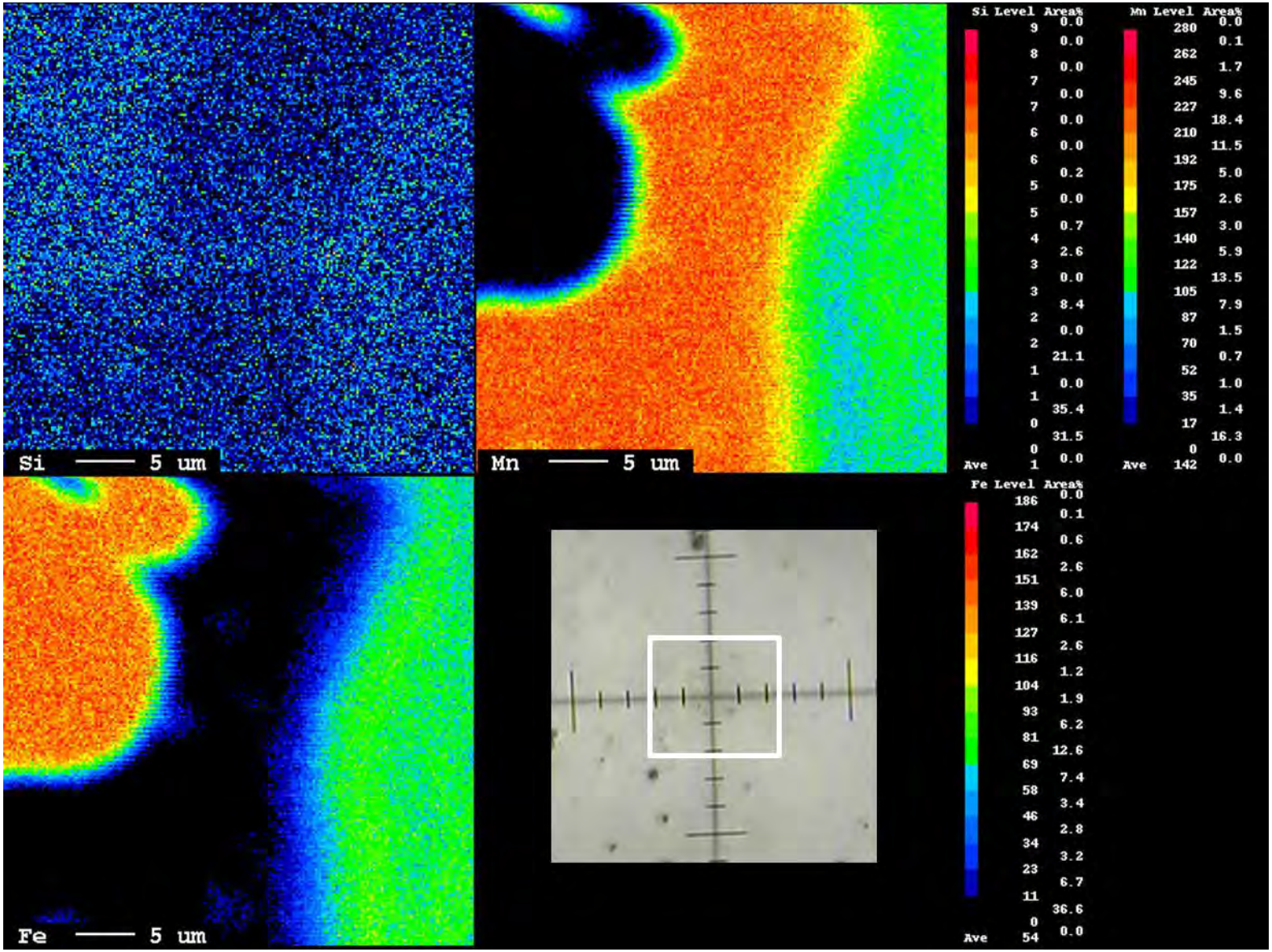

Figure 62: Sample C5 from Kasteelpoort Path shows evidence for multiple iron and manganese precipitates which are not defined in the homogeneous texture of the reflected light image.

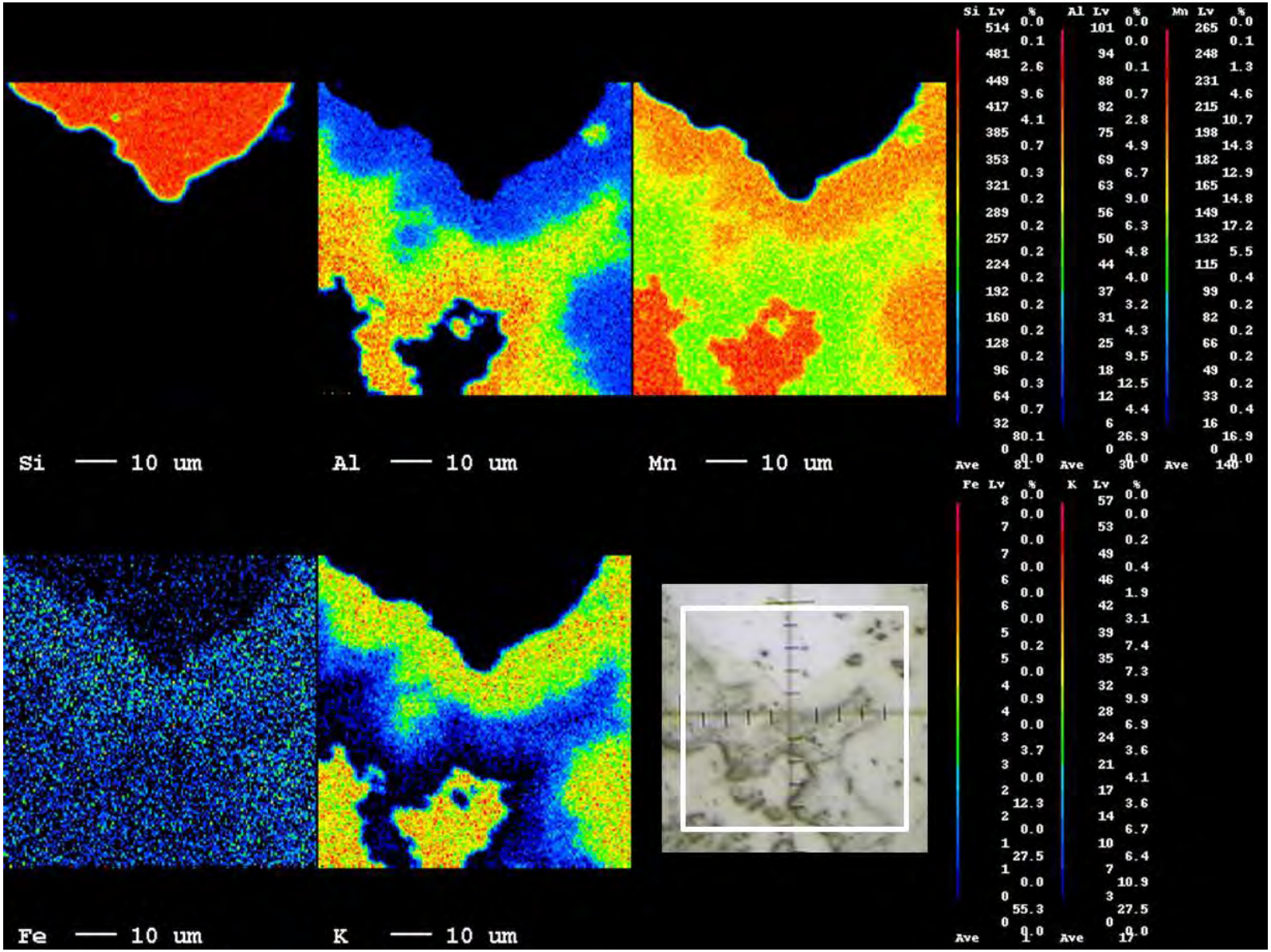

Figure 63: Four compositionally different precipitates of high concentrate manganese in sample 8 from Skeleton Gorge Site 3 and 4.

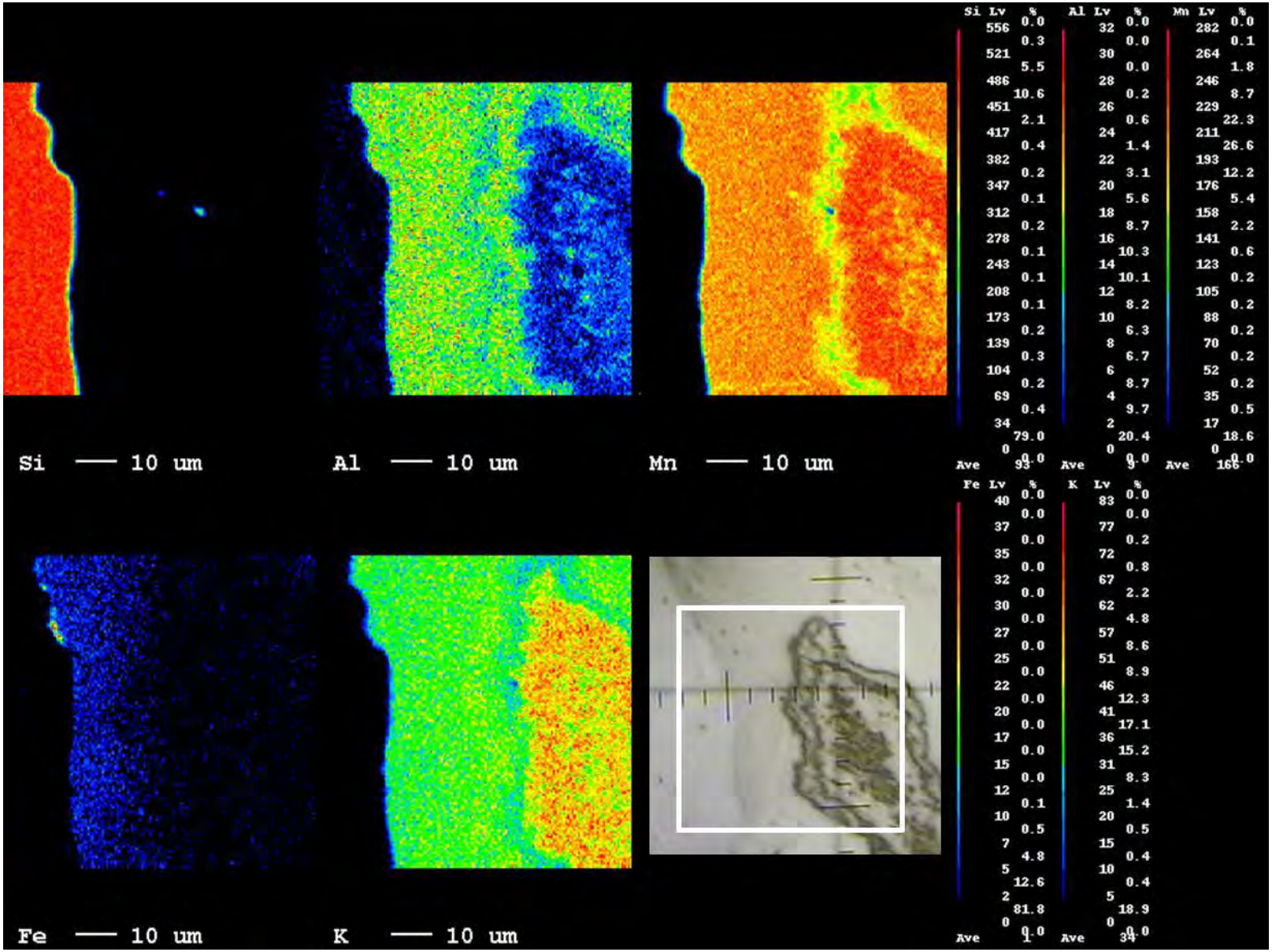

Figure 64: Three compositionally different precipitates of high concentrate manganese in sample 10 from Skeleton Gorge Site 3 and 4.

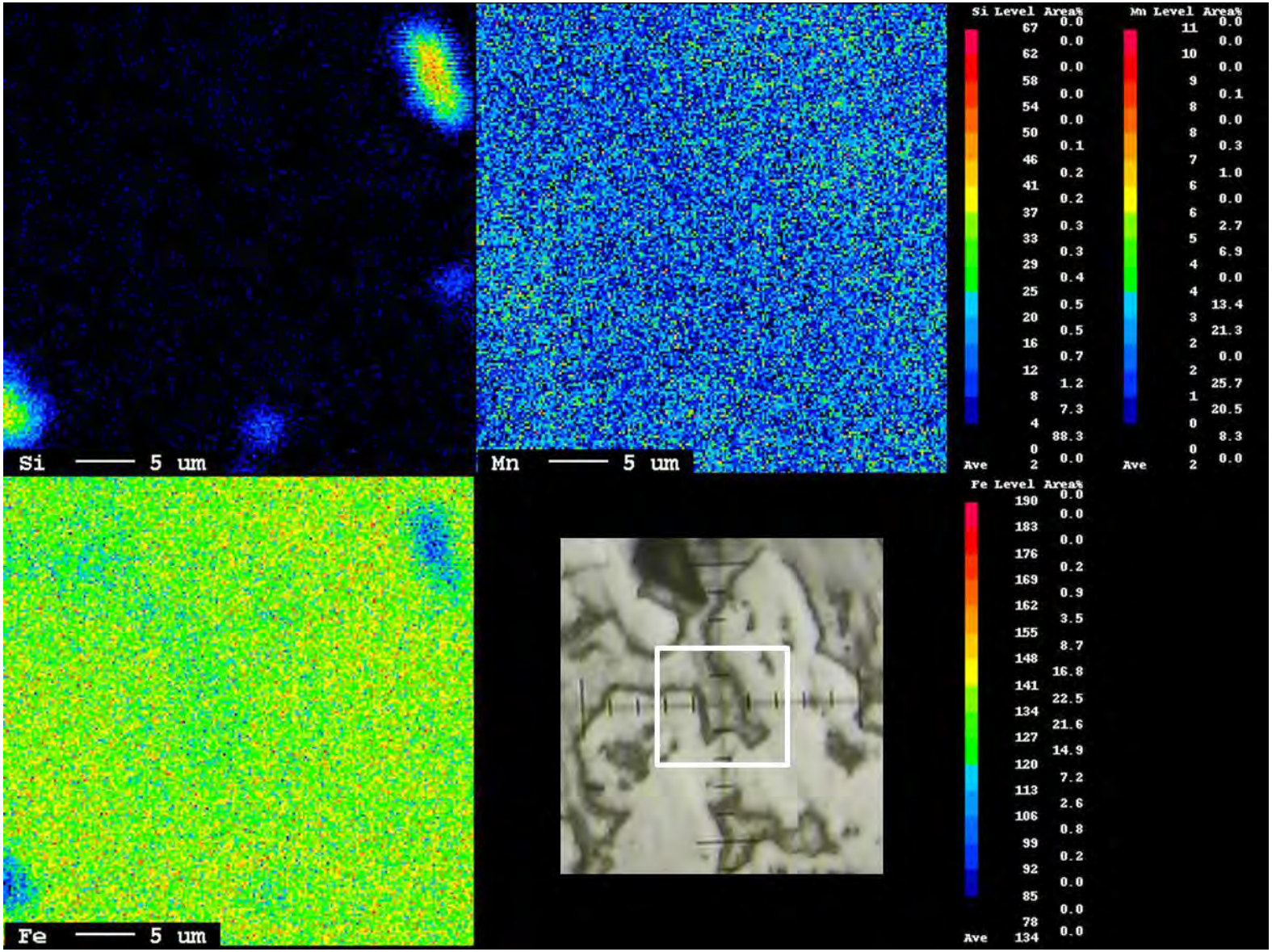

Figure 65: Textural variations shown in lower right image that do not correspond to chemical differences, sample B6 from Skeleton Gorge.

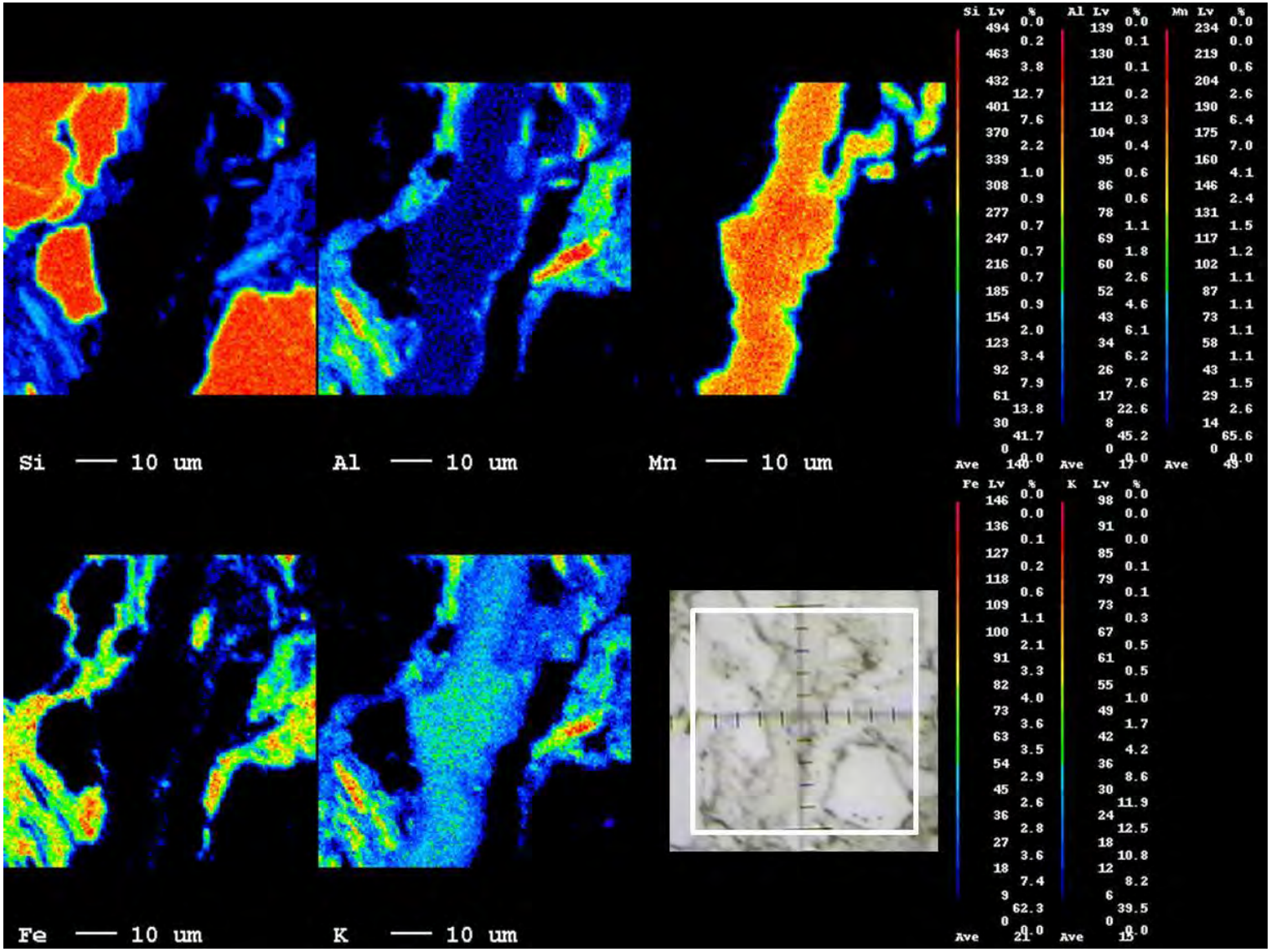

Figure 66: Sample 10 from Skeleton Gorge Site 3 and 4, showing nearly iron deposition surrounded by quartz and mica, and manganese deposition isolated in the centre. Note that high manganese area is also enriched in potassium which is reflecting the composition of the manganese mineral (refer to following section).

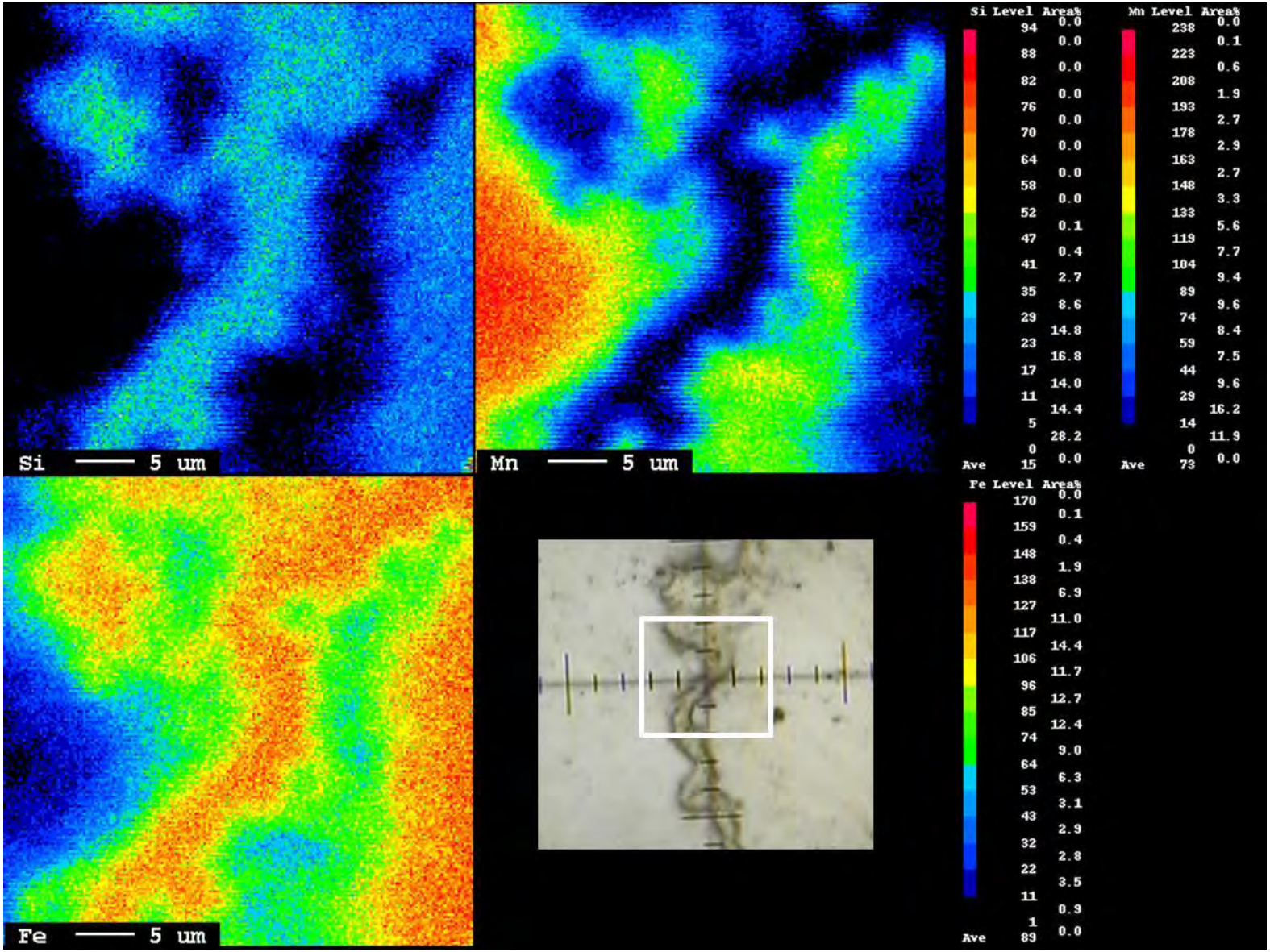

Figure 67: Sample E4 from Hout Bay, showing silica sharing precipitation space with the iron.

4 DISCUSSION

Based on Harrison's classification system (Harrison, 1998) and the results presented in this thesis, the deposits of manganese found throughout the Cape Peninsula are hypothesised to be Type 1 low-temperature hydrogenous deposits, where the manganese is sourced from the reduction of manganese in Peninsula Fm soil profiles and bedrock. Joint sets and faults throughout the bedrock act as conduits and focusing mechanisms for the flow of reduced groundwaters. When these groundwaters seep out of the bedrock their reduced iron and manganese are oxidised resulting in the precipitation of the iron and manganese oxide cements. The discussion which follows presents the evidence to support the above hypothesis that the Cape Peninsula manganese deposits are Type 1.

4.1 Lateral Secretion as a Depositional Model

Lateral secretion, as part of Type 1 deposits, is proposed here as the likely mechanism for the deposition of the Cape Peninsula manganese deposits. The low-temperature fluid flow of lateral secretion starts with rain water. The rain water falls to ground and gets reduced as it percolates through the organic-rich upper layers of the soil. The humic-rich horizon of the soil is reducing as a result of microbial degradation of the organic material which consumes oxygen and releases CO_2. The oxygen-depleted water becomes more acidic from the CO_2 generated in the organic rich soil waters by forming carbonic acid from the elevated soil pCO_2 measured to be 100 times greater than atmospheric pCO_2 in some soils (Compton, 2004; Graham et al., 1988; Karberg et al., 2005; Sparks, 2003). Because the TMG contains no carbonate and few other acid neutralising minerals, such as feldspar, the soil waters are acidic with stream waters draining the TMG having measured pH values of between 3.5 and 4.5 (Bergh, 2012; Netili, 2007; Smit, 2003). The microbial degradation of soil organic matter reduces the oxygen content of soil and ground waters and these acidic, reducing waters then leach out metals from the soil and underlying bedrock as it flows through the soil and into the fractures of the underlying bedrock. These metals migrate along the hydrologic flow paths within the soil and bedrock until these fluids emerge at the surface and the metals precipitate out as the waters equilibrate with the oxygen-rich atmosphere. Points of oxidation are where the water intersects oxygen again, primarily when it comes into contact with the atmosphere as it exits springs and seeps. The metals will precipitate from the water as it flows out of the bedrock, adding layer upon layer of metal oxides.

Compton (2004) proposed a basic lateral secretion model occurring within the Cape Peninsula (Figure 1). He proposed a reduction-oxidation (redox) reaction which included the release of potassium ion from the dissolution of minerals. The mineral depicted in Figure 1 is potassium feldspar but because little if any potassium feldspar was observed in the Peninsula Formation sandstone, it is here proposed that most of the potassium is released from the dissolution of mica minerals which were described in Chapter 3. The dissolution of mica and release of potassium is the most likely source of the potassium required for the

formation of the principal manganese mineral found on the Cape Peninsula, cryptomelane.

There are three critical aspects to the lateral secretion depositional model in the Cape Peninsula: finding a redox reaction to fit the lateral secretion model, showing the link between the fluids and the manganese and, finally, showing that the redox reaction and the fluid flow paths are consistent with field observations.

It is also possible that the lateral secretion model is just the secondary process to the formation of the manganese, and that these are Type 8 supergene enriched sandstone claystone deposits, where the supergene enrichment is caused through lateral secretion.

4.1.1 Field Evidence Supporting the Lateral Secretion Model

The discussion above focuses on establishing a link between the water and the manganese rich deposits, and in outlining how that a redox reaction can be fit to the depositional environment. What has not been shown is evidence of the redox reaction in the field. The following discussion shows that field mapping, and thin section and microprobe analysis support the redox, lateral secretion model of manganese deposition.

In the field, iron staining was commonly observed to extend deeply recessed into the rocks (Figure 13) and in heavily weathered exposures where the surface material had been removed (Figure 16 – right hand image). At the scale of thin section analysis, minor iron staining was commonly observed within tightly cemented and only slightly weathered sandstone (Figure 46) whereas manganese staining was not. Microprobe analysis shows that iron staining tends to occur along very narrow veins in the rocks, including relatively unweathered sandstone samples (Figures 56 and 57). These observations suggest that, in comparison to manganese, the iron staining occurs deep within the bedrock. This suggests that during periods when the area had active fluid flow, and was unweathered, the iron staining would have occurred deep within the rock in a then narrow void within the rock where oxygen penetration from the surface would have been minimal.

The road cut at the Rooi Els site has revealed the deep interior nature of the manganese deposit (Figure 27). Massive, thick deposits of manganese occur at the surface and diminish into the bedrock. The number and width of fractures within the Peninsula Fm bedrock decrease from the surface to the interior of the cut exposure and reveal that iron tends to occur within the fine fractures of the interior whereas manganese tends to occur in the outermost, larger fractures near the surface. For example, Figure 47 (right hand image) was taken of sample B4 from the Rooi Els site. This sample was collected from the solid rock portion of the Rooi Els manganese exposure, near to where the addit is. While manganese deposition is prominent in this exposure, it is mainly concentrated in large bedrock void spaces while the iron occurs in small fractures and void

spaces located on the edge of the large voids (Figure 47 – left hand image). This same pattern is reflected in the microprobe images of samples C6 and C2 (Figures 56 & 57), with the iron occupying minor void spaces along grain boundaries where no manganese is found. From these observations it can be concluded that the iron is precipitating out first within small void spaces deep within the bedrock.

The lateral secretion model proposes that as the fracture dimensions increase with proximity to the exposed bedrock face, the bedrock void spaces increase and the degree of iron precipitation increases, until a cross over point is reached where significant manganese precipitation occurs with the iron and then becomes dominant approaching the surface. This crossover from iron to manganese is the point where fluids become saturated with sufficient oxygen to raise the Eh to precipitate the manganese out of solution. The observations in the field agree with this, between the addits in Hout Bay and Rooi Els, and the massive surface precipitation in Skeleton Gorge, all three sites concur with the increase in precipitation of the manganese and decrease in iron precipitation with an increase in bedrock void space approaching the exposed bedrock face. Figure 58 of sample B4 which was collected from Rooi Els along the addit shows that as the void space increases, the amount of iron precipitating tails off, while the manganese precipitation increases.

4.1.2 Redox Reaction of Manganese and Iron

Supporting the idea that the manganese within these deposits is formed through a redox reaction is the correlation of molybdenum and manganese (Figure 68). From Adelson et al. (1999) and Drahota et al. (2010), the presence of enriched molybdenum within a marine or fluvial environment is attributed to molybdenum following manganese during manganese reduction and oxidation through the natural anoxic/oxic boundaries. The redox reaction affects the manganese contained within these fluvial or marine environments, with the molybdenum following the manganese throughout the cycle. Molybdenum only leaves the redox cycle during the reduced phase when it interacts with organic thiols or concentrated H_2S and then gets taken up within the sediment profile. Decreasing oxygen within the marine or fluvial environment results in a large anoxic region, and more free molybdenum is taken up within the sediment profile (Adelson et al., 1999). The correlation of molybdenum and manganese within the Cape Peninsula suggests a similar redox process, albeit in a different environment and reversed order. Without significant amounts of H_2S or organic thiols, the reduced molybdenum remains in solution and combines with the manganese during the oxidation of the manganese.

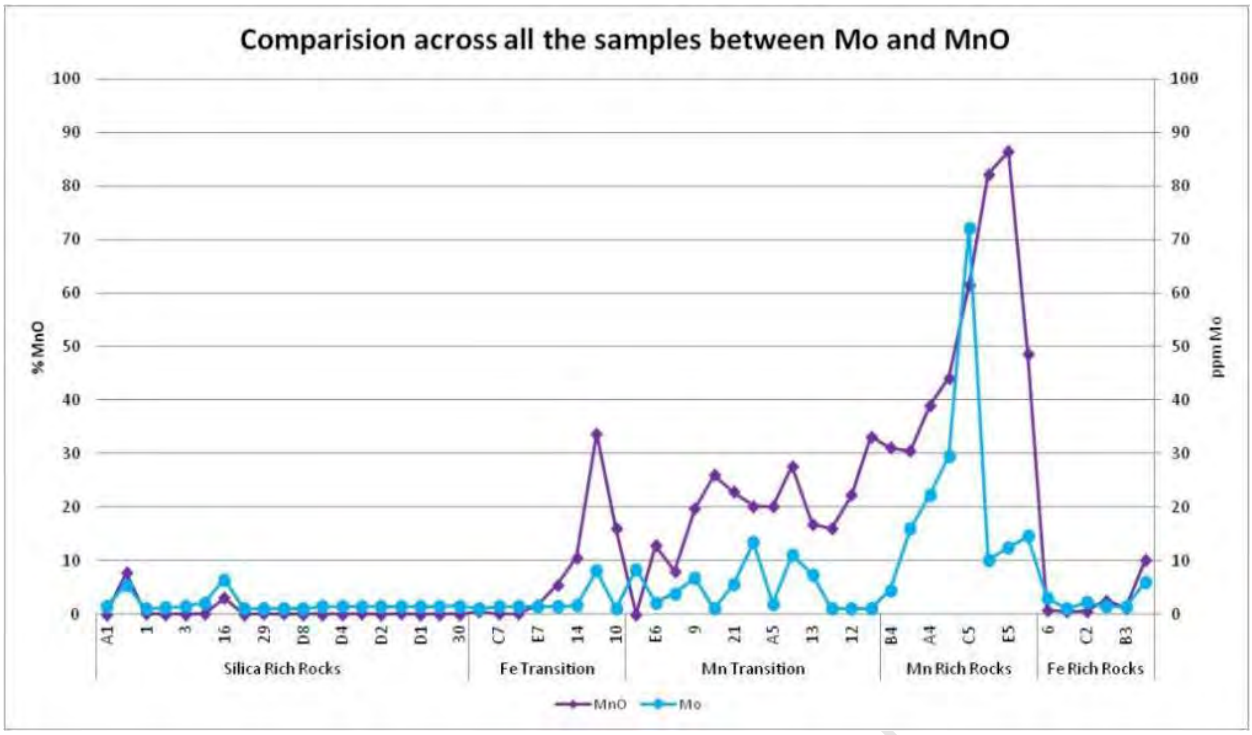

Figure 68: Correlation of molybdenum and manganese suggesting the presence of a redox reaction.

Along with the positive correlation of the molybdenum and manganese, is the fact that the dissolution of manganese in shallow soil profiles and iron in deeper soil profiles (Figure 69) is commonly observed (Martin, 2003). The dissolution of manganese coupled with the correlation between molybdenum and manganese suggests that a redox reaction is taking place within the Cape Peninsula.

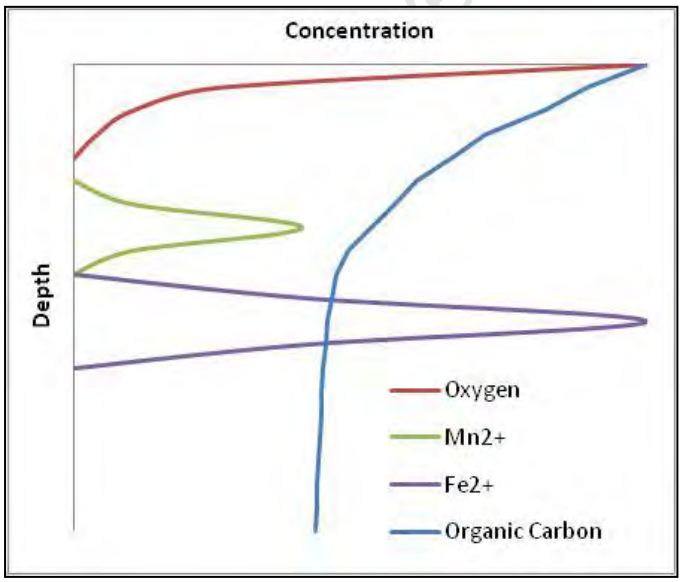

Figure 69: Dissolution pattern within an average soil profile with depth. Adapted from Martin (2003).

Redox reactions of manganese and iron hinge around the reduction of Mn(IV) and Fe(III) to Mn(II) and Fe(II) and then the oxidation back to Mn(IV) and Fe(III). Redox reactions involving manganese and iron are common in the natural environment with soluble manganese and iron occurring in ground water. In the event that this soluble manganese and iron in the anaerobic ground water encounters oxygen, the manganese and iron come out of the solution as highly insoluble oxides (Lovley, 1991; Graham et al., 1988). Based on the fact that the water flows through an organic rich soil horizon where carbonic acid is formed, Figure 70 shows the assumed redox reactions, with the formate (the anion in the formation of formic acid) being CO_2.

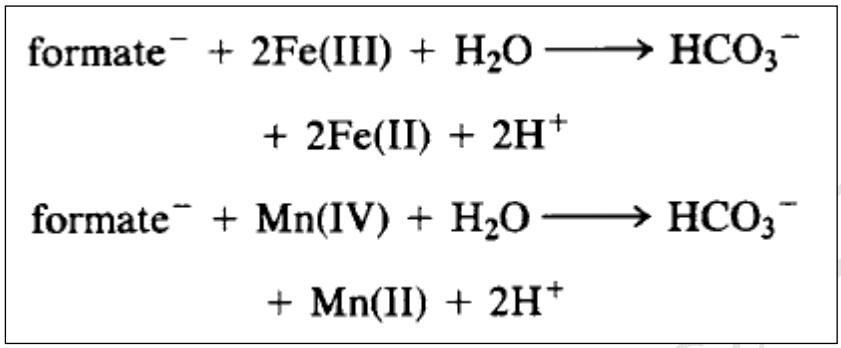

Figure 70: Redox equations of the reduction of manganese and iron within the soil horizon (Lovley, 1991).

While this is an applicable redox reaction to fit the environment, this does not necessarily mean that the environment is conducive to the reduction of the solid Mn(IV) into soluble Mn(II) and or the solid Fe(III) into soluble Fe(II), or that a redox reaction could form cryptomelane, the manganese mineral associated with the deposits. Synthesis of cryptomelane in a laboratory is carried out through redox reactions involving potassium permanganate and adjustments made to the pH of the fluids (Barrio et al., 2007; Banerjee et al., 2009; Feng et al., 2011), while in the natural environment the alteration sequence of manganese oxides, Mn(II), to higher order more stable oxides, Mn(IV), goes through a cryptomelane phase through a natural redox reaction (Nahon et al., 1989). All of this indicates that the formation of cryptomelane through a redox reaction is possible.

The reduction of manganese and iron will depend on the location of the manganese and iron redox reactions within the Eh-pH space of the environment. Eh-pH diagrams show the stability of different compounds at specific temperatures and pressures given changing proton states (pH) and changing electron states, or the state of the free voltage of the environment (Eh). The pH measure is between 0 (acidic) and 14 (basic) and where 7 represents a neutral environment. A lower pH means that there is an excess of free protons and a higher pH means that there is a shortage of free protons. The Eh measure is between 1.2 (oxidised) and -0.8 (reduced) where 0 denotes an environment

with no electron potential. A low Eh means the environment is reducing resulting in the loss of electrons, while a high Eh means the environment is oxidising resulting in the gain of electrons (Martin, 2003). Simplified this means that the Eh-pH of the environment is dependent on the activity level of oxygen (Eh) and the activity of the hydrogen ion (pH) of the fluids within which the manganese and iron occur (Martin, 2003).

While pH testing of the water was not conducted in this study, the pH of the fynbos dominated catchment areas of the Western Cape has been shown in other studies to be 3.5 − 4.5 versus the rainwater pH in the same region of 5.6 (Bergh, 2012; Compton, 2004; Netili, 2007; Smit, 2003). The relatively low pH of streams draining the TMG supports the initial phase of the lateral secretion model where the combination of the soils and rain water form a weak carbonic acid within the ground water system that generally lacks minerals to neutralise the acidic (low pH) waters. The measured values of pH reported in the literature of 3.5 to 4.5 give a range to predict the position of a typical fynbos TMG environment similar to the study area on the Eh-pH diagram. The Eh will depend on what stage within the lateral secretion model the fluid is in. At the initial reducing stage when the manganese is being dissolved, the Eh will be very low and when the fluids reach the seeps and springs and the fluids are re-oxygenated the Eh will be high.

Below are two Eh-pH diagrams (Figure 71) representing the thermodynamic properties of manganese and iron at 1 atm and 25^{O}C (Dill et al., 2010). The yellow shaded areas represent solid phases, the red lines boundaries between the solid phases, the blue shaded areas represent aqueous phases and the dashed lines show the boundaries of stability of water. Hematite represents the solid oxide of Fe (III) and pyrolusite represents the solid phase of Mn(IV).

Of the manganese occurring within the compound cryptomelane, 90% of it is Mn(IV) (Gruner, 1943) which is pyrolusite ($Mn^{4+}O_2$, WEB4), making the pyrolusite stability field a good indicator of the cryptomelane stability field. Based on a starting pH of 5.6 (rainwater) and a final pH of 3.5 (rivers flowing in streams off Table Mountain fed by surface and groundwater flow) and a Eh pattern reflecting the entry into the soil profile and exiting at the seeps of the fluids, the green line would represent a possible evolution of the fluids within Table Mountain on their flow path from the surface soil cover through the bedrock and then exiting out of a seep.

This redox process also affects the silica, this was noticed in the iron embayments within quartz of the thin sections (Figure 47) and the shared precipitation of iron and silica in the microprobe images (Figure 67). Harder (1976) and Bennet et al. (1988) both showed how low temperature dissolution of quartz followed by the formation of iron alumino-silicate minerals was possible. It is suggested that this is the methodology by which the embayments are being formed, and by which the iron and silica are sharing the same void space.

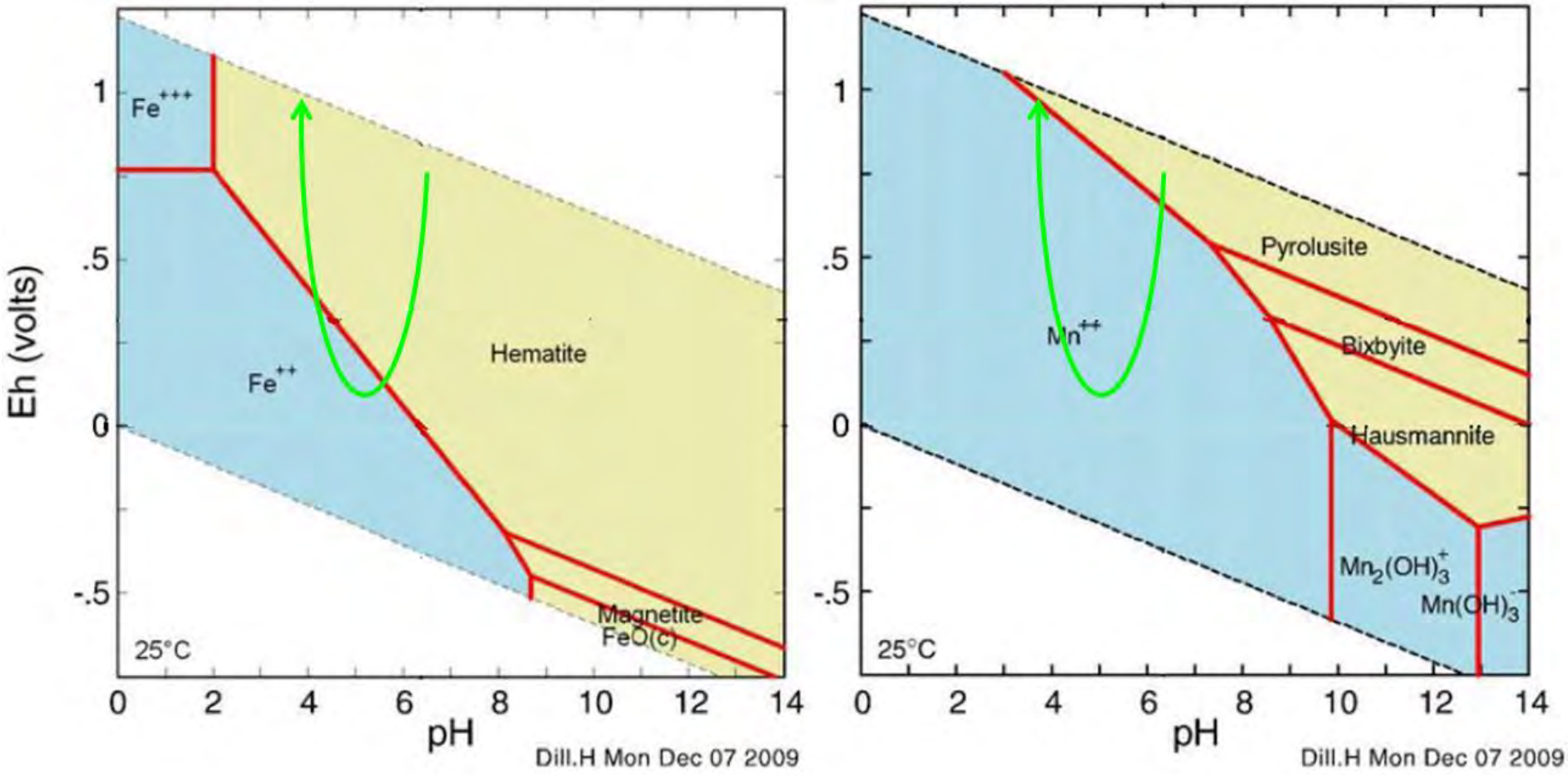

Figure 71: Eh-pH diagrams for manganese and iron (Dill et al., 2010). The blue represents aqueous phases, the yellow solid phases and the red lines boundaries between the different compounds. The white represents where the fluid would become unstable. The green line shows the suggested evolution of the fluids moving through the TMG as rainwater forms subsurface groundwater which eventually emerge at surface seeps.

The flow path and changing redox conditions are depicted in Figure 72. Rainwater will have an initial pH of around 5.6 and a relatively high Eh from dissolved free oxygen in equilibrium with the oxygen-rich atmosphere. Iron and manganese oxide minerals will both be stable in the solid form in contact with surface rainwaters. The bacterial degradation of soil organic matter removes free oxygen and releases CO_2 in subsurface, organic-rich soils. As the rain water percolates into such soils it will re-equilibrate with the CO_2-rich and O_2-depleted soil atmosphere, taking up CO_2 and losing O_2 to become more acidic with a lower pH and more reducing with a lower Eh than rainwater. The loss of O_2 and drop in Eh causes the manganese oxide, Mn (IV), to become unstable and react with the excess electrons to form Mn (II) which is soluble in acidic water. As the fluids move deeper into the soil profile the low Eh results in the Fe (III) no longer being stable and it too gains an electron and becomes soluble Fe(II).

These metal rich fluids then move through the regolith and bedrock fractures as groundwater where the low Eh and pH is maintained and the Mn(II) and Fe(II) remain in solution. These fluids, with their low pH and low Eh, will alter mica minerals encountered along their flow path through the Peninsula Formation bedrock and other ions such as potassium, sodium and magnesium will be introduced into the fluid. These waters may also leach more iron and manganese from minerals present in the bedrock. As the fluids flow laterally and approach a seepage point they will encounter oxygen that has penetrated into the cracks and open pores of the bedrock resulting in an increase in Eh until the Fe(II) becomes unstable and precipitates out as Fe(III) within the open cracks and pores of the bedrock. The Eh will continue to increase as these fluids approach the surface with a sudden increase in Eh as the fluids exit the bedrock and encounter free oxygen present in the atmosphere.

The increasing Eh will result in an increase in precipitation of Fe(III) within the increased open pore space associated with the proximity to the weathered portion of the outcrop face and the seepage point. As these fluids exit the bedrock and the Eh increases dramatically, the Mn(II) will become unstable and precipitate out as Mn(IV) on the surface of the rocks, bonding with the available potassium to form cryptomelane. Most of the manganese in the cryptomelane will be Mn(IV) but some will occur as Mn(II). It is assumed that due to the preferential precipitation of the Fe(III) within the bedrock at relatively low oxygen levels most of the iron comes out of the fluid before the manganese. By the time the fluid reaches the bedrock face, most of the iron has already been removed and manganese remains to precipitate out near or upon the surface exposure of the bedrock. The above would explain the field observation of iron rich early precipitation followed by more massive manganese precipitation seen in this study. This same phenomenon has been seen more commonly in volcanogenic sources of lateral secretion deposited manganese (Harrison, 1998), but also shown to exist in sedimentary processes (Krauskopf, 1957).

As the fluids exit the surface seeps and join the streams flowing off the mountain the Eh will stabilise and remain high, but some of the remaining Fe(II) and Mn (II) stays in solution as seen in the water ICP-MS results (Table 21).

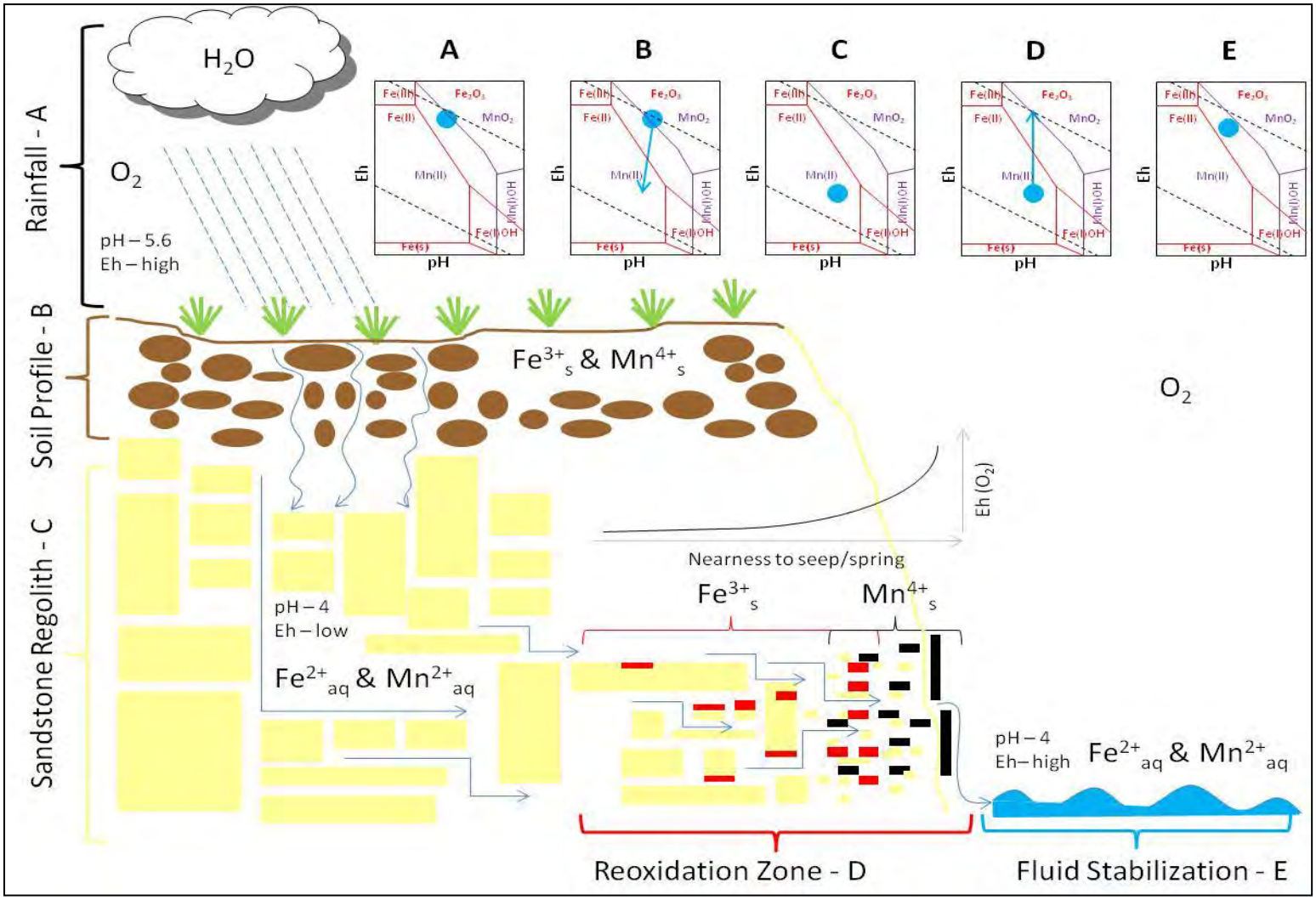

Figure 72: Schematic showing the change in Eh-pH for Mn and Fe during the flow path of the fluids with the lateral secretion model. Rainfall (A) percolates through the soil profile and becomes acidic and reducing and leaches Mn and Fe from the soil into solution (B). The fluid continues to move through the regolith and bedrock fracture fluid pathways dissolving additional Mn and Fe as well as K from mica mineral dissolution (C). When the fluid eventually flows laterally to an oxidation front where first Fe and then Mn are precipitated out as oxides Mn(IV) and Fe(III) (D) and finally the fluids stabilise with streams carrying the remaining Mn(II) and Fe (II) in solution.

4.1.3 Environment of Manganese Deposition

The hypothesis above implies that the manganese and iron were deposited in a low-temperature fresh water seep environment. Manganese can be deposited under multiple fluid environments, low or high temperature, and marine or fresh water. To test which of these environments apply to the manganese deposits of this study, various elemental comparisons and ternary plots were built in order to isolate the environment. As this was designed to test the manganese and iron rich deposits, the results from the unmineralised source rocks were excluded from all graphs (Table 23). Figure 73 differentiates between fresh water, shallow marine and marine waters (Nicholson, 1992; Gültekin, 1998). The basic definition of marine water is water containing more than 1000 ppm of dissolved solids and fresh water has less than 1000 ppm of dissolved solids (Brookhart et al., 1958). Nicholson's (1992) classification of manganese ores forming within a fresh or saline environment is dependent on the natural salts present in the fluids. The most common salts are magnesium and sodium (Swenson, 2012) and higher portions of these salts will result in the fluid being classified a marine fluid. All samples fall into the fresh water category (Figure 73).

Table 23: Element composition of highly enriched manganese rocks plotted in Figures 73-75.

	Sample	Figure 63		Figure 64		Figure 65		
	No	Na	Mg	Th	U	Co x 100	Mn	Fe
Fe Transition	**31**	0.1	0.1	3.2	0.9	2.3%	13.1%	84.6%
	C7	0.1	0.1	4.3	1.9	11.7%	3.7%	84.6%
	C6	0.0	0.1	15.3	2.9	6.0%	2.3%	91.6%
	E7	0.1	0.1	0.9	2.8	10.1%	10.6%	79.2%
	B2	0.1	0.1	7.3	2.3	6.1%	36.3%	57.6%
	B6	0.2	0.1	2.1	11.5	1.8%	81.4%	16.8%
Mn Transition	**E6**	0.4	0.1	3.9	2.2	9.0%	87.2%	3.8%
	25	0.0	0.1	4.9	1.5	0.3%	96.3%	3.4%
	A5	0.2	0.1	4.3	5.2	2.6%	74.1%	23.3%
Mn Rich	**B4**	0.4	0.1	7.7	3.7	18.0%	80.0%	2.0%
	A4	0.2	0.1	4.9	3.8	2.3%	92.0%	5.7%
	A6	0.2	0.1	1.3	1.4	1.4%	95.7%	2.9%
	C5	0.4	0.1	0.2	18.1	1.4%	83.0%	15.6%
	E3	0.3	0.1	1.7	1.9	4.9%	94.9%	0.3%
	E5	0.2	0.1	0.1	1.2	4.3%	95.6%	0.1%
	E8	0.5	0.1	6.4	11.4	4.0%	75.6%	20.4%
Fe Rich	**C2**	0.1	0.1	1.2	3.3	6.4%	1.6%	92.0%
	E2	0.3	0.1	1.0	0.6	9.8%	8.3%	82.0%
	B3	0.1	0.1	21.2	35.6	2.2%	3.7%	94.1%
	E4	0.1	0.1	1.8	9.6	16.3%	21.9%	61.8%

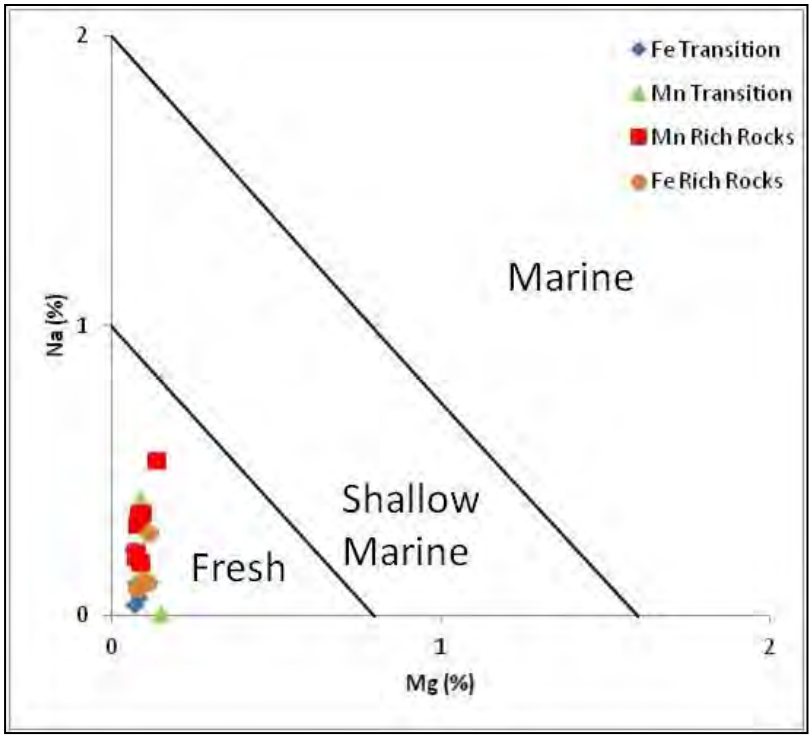

Figure 73: Environment classification of the manganese deposits of this study based on Nicholson (1992). Na content of the ores is plotted against the Mg content to differentiate between fresh, shallow marine and marine deposits.

Nicholson's (1992) work also showed the most reliant method of differentiating between hydrothermal and hydrogenous deposits across all depositional environments. Hydrothermal refers to hot water (>25^{O}C); hydrogenous (supergene) refers to cold (<25^{O}C) water, as described by Lindgren (1933). To differentiate between the two, Nicolson (1992) plotted As+Cu+Mo+Pb+V+Zn against Co+Ni. As zinc and arsenic were not evaluated in this study, two sets of graphs from Bonatti et al. (1972) were used instead.

The graphs from Bonatti et al. (1972) are commonly applied to deep water formations of manganese such as manganese nodules but are still useful in differentiating between hydrothermal and hydrogenous manganese. Bonatti et al. (1972) showed that the ratio between U/Th could be used to determine if manganese nodules formed through hydrogenous or hydrothermal means, as higher contents of thorium in a nodule would suggest a slower rate of growth and thus a hydrogenous component (Brink et al., 1996). The uranium and thorium contents of the samples from this study indicate that the deposits are predominantly hydrogenous rather than hydrothermal in origin (Figure 74).

As per Nicholson's (1992) work, the presence of additional cobalt is an indication of a hydrogenous origin to the manganese (Balaram et al., 2012). The ternary diagram in Figure 75 shows that the half of the points lies convincingly within the hydrogenous field. It is important to bear in mind that these plots are designed for a marine manganese deposit, however, with the combined U/Th and the ternary diagram it can be stated that the fluvial environment is hydrogenous.

These results are consistent with the lateral secretion depositional model as outlined in the previous section with manganese and iron oxide deposited from low-temperature (hydrogenous) fresh waters. Thus these deposits are not Type 1 hydrothermal deposits.

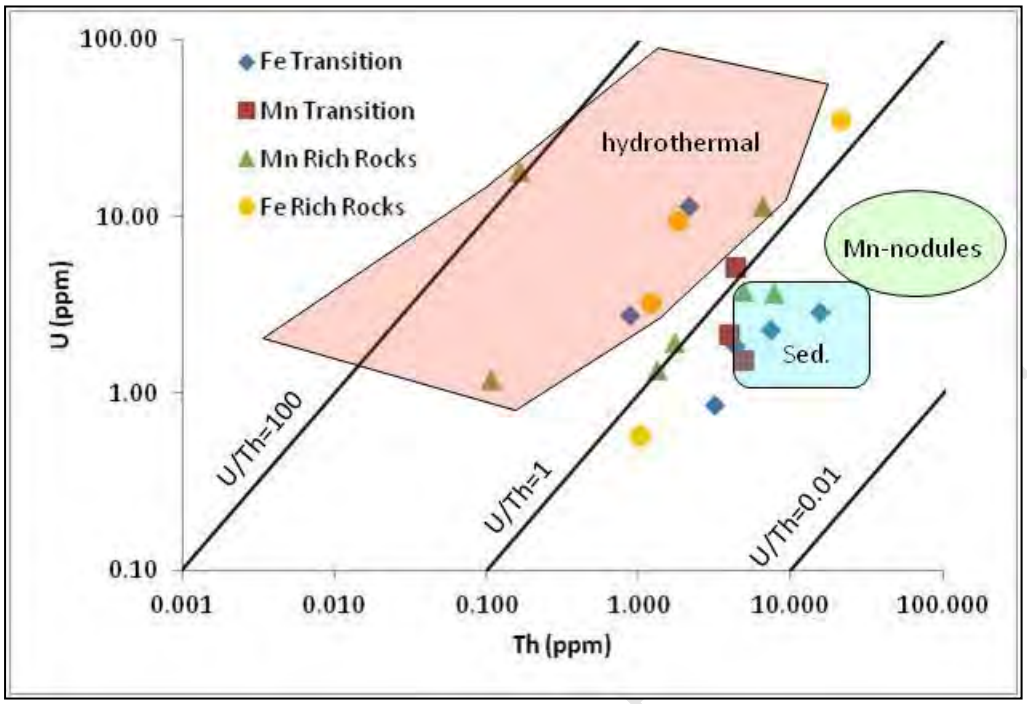

Figure 74: Uranium vs. thorium content of samples from Table 23 compared to fields of manganese formation defined by Bonatti et al. (1972).

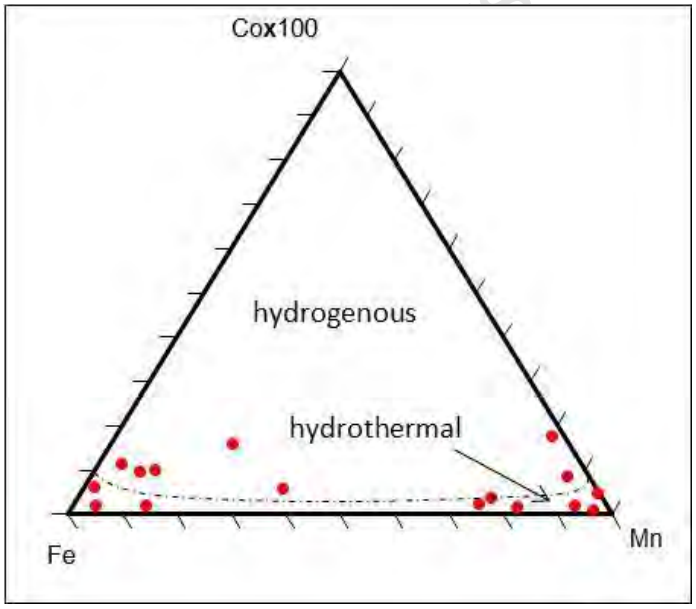

Figure 75: Ternary plot as devised by Bonatti et al. (1972) differentiating between hydrothermal and hydrogenous manganese formation. Samples from this study (Table 23) plotted as red points.

4.2 Fluid Flow Dynamics

The following section discusses how the fracture porosity of the rocks, the faults within the depositional sites, and finally the overall fluid dynamics of the depositional sites influence the location and degree of manganese and iron deposition.

4.2.1 Porosity of the Rocks

The lateral secretion model requires that the bedrock (including soil and regolith) be sufficiently porous and permeable to allow the flow of fluids. In some of the depositional sites there appeared to be aquitards or aquicludes, the siltstone layer within the Skeleton Gorge site for example (Figure 15), which restrict and influence the flow of groundwater to seep sites. Porosity and permeability tests were not conducted as part of this study, but through a literature review and the field observations it is possible to come to the following conclusions about the aquifers and aquitards that affect the flow paths.

Aquifers

Of the five rock formations on the Cape Peninsula only the fractured Peninsula Fm and unconsolidated Quaternary sediments have the potential to be aquifers. Based on field observations, all of the manganese rich deposits occur within the Peninsula Fm sandstone or in Quaternary alluvium overlying the Peninsula Fm, so this implies the Peninsula Fm is the best aquifer through which to transport the manganese rich fluids. At Rooi Els the manganese deposit occurs within the talus slope. The talus slope is a Quaternary sedimentary deposit, the material in the talus slope is made up of Peninsula Fm sandstone, but its effective porosity will be completely different from that of bedrock Peninsula Fm sandstone being made up of unconsolidated gravel and sand sized material.

Porosity is the measure of the pore spaces in a rock. Permeability is the measure of how easily a fluid can move though a rock. A rock might have a high porosity, but a low permeability, making it a poor aquifer. It is the combination of both porosity and permeability, the effective porosity, which makes a good aquifer (WEB2). Table 2 shows the effective permeability based on averages from global samples. Aeolian sand was included in this table in order to give some sort of frame of reference for comparison. As can be seen the aeolian sand, which is a loose unconsolidated sediment, has an effective porosity of 0.38, which, when compared to the other mediums is close to the medium grained sandstone of 0.27.

From these global estimates it is possible to see that the sandstone is a much better aquifer than even the unconsolidated sediments of the talus slope. This makes it likely that the Peninsula Fm is an aquifer through which the fluids are moving. It is important to note however, that the Peninsula Fm sandstone has

lower porosity than shown above as it is tightly cemented; but that this is offset by additional fracture porosity as these rigid hard rocks are highly fractured in places allowing for the effective through flow and storage of water (Jia et al., 2009). Based on Jia et al. (2009) the effect of the cementation is marginally offset by the fractures occurring in the Peninsula Fm sandstone, the end result being that the unconsolidated talus slope will have a higher effective porosity than the Peninsula Fm sandstone. Out of the potential aquifers existing in the bed rock, the studies from Jia et al. (2009) and Blake et al. (2010) show that the only plausible bed rock aquifer in the study area is the fractured Peninsula Fm, with the Cape Granite Suite, and Malmesbury Group acting as aquitards (Figure 76).

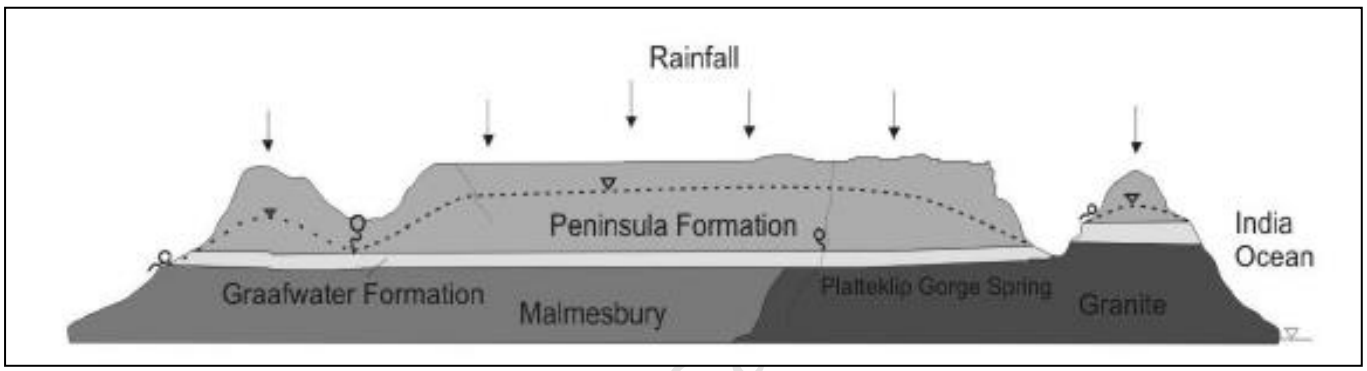

Figure 76: Groundwater flow paths through aquifers and around aquitards within Table Mountain, from Jia et al. (2009).

Aquitards

While the aquifers allow for the flow of the fluids, the faults which bound the deposits could either be aquitards or aquifers. From observations in Skeleton Gorge it was noticed that the fault which runs along the gorge valley separates manganese rich deposits on the northern slopes from relatively minor manganese deposits on the southern slopes. Within the fault breccia, Site 8, only minor iron staining was noticed. Due to overgrowth and rock falls it was not possible to follow the bedrock laterally away from the valley floor breccia.

Not only did the fault appear to influence the distribution of manganese within Skeleton Gorge, but within Site 3 & 4 of Skeleton Gorge there is a siltstone layer (Figure 15) inside the overhang within the Peninsula Fm sandstone. The thin section analysis of the siltstone layer showed that it is rich in clays and highly cemented, the field observations showed very little fracturing within the siltstone and that there is no manganese below it, suggesting that it acts as an aquitard forcing groundwater to flow laterally to the manganese rich seeps above it. Table 2 shows the effective porosity of the proposed aquitards in the study areas.

By reviewing these potential aquitards against the proposed aquifer, Peninsula Fm sandstone, it is possible that the uncommon and discontinuous siltstone layers within the Peninsula Fm and the underlying Graafwater Fm, Cape Granite

Suite and Malmesbury Group would all act to retard the flow of water, and could potentially act as aquitards, forcing groundwater flowing through the Peninsula Fm to flow laterally along the contact to exit eventually at surface seeps. It is proposed that fault breccia would act as an aquitard and retard the flow across the fault and instead guide the fluids along the fault surface until the waters exit at the surface. This would make faults a key factor in the large scale precipitation of manganese and iron oxides.

4.2.2 Fault Bounded Deposits

Most faults in the study area are normal faults that formed during the extensional breakup of Gondwana circa 130 Ma (Anhaeusser et al., 2006). The offset on the faults is moderate but they define the occurrence of most of the mountain gorges and valleys in the study area. From the field descriptions and the geological maps it is known that deposits occur around areas where there are faults. The proposed influence of faults on the deposition of manganese rich deposits is represented schematically in Figure 78, modelled on the case of the Skeleton Gorge site. The faults create areas of weakness in the competent rock, and as such these areas of weakness are exploited with weathering and erosional processes and gorges are created. Thus the faults create a physical focal point in the topography where the manganese deposits can occur and assist in the channelling of groundwater flow through the highly fractured rock surrounding the fault.

Not only are the effects of the faults visible on a macro scale (with the formation of the gorges) but also within the microscopic scale (Figure 79). The rock samples from the control group showed the typical Peninsula Fm quartz grains un-fractured, sub rounded to rounded grains while the samples taken from the Sample Sites showed quartz grains with fractured sub angular grains. The shape of the grain changes to angular and the fracture intensity increases closer to the faults which occur within the sample sites.

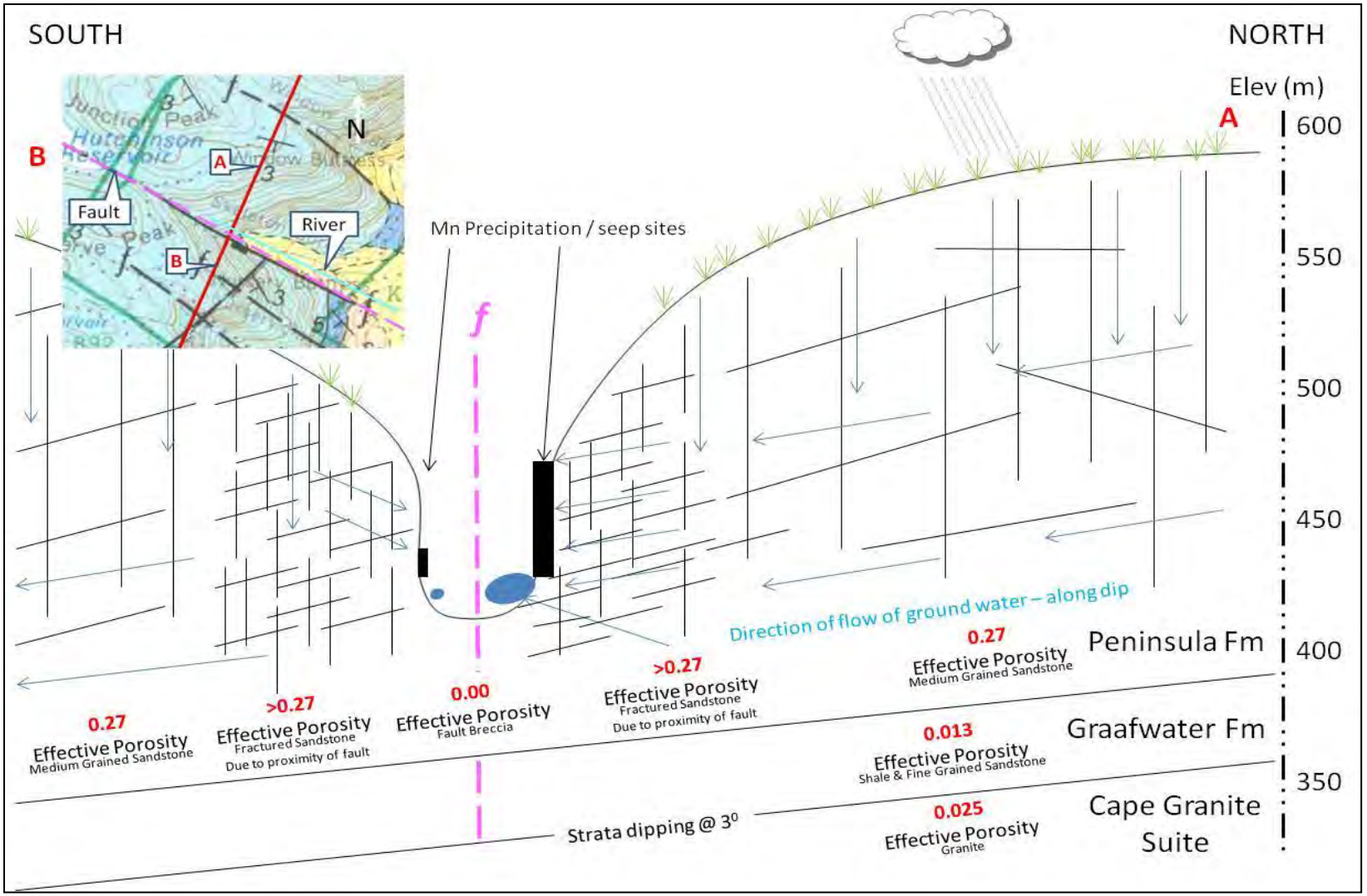

Figure 77: Cross section of the Skeleton Gorge deposit (as shown in the geological map insert, A-B) showing the influence of the fault on the fluid dynamics of the deposit. The blue arrows indicate the approximate fluid flow paths. Rainwater moves into the aquifer (Peninsula Fm) and then flows along dip above the less porous Graafwater Fm and Cape Granite Suite Fm, towards the more porous faulted bedrock which allows for faster and higher levels of fluid flow. Finally the fluids reach the fault zone which acts as an aquitard forcing the fluids to seep out of the rock.

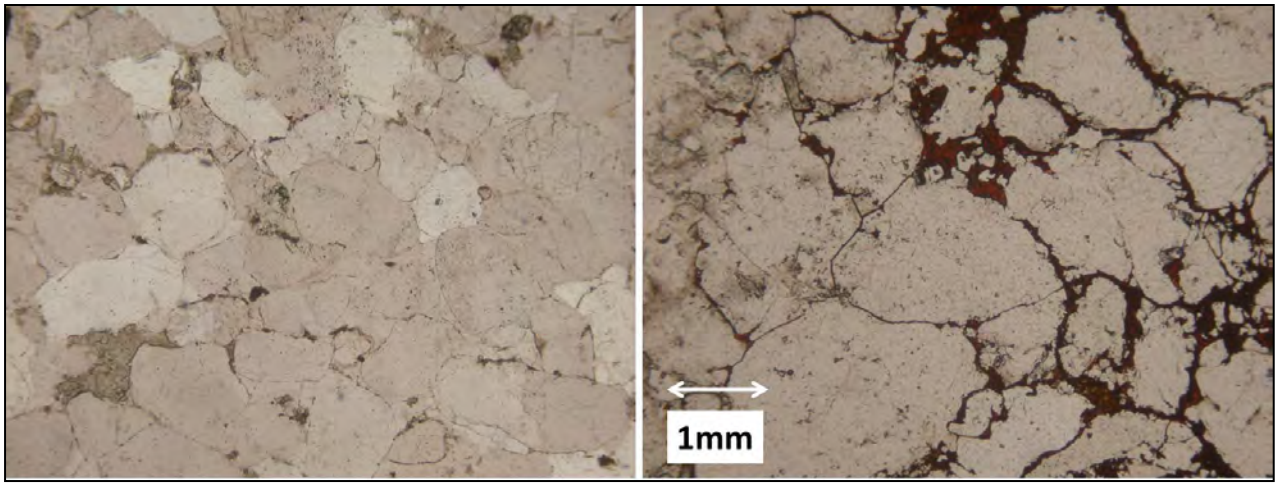

Figure 78: Thin Section of sample D3 of Peninsula Fm sandstone (left) sample B6 (right) in plane light. Sample D3 shows the typical rounded to subrounded quartz grains, while B6 shows more subangular quartz grains with a higher degree of fractures.

The hypothesis that faults bound these deposits was only tested once during the field mapping by following the fault line of Skeleton Gorge to the other side of Table Mountain. This resulted in the discovery of the Kasteelpoort Gorge manganese and iron deposit. While it is not as extensive as the Skeleton Gorge deposit, the fact that it exists along the same fault suggests that the fault in some manner assists in the precipitation of the manganese. This suggests that at every fault location within Peninsula Fm sandstone, where there is a gorge, some large scale manganese and iron deposit, larger than just the normal superficial surface coating, should be found.

Apart from Skeleton Gorge and Kasteelpoort Path, Hout Bay was the only other deposit where a fault could definitively be seen at the depositional site (Figure 32). The Kommetjie manganese deposit is not in place and therefore difficult to determine the influence of the local faults on its deposition, and the Rooi Els deposit was too laterally extensive and covered in talus slope material. For Kommetjie however, at point 2 of Figure 29 a fault line can be seen that if continued would run through the location of the Kommetjie deposit, suggesting a potential link to the fault structure during the deposition of the deposit.

The Skeleton Gorge and Kasteelpoort Path manganese deposits appear to be recent, with unweathered surfaces over weathered surfaces, and are clearly aligned with a fault. The deposits were both concentrated to the northern, up dip portion of the gorges, with the fault running through the centre of the gorge. The southern, down dip portion of the gorge had no major manganese or iron precipitation with the exception of thin coatings on some boulders. The fault therefore appears to control where major manganese precipitation occurs with most manganese concentrated on the northern (down dip) rather than southern (up dip) side of the fault.

In summary, while the faults may become a weak point within the overall geology, and form a topographical feature in terms of a gorge, most importantly

they do not allow the manganese rich fluids to flow further down dip because of the low effective porosity of the fault breccia. Instead, the fault breccia forces flow along the fault surface where the rock is fractured and more porous, concentrating the fluids into a single location, until the fluids exit the rock, generally at a topographical feature (e.g., a valley) formed by the fault.

4.2.3 Mass Balance

Is there sufficient manganese and iron within the water that feeds some of these sites to form the deposits observed? The manganese and iron concentrations, determined by ICP-MS analysis of waters associated with the sites, were compared to the size of the manganese and iron deposits at Skeleton Gorge to try and answer this question.

The concentrations of manganese and iron (Table 21) show that water found along the Skeleton Gorge is above the standard average for water around the world. For example, the manganese concentration in river waters in the USA ranges from 11 – 51 $\mu g.l^{-1}$ (WHO, 2011) which is 0.011 – 0.051 ppm and the iron concentration in river waters in USA is 0.7 $mg.l^{-1}$ (WHO, 1996) which is 0.7 ppm. This means that the iron and manganese concentrations across the gorge are between 100 – 100000 times greater than average river waters from the USA.

Table 24 shows a rough calculation used to determine if the flow rates of the seeps and streams coupled with the high concentration of manganese in the water would be sufficient over time to form the deposits. This calculation does not take into account erosion of the deposits and does not include iron. The size of the iron deposit in Skeleton Gorge is difficult to estimate as most of the iron is not exposed in Skeleton Gorge. By analogy with other sites such as Rooi Els it is assumed that the iron in Skeleton Gorge occurs deeper into the bedrock than the surface manganese deposits.

Table 24: Calculation of time required to form the Skeleton Gorge manganese deposit from present-day waters.

	Units	Lowest	Average	Highest
Average Flow Rate	($l.min^{-1}$)	4	4	4
Manganese Concentration	(ppm)	3	149	1 006
	($g.l^{-1}$)	0	0.1	1
	($g.min^{-1}$)	0	1	4
Manganese Deposit	Size (m^3) (150m x 30m x 0.02m)	90	90	90
	Tonnes @ 4.36$g.cm^{-3}$	392	392	392
	Tonnes of Manganese present (60% of Cryptomelane compound)	233	233	233
	Grams	233 035 959	233 035 959	233 035 959
Time taken to form deposit	(minutes)	22 742 888 230	390 638 954	57 921 440
	(years)	43 270	743	110

The size of the manganese deposit was estimated from Sites 3 & 4 as this was the largest established site within the area where water was analysed. The manganese deposit at Sites 3 & 4 was estimated to be 150 m wide x 30 m high x 0.02 m thick giving a total of 90 m^3 of manganese rich rock. This volume was converted to tonnes using a cryptomelane density of 4.36 $g.cm^{-3}$ (WEB3) as this was determined through XRD to be the dominant manganese mineral, giving 392 tonnes of cryptomelane ore. An assumption was then made that the entire deposit is cryptomelane and the cryptomelane tonnes were converted to pure manganese tonnes by determining the weight percentage of manganese within cryptomelane. The flow rate at the deposit site was an average of both the summer and winter flow rates as established from seeps coming out of the rock face near to site 3, this was determined to be 4 litres per minute. It is not possible to determine the concentration of the manganese in the water prior to it exiting the face (concentration of manganese in the ground water), so the manganese concentration was based on three possibilities, the lowest concentration, the highest and the average from all the water samples taken (Table 24). Knowing the amount of manganese in the water, the rate of flow, and the amount of manganese within the deposit gave the time taken to form the deposit.

Based on these calculations the Skeleton Gorge deposit could have formed between 110 and 43 000 years using the highest and lowest manganese ion concentration, respectively. While at the lowest concentrations this is a long period, both the average and maximum concentrations form the deposit in an exceptionally short period of geological time less than a thousand years. The rate of manganese deposition is much faster than the rate of rock face erosion which is probably on the order of 10 m/myr (Brown et al., 2008) and it is the relatively slow rate of erosion compared to deposition that allow for the formation of these large scale manganese deposits.

This shows that present-day waters have enough dissolved manganese to potentially account for the historical and on-going regional deposition of the manganese deposits. There is still a question as to what causes certain areas to be high in manganese, and others not considering that the Cape Peninsula is full of small streams, seeps and springs the majority of which are not associated with significant manganese deposition. Thus while the water studied in Skeleton Gorge shows that the flow of water is a contributing factor in delivering the manganese to the site, it is not the only factor in the formation of a relatively large scale deposit.

4.3 Type 1 or Type 8 Deposit

It has now been shown that the fluvial environment supports the lateral secretion model, and would supply sufficient volumes of manganese to form the deposits. It can thus be conclusively stated that lateral secretion plays a role in these manganese deposits. However, whether lateral secretion (Type 1) is the classification of these deposits or if supergene enriched sandstone claystone (Type 8) through a lateral secretion process is the classification of these

deposits, has not been shown. The following section will define whether or not these are Type 1, or Type 8 deposits.

4.3.1 Source of the Manganese

One of the critical components to the formation of these deposits is the source of the manganese. If the source lies outside of the sandstone then that would immediately point to this not being a Type 1 deposit. It has been shown that the manganese is mobilised during reduction in the soil profile and extending into the bedrock below; however, which of the available bedrock types present in the Cape Peninsula is the most likely to supply the manganese that ends up in the manganese deposits? Graham et al. (1988) reported on the amount of manganese locked up in common mineral assemblages and then, based on the mineral data, shows the amount of manganese expected to occur within common rock types. This does not discuss the ease with which the different mineral assemblages could release the captured manganese and purely looked at the amount of captured manganese. Table 25 shows the common minerals which occur in Cape Granite, Peninsula Fm sandstone and the Graafwater Fm sandstone and mudstone and Malmesbury Group shale.

In terms of total manganese content the most likely source rock for manganese would be shale of the Malmesbury Group, then granite typical of the Cape Granite, then muddy sandstone of the Graafwater Fm, then quartz arenite sandstone of the Peninsula Fm. The other factor in addition to how much manganese is contained in these different rock types is how easily the manganese is released and potentially mobilised to the reducing groundwater flow. Because both the Cape Granite Suite and the Malmesbury Group shale bedrock have low effective porosity, the manganese contained within these rock types can only be released in weathered soil profiles and leaching from their much larger bedrock manganese reservoir would be limited by the extent to which groundwaters can penetrate and leach them of manganese. This suggests that either the Graafwater Fm or the Peninsula Fm is the primary source rock for manganese.

Table 25: Manganese abundance in common rocks based on manganese content of common mineral assemblages. Adapted from Graham et al. (1988).

Rock Type	Mineral Assemblages (**ABUNDANT**) (subordinate)	Manganese Concentrations of Minerals($mg.kg^{-1}$)		Manganese Concentrations of Rock ($mg.kg^{-1}$)
		Range	Average	
Granite	**K – Feldspar**	**4-100**	**15**	400
	Quartz	**<100**	**10**	
	Ca – Feldspar	10-400	60	
	Biotite	100-100000	2000	
	Amphibole	100-6500	2000	
Sandstone	**Quartz**	**<100**	**10**	170
	K – Feldspar	**4-100**	**15**	
	Ca – Feldspar	**10-400**	**60**	
	Muscovite	**80-400**	**200**	
Shale	**Quartz**	**<100**	**10**	600
	K – Feldspar	**4-100**	**15**	
	Muscovite	**80-400**	**200**	
	Biotite	**100-100000**	**2000**	

The field observations confirm this assessment of effective bedrock porosity/permeability with no manganese deposits associated with granite or Malmesbury Group shale exposures; manganese deposits are all associated with the Peninsula Fm quartz arenite sandstone. Figure 79 and Table 26 show the bulk rock chemistry for Peninsula Fm and Graafwater Fm samples. From these data it appears that the concentrations of manganese in the Peninsula Fm and Graafwater Fm are too low to be the source of manganese deposits which have concentrations as high as 86wt% MnO. The Peninsula Fm and Graafwater Fm have similar bulk rock manganese contents of 0.038 wt% MnO. While this concentration is low, this is higher than the expected amount of manganese present in quartz arenite sandstone of 0.023 wt% MnO as suggested by Graham et al. (1988). The iron, aluminium and potassium values show a noticeable increase from Peninsula Fm to the Graafwater Fm reflecting the muddier content of the Graafwater Fm. The greater potassium content of the Graafwater Fm may

be important as a source of potassium in the manganese mineral cryptomelane which makes up the deposits. Despite their low bulk rock manganese concentrations, the volume of water rock interaction of the Peninsula Fm and Graafwater Fm needs to be taken into consideration as reflected in their effective bedrock porosity.

Table 26: Major elements of unmineralised TMG rocks (wt%).

	Peninsula Fm					Graafwater Fm				
Sample	A1	B1	D3	D4	**AVERAGE**	D1	D2	D9	D10	**AVERAGE**
SiO_2	94.36	94.30	96.32	95.72	**95.17**	89.16	93.46	88.55	82.09	**88.32**
Al2O3	2.70	3.18	1.11	0.98	**1.99**	6.15	3.19	4.28	9.07	**5.67**
K_2O	0.65	0.75	0.25	0.18	**0.46**	1.66	0.81	2.06	3.76	**2.07**
Fe_2O_3	0.50	0.48	0.93	0.99	**0.73**	0.86	0.60	1.40	2.57	**1.36**
MnO	0.03	0.05	0.03	0.04	**0.04**	0.03	0.03	0.06	0.04	**0.04**

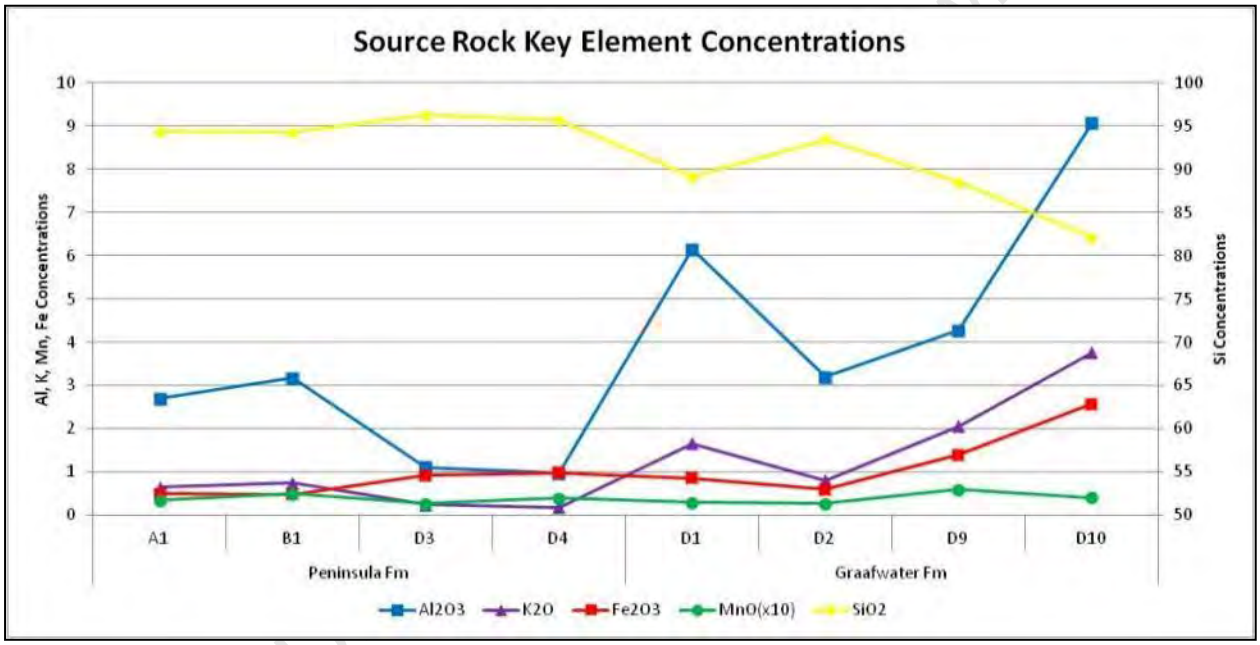

Figure 79: Concentrations of the key elements within possible source rocks of the manganese deposits. Due to the low concentrations of the manganese (MnO) it was multiplied by a factor of ten in order to show the variations on the graph.

Table 27 shows a rough calculation of the potential volumes of manganese that could be produced from the concentrations of manganese and iron in Table Mountain rocks of the Peninsula and Graafwater formations. It is important to note that if the Peninsula Fm and Graafwater Fm are the source of the manganese, then the values that were found during the sampling were already depleted, and that this calculation assumes that all the bedrock will act as a source. However, this is dependent on the fracture porosity which will determine the water to rock ratio or the extent to which the groundwater interacts with the bedrock. However, even with these potentially depleted values and assuming 1% exposure of the bedrock to the groundwater fluids there are more

than sufficient amounts of manganese remaining within Table Mountain bedrock to supply all the manganese deposits found throughout the Cape Peninsula. Therefore, the amount of manganese in the bedrock of the Peninsula Fm and Graafwater Fm are sufficient as a source of manganese for the deposits, but due to the field observations placing all of the deposits within the Peninsula Fm and the better effective porosity of the Peninsula Fm, it is concluded that the Peninsula Fm sandstone is the source rock. This suggests that it is still possible for these deposits to be a Type 8 deposit.

Table 27: Approximate volume calculations of potential total manganese in the Peninsula Fm and Graafwater Fm.

		Peninsula Fm	Graafwater Fm
Thickness around Table Mountain		400	100
Dimensions of Table Mountain up to Skeleton Gorge (Ground water feeder range)	Length (m)	3,000	3,000
	Width (m)	3,000	3,000
	Area (m^2)	9,000,000	9,000,000
Volume of Rock		3,600,000,000	900,000,000
Tonnes of Rock (assume SiO_2 density of 2.62g.cm^{-3} - WEB 5)		9,432,000,000	2,358,000,000
Average Concentration of MnO		0.038%	0.039%
Tonnes of Potential Manganese from Source Rocks		3,584,160	919,620
1% (Assumed Exposure of Groundwater due to Fractures		35,842	9,196

4.3.2 Type 8 Deposit

A sandstone claystone Type 8 deposit was described by Harrison (1998) as a shallow marine deposit formed on the rims of an anoxic basin during a transgression. The common rock formations are sandstone, siltstone, claystone and some marls, generally representing a transgressive cycle. The host rock contains the manganese in thick stratiform layers, and occasionally multiple thin stratiform layers or lenses, in both cases these layers are laterally extensive.

The manganese itself is commonly cryptomelane and can have an abnormally high phosphorus content. The average grade of the in situ manganese is 20-40%, with the average size being 7.3 Mt.

The supergene enriched sandstone claystone deposit follows the same principles, except that it has been supergene enriched post the formation of the sandstone claystone host rock. Long term lateritic process will produce the highest yielding and highest grade ores. The grade of these ores is not specified.

The Peninsula Fm sandstone deposit was formed during a marine regression, in a fluvial environment (Anhaeusser et al., 2006) and the in situ grade of the manganese is only 0.038% MnO. So while the Peninsula Fm sandstone is the source of these deposits, this is coincidental to the type classification. As these cannot be classified as Type 8 deposits, it is possible to state that they are Type 1 deposits.

4.4 REE Analysis

The REE analyses can provide signatures of the source (silica rich) and mineralised (manganese rich) rocks to help assess the source of the manganese and how variable the REE signatures are among the different sample types and areas studied. Figures 40 and 41 show the PAAS normalised REE patterns from ICP-MS analyses for the different types, and for different sites, respectively. From these results a large amount of variation within the REE patterns is seen.

The iron and manganese transition samples have enriched LREE and depleted HREE relative to the source rock (silica rich samples and Contour site) samples. Conversely the iron and manganese rich samples have depleted LREE and enriched HREE relative to the source rocks. Kasteelpoort Path, Skeleton Gorge, the Contour Path and Rooi Els have similar REE patterns whereas Hout Bay and Kommetjie have distinct patterns. Hout Bay has depleted LREE and enriched HREE. Kommetjie has enriched HREE.

Kasteelpoort Path and Skeleton Gorge samples were compared against the proposed source rock samples (Peninsula Fm samples D3 & D4). This revealed that there is a significant difference between the REE patterns for the manganese enriched samples while the iron rich samples are significantly enriched, specifically in the LREE (Figure 80).

This preferential uptake of LREE by iron, coupled with the iron precipitating out of solution first, results in a LREE depleted fluid during the precipitation of the manganese and LREE relative depleted manganese. Based on the individual iron and manganese rich plots, it is the presence of iron which causes the major LREE enrichment within the deposits, similar to the results seen by Compton et al. (2003).

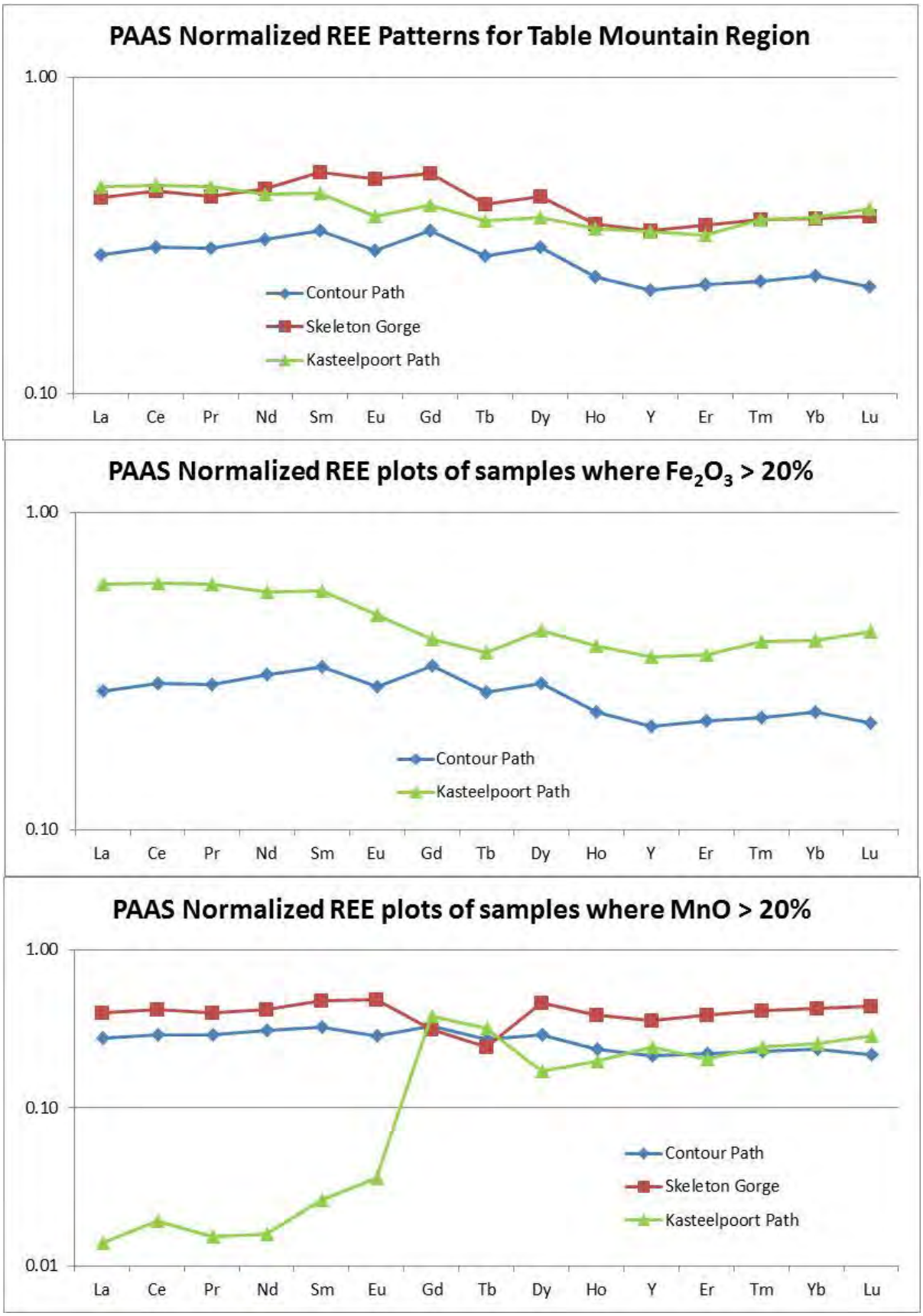

Figure 80: PAAS normalised REE plots of the Table Mountain Region Sites.

The variation in REE patterns may be attributable to variations in the REE signature of the source (silica rich) rocks of the different Sites, to variations over time of the fluids involved in the deposition of the manganese and potentially the different lateral secretion types. The source rocks of Hout Bay and Kasteelpoort are similar but different from the similar source rock REE patterns of the Contour Path, Rooi Els and Skeleton Gorge (Figure 81). The major difference is the Hout Bay and Kasteelpoort source rocks are less depleted in the LREE compared to the other sites.

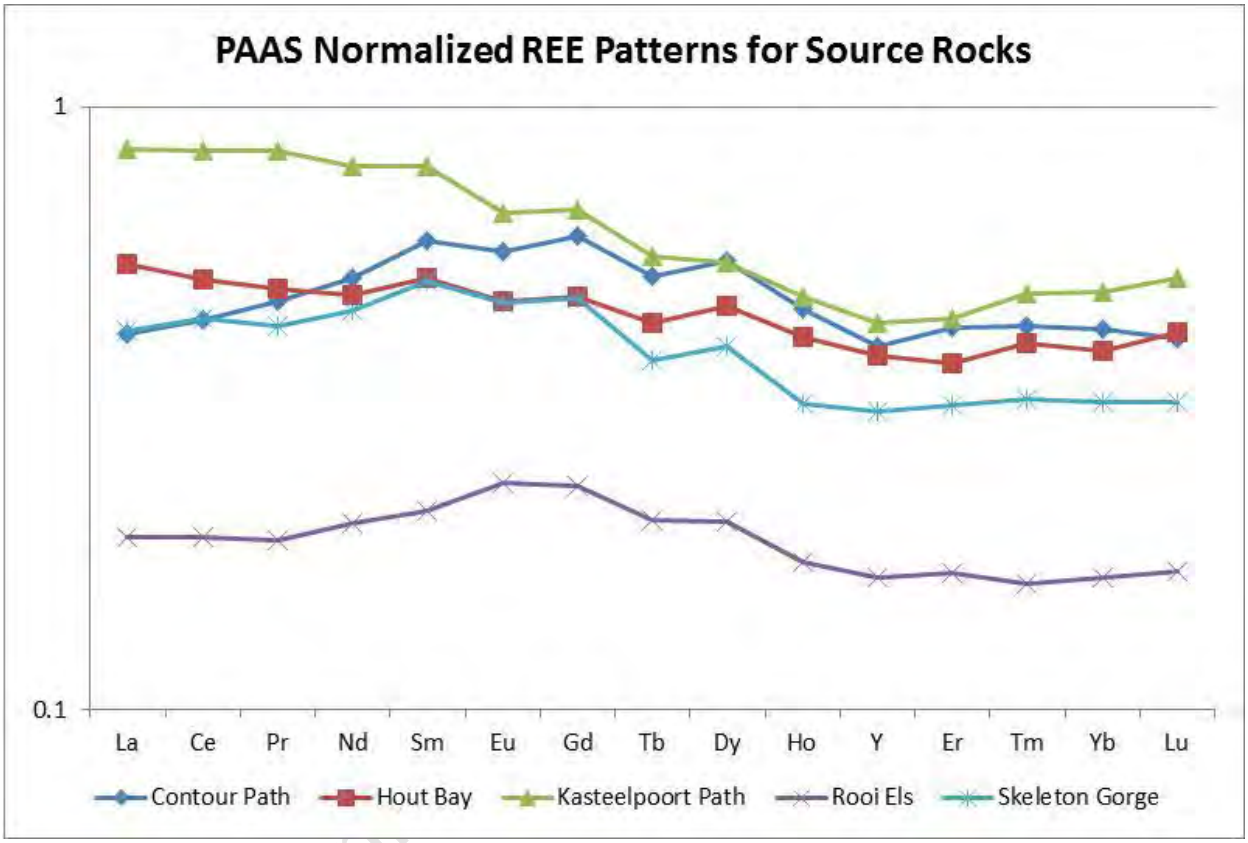

Figure 81: Source (silica rich) rock PAAS normalised REE patterns from ICP-MS analyses.

In summary the REE patterns show that many of the manganese deposits have a similar REE pattern to the proposed Peninsula Fm silica rich rocks but have a greater REE content than the source rock. In some of the sites however the manganese samples are not enriched relative to the source rocks and this may reflect the modification of the REE pattern during the deposition of the manganese deposits as indicated by the variable REE patterns related to the amount of iron and manganese content. Ultimately the variable source rocks REE and changes in the fluids involved, and in the lateral secretion mechanism results in variations in the REE pattern.

5 CONCLUSION

Harrison (1998) defined 8 different types of manganese deposits based on the depositional environment; the study did not differentiate between the manganese texturally or chemically. All of these deposit types are economic in some form, either as large scale mining, or as small artisanal mining. Most studies of manganese are focused on the large scale economic deposit types (Types 4, 7 and 8) but the other types of manganese deposition are important in terms of understanding the geochemical behaviour of manganese in different environments. The manganese deposits within the Cape Peninsula were economic in the early 1900's (Welsh, 1917) but because of their small size and varying grades the mining of these deposits soon stopped. While no longer economic they are of interest, especially as no work has focused on the origin, type or the regional geological setting of the Cape's manganese deposits.

This study focused on the Cape Peninsula and its many small scale superficial vein and surface coatings of manganese and iron. Five relatively large deposits were analysed at Skeleton Gorge, Kommetjie, Hout Bay and Rooi Els, and one previously unknown deposit at Kasteelpoort Path. Not only are there chemical variations among the sites, both in bulk rock chemistry and the REE patterns, but there are also variations to the depositional setting. Three depositional settings were established, veined deposits, surface deposits and talus slope deposits. It was shown that chemically there are subtle differences between the depositional settings but that the mechanism controlling the deposition was the same. The differences came from variations within the local geology.

Vein deposits occur throughout the region, but are mainly recessed deep within the rock, where the fracture spacing increases substantially then large scale manganese deposition can occur, resulting in feasible artisanal mining of the manganese. Both surface and talus slope deposits occur once the fluids exit the bedrock. Thus all sample sites had a component of vein deposits.

The surface deposit occurs when the fluids exit the bedrock onto a rocky outcrop, while the talus slope deposit occurs when the fluids exit the bedrock into loose unconsolidated sediment, a talus slope off of the edge of a mountain. In both cases the size of the deposit is dependent on the amount of fluid flow, the concentrating mechanism and the rate of erosion.

The primary manganese mineral is cryptomelane, established through conclusive XRD profiles and the strong correlation of potassium and manganese. The manganese to potassium molar ratio of the samples from this study is higher than that predicted for ideal cryptomelane (KMn_8O_{16}) and is most likely the result of substitution of sodium and other elements for potassium in the mineral.

While it was shown that there is plenty of manganese and iron in the major rock types in the Cape Peninsula, to act as the source of the iron and manganese in the deposits fluids need to be able to access this manganese and iron and transport it away. Through analysis of the estimated porosity of the different rock formations in the study area, the Peninsula Fm sandstone is the only one

that could act as an aquifer allowing the movement of groundwater to leach the manganese and iron locked up within the rock matrix. Based on the manganese present within the unmineralised Peninsula Fm sandstone there is sufficient manganese to form the deposits found even assuming water to rock ratios of 1%.

Based on elemental plots and the elemental ratios it was established that the manganese was deposited in a hydrogenous fresh water environment. Not all of the manganese deposits had flowing water, but those that did showed signs of fresh deposition of manganese, and all of the Sites were down dip of a potential water source. By sampling the water within the Skeleton Gorge Site it was possible to conclusively show that the water has sufficient volumes of manganese to form the deposits in a relatively short space of time, 110 – 43 000 years.

While the Cape Peninsula is covered in Peninsula Fm rocks, and multiple streams, the occurrence of large manganese deposits are rare. This is where the third factor becomes important, a concentrating mechanism. This was mostly in the form of a fault; the fault gauge has a very low porosity, acting as an aquitard, while the rocks adjacent to the fault have a higher porosity due to increased fracture spaces. This results in increased fluid flow along the fault structure until the groundwater exits at a spring.

The formation of these deposits is dependent on three factors, being hosted by the Peninsula Fm sandstone, occurring on a down dip slope and having a concentrating mechanism. Being hosted by the Peninsula Fm sandstone speaks to three factors, mobility of the manganese within the sandstone due to its high porosity, the fact that the Peninsula Fm acts as a relief feature, and the fact that the manganese is leached out of the Peninsula Fm. Thus the Peninsula Fm is the start of the formation of these deposits with reduced fluids flowing into the Peninsula Fm, leaching out manganese, then moving through the Peninsula Fm and then finally exiting out of the Peninsula Fm at seeps or springs at a gorge or cliff face.

The requirement of the deposit to occur on a down dip slope is purely to assist with the flow of the fluids through the Peninsula Fm, this also helps to concentrate the fluids and build up the scale of the manganese deposit. While it is possible for deposits to occur against the dip of the bedrock (southern side of Skeleton Gorge) these deposits will be minor deposits. All other deposits occur on a down dip slope. Even Kasteelpoort Path and Rooi Els where the bedrock dips away are considered to be down dip deposits, as they occur within the talus slope which has formed on the flanks of the mountain and are natural down dip features.

Kasteelpoort Path, most of Rooi Els and most of Skeleton Gorge are small scale deposits. It takes the addition of the third factor to form large scale deposits, a concentrating mechanism. This concentrating mechanism forces all the fluids to seep out at a single point, increase the amount of fluids containing manganese and iron, and in turn increasing the amount of manganese and iron deposited.

It is the combination of these three factors which creates the large scale deposits, a faulted up dip Peninsula formation may still create manganese or iron deposit, but it will be small.

The geomorphology of the sites is important in understanding the overall dynamic of the lateral secretion model of deposition. The chemistry and transport of the manganese and iron revolves around their thermodynamic properties. Through an understanding of the pH of the waters involved and the Eh of the different portions of the lateral secretion model, it was possible to plot a proposed sequence of the manganese and iron dissolution and precipitation throughout the lateral secretion process. The initial presence of the rain water within the soil profile becoming acidic and losing oxygen causes the soil profile to become reductive and manganese and iron are dissolved into the fluid. These reduced fluids then move through the regolith and fractured bedrock until an aquitard is encountered which forces the fluids to exit as a surface seep or spring where the iron and manganese precipitate out as oxides in the high Eh environment.

Iron requires a lower Eh to precipitate out that manganese resulting in iron precipitating out within the cracks and voids present within the regolith near to the seepage point. As the fluids move closer to the seepage point the Eh will continue to rise, resulting in more iron precipitating out, and some manganese beginning to precipitate out. By the time the fluids reach the seepage point, most of the iron within the fluids will have precipitated out, and the Eh will have risen to very high levels, forcing the manganese to precipitate out on the surface of the rock in very high concentrations. This progression of joint and vein filled iron to massive manganese deposits was corroborated by the field observations, petrographic analysis and microprobe analysis.

REE plots show that the different classified rocks, manganese rich through to silica rich, and the different sites had large variability which was attributed to differences in the source rock chemistry, age and dynamic of the deposits. Based on the REE plots of the sites on Table Mountain, Kasteelpoort Path and Skeleton Gorge it was established that the presence iron results in an enriched REE pattern.

In summary, the deposits found in the Cape Peninsula can be classified as hydrogenous fresh water deposits formed through lateral secretion where the primary mineral formed is cryptomelane. Based on Harrison's (1998) classification system this means that they are a Type 1 deposit.

The results of this study assist in understanding the formation of manganese deposits particularly the low temperature remobilisation of manganese by surface and groundwater processes. What it does not answer is whether or not such deposits are economical. Based on Harrison's (1998) classification system some Type 1 deposits are economical, and historically the Cape Peninsula had economic manganese mines. Table 28 shows the Cape Peninsula manganese deposits (where MnO > 20%) in comparison to other deposits from around the globe. From this table it is possible to see that the Cape Peninsula deposit, while having excellent manganese grades, has relatively high concentrations of

phosphorus and silica, which are deleterious elements making the deposits in the Cape Peninsula mostly of academic interest.

Table 28: Worldwide manganese deposits compared with the Cape Peninsula deposits, adapted from Schaefer et al. (2001).

Deposit Type	TYPE 8A		TYPE 8B	TYPE 8D		TYPE 8E		TYPE 8F			GLOBAL AVERAGE	TYPE 1
Deposit	Nikopol (Ukraine)		Gr. Eylandt (Australia)	Moanda (Gabon)	Azul (Brazil)	Molango (Mexico)	Urkut (Hungary)	Kalahari Manganese Field (South Africa)		Urucum (Brazil)		Table Mountain
Ore Type	Carbonate	Oxide	Oxide	Oxide		Carbonate		Carbonate	Oxide	Oxide		Oxide
Manganese	23.80	51.20	49.00	51.50	48.50	27.00	38.50	38.50	46.00	46.10	**42.01**	39.36
Iron	1.30	0.57	3.30	2.80	5.80	7.10	5.30	3.30	12.60	11.40	**5.35**	7.39
SiO_2			5.80	2.01	2.50	13.30	4.40	4.10	4.70	2.70	**4.94**	39.49
TiO_2				0.21				0.06	0.05		**0.11**	0.22
AL_2O_3			3.50	5.60	5.20	2.50		0.20	0.30	1.50	**2.69**	3.47
P_2O_5	0.18	0.25	0.09	0.11	0.08	0.10	0.11	0.01	0.02	0.17	**0.11**	0.89
CO_2	32.40					28.00		15.00			**25.13**	
Manganese/Iron	18.30	89.80	14.90	18.00	8.40	3.80	7.30	11.70	3.70	4.00	**17.99**	5.33

REFERENCES

Adelson, J.M., Heltz, G.R., Miller, C.V., 1999, Reconstructing the rise of recent coastal anoxia; Molybdenum in Chesapeake Bay sediments: *Geochimica et Cosmochimica Acta*, v. 65, p. 237-252.

Anhaeusser, C.R., Johnson, M.R., Thomas, R.J., 2006, The Geology of South Africa 2nd Edition: *The Geological Society of South Africa, Johannesburg.*

Balaram, V., Chandrasekharam, D., Gurav, T., Kaisary, S., Kota, D., Mudholkar, A.V., Paropkari, A.L., Prakash, L.S., Raju. K.A.K., Ray, D., Satyanarayanan, M., Sreenivas, B., 2012, Distribution of REEs and yttrium among major geochemical phases of marin Fe-Mn-oxides: Comparitive study between hydrogenous and hydrothermal deposits, *Chemical Geology*, v. 312-313, p. 127-137.

Banerjee, A., Bhowmilk, P.K., Cheney, M.A., Jose, R., Okoh, J.M., Qian, S., 2009, Synthesis and Characterization of Birnessite and Cryptomelane Nanostructures in Presence of Hoffmeister Anions: *Journal of Nanometals*, v. 2009.

Barrio, I., Centeno, M.A., Frias, D., Lopez, T., Montes, M., Nousir, S., Odriozola, J.A., 2007, Synthesis and characterization of cryptomelane- and birnessite-type oxides: Precursor effect: *Materials Characterization*, v. 58, p. 776–781.

Bennet, P.C., Hasset, J.P., Melcer, M.E., Siegel, D.I., 1988, The dissolution of quartz in dilute aqueous solutions of organic acids at 25°C, *Geochemica et Cosmochimica Acta*, Vol. 52, issue 12, p. 3023

Bergh, E., 2012, A one-year, postfire record of element deposition and cycling in the Kogelberg sandstone fynbos mountain ecosystem of the Western Cape, South Africa, Unpublished MSc Thesis *Department of Geological Sciences, Faculty of Science, University of the Cape Town*.

Beukes, N.J., Gutzmer, J., 2002, Iron and Manganese Ore Deposits: Mineralogy, Geochemistry, and Economic Geology, *Encyclopaedia of Life Support Systems, UNESCO*, Section 5.15.6.2

Blake, D., Hartnady, C., Mlisa, A., 2010, Large scale quantification of aquifer storage and volumes from the Peninsula and Skurweberg Formations in the southwestern Cape, *Water SA, Young Water Professionals Special Edition 2010*, v. 36, n. 2

Bonatti, E., Kraemer, T., Rydell, H.S., 1972, Classification and genesis of submarine iron-manganese deposits, *in* Horn, D., ed., Ferromanganese deposits on the ocean floor: *National Science Foundation, Washington, D.C.,* p. 149-166.

Brink, S.E., Cleland, J.M., McSwiggen, P.L., Melcher, F., Morey, G.B., 1996, Hydrothermal Systems in Manganese-rich Iron-formation of the Cuyana North Range, Minnesota: Geochemical and Mineralogical Study of the Gloria Drill Core, *Minnesota: Minnesota Geological Survey Report of Investigations* n 46.

Bortleson, G.C., Lee, G.F., 1974, Phosphorous, iron, and manganese distribution in sediment cores of six Wisconsin lakes, *Limnology and Oceanography,* v. 19, p. 794-801.

Brookhart, J.W., Langford, R.H., Robinove, C.J., 1958, Saline-Water Resources of North Dakota, *United States Government Printing Office, Washington.*

Brown, R., Tinker, J., de Wit, M., 2008, Mesozoic exhumation of the southern Cape, South Africa, quantified using apatite fission track thermochronology, *Tectonophysics,* v. 455, issue 1-4, p. 77-93.

Bryant, M., Hope, D., 2012, June 2012 Mineral Resource & Ore Reserve Competent Persons Report: Manganese CSG, GEMCO, *BHP Billiton*.

Burgers, C., Harris, C., Miller, J., Rawfoot, F., 2010, O- and H-isotope record of Cape Town rainfall from 1996 to 2008, and its application to recharge studies of Table Mountain groundwater, South Africa: *Geological Society of South Africa*, p. 33-56.

Compton, J.S., Smith, M., White, R.A., 2003, Rare earth element behaviour in soils and salt pan sediments of a semi-arid granitic terrain in the Western Cape, South Africa: *Chemical Geology*, v. 201, p. 239-255.

Compton, J.S., 2004, The Rocks and Mountains of Cape Town: *Double Storey, Cape Town.*

Cox, D.P., Singer, D.A., 1986, Mineral deposit models. *US Geological Survey Bulletin*, n 1693.

Cunat, P.J., 2004, Alloy Elements in Stainless Steel and Other Chromium-Containing Alloys, *The European Stainless Steel Development Association*, p. 1-24.

Diamond, R.E., Harris, C., 2000, Oxygen and hydrogen isotope geochemistry of thermal springs of the Western Cape, South Africa: Recharge at high altitude? *Journal of Earth Sciences*, Vol. 31, issue3-4, p. 467-481.

Dill, H.G., Hanse, B., Keck, E., Weber, B., 2010, Cryptomelane: A tool to determine the age and the physical chemical regime of a Plio-Pleistocene weathering zone in a granitic terrain (Hagendorf, DE Germany): *Geomorphology*, v. 121, p. 370-377.

Duncan, A.R., Marchant, J.W., Willis, J.P., 1978, Geochemistry of the TMG, I: Aspects of the Origin of the Hout Bay Manganese Deposit: *South African Journal of Geology*, v. 81, p. 179-184.

Drahota, P., Grygar, T., Mihaljevic M., Pertold, Z., Rohovec, J., 2010, Seasonal variations of Zn, Cu, As and Mo in arsenic-rich stream at the Mokrsko gold deposit, Czech Republic: *Environmental Earth Science*, v. 62, p. 429-441.

Feng, X., Li, Q., Liu, F., Qiu, G., Tan, W., Yu, Y., 2011, Oxidation behaviour and kinetics of sulphide by synthesized manganese oxide minerals: *Journal of Soils and Sediments, December 2011*, v. 11, issue 8, p. 1323−1333.

Fleischer, M., Hewett, D.F., 1960, Deposits of Manganese Oxides: *Economic Geology*, v. 55, p. 1-53.

Graham, R.D., Hannan, R.J., Uren, N.C., 1988, Manganese in Soils and Plants, *Kluwer Academic Publishers,* v. 1, p. 1-55.

Gruner, J.W., 1943, The Chemical Relationship of Cryptomelane (Psilomelane), Hollandite, and Coronadite: *American Mineralogist*, v. 28, n, 9-10, p.497-506.

Gültekin, A., 1998, Geochemistry and Origin of the Oligocene Binkiliç Manganese Deposit; Thrace Basin, Turkey: *Tubitak Journals of Earth Sciences*, v. 7, p. 11-23.

Harder, H., 1976, Synthesis of Iron Layer Silicate Minerals Under Natural Conditions, *Clays and Clay Minerals*, vol. 26, no. 1, p. 65-72.

Harrison, P., 1998, Description of the Various Manganese Deposit Types, *Unpublished Internal Samancor (South African Manganese Corporation) Document*, v. 3, p 1-53.

Hutcheson, P., 2004, Geology of the Coastal Terrace between Strand and Kleinmond, Unpublished Honours Thesis *Department of Geological Sciences, Faculty of Science, University of the Cape Town*.

Jia, H., Lin, L., Xu, Y., 2009, Groundwater Flow Conceptualization and Storage Determination of the TMG (TMG) Aquifers: *Water Research Commission,* WRC Report No. 1419/1/09

Karberg, N.J., King, J.S., Friend, A.L., Pregitzer, K.S., Wood, J.R., 2005, Soil carbon dioxide partial pressure and dissolved inorganic carbonate chemistry under elevated carbon dioxide and ozone: *Oecologia*, v 142, p 296-306.

Krauskopf, K.B., 1957, Seperation of manganese from iron in sedimentary processes: *Geochimica et Cosmochimica Acta,* v. 12, p 66−84.

Laznicka, P., 1992. Manganese deposits in the global lithogenetic system: quantitative approach. *Ore geology reviews*, v.7, p 279 - 356.

Lindgren, W., 1933, Mineral Deposits: *McGraw Hill, 4th Edition, London.*

Lindstad, T., Olsen, S.E., Tangstad, M., 2007, Production of Manganese Ferroalloys, *SINTEF and Tapir Academic Press*, v. 1, p. 1−27.

Lovley, D., 1991, Dissimilatory Fe(III) and Mn (IV) Reduction, *Microbiological Reviews*, v. 55, no 2, p. 259−287.

Machamer, J.F., 1987. A working classification of manganese deposits. *Mining Magazine*, October, p 348-351.

Martin, S., 2003, Environmental Catalysis: Chapter 4: Precipitation and Dissolution of Iron and Manganese Oxides, *Taylor & Francis.*

Maynard, J., 2010, The Chemistry of Manganese Ores through Time: The Signal of Increasing Diversity of Earth-Surface Environments: *Economic Geology*, v. 1, p. 535–552.

McLennan, S.M., Taylor, S.R., 1985, The Continental Crust: Its Composition and Evolution. *Blackwell, Oxford*.

Moriyama, T., Panigrahi, M.K., Pandit, D., Watanabo, Y., 2008, Rare Earth Element Enrichment in Late Archean Manganese Deposits from the Iron Ore Group, East India: *Resource Geology*, v. 58, issue 4, p. 402–413.

Nahon, D., Parc, S., Tardy, Y., Vieillard, P., 1989, Estimated solubility products and fields of stability for cryptomelane, nsutite, birnessite, and lithiophorite based on natural lateritic weathering sequences: *American Mineralogist*, v. 74, p. 466–475.

Netili, K.F., 2007, A Preliminary Understanding of Deep Groundwater Flow in the TMG (TMG) Aquifer System, Unpublished MSc Thesis - *Department of Earth Sciences, Faculty of Science, University of the Western Cape*.

Nicholson, K., 1992, Contrasting Mineralogical - Geochemical Signatures of Manganese Oxides: Genesis to Metallogenesis: *Economic Geology*, v. 87, p. 1253–1264.

Robb, L.J., 2005, Introduction to Ore-Forming Processes, *Blackwell Science Ltd*, *Victoria, Australia*, v. 1, p. 129–214.

Roy, S., 1981. Manganese deposits. *Academic Press*, p 458.

Roy, S., 1988, Manganese metallogenesis: a review. *Ore geology reviews*, v 4, p 155-170.

Roy, S., 1992, Environments and processes of manganese deposition, *Economic Geolology*, v 87, n 5, p 1218-1236.

Roy, S., 1997, Genetic diversity of manganese deposition in the terrestrial geological record, *Geological Society, London, Special Publications*, v. 199, p. 5-27.

Schaefer, M.O., Beukes, N.J., Gutzmer, J., 2001, Late Paleoproterozoic manganese rich oncoids: Earliest evidence for microbially mediated manganese precipitation: *Geology*, v. 29, p. 835-838.

Smit, A., 2003, Geochemistry of pristine fynbos ecosystem in the Harold Porter National Botanical Gardens and Kogelberg biosphere reserve, Unpublished MSc Thesis – *Department of Geological Sciences, Faculty of Science, University of the Cape Town*.

Sparks, L., 2003, Environmental Soil Chemistry: *Academic Press, London.*

Swenson, H., 2012, Why is the Ocean Salty?: *General Interest Publications of the US Geological Survey.*

Tangstad, M., Calvert, P., Brun, H. & Lindseth, A.G., 2004, Use of Comilog ore in ferromanganese production. *Proceedings of the Tenth International Congress on Ferroalloys (INFACON 10), Cape Town, 1-4 February 2004,* p. 213-222.

The Joint Ore Reserves Committee of The Australasian Institute of Mining and Metallurgy, Australian Institute of Geoscientists and Minerals Council of Australia (JORC)., December 2004, The Australasian Code for Reporting Exploration Results, Mineral Resources and Ore Reserves (The JORC Code): *JORC*.

United Nations Publications, 2003, Commodity Yearbook 1995-2000, ISBN 92-1-012050-7.

Welsh, A.B., 1917, Report on the manganese Deposits in the South-West Districts of the Cape Province: Cape Times Limited, *Government Printers*.

World Health Organization (WHO), 1996, Iron in Drinking Water, Guidelines for drinking water quality WHO/SDE/WSH/03.04/08.

World Health Organization (WHO), 2011, Manganese in Drinking Water, Guidelines for drinking water quality WHO/SDE/WSH/03.04/104/Rev/1.

Websites

WEB 1 – http://www.indexmundi.com/en/commodities/minerals/manganese/manganese_t8.html

WEB 2 – http://web.ead.anl.gov/resrad/datacoll/porosity.htm

WEB 3 – http://www.webmineral.com/data/Cryptomelane.shtml

WEB 4 – http://www.webmineral.com/data/Pyrolusite.shtml

WEB 5 – http://www.webmineral.com/data/Quartz.shtml

WEB 6 – http://wisconsingeologicalsurvey.org/porosity_density/about_porosity_density.htm

WEB 7 – http://www.worldsteel.org/media-centre/press-releases/2011/april-sro.html

APPENDIX A

Number of microprobe maps and line scans generated for primary samples.

Sample Number	Number of maps constructed (80µm by 80µm)	Number of line scans done	Sample Locality
A5	5	1	Skeleton Gorge
B1	2	0	Rooi Els
B2	2	3	
B4	7	0	
B5	1	0	
B6	4	0	
B7	6	0	
C1	3	3	Kasteelpoort Path
C2	2	0	
C3	2	0	
C4	1	0	
C5	7	5	
C6	4	3	
D1	2	0	Contour Path
D2	2	0	
D3	2	0	
D4	2	0	
E3	2	3	Hout Bay
E4	4	2	

Number of microprobe maps and line scans generated for secondary samples.

Sample Number	Number of maps constructed (150µm by 150µm)	Number of line scans done	Sample Locality
1	2	0	Skeleton Gorge
3	3	0	
5	2	0	
7	2	0	
8	7	0	
10	8	7	
11	3	0	
14	2	2	
16	5	3	
19	2	0	
20	9	2	
23	5	0	
25	2	0	
27	3	0	
29	2	3	
30	4	0	
31	2	0	
A2	3	0	
A3	3	2	
A5	6	0	

APPENDIX B

Petrographic analyses of initial samples.

Sample Number	Location	Hand Held Description	Thin Section Description	Percentages
A1	Skeleton Gorge	Quartz	Large grains, almost no fracturing present	Quartz - 98%
		Mica	Appears to be overprinting and replacing quartz	Mica - Trace
		Isotropic Mineral	Detrital grain of isotropic mineral	Manganese - Trace
		Iron	Staining of the edges of some of the quartz grains that have fracturing	Iron - Trace
A2		Quartz	Highly fractured grains, almost angular due to fractured nature	Quartz - 80%
		Mica	Very rare, remains inbetween few remaining grain boundaries	Mica - Trace
		Iron	Due to more fractures, more exploitable crevices, thus more staining around quartz grains	Iron - 15%
		Manganese	Starting to intruse into the fractures occuring in the quartz, iron dominant still	Manganese - 5%
A3		Quartz	Grains are fractured along edges, but in the centre, some embayements also present	Quartz - 65%
		Iron	Occurs in the embayments and stains the quartz	Iron - Trace
		Manganese	Prevalent everywhere, completely isolates the quartz grains from eachother	Manganese - 35%
A4		Quartz	Grains are fractured along edges, but in the centre, some embayments also present	Quartz - 50%
		Iron	Occurs in the embayments and stains the quartz	Iron - Trace
		Manganese	Prevalent everywhere, completely isolates the quartz grains from eachother	Manganese - 50%
A5		Quartz	Highly fractured, very small, isolated	Quartz - Trace
		Iron	Occurs in concentric layered circular structures, almost like growth rings, occaisionally the centre is empty	Iron - 15%
		Manganese	Appear to be embayments in the iron, with the manganese replacing it	Manganese - 85%
A6		Quartz	Highly fractured and broken down into smaller grains	Quartz - 55%
		Iron	Only occurs in grain boundaries and as staining of the quartz occaisionally	Iron - 10%
		Manganese	Occaisionally causing as veins, have intensely fractured and broken up quartz grains	Manganese - 35%
A7		Quartz	Shows bimodal qualities, half fractured, isolated, broken up and the other half not	Quartz - 60%
		Iron	Only occurs in the unfractured quartz by staining the cementation material	Iron - Trace
		Manganese	The other half of the quartz is surrounded by manganese	Manganese - 40%

B1	Rooi Els	Quartz	Large grains, almost no fracturing present	Quartz - 88%
		Mica	Appears to be replacing quartz	Mica - 10%
		Manganese	Occurs within grain boundaries replacing mica	Manganese - Trace
		Iron	Occurs within grain boundaries replacing mica	Iron - Trace
B2		Quartz	Not very fractured, but quartz grains smaller than usual and isolated from eachother	Quartz - 30%
		Iron	Dominates the rock, but not the quartz grains, against the norm	Iron - 45%
		Manganese	Only occurs as rings around quartz grains, against norm	Manganese - 25%
		Green Mineral	Detrital in origin	Green Mineral - Trace
B3		Iron	Generally froms concentric layered circles, otherwise forms isolated points in manganese	Iron - 65%
		Manganese	Boundary between iron and manganese sharp, with no manganese in the iron, but some iron in the manganese	Manganese - 35%
B4		Quartz	Bimodality occurs again, one part highly fractured smaller grains, the other not fractured larger grains	Quartz - 50%
		Iron	Occurs in the fractures of the quartz or stains the quartz	Iron -Trace
		Manganese	Covers a lot of the rock, filling in the gaps from the fracturing, veined manganese present as well	Manganese - 50%
B5		Quartz	Chert type substance	Quartz - 100%
B6		Quartz	Bimodality occurs again, one part highly fractured smaller grains, the other not fractured larger grains	Quartz - 70%
		Iron	Occurs in the fractures of the quartz or stains the quartz or is massive and causing embayments into quartz	Iron -10%
		Manganese	Covers a lot of the rock, filling in the gaps from the fracturing, minor veined manganese present as well	Manganese - 20%
B7		Quartz	Bimodality occurs, one part highly fractured smaller grains, the other not fractured larger grains with Mica	Quartz - 65%
		Mica	Covers only one section of the rock, same section as the iron, no replacement of mica by the manganese	Mica - 5%
		Iron	Only occurs in one section of the rock, replacing the Mica, this is the non fractured section of quartz	Iron -Trace
		Manganese	Covers a lot of the rock, filling in the gaps from the fracturing, does not extend into the Mica section, veined manganese present as well	Manganese - 30%

C1	Kasteelpoort Path	Quartz	Appear to be unalteriron, almost no fracturing present, and very little replacement also	Quartz - 40%
		Carbonate	Appears to be numerous large detrital pieces of carbonates	Carbonate - 5%
		Iron	Occurs as staining of the grain boundaries of the quartz	Iron - Trace
		Manganese	Fills in the contacts between the quartz, not forcing fractures or grains apart	Manganese - 55%
C2		Quartz	Bimodality, smaller more fractured grains with manganese isotropic minerals, larger more cohesive grains without	Quartz - 75%
		Iron	Generally appears to be only affecting the cementation material of the quartz, not very dominant	Iron -5%
		Manganese	Dominant in the more fractured side of the thin section, filling in the spaces and gaps of the quartz, minor veined manganese present as well	Manganese - 20%
C3		Quartz	Quartz is highly fractured and broken up, has very little cohesion	Quartz - 50%
		Iron	Occurs in grain boundaries and generally only as a fine staining	Iron -Trace
		Manganese	The fracturing has been exploited and manganese dominates these areas, minor veined manganese present as well	Manganese - 50%
C4		Quartz	Quartz is highly fractured and broken up, has very little cohesion	Quartz - 50%
		Iron	Occurs in grain boundaries and generally only as a fine staining	Iron -Trace
		Manganese	The fracturing has been exploited and manganese dominates these areas, minor veined manganese present as well	Manganese - 50%
C5		Iron	Concentric layering present again, coupled with occaisional holes in the centre of the rings	Iron -35%
		Manganese	Contact between manganese and iron sharp, no crossing by either	Manganese - 65%
C6		Quartz	Quartz is not fractured, has no embayments, there is a large vein just cutting straight through the middle	Quartz - 60%
		Mica	Occurs in the cementation material of the quartz	Mica - Trace
		Aplite	Crystalline mineral occuring in the vein, perfectly euhedral	Aplite - 10%
		Iron	Staining of the grain boundaries of the quartz	Iron -10%
		Manganese	Doesn't cross outside the boundaries of the vein, inside these boundaries it encompasses the Aplite	Manganese - 20%
C7		Quartz	Quartz is not fractured, has no embayments, there is a large vein just cutting straight through the middle	Quartz - 60%
		Mica	Occurs in the cementation material of the quartz	Mica - Trace
		Aplite	Crystalline mineral occuring in the vein, perfectly euhedral	Aplite - 10%
		Iron	Staining of the grain boundaries of the quartz	Iron -10%
		Manganese	Doesn't cross outside the boundaries of the vein, inside these boundaries it encompasses the Aplite	Manganese - 20%

D1	Contour Path	Quartz	Equigranular, sub rounded to sub angular, typical arenite	Quartz - 80%
		Mica	Makes up the cementation material, inbetween the quartz grains	Mica - 15%
		Isotropic Mineral 1	Occurs as small detrital fragments, very rounded, sometime encompassed by cementation material	Isotropic Mineral 1 - Trace
		Isotropic Mineral 2	Angular and jagged, occurs only within the cementation material	Isotropic Mineral 2 - Trace
D2		Quartz	Equigranular, sub rounded to sub angular, typical arenite	Quartz - 98%
		Mica	Makes up the cementation material, inbetween the quartz grains	Mica - Trace
		Isotropic Mineral 1	Occurs as small detrital fragments, very rounded, sometime encompassed by cementation material	Isotropic Mineral 1 - Trace
		Isotropic Mineral 2	Angular and jagged, occurs only within the cementation material	Isotropic Mineral 2 - Trace
D3		Quartz	Equigranular, sub rounded to sub angular, typical arenite	Quartz - 98%
		Mica	Makes up the cementation material, inbetween the quartz grains	Mica - Trace
		Isotropic Mineral 2	Angular and jagged, occurs only within the cementation material	Isotropic Mineral 2 - Trace
D4		Quartz	Equigranular, sub rounded to sub angular, typical arenite	Quartz - 98%
		Mica	Makes up the cementation material, inbetween the quartz grains	Mica - Trace
		Isotropic Mineral 2	Angular and jagged, occurs only within the cementation material	Isotropic Mineral 2 - Trace

E1	Hour Bay	Iron	Concentric layered circles which do not touch or interact, suggests zoning , or pulses of fluids	Iron - 100%
		Iron	Similar to C5, except the manganese is dominant. Iron still shows zonation, and is blotchy	Iron - 65%
E2		Manganese	Contact still sharp, no crossing by either party	Manganese - 35%
E3		Manganese	Layers are visible when looking at the section with the naked eye, not with microscope due to isotropy	Manganese - 100%
		Iron	Appears to be a solid mass with no layering , except along the manganese veins, here a lighter iron band occurs	Iron - 65%
E4		Manganese	Massive veined manganese, appears silver in hand specimen, is completely isotropic	Manganese - 35%
E5		Manganese	Layers are visible when looking at the section with the naked eye, not with microscope due to isotropy	Manganese - 35%
		Quartz	Bimodality, mostly not fractured and larger grains size, other parts heavily fractured and smaller grain size	Quartz - 60%
E6		Manganese	Fractured quartz surrounded in manganese	Manganese - 35%

E7	Kommetjie	Quartz	Not very fracture, but not very cohesive either	Quartz - 55%
		Iron	Iron fills in grain boundaries, fractures and stains the quartz, covers the rock	Iron - 40%
		Manganese	Only occurs sporadically where a large fracture has occuriron in the quartz	Manganese - 5%

Petrographic analyses of secondary samples.

Sample Number	Location	Hand Held Description	Thin Section Description	Percentages
1	Sample Site 1	Sandstone, slightly weathered	Medium to small sized particles of quartz, grains are sub rounded to sub angular. Some clay and mica minerals evident in between some of the quartz clasts. Some rounded isotropic minerals noticed.	Quartz – 95% Mica – 1% Weathered material – 2% Isotropic Mineral – 2%
2	Sample Site 1	Sandstone, slightly weathered	Medium to small sized particles of quartz, grains are sub rounded to sub angular. Some clay and mica minerals evident in between some of the quartz clasts. Some rounded isotropic minerals noticed.	Quartz – 95% Mica – 1% Weathered material – 2% Isotropic Mineral – 2%
3	Sample site 2	Manganese coated sandstone	Small grained sub angular quartz grains with some clay inbetween the quartz grains. Some micas also present, and some isotropic minerals (both rounded and not).	Quartz – 85% Mica – 1% Weathered material – 10% Isotropic Mineral – 2%
5	Sample site 2	Manganese coated sandstone	Small grained sub angular quartz grains with some clay inbetween the quartz grains. Some micas also present, and some isotropic minerals (both rounded and not).	Quartz – 85% Mica – 1% Weathered material – 10% Isotropic Mineral – 2%
7	Sample site ¾	Extensive surface coating	Sub rounded to sub angular medium grained quartz grains, with both iron and manganese occuring within the matrix material. Where the manganese occurs the quartz is less present, where the iron occurs the quartz is more dominant.	Quartz – 50% Iron – 25% Manganese – 25%
8	Sample site 3/4	Extensive surface coating	Small to very small angular quartz fragments held together by a matrix of manganese material. It appears as if the manganese material is replacing the quartz, creating embayments in the quartz crystals. Trace amounts of iron are present along the cracks and margins of some of the quartz grains.	Quartz – 50% Manganese – 50% Iron – Trace
10	Sample site 3/4	Siltstone and manganese	Very small angular quartz grains within a brown to reddish brown matrix. In some cases the reddish brown matrix appears to be iron stained. Some portions of the quartz have a manganese matrix instead. There is no discernable difference between the two matrix's.	Quartz – 35% Red Matrix – 45% Manganese – 20%
11	Sample site 3/4	Replacement/surface coating	Very small quartz fragments, sub angular. Surrounded by manganese.	Quartz – 20% Manganese – 80%
14	Sample site 3/4	Replacement/surface coating	Fine grained quartz, angular and fractured grains. Matrix appears to be mainly iron, with some manganese veins.	Quartz – 80% Iron – 15% Manganese – 5%

16	Sample site 3/4	Manganese veins in sandstone	Medium to small grained sub rounded quartz, with some clay minerals and some rounded isotropic minerals. There is one long fracture running the length of the thin section. Along the margins of this fracture the quartz is severly fracture parallel to the fracture. The degree of fracturing decreases as on moves away from the fracture. Within the fracture there is only manganese.	Quartz – 70% Clay minerals – 10% Manganese – 20%
19	Sample Site 5	Granular Manganese	Small to very small angular quartz fragments held together by a matrix of manganese material. It appears as if the manganese material is replacing the quartz, creating embayments in the quartz crystals. Trace amounts of iron are present along the cracks and margins of some of the quartz grains.	Quartz – 50% Manganese – 50% Iron – Trace
20	Sample site 5	Sandstone with manganese veins	Medium to small quartz fragments. There are two sections to this thin section, the fine grained portion, and the coarser grained side. The coarser grained portion has the iron as a matrix, and is quartz clast dominant. The finer grained portion is matrix dominant and the matrix is manganese. There appears a sharp contact between the two zones.	Quartz – 50% Manganese – 30% Iron – 20%
23	Sample site 5	Granular Manganese	Small to very small angular quartz fragments held together by a matrix of manganese material. It appears as if the manganese material is replacing the quartz, creating embayments in the quartz crystals. Trace amounts of iron are present along the cracks and margins of some of the quartz grains	Quartz – 50% Manganese – 50% Iron – Trace
25	Sample site 6	Sandstone	Medium sub rounded quartz grains with some clay and mica present. Trace isotropic minerals present as well.	Quartz – 85% Mica – 5% Weathered material – 5% Isotropic Mineral – trace%
27	Sample Site 8	Breccia with Iron and Manganese staining	Medium to small grained sub rounded quartz grains. Running through the rock are fractures that have in some instances split the quartz grains in two. Occasionally there is breccia within the fractures, however the fractures are mainly filled with a iron and some manganese.	Quartz – 70% Iron – 25% Manganese – 5%
29	Sample Site 8	Breccia with Iron and Manganese staining	Medium to small grained sub rounded quartz grains. Running through the rock are fractures that have in some instances split the quartz grains in two. Occasionally there is breccia within the fractures, however the fractures are mainly filled with a iron and manganese. The majority of the isotropic minerals are iron.	Quartz – 70% Iron – 25% Manganese – 5%
30	Sample site 3/4	Siltstone	Very fine grained siltstone, layering evident. Some carbonaceous layers also evident. Clay minerals abundant, and mica's also present.	Quartz – 50% Clay – 35% Mica – 5% Carbonaceous material – 10%
31	Sample site 3/4	Sandstone	Small to medium grained sub angular quartz crystals. Some clay minerals present, almost no isotropic minerals noticed though.	Quartz – 95% Weathered material – 4% Isotropic Mineral – 1%

APPENDIX C

Additional XRD analyses.

Sample A4.

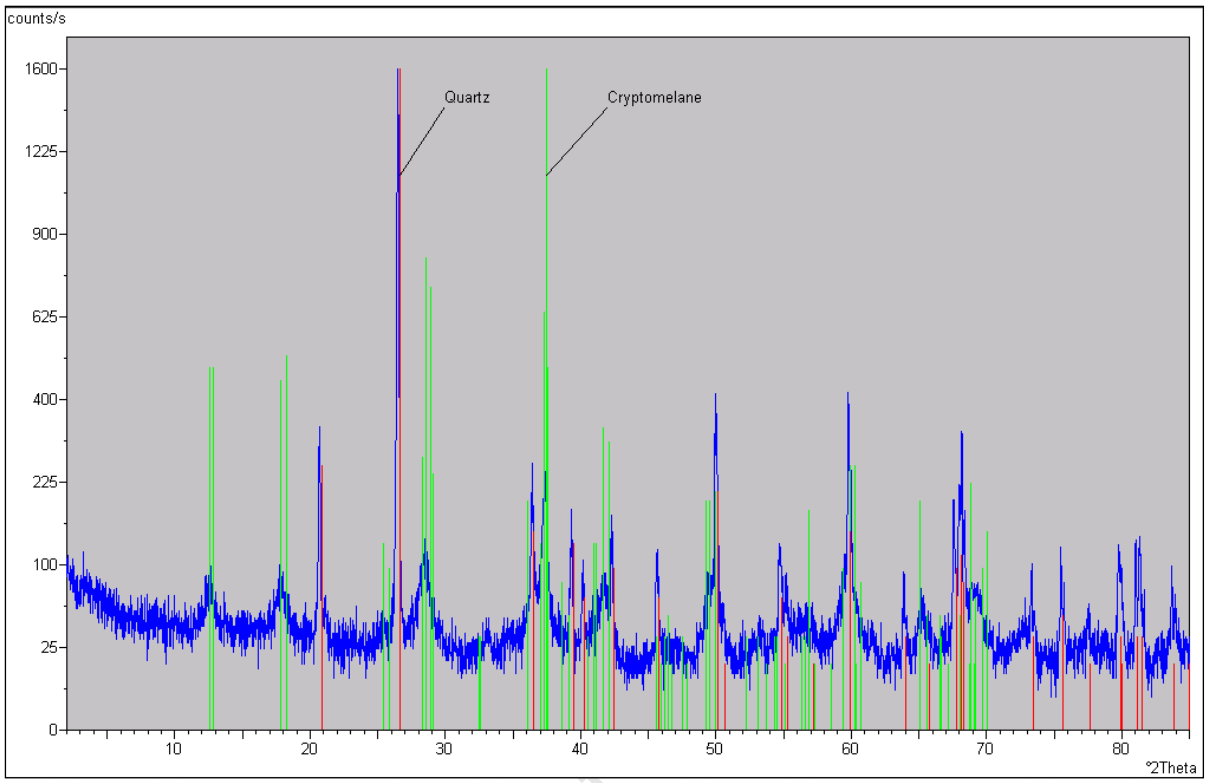

Sample E6.